**US Army Corps
of Engineers**
Waterways Experiment
Station

Comparison Between Third- and Second-Generation Ocean Wave Models

by   Steven M. Bratos

**US Army Corps
of Engineers**
Waterways Experiment
Station

INFORMATION
TECHNOLOGY
LABORATORY

–N–

HEADQUARTERS
BUILDING

MAIN
ENTRANCE

COASTAL &
HYDRAULICS
LABORATORY

GEOTECHNICAL
LABORATORY

ENVIRONMENTAL
LABORATORY

FOR INFORMATION CONTACT:
PUBLIC AFFAIRS OFFICE
U.S. ARMY ENGINEER
WATERWAYS EXPERIMENT STATION
3909 HALLS FERRY ROAD
VICKSBURG, MISSISSIPPI 39180-6199
PHONE: (601) 634-2502

STRUCTURES
LABORATORY

SCALE
500   0   500 m

AREA OF RESERVATION < 2.7 sq km

PREFACE

The investigation described herein was authorized as a part of the Civil Works Research and Development Program by the Headquarters, U.S. Army Corps of Engineers (HQUSACE). Work was performed under the Modeling the Evolution of Wave Spectra in Shallow Water work unit (No. 32869), which is part of the Coastal Navigation and Storm Damage Reduction Program, and the Rapidly Installed Breakwater System (RIBS) work unit, which is part of the Logistics Over the Shore (LOTS) Program, at the Coastal and Hydraulics Laboratory (CHL) of the U.S. Army Engineer Waterways Experiment Station (WES). Messrs. John Bianco, Charles Chesnutt, and Barry Holiday were HQUSACE Program Monitors.

The study was conducted from 1 January 1995 through 31 June 1997 by Mr. Steven M. Bratos, Research Division (RD), CHL. This report is substantially the same as the thesis submitted to Texas A&M University by Mr. Bratos in partial fulfillment of the requirements for a Master of Science degree in Ocean Engineering. Drs. Robert E. Randall, Texas A&M University, and Edward F. Thompson, WES, were thesis advisors.

This study was performed under the general supervision of Dr. James R. Houston, Director, CHL; Mr. Charles C. Calhoun, Jr., Assistant Director, CHL; and Ms. Carolyn Holmes, Program Manager, Coastal Navigation and Storm Damage Reduction Program, CHL. During the course of the study, direct supervision was provided by Mr. H. Lee Butler, Chief, RD (retired). At the time of final preparation of this report, direct supervision was provided by Mr. C. E. Chatham, Jr., Chief, Navigation and Harbors Division.

At the time of publication of this report, Director of WES was Dr. Robert W. Whalin. Commander was COL Robin R. Cababa, EN.

TABLE OF CONTENTS

Page

LIST OF FIGURES

FIGURE   Page

FIGURE   Page

LIST OF TABLES

CHAPTER I

INTRODUCTION

1.1 Objective

The objective of this research is to investigate and document the performance of the two spectral wave models used at the US Army Waterways Experiment Station. The models differ significantly in complexity and computing requirements, but differences in the accuracy of wave estimations are less clear. High-quality wind fields, with detailed spatial and temporal resolution are used to force the models in an effort to isolate the true differences between the model formulations and subsequent performance. The two wave models used in this study are WISWAVE (Hubertz 1992), a second generation (2G) model, and a third generation (3G) model, 3GWAM: Cycle 4 (WAMDI 1988). Throughout this report, WISWAVE and 3GWAM: Cycle 4 are referred to as "WIS" and "WAM" respectively. A battery of statistical tests is used to compare the models to in situ measurements, in deep water, over a wide variety of meteorological and wave scenarios.

1.2 Review of Wind Wave Modeling

a. Birth of wave prediction tools

The development of theories for ocean waves began in the early 1940's during World War II. Effective planning for amphibious operations required accurate prediction of wave conditions. In response to this need Sverdrup and Munk (1947) offered a practical wave forecasting theory based on wave energy growth and decay, and they were among the first to use a statistical wave

---

This thesis follows the style and format of the *Journal of Atmospheric and Oceanic Technology*.

parameter, called the significant wave height. Bretschneider (1952) provided further modification to the Sverdrup and Munk (1947) theory, and Pierson et al. (1955) advanced the theory with the introduction of the wave energy spectrum as a function of wind. Since this development, research has focused on refining specifications for the shape of the wave spectrum for a given wind and the appropriate treatment of nonlinearities in a linear model.

b. First generation modeling

The realization that waves are a random process and hence more accurately represented by frequency-direction spectra rather than in terms of a wave height and period, led to the development of numerical wave prediction models based on the transport equation for two-dimensional wave spectra (Gelci et al. 1957). These models are referred to as first generation (1G) wave models. The transport or energy balance equation is given by:

$$\frac{\partial F}{\partial t} + \vec{c_g} \cdot \nabla F = \Sigma S_i \tag{1}$$

where F is the two dimensional wave spectrum, and is a function of frequency f, direction θ, the spatial coordinates x and y and time t. The group velocity (c_g) is a function of x and y. The second term on the left side of the equation, $\vec{c_g} \cdot \nabla F$, represents the effects of wave propagation. The source/sink term on the right side, $\sum S_i$, represents the effects of all processes that add or remove energy. These include the atmospheric input, S_{in}, and high frequency dissipation, S_{ds}.

The atmospheric input, S_{in}, is represented by a combined Phillips (1957) and Miles (1957) term. Phillips' resonance model considers turbulent pressure fluctuations on the surface. Miles' shear flow model neglects the turbulent fluctuations and considers the mean flow and the waves. The resonance model produces a linear growth of waves and provides a broad-spectrum energy

input in the early stages of wave growth. In Miles' model the interaction between the mean flow and waves provides a frequency dependent feedback and produces exponential wave growth. These mechanisms form the relationship for growth of waves through atmospheric input.

In nature there is a limit to the height that waves can grow. Using only the Miles-Phillips mechanism there is a potential for infinite wave growth. In order to limit the growth process, a mechanism that removes energy is required. Phillips (1958) proposed that one such mechanism is wave breaking and developed the concept of the universal equilibrium range of the spectrum. The universal equilibrium range is defined as the high frequency region of a spectrum where energy densities are limited due to local wave breaking that dominates over wind effects. This effect is represented as the high frequency dissipation term, S_{ds}. Pierson and Moskowitz (1964) extended the work of Phillips (1958) to formulate a limit for a fully developed wave spectrum which is based on the maximum amount of energy per frequency attainable for a given wind.

Hence, by the late 1950's, a theoretical basis for wind-wave growth was established from the concept of the Miles (1957) and Phillips (1957) mechanisms. Phillips (1958) limit for spectral densities reasonably capped the growth, and together with the wind-wave growth mechanism formed the basis for 1G models.

c. Second generation modeling

During the late 1960's through the early 1970's two avenues were pursued in the study of ocean wave mechanics that had a significant impact on the future of wave models. First, definitive wave measurement programs such as, the JONSWAP field experiment (Hasslemann et al. 1973), and Mitsuyasu (1968,1969), were undertaken. Secondly, theoretical work of Hasselmann (1962,1963a,1963b) on the introduction of a non-linear wave-wave interaction formed the basis of a fundamental change in understanding of the processes that controlled the spectral energy balance.

Hasselmann et al. (1973) and Mitsuyasu (1968) wave growth experiments showed that the high frequency equilibrium spectrum did not have a universal value as suggested by Phillips (1958). Instead, it was observed that a relationship existed between Phillips' equilibrium constant, α, and nondimensional fetch. This indicates that the high frequency equilibrium spectrum is controlled by more than just local wave breaking.

Prior to these experimental field studies, Hasselmann (1962,1963a,1963b) introduced the theory of nonlinear wave-wave interaction. Hasselmann showed mathematically that waves interact with each other spreading energy over the spectrum. Energy at the spectral peak transferred to regions of lower and higher frequency on either side of the spectral peak. While Hasselmann's nonlinear wave-wave interaction theory was presented in the early 1960's, its importance was not appreciated until discrepancies between field data and 1G model results were clearly documented. The nonlinear wave-wave interaction mechanism explained behavior found in the experimental studies. Parameterized solutions of Boltzman integrals (Hasselmann 1962), provided approximations of the nonlinear wave-wave interaction term, S_{nl}, and became the basis for second generation (2G) models.

In 2G models, the spectral energy balance consists of an atmospheric input, S_{in}, a dissipation, S_{ds}, and a nonlinear wave interaction, S_{nl}, source term. WISWAVE (WIS) (Hubertz 1992), one of the two models considered in this study, is an example of a 2G model. The model is presently used in the Corps of Engineers' long-term wave hindcast studies (Hubertz et al. 1993).

d. Third generation modeling

While 2G models have been widely used for the past 20 years and provide useful results for synoptic scale wind fields, they have several shortcomings. These deficiencies were summarized, through a controlled series of tests using a variety of 2G models, in the Sea Wave

Modelling Project (SWAMP 1985) wave model comparison study. All source terms were parameterized representations. However, the most restrictive assumption in 2G models is the requirement for an a priori limiting form of the frequency spectrum. The simplified nonlinear transfer parameterization requires the spectral shape to have predetermined limits. To obtain useful results, the models required significant tuning for different scenarios to obtain source term balance and approximately simulate JONSWAP growth rates. Many different formulations of the source terms are used in 2G models, including momentum flux and energy balance, but for the most part all consider these solutions as lumped mass conservation processes with the peak frequency changing via equational forms. The 2G models are unable to accurately simulate complex wind waves generated by rapidly changing wind fields such as hurricanes and small scale cyclones or frontal passages. These models also have difficulty simulating the change from wind-sea to swell.

Because of these deficiencies and uncertainties in 2G models, including an order of magnitude difference found in results of simple tests between 2G models, the SWAMP (1985) study recommended the development of 3rd generation (3G) models where the wave spectrum is determined by integration of the spectral transport equation without restrictions on the spectral shape. This requires discrete approximations, in frequency and direction, of all source terms commensurate with the resolution of the modeled spectrum. By using a more detailed description of the nonlinear wave-wave interaction source term, 3G models avoid the need for preset limits to the spectral shape. The most widely known 3G model is 3GWAM (WAM) (WAMDI Group 1988), the second model chosen for this investigation.

1.3 Motivation

Even though WIS and WAM have been compared in previous studies (Cardone et al. 1996), this study is the first direct comparison where frequency and direction are discretized

identically, no wind field interpolation is required and wave model grids are not nested. Nesting the grid of primary interest inside a larger domain grid allows the use of boundary conditions to represent wave energy originating from outside the primary grid but this adds another source of error in comparing the models' performance. The wind fields that are used in this comparison study are the highest quality available for wave modeling. These high-quality wind fields minimize the errors in the wave models due to wind input and therefore allow more insight into wave model deficiencies. In most studies, only mean wave parameters are used to evaluate model performance. This comparison study is unique in that frequency spectra and frequency-direction spectra have also been used to evaluate the performance of the wave models. Third generation (3G) models, due to less parameterization, are more computationally intensive than 2G models, however WIS requires an order of magnitude more memory than WAM. A comparison of WIS (2G) and WAM (3G) model performance forms a basis for determining the relative merits of each model.

CHAPTER II

WAVE MODEL AND WIND FIELD DESCRIPTION

2.1 Wave Models

a. Spectral transport equation

Both WIS and WAM describe the evolution of a two-dimensional ocean wave spectrum

through the integration of the spectral wave transport equation given by

$$\frac{\partial F}{\partial t} + (\cos\phi)^{-1} \frac{\partial}{\partial \phi} (\dot{\phi}\cos\phi F) + \frac{\partial}{\partial \lambda} (\dot{\lambda}F) + \frac{\partial}{\partial \theta} (\dot{\theta}F) = S \tag{2}$$

where F $(f, \theta, \phi, \lambda, t)$ is the two-dimensional wave energy spectrum and is a function of frequency f,

direction θ, and time t, in a spherical coordinate system with ϕ representing latitude and λ

representing longitude. The latitude and longitude components of group velocity are represented

by $\dot{\phi}$ and $\dot{\lambda}$ respectively and $\dot{\theta}$ is the rate of change of direction due to great circle propagation. The

source/sink term S includes the wind input S_{in}, nonlinear wave-wave interaction S_{nl}, and the wave

dissipation S_{ds}. The spectral transport equation describes the change in wave energy over a

spherical coordinate system due to these source terms. The representation of these source terms is

the main difference between the two models. The following sub-sections describe each model's

source term implementation and numerical schemes followed by a discussion of some simple test

cases used to illustrate model differences.

b. WIS source terms

As a 2G model, WIS is based on the assumption that the dynamic balance between wind

input and nonlinear energy flux due to wave-wave interactions dominates the transport equation so that the wave spectrum maintains an f^{-4} equilibrium shape. The source terms in this model are described in Resio and Perrie (1989). S_{in} includes a linear and exponential growth term and is given by $S_{in} = A + BF$. The exponential term, B, is a function of the wind speed, U. S_{nl} is represented as an energy transfer from the midrange frequencies to the forward face (low frequency side) of the spectrum. This energy transfer is based on momentum flux onto the forward face which is a constant proportion of the momentum flux transferred out of the midrange frequencies. The energy transfer is calculated in terms of the migrating peak frequency which defines the forward face and midrange portions of the spectrum. Energy and peak frequency are calculated in terms of the friction velocity, U_*. The drag law used to calculate U_* from U_{10}, the wind speed at a 10 m elevation, is that of Large and Pond (1981). Wave-wave interactions also transfer some energy to the high frequency region where it is assumed to be lost due wave breaking. S_{ds} removes all energy above a threshold frequency.

c. WAM source terms

For 3G models such as WAM, the energy transfer due to wave-wave interactions is not assumed to be dominant enough to control the shape of the spectrum. The source terms are defined explicitly and their balance is integrated over time to give an evolving wave spectrum. Limits to spectral growth and arbitrary spectral shapes up to about twice the peak frequency, f_p, are not applied. Instead energy in the spectrum is allowed to vary according to the source term estimates. A parametric form is still used for the high frequency region. WAM is described by the WAMDI-Group 1988.

This is the fourth cycle of WAM. This version uses the S_{in} described by Janssen(1991). The most significant difference between the S_{in} terms in WIS and this version of WAM is that the

growth rate is calculated as a function of the sea surface roughness as well as the wind. Janssen's method enhances young wind sea growth over older wind sea growth. S_{in} is a quadratic function of the friction velocity, U_* which is related to the roughness and roughness is related to the wave height or sea state. The drag law used in WAM is that of Wu(1982). S_{nl} is represented by a parameterization of the exact nonlinear wave-wave interactions described by Hasselmann et al. (1985) and is referred to as the Discrete Interaction Approximation (DIA). The whitecapping dissipation term S_{ds} removes energy from the high frequency region due to wave breaking and is proportional to f^4.

d. Numerical schemes

The numerical schemes used in wave models can introduce computational dispersion and dissipation which can cause misinterpretation of the model's physical behavior. This can affect the growth rate, response to shifting winds, propagation of swell, and the interaction between wind sea and swell. Therefore, it is important to understand the errors due to numerical schemes when interpreting wave model results. The numerical scheme used by both models for propagation is a first order upstream difference in time and space. Tolman (1992), Lin and Huang (1996), and Bender (1996) showed that the WAM implementation of this scheme is highly dissipative and have proposed higher order schemes to reduce this numerical error. The source terms in WAM are integrated using a second order implicit scheme. Another difference between the models is the treatment of the wind input over time. WIS interpolates the wind input, which has 1 hour increments, down to the model time step which is 600 sec. WAM keeps the wind constant between input intervals.

e. Simplified test cases

In order to isolate differences between some of the models' properties, three simple test cases were run. The cases consist of fetch and duration limited wave growth and response to shifting winds. The results of these tests provide a basis for discussion of model performance during the storm events in Chapter IV.

Cases I and II are concerned with fetch and duration limited wave growth for uniform stationary wind speeds of 5 m/s to 30 m/s in increments of 5 m/s blowing orthogonally across the
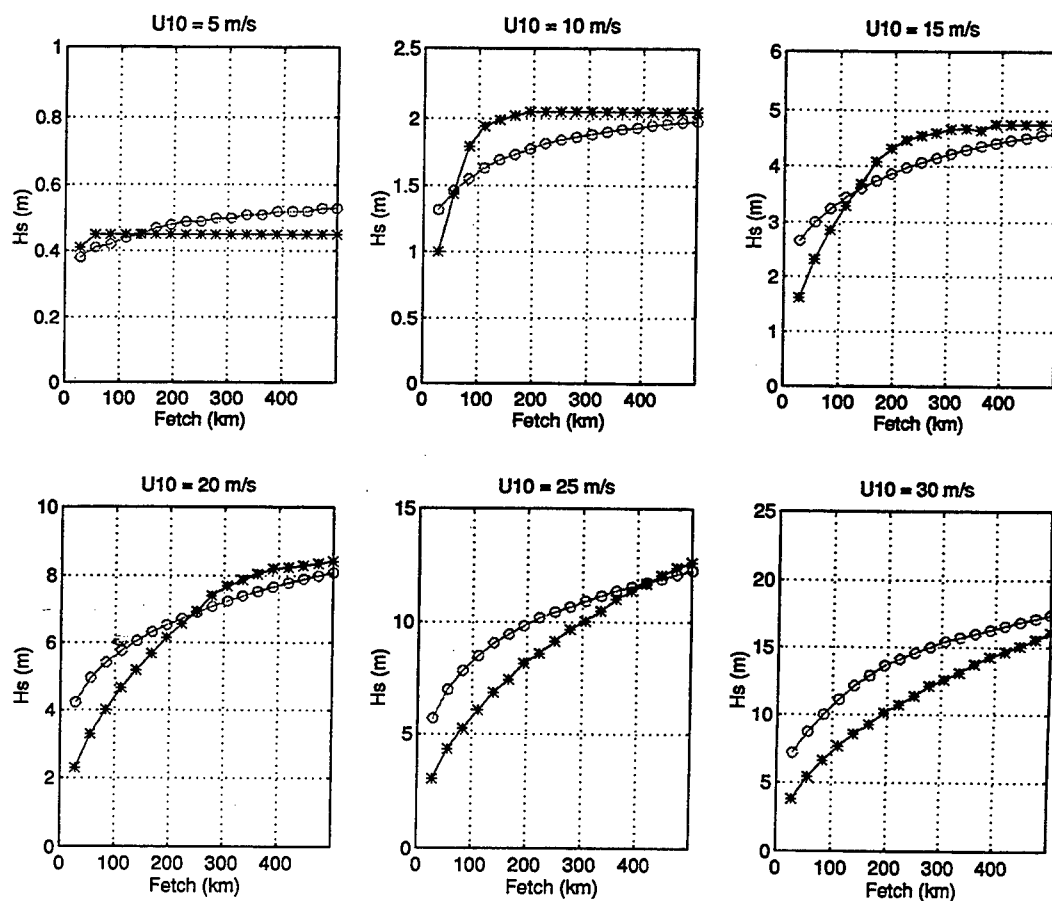
Figure 1. Fetch limited growth test Case I, H_s vs. fetch (WAM = O, WIS = *).

grid domain. Fetch limited growth curves were obtained over the 500 km grid after a sufficiently long simulation time of 300 hrs. Evolution of the wave field over time at a 500 km fetch provided the duration limited growth curves.

Figure 1 shows the fetch limited growth results of Case I. For a 5 m/s wind speed there is little difference between each model's growth. A maximum H_s difference of less than 0.1 m occurs at the longest fetch. For a 10 m/s wind speed the WAM H_s is slightly above that of WIS for short fetches, then the WIS H_s increases to nearly 0.5 m above that of WAM for a fetch of 100 km and remains above the WAM H_s until a fetch of 500 km is reached. As wind speed increases, a similar relationship between the growth curves of the two models can be seen except that the fetch at which the WIS growth exceeds that of WAM increases and the amount of exceedance decreases to the point where WIS growth never surpasses WAM at the highest wind speed. For wind speeds between 10 m/s and 20 m/s the WIS growth is above that of WAM for fetches greater than about 50 km to 250 km with differences of up to 2.0 m. For wind speeds of 25 m/s and 30 m/s the WAM H_s exceeds that of WIS for fetches less than 400 km and 500 km respectively with differences of up to 2.5 m and 4.0 m.

Figure 2 shows the peak frequency as a function of fetch. With increasing fetch the peak frequency migrates toward lower frequencies. For all wind speeds, the WIS peak frequency is higher than that of WAM over the entire fetch. With the exception of the 5 m/s and 10 m/s wind speeds, the differences range from about 0.05 hz to 0.01 hz for fetches of 25 km to 500 km. For the 5 m/s wind speed WIS reaches a minimum peak frequency of 0.3 hz for fetches greater than 50 km while the WAM peak frequency continues to decrease over the entire fetch. This behavior in WIS is due to a Pierson-Moskowitz growth limit used in the model, which limits the peak frequency.
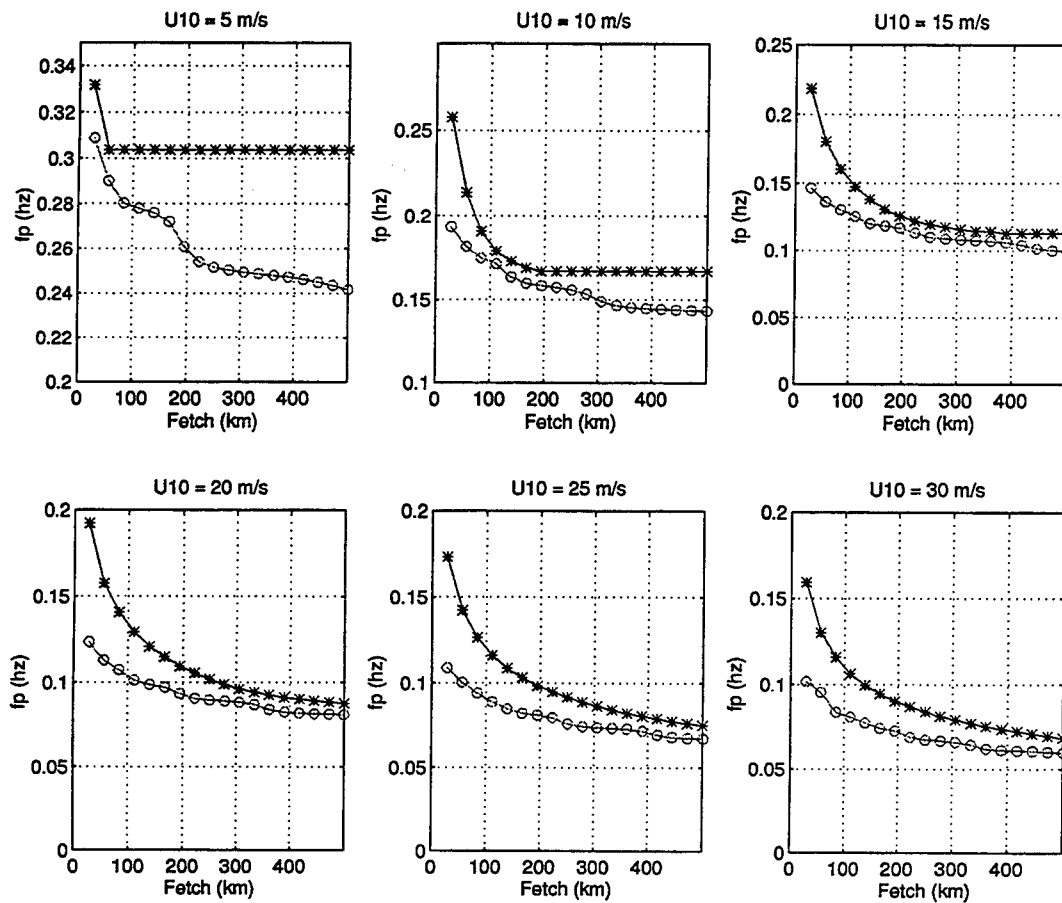
Figure 2. Fetch limited growth test Case I, f_p vs. fetch (WAM = O, WIS = *).

Figure 3 shows the duration limited H_s as a function of time. For the 5 m/s wind speed the WAM H_s decreases from 1.0 m to 0.5 m over a 60 hour duration while the WIS H_s increases from 0.0 m to near 0.5 m. The significant difference in the H_s between the models at the minimum duration is due to an artificial initial condition in the WAM version tested. For wind speeds of 10 m/s to 25 m/s, differences between the models are similar, with the WAM growth rate being greater than that of WIS during the duration limited period. Both models converge to about the same value
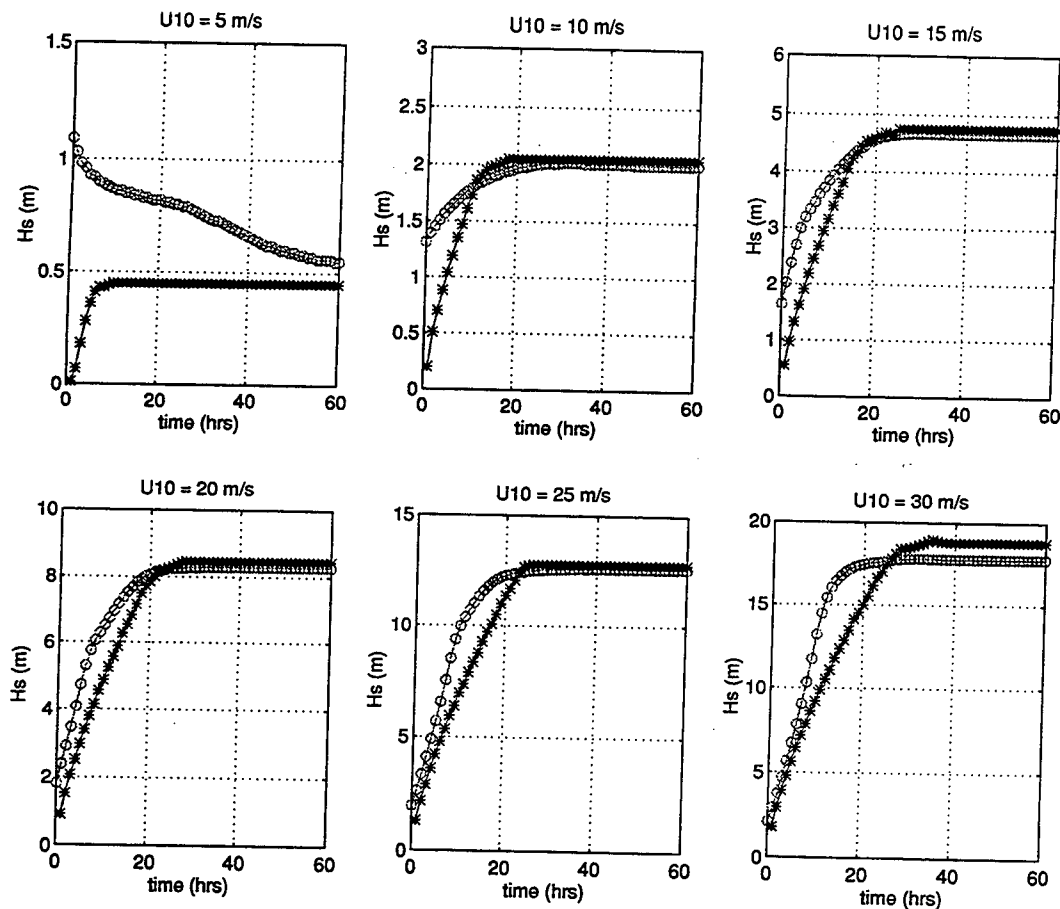
Figure 3. Duration limited growth test Case II, H_s vs. time (WAM = O, WIS = ✱).

for fully developed conditions within a 10 hr to 20 hr duration except for low wind speeds. For the 30 m/s wind speed, the WIS H_s converges to a value about 1.0 m higher than that of WAM but with 10 hours more duration.

Figure 4 shows the peak frequency as a function of duration for the six wind speeds. Just as in the fetch limited case, the WIS peak frequency is higher than that of WAM over the entire duration although they are very similar beyond about 24 hrs. The 5 m/s wind speed shows unusual behavior for both models and may be due to problems with growth rates at low wind speeds or limits set on the energy or frequency in the case of WIS. The differences between the two models'
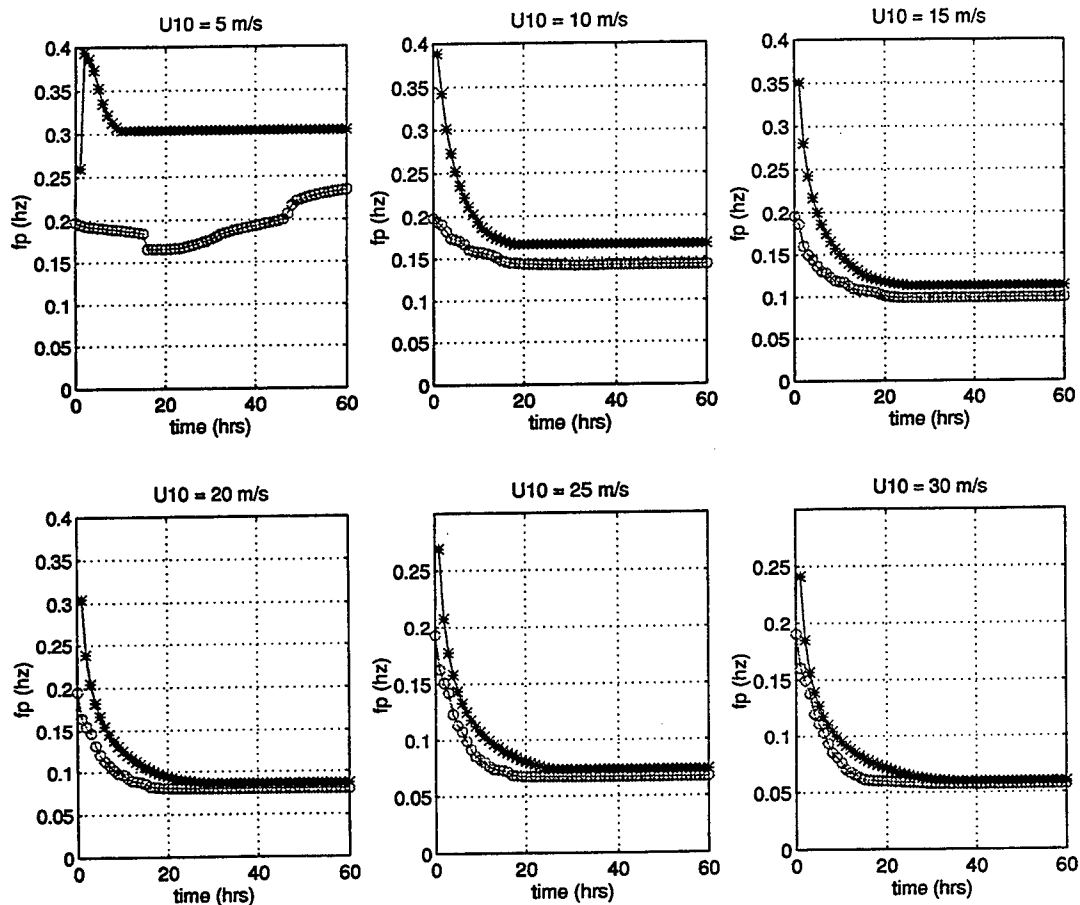
Figure 4. Duration limited growth test Case II, f_p vs. time (WAM = O, WIS = *).

peak frequencies range from 0.2 hz to 0.05 hz at the minimum duration with and converge to about

the same value within 24 hrs.

Case III considers response of the wave models to a shifting wind. A constant uniform

wind speed of 20 m/s is applied to the grid for 48 hours. Then the wind direction is gradually

turned 90° over a 6 hr period into a cross wave direction and held constant. This idealized test is

intended to show model behavior during the passing of moderately sized storm events. During

actual storm events there is normally a change in wind speed also. Another more extreme wind

shift occurs with the passage of strong fronts. In these situations, the wind speed change and

direction shift, about 180°, over time are more dramatic, occurring over a period of several hours.

Figure 5 shows the results of this test with peak wave direction plotted as a function of time. The models are equally responsive during the first 5 hours of the wind shift where the peak wave direction shifts 25°. After this WIS continues to shift at approximately the same rate until reaching the new wind direction, within several degrees, after 12 hours. The WAM rate of peak wave direction shift, however, decreases to near zero for several hours before resuming the previous rate of change. The WAM rate of direction change begins to decrease again within about 20° of the new wind direction and also overshoots the new direction by about 5°. Where WIS required about 12 hours to shift to the new direction, WAM required about 27 hours. Results from wind speeds of 10 m/s and 15 m/s (not shown) were similar except that no overshoot occurrs for the lower wind speeds.
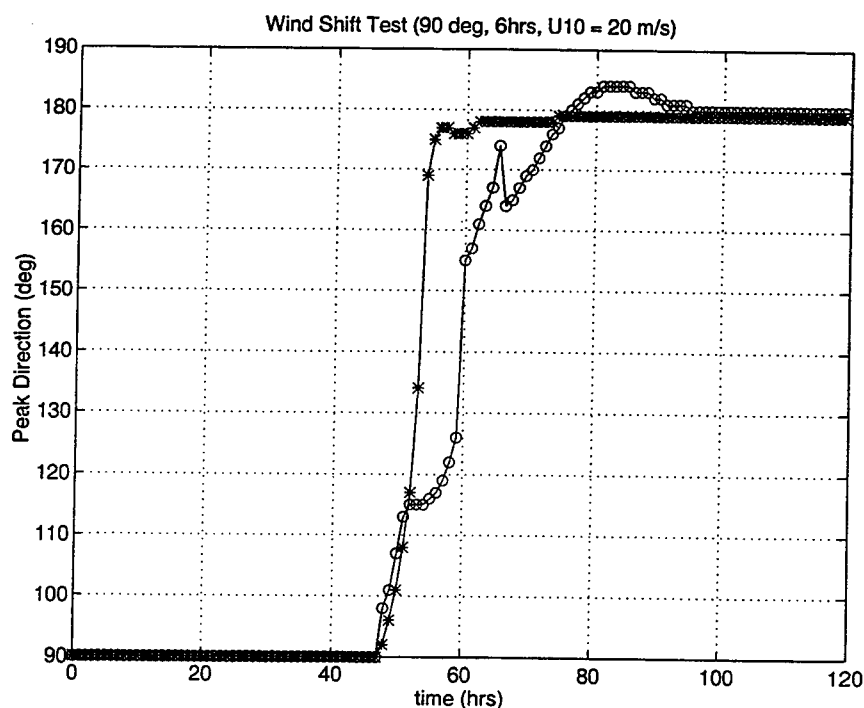
Figure 5. Shifting wind direction test Case III (WAM = O, WIS = *).

2.2 Wind Fields

In order to examine model performance, five historical storms are run for each model. The storms are all extra-tropical events which occurred along the US Atlantic coast. These storm events were chosen because high-quality windfields are available and they represent a variety of conditions ranging from extreme events to more moderate and variable conditions characterized by sea and swell, shifting winds, and cold front passages. Table 1 lists the storms and their respective dates. Three of the storms occurred during the Surface Wave Dynamics Experiment (SWADE) (Weller et al. 1991) intensive operation periods (IOP) and are labeled IOP1, IOP2, and IOP3. The

Table 1. Storms for model/buoy comparison.

IOP1	October 20 -31, 1990
IOP2	January 7 - 15, 1991
IOP3	February 23 - March 9, 1991
Halloween Storm	October 25 - November 1, 1991
Storm of the Century	March 11 - 17, 1993

remaining two storms, the "Halloween Storm" and the "Storm of the Century", were significant events causing flooding and damage along the Atlantic seaboard. The Halloween Storm was also a unique event in that the extra-tropical system absorbed a hurricane during development. The results of model runs for these storms are used to generate statistics for comparison to National Data Buoy Center (NDBC) buoy wave data. The following describes the analysis method used to produce these wind fields. All five historical wind fields used for this study were developed by Oceanweather, Inc., using classical manual kinematic and objective analysis techniques (Cardone

et al. 1980 and Cardone 1992). Surface analysis fields are derived from measured meteorological data distributed over the area of interest. The winds are derived as a blend of surface winds transformed from boundary layer pressure and temperature fields using a marine planetary boundary layer model and winds derived from kinematic analysis. Hand kinematic analysis is employed in order to retain continuity between wind field approximation at successive times. The kinematic analysis did not extend much past Cape Hatteras, NC.

CHAPTER III

PROCEDURE

3.1 Model Setup

In setting up the models, the goal was to implement each as identically as possible in order to avoid differences in performance due to inconsistent discretization of space, time, frequency or direction. Toward that end, both models were set up with 25 frequency bands, 24 direction bands, and a time step of 600 sec. Note that WAM allows different time steps for propagation, wind input, and wave growth. The wind fields used to drive the models were gridded on a 1/2° latitude and longitude spatial resolution with a 1 hour temporal resolution. In order to remove uncertainties introduced by wind field interpolation, the wave models were implemented with the same spatial and temporal resolution as the wind fields. As mentioned in Chapter II, WIS interpolates the 1 hour wind input down to the model time step.

The model grids, located over the continental shelf off the US Atlantic coast, are identical for WIS and WAM during the five simulations. For IOP1 and IOP3, a 63 by 49 grid ranging in latitude from 24°N to 48°N and longitude from 51°W to 82°W was used (Figure 6). For IOP2, the "Halloween Storm" (HOS) and the "Storm of the Century" (SOC), a 105 by 89 grid ranging from 23°N to 67°N latitude and from 30°W to 82°W longitude was used (Figure 7). Since shallow water effects are not investigated in this study, both models were run in the deepwater mode. No provision was made to capture the far field wave energy which would come from storm events outside the grid domain.
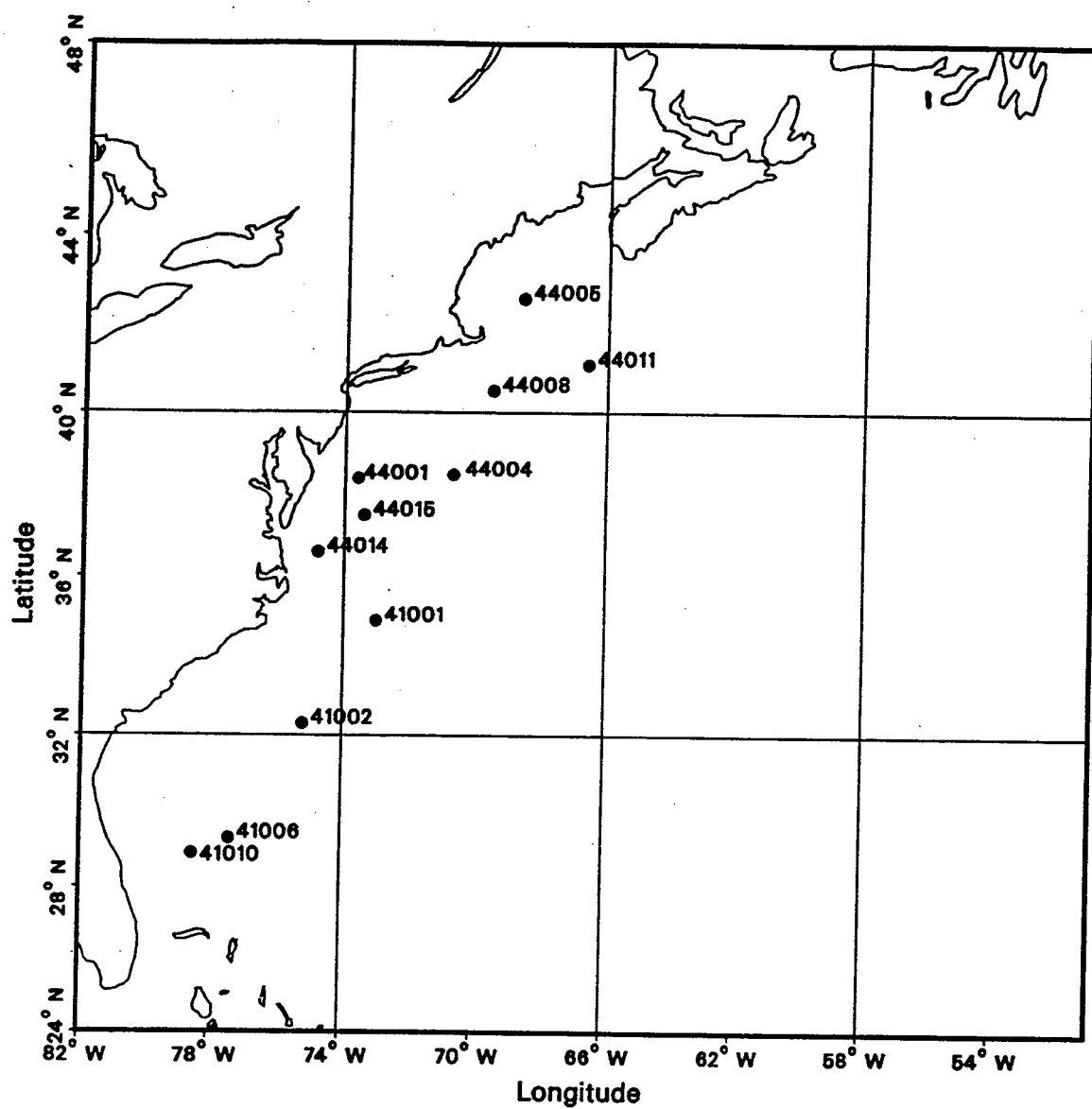
Figure 6. Model domain and buoy locations for IOP1 and IOP3.
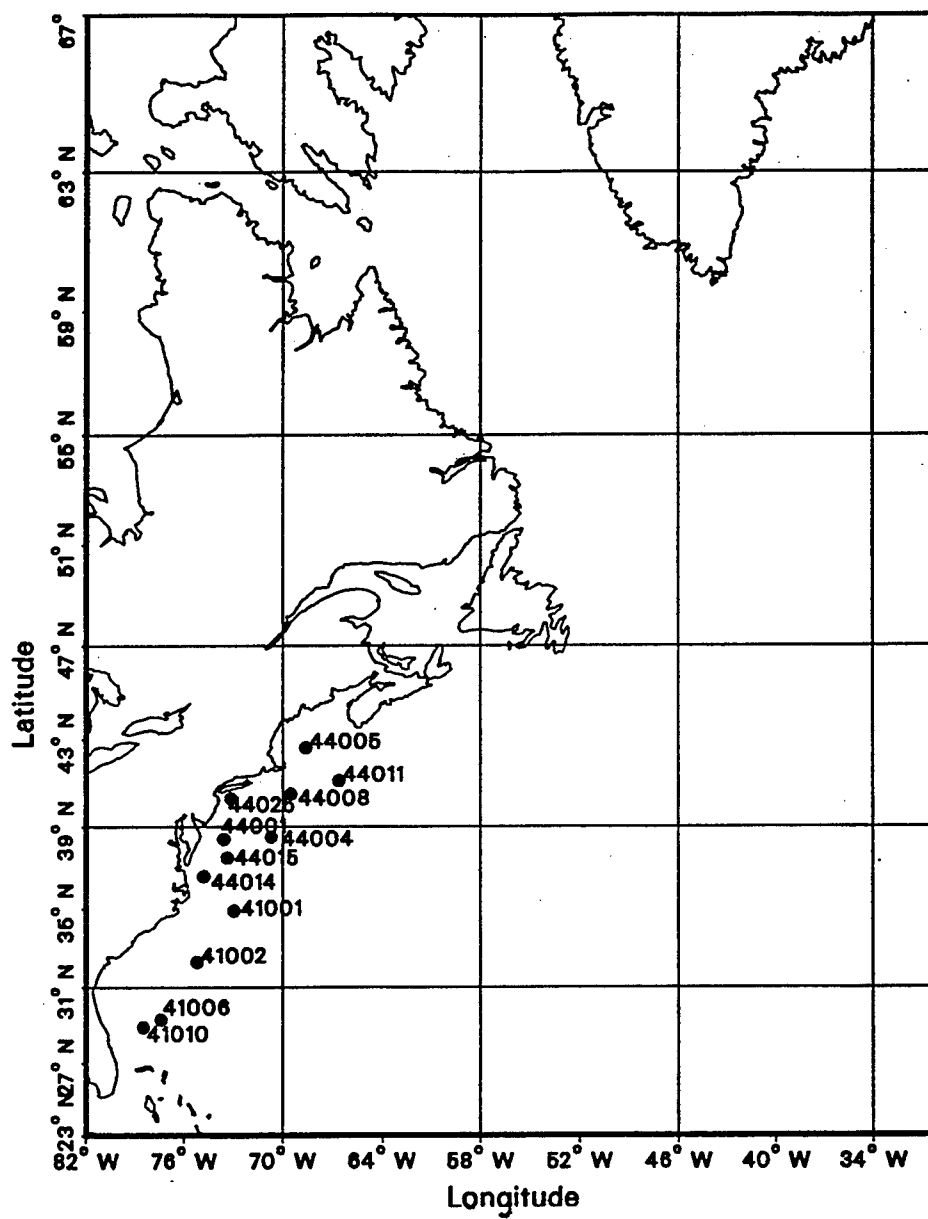
Figure 7. Model domain and buoy locations for IOP2, HOS, and SOC.

Also no spin-up of the models was made to ensure the beginning simulation conditions were consistent with measurements. The statistical calculations were applied 48 hours after the beginning of each simulation.

Differences between models in the method for calculating integrated properties introduces another ambiguity in comparing the relative performance of the models. In order to eliminate this difference, the WIS output subroutine was modified so that both of the models' integrated properties are based on the same method. The integrated properties, significant wave height, mean and peak period, and mean and peak direction are calculated as follows (Cardone et al. 1996):

$$H_s = 4 \left[\int_0^{2\pi} \int_0^{\infty} F(f,\theta) \, df \, d\theta \right]^{1/2} \qquad (3)$$

$$f_m = \left[\frac{\displaystyle\int_0^{2\pi} \int_0^{\infty} f^{-1} F(f,\theta) \, df \, d\theta}{\displaystyle\int_0^{2\pi} \int_0^{\infty} F(f,\theta) \, df \, d\theta} \right]^{-1} \qquad (4)$$

$$f_p = parabolic\ fit\ of\ \frac{dE(f)}{df} = 0\ , where\ E(f) = \int_0^{2\pi} F(f,\theta) \, d\theta \qquad (5)$$

$$T_m = f_m^{-1} \qquad (6)$$

$$T_p = f_p^{-1} \qquad (7)$$

$$\theta_m = \tan^{-1} \frac{\int_0^{2\pi} \int_0^{\infty} \sin\theta \, F(f,\theta) \, df \, d\theta}{\int_0^{2\pi} \int_0^{\infty} \cos\theta \, F(f,\theta) \, df \, d\theta} \qquad (8)$$

$$\theta_p = parabolic\ fit\ of\ \frac{\partial F(f_p,\theta)}{\partial \theta} = 0 \qquad (9)$$

3.2 Analysis

In order to assess accuracy of the wave models, model results are compared to National Data Buoy Center (NDBC) wave data. Analysis of the results is divided into three phases. First a qualitative comparison is made between model estimates and buoy data for the integrated parameters: significant wave height H_s, mean wave period T_m, peak wave period T_p, peak wave direction θ_p, directional spreading coefficient, wind speed, and wind direction. Second, a series of statistical tests is applied to the integrated wave properties including mean, bias, RMS error, scatter index and correlation coefficient. Finally, a comparison of the pattern correlation between model and buoy directional wave spectra is made.

The following statistics were computed for the scalar parameters, significant wave height, period, and wind speed (Cardone et al. 1996). The symbols B and M indicate buoy and model parameters respectively, and the symbol $<...>$ indicates the "mean".

Mean Buoy and Model $\qquad\qquad\qquad \bar{B} = <B> \ , \ \bar{M} = <M>$

Bias (Model - Buoy) $\qquad\qquad\qquad <M-B>$

Mean absolute difference	$<\lvert M - B \rvert>$
Root-mean-square error (RMSE)	$<(M-B)^2>^{1/2}$
Scatter Index (SI)	$\dfrac{RSME}{\bar{B}}$
Correlation Coefficient (CC)	$\dfrac{<(B-\bar{B})(M-\bar{M})>}{<(B-\bar{B})^2>^{1/2} <(M-\bar{M})^2>^{1/2}}$

For the vector quantities, wind direction and mean and peak wave direction, the statistics were calculated as (Cardone et al. 1996):

Mean scalar buoy and model	$\tan^{-1}\left[\dfrac{<\sin\theta_B>}{<\cos\theta_B>}\right]$, $\tan^{-1}\left[\dfrac{<\sin\theta_M>}{<\cos\theta_M>}\right]$
Mean vector buoy and model	$\tan^{-1}\left[\dfrac{<u_B>}{<v_B>}\right]$, $\tan^{-1}\left[\dfrac{<u_M>}{<v_M>}\right]$
Mean vector difference	$<\theta_B - \theta_M>$

In order to calculate the buoy mean and peak wave direction and perform the pattern correlation, the cross power spectral density matrix (CPSD), reported by the buoy, must be converted to a 2-D spectrum using a combination of the Maximum Likelihood Method and Longuet-Higgins et al. (1961) method.

The NDBC pitch-roll-heave buoys measure vertical acceleration, or in the case of buoy 44014, surface elevation, and North-South slope and East-West slope. These quantities are reported in the form of a cross power spectral density matrix for each frequency ranging from 0.01 to 0.40 hz at a 0.01 hz interval every hour. Because the buoy hull does not follow the wave

motions perfectly, there is a hull response present in the CPSD which must be corrected. This is accomplished by adjusting the CPSD to agree with linear theory.

The 2-D buoy spectrum with 40 frequency bands and 72 direction bands is estimated using the Maximum Likelihood Method (MLM) (Capon 1969; Isobe et al. 1984; Brissette and Tsanis 1994) applied to the CPSD. More accurate methods for estimating the 2-D spectra from pitch-roll-heave buoys exist, but the MLM method's computational efficiency and robust behavior make it a practical choice for processing large amounts of data. One important MLM deficiency is that it consistently overpredicts the actual wave field spread (Brissette and Tsanis 1994).

The MLM is valid as long as the CPSD matrix at each frequency is positive definite. If the determinant of the CPSD at a single frequency is less than zero then the directional distribution is set to the average of the distributions at the adjacent frequencies. If two or more adjacent frequencies have CPSDs which are not positive definite then the Longuet-Higgins et al. (1961) method for estimating directional spectra is used.

The directional spreading coefficient was calculated by applying the Kuik et al. (1988) method to the model 2-D wave spectra and the buoy directional Fourier coefficients and is briefly shown here. Also to calculate the directional spread, the directional Fourier coefficients, also reported by the buoy, must be converted to standard Fourier coefficients.

$$\theta_0 = \tan^{-1}\left(\frac{b_1}{a_1}\right) \tag{10}$$

$$
\begin{aligned}
m_1 &= \int_0^{2\pi} \cos\left(\theta - \theta_0\right) F(\theta)\, d\theta \\
&= a_1 \cos(\theta_0) + b_1 \sin(\theta_0) = (a_1^2 + b_1^2)^{1/2}
\end{aligned} \tag{11}
$$

where θ_o is the vector mean wave direction, a_1 and b_1 are the lowest Fourier coefficients, and m_1 is the first centered Fourier coefficient. The directional spreading coefficient or circular width is given by the second order circular moment:

$$\sigma = \{ 2 (1 - m_1) \}^{1/2} \tag{12}$$

The final basis for comparison of the models is a pattern correlation between the model and buoy directional wave spectra. This is a measure of the correlation between the model and buoy spectral shape. The pattern correlation analysis consists of the following five steps. First the buoy spectrum is interpolated onto the model frequency and direction bins. The buoy spectrum is discretized into 40 frequency and 72 direction bins while the model has 25 frequency bins and 24 direction bins. Next the mean wave direction for the model and interpolated buoy spectra are calculated, and the buoy spectrum is rotated to match the model mean direction. The mean wave frequencies are then calculated for the model and buoy, and the buoy spectrum is translated to match the model mean frequency. The final adjustment is to scale the resulting buoy spectrum by the ratio of the total energy in the model and buoy spectrum. Finally, the correlation coefficient between the adjusted buoy spectrum and the model spectrum is calculated on a bin by bin basis. The correlation coefficient is given by (Shay et al. 1996):

$$r = \frac{\sum_{i=1}^{m} (E_{b_i} - \bar{E}_b)(E_{b_i}' - \bar{E}_b')}{\sqrt{\sum_{i=1}^{m} (E_{b_i} - \bar{E}_b)^2 (E_{b_i}' - \bar{E}_b')^2}} \tag{13}$$

where E_b is the energy per bin of the buoy wave spectrum and E_b' is the energy per bin of the model wave spectrum. The overbar indicates the mean energy over i, which represents the individual frequency and direction bins. The value of r ranges between 1 and -1. When r > 0, the buoy and model energy distribution are positively correlated. When r = 0, E_b and E_b' are uncorrelated. In addition to the pattern correlation coefficient, the error due to interpolation of the buoy spectrum is calculated for total energy, mean frequency, and mean direction.

CHAPTER IV

MODEL RESULTS

4.1 IOP1

a. Synoptic weather conditions

In this section a general description of the meteorological systems which affected the model domain during IOP1 is presented. A more detailed description may be found in Cardone et al. (1995). Three weather systems passed through the area during the simulation period which are of primary interest. All times are given in the Universal Time Coordinate (UTC) convention.

The first weather system of interest to pass through the model domain formed on the South Carolina coast on 23 October. The center of this low pressure system moved northeast along the US Atlantic Coast for the next 48 hours. Figure 8 shows the movement of the low pressure center and the associated front for this period and the isobars corresponding to 0000 UTC 24 October. A maximum windspeed of 17 m/s was recorded at 44015. The maximum recorded H_s ranged from about 3.0 m to 4.5 m for the buoys included in this study.

The second weather system to pass through the model area was the most intense storm. This system also formed along the South Carolina coast on 25 October, but was more complex in that it was comprised of two low pressure centers. The first one formed along the South Carolina coast while the second, a more intense low, formed later and further north and trailed the first low. Figure 9 shows the isobars for 0000 UTC 26 October and the two low pressure center paths from 25 to 27 October. A maximum wind speed of about 25 m/s was measured at 44015 and 41001. The maximum measured H_s ranged from 4.5 m to 9.0 m for all buoys.

The third system to pass through the model domain formed along the New England coast
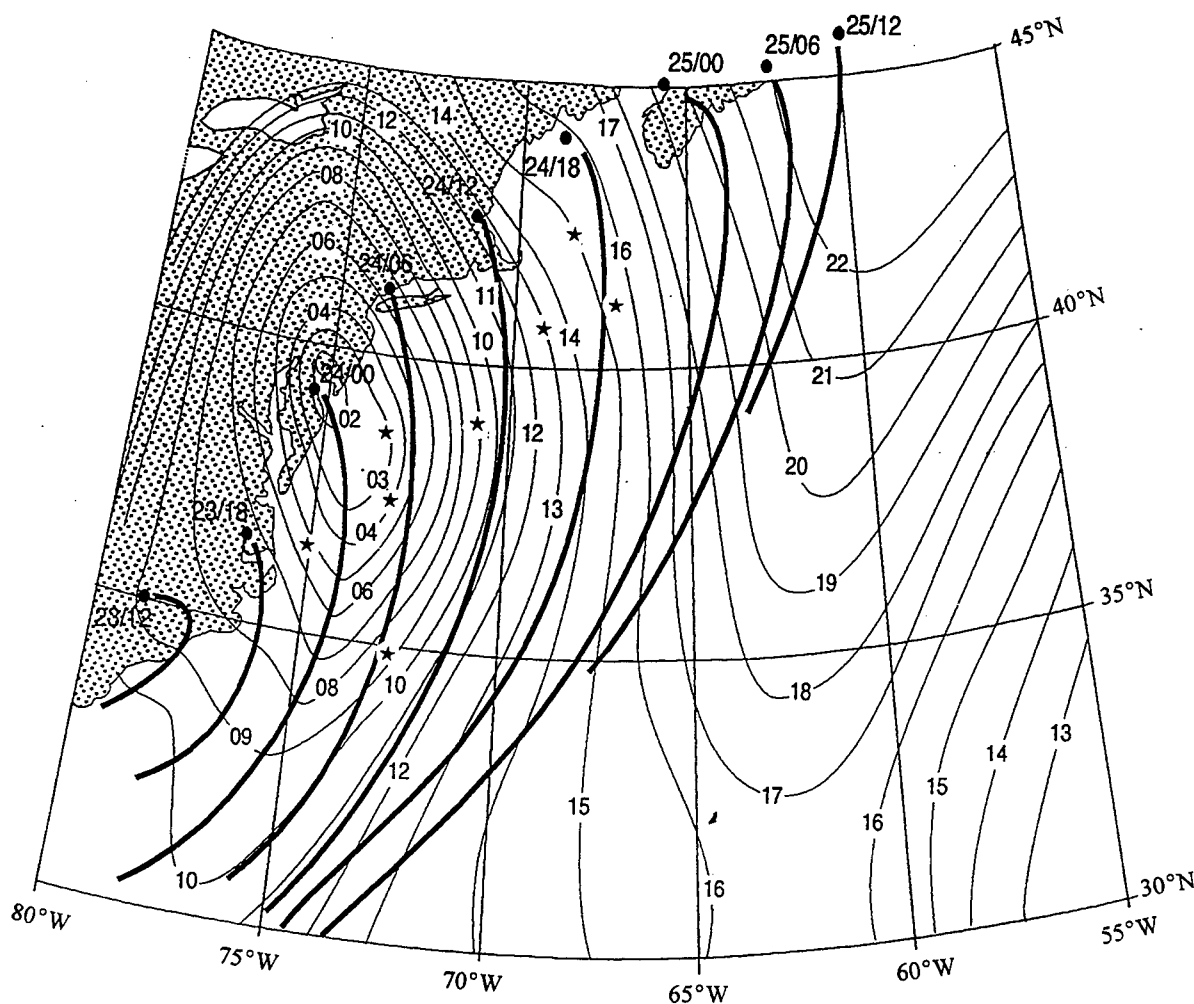
Figure 8. IOP1 isobars on 24 October 1990 and time evolution of storm centers and frontal boundaries for 23-25 October. Buoy locations indicated by ★ (adapted from Cardone 1995).

on 29 October and moved northeast. This system created a situation with new wave growth in the presence of an existing swell from the previous system. Maximum measured wind speeds were about 17 m/s and the maximum H_s ranged from 3.0 m to 5.0 m for all buoys.

Several other meteorological features existed which were of less importance but impacted the model domain. In the beginning of the simulation, swell energy, with a H_s of 1 m to 2 m and T_p of 8 sec to 10 sec, existed at all buoy locations. The origin of this swell energy, based on buoy
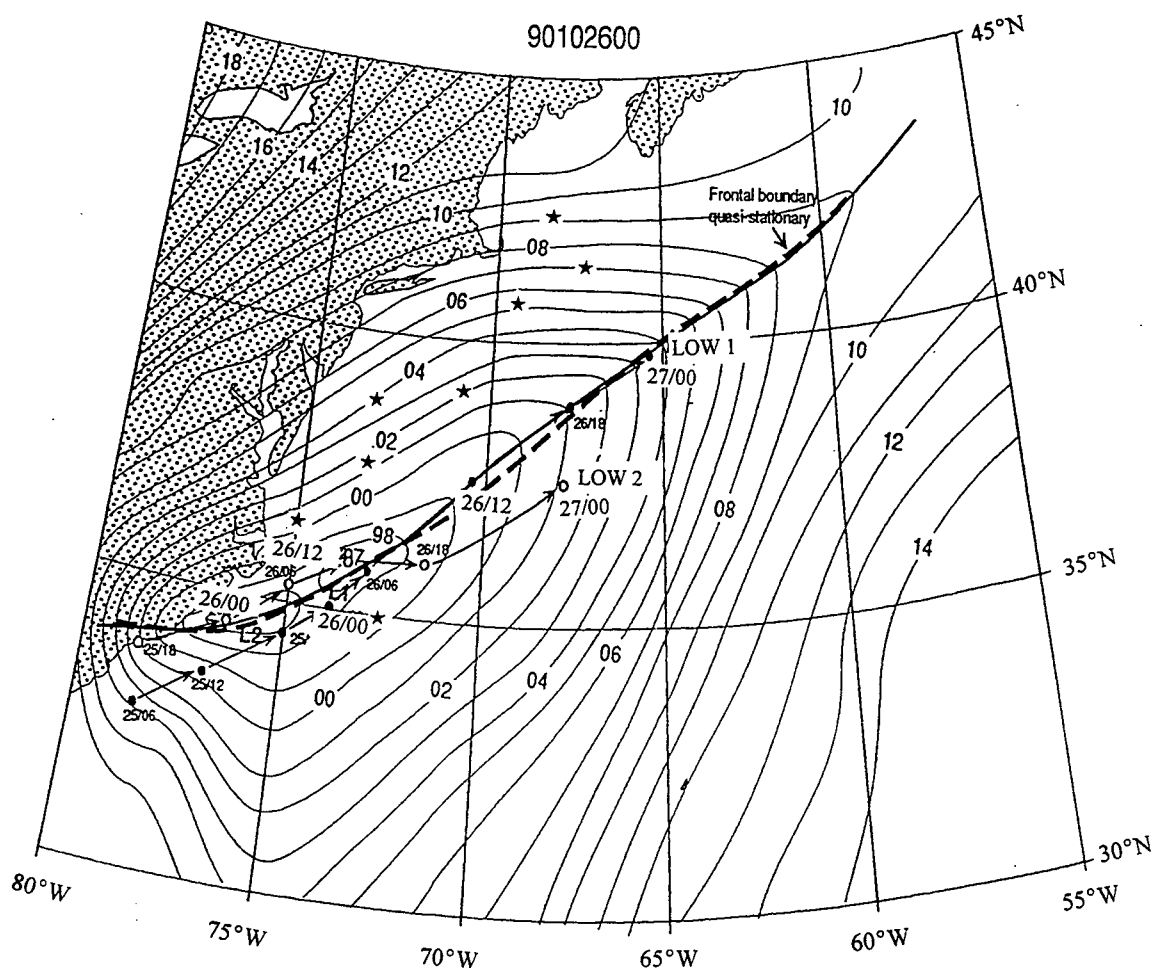
Figure 9. IOP1 isobars for 26 October. Frontal boundary and evolution of two low pressure systems. Buoy locations indicated by ★ (adapted from Cardone 1995).

wave directions, is apparently in the North Atlantic partially outside the model domain. A source of swell in the southern half of the domain was the tropical storm *Nana*, located about 30°N and 60°W on 20 October (Cardone et al. 1995). This system was present within the model domain from the beginning of the simulation, 20 October, to about 22 October. Another system which affected the model domain was a low pressure system which moved over Nova Scotia causing peak wind speeds at 44005, 44008, 44011, and 44004 of 10 m/s to 12 m/s on 20 October.
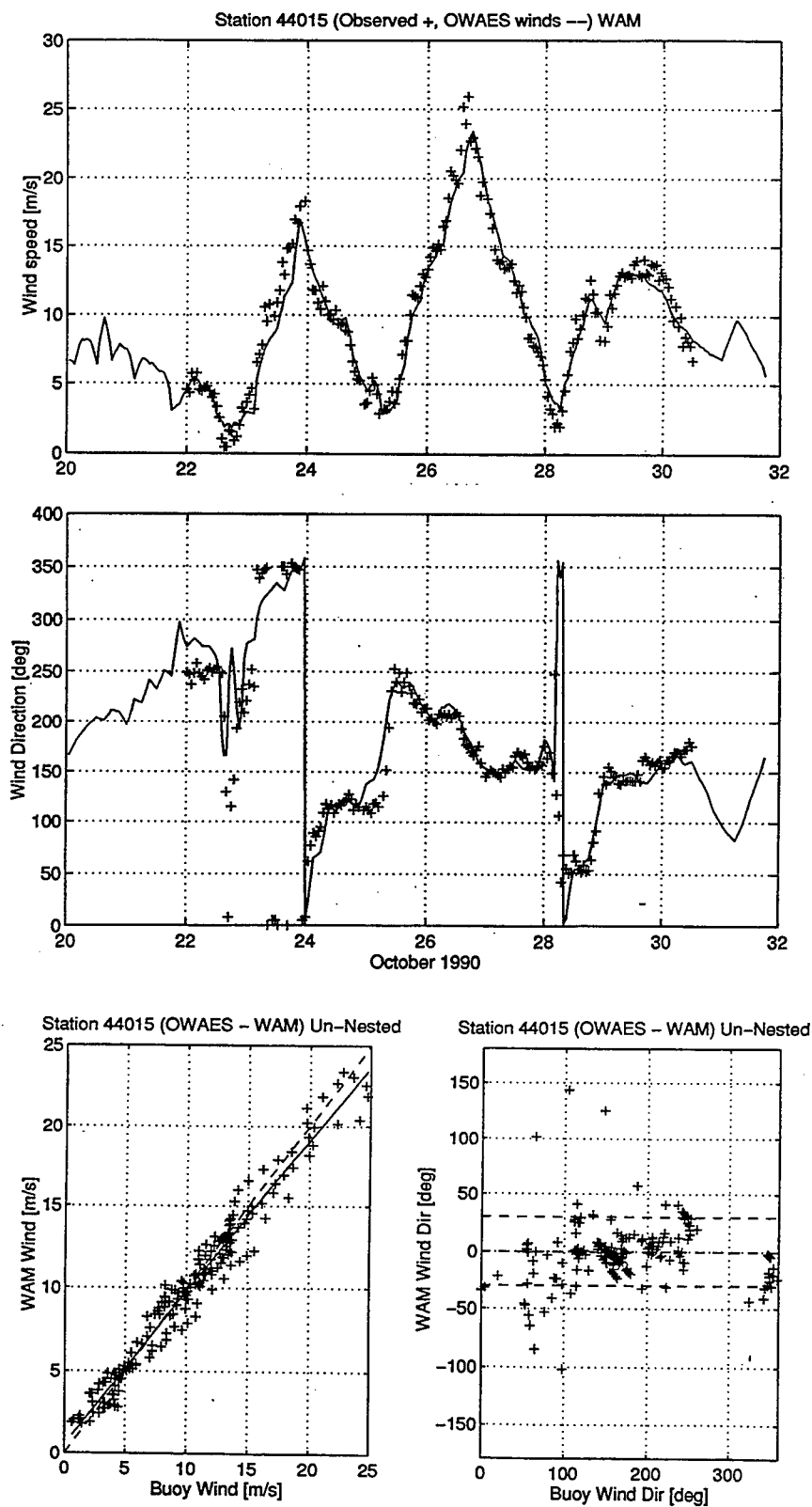
Figure 10. Wind time history and scatter plots at 44015 for IOP1.

b. Winds

The time histories shown in Figure 10 illustrate the excellent agreement the simulated wind speed and direction have with that measured at 44015, which is located in the central SWADE area. The three systems discussed previously are evident with peak wind speeds on about the 24th , 27th, and 29th. The timing of the increasing and decreasing wind speed and shifting of the wind is very good. There is however a small under prediction of the peak wind speeds ranging from 1 m/s to 3 m/s. Scatter plots of wind speed and direction in Figure 10 show only a very slight bias toward the buoy for higher wind speeds and wind directions which are for the most part within ± 30° of the buoy. Statistics for the winds are quantified later along with wave parameters.

As mentioned in Chapter II, the kinematic analysis (KA) was not applied to the part of the model domain which is roughly south of 30°N latitude. Buoys 41006 and 41010 are below this latitude and the resulting decrease in accuracy of the wind speed is evident in the wind speed scatter plot shown in Figure 11, for 41006. Both magnitude and timing errors are present in the
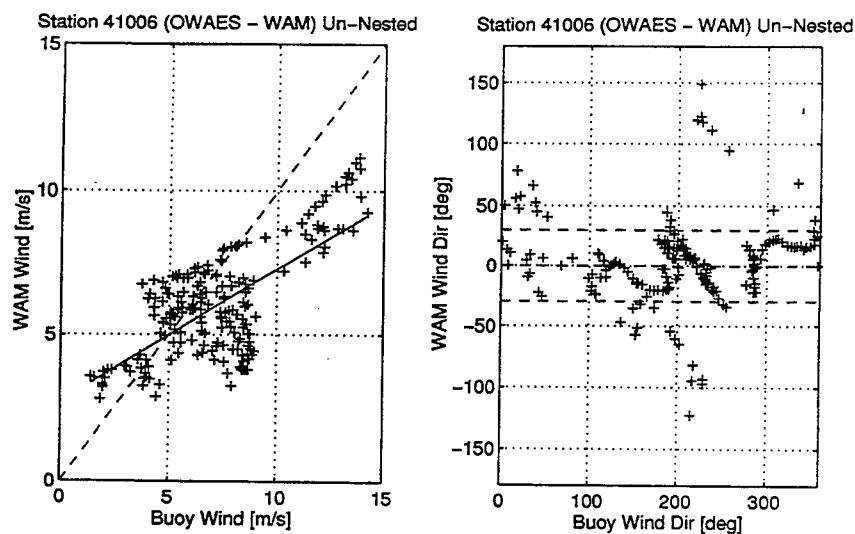
Figure 11. Wind speed and direction scatter plots at 41006 for IOP1.
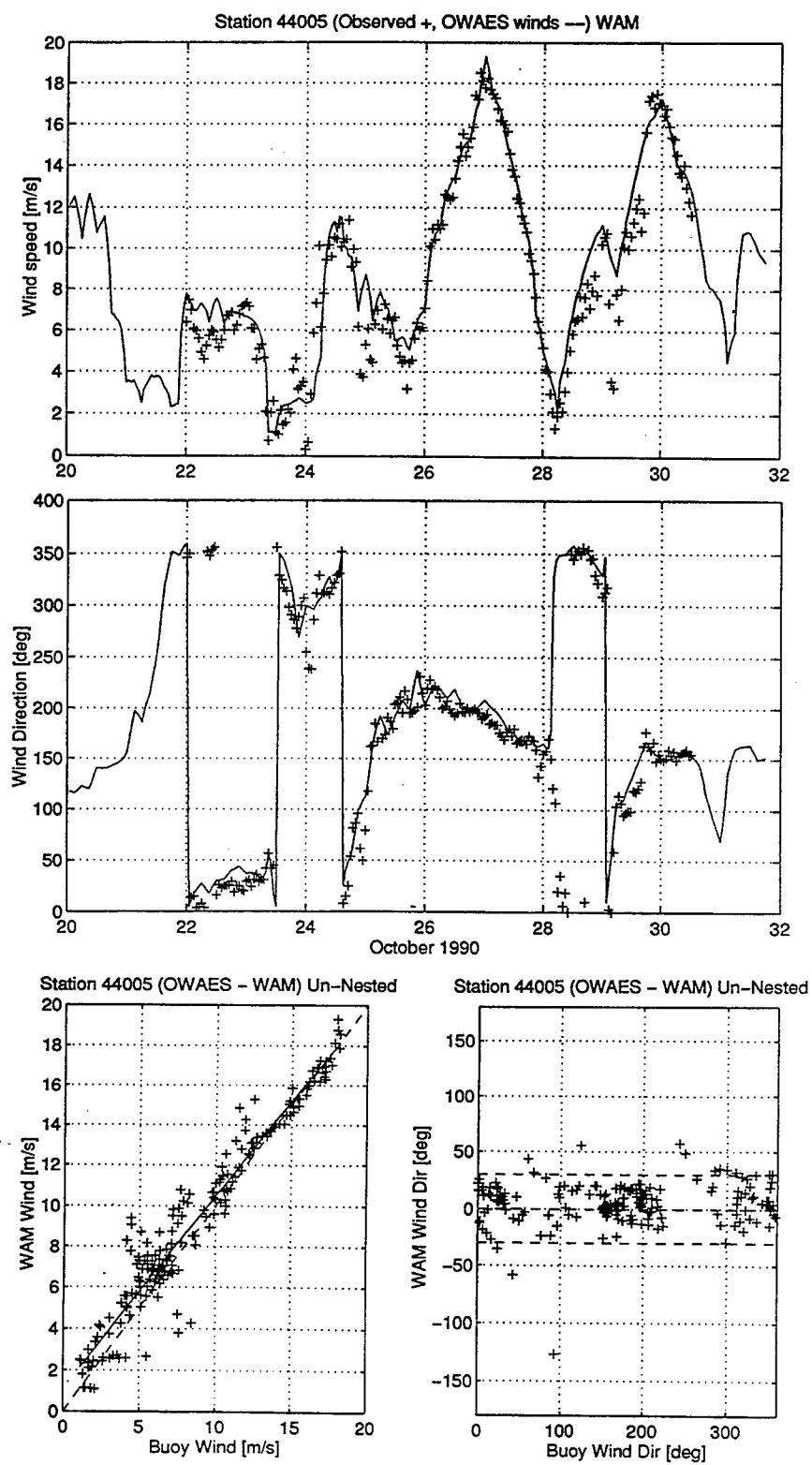
Figure 12. Wind time history and scatter plots at 44005 for IOP1.

wind speed time histories for both buoys. This can be seen in the increase in bias toward the buoy for the wind speed scatter plot. The wind direction on the other hand has about the same accuracy as the locations within the KA area.

The northern area of the model domain is within the KA area but has sparse measured data relative to the central SWADE area. This results in some decrease in accuracy of the simulated wind speed, which is evident in the time history and scatter plots shown in Figure 12, for location 44005. Plots for all locations considered are in Appendix A.

c. Wind and wave statistics

One indication of the general performance of the models is given by the statistics of the integrated properties, windspeed at a 10 m elevation, U_{10}, significant wave height, H_s, and peak wave period , T_p. Note that the calculation method for the statistics is presented in Chapter III. Statistical performance of the models should be judged with consideration for the error inherent in the measurements. Scatter for typical buoy measurements is about ± 12% for H_s and ± 9% for T_p (Donelan and Pierson 1983).

In Table 2 the quality of the simulated wind speed can be seen in the RMS Error which ranges from 1.0 m/s to 1.5 m/s with the exception of the previously mentioned locations 41006 and 41010. Excluding the two southern locations, simulated wind speed has, for the most part, a small positive bias ranging up to 0.87 m/s. The scatter index (SI) ranges from 10% to 19% and the correlation coefficient, at 0.97 to 0.98, is high.

Tables 3 shows the H_s statistics for WAM and WIS. Considering all but the two southern most locations, the RMS Error tends to be slightly smaller for WAM, ranging from 0.4 m to 0.5 m, than WIS which ranges from 0.4 m to 0.8 m . However WAM has a negative bias, ranging from -0.03 m to -0.5 m, while WIS has a positive bias, ranging from 0.01 m to 0.30 m. The SI for

Table 2. Statistics of measured and hindcast wind speed for IOP1.

Buoy	Mean Buoy (m/s)	Mean Model (m/s)	Bias (m/s)	Abs Err (m/s)	RMS Err (m/s)	SI (%)	CC	# pts
44005	8.67	9.24	0.57	0.93	1.32	15	0.97	203
44011	8.85	9.31	0.46	1.01	1.48	17	0.97	198
44008	8.39	9.25	0.87	1.29	1.59	19	0.97	200
44004	9.56	9.59	0.03	0.87	1.05	11	0.98	203
44001	8.49	8.62	0.13	0.89	1.12	13	0.97	121
44015	10.14	9.94	-0.20	0.82	1.06	10	0.98	199
44014	8.82	9.23	0.42	0.80	1.04	12	0.98	203
41001	9.01	9.14	0.12	0.81	1.06	12	0.97	204
41006	7.24	6.01	-1.23	1.90	2.37	33	0.69	203
41010	7.64	6.09	-1.55	2.31	2.93	38	0.57	203

SI - scatter index   CC - correlation coefficient

Table 3. Statistics of measured and hindcast H_s for IOP1.

Buoy	WAM							WIS						# pts
	Mean Buoy (m)	Mean Model (m)	Bias (m)	Abs Err (m)	RMS Err (m)	SI (%)	CC	Mean Model (m)	Bias (m)	Abs Err (m)	RMS Err (m)	SI (%)	CC	
44005	2.09	2.03	-0.05	0.33	0.41	20	0.95	2.41	0.33	0.53	0.70	33	0.94	203
44011	2.81	2.38	-0.43	0.48	0.57	20	0.98	2.83	0.02	0.50	0.64	23	0.96	198
44008	2.45	2.37	-0.07	0.41	0.49	20	0.97	2.69	0.25	0.58	0.80	33	0.95	200
44004	2.99	2.51	-0.48	0.53	0.59	20	0.98	2.79	-0.20	0.31	0.40	13	0.98	203
44001	2.31	2.09	-0.22	0.36	0.46	20	0.96	2.30	-0.01	0.33	0.48	21	0.95	121
44015	2.63	2.52	-0.12	0.34	0.41	16	0.97	2.79	0.16	0.40	0.51	19	0.96	199
44014	2.36	2.33	-0.03	0.36	0.44	18	0.96	2.63	0.27	0.42	0.59	25	0.96	203
41001	2.64	2.50	-0.14	0.36	0.43	16	0.97	2.78	0.14	0.32	0.44	17	0.96	204
41006	2.07	1.55	-0.52	0.67	0.84	41	0.67	1.74	-0.33	0.53	0.67	32	0.74	203
41010	1.87	1.50	-0.37	0.57	0.71	38	0.69	1.68	-0.19	0.43	0.56	30	0.74	203

SI - scatter index   CC - correlation coefficient

WAM is generally lower, ranging from 16% to 20%, while the SI for WIS ranges from 13% to 33%. The correlation coefficients (CC)are similar for both models and vary between 0.94 and 0.98.

Table 4 shows the T_p statistics for WAM and WIS. Again, excluding the two southern locations, in general the statistics are similar for both models. Both models exhibit a consistent negative bias, ranging from -0.52 sec to -1.37 sec for WAM and -0.25 sec to -1.08 sec for WIS. WIS has a consistently smaller negative bias than WAM except for 44011 and 44008. The RMS Error for WAM is smaller than WIS for all but 44014. The difference in RMS Error between the models ranges from 0.01 sec to 0.42 sec. The SI are similar for both models, except for 44008 and 44011, and ranges from 17% to 29%. For 44008 and 44011 the SI for WAM is about 5% to 7% lower than for WIS. The CC for both models are very similar and range from 0.43 to 0.84.

Table 4. Statistics of measured and hindcast T_p for IOP1.

| Buoy | WAM | | | | | | | WIS | | | | | | |
	Mean Buoy (s)	Mean Model (s)	Bias (s)	Abs Err (s)	RMS Err (s)	SI (%)	CC	Mean Model (s)	Bias (s)	Abs Err (s)	RMS Err (s)	SI (%)	CC	# pts
44005	8.27	7.46	-0.81	1.61	2.32	28	0.43	7.47	-0.80	1.83	2.41	29	0.45	203
44011	8.73	7.96	-0.76	1.18	1.51	17	0.76	7.96	-0.76	1.53	1.93	22	0.70	198
44008	8.88	8.11	-0.77	1.19	1.62	18	0.71	8.06	-0.82	1.68	2.18	25	0.62	200
44004	9.12	8.14	-0.98	1.10	1.55	17	0.84	8.22	-0.90	1.13	1.65	18	0.84	203
44001	9.05	7.68	-1.37	1.88	2.44	27	0.60	7.96	-1.08	2.00	2.50	28	0.61	121
44015	9.10	8.13	-0.97	1.30	1.75	19	0.78	8.50	-0.61	1.29	1.76	19	0.77	199
44014	8.83	8.06	-0.77	1.33	1.88	21	0.72	8.55	-0.27	1.41	1.82	21	0.74	203
41001	8.80	8.28	-0.52	1.08	1.54	17	0.83	8.55	-0.25	1.11	1.56	18	0.81	204
41006	9.93	8.64	-1.29	1.70	1.91	19	0.84	8.82	-1.11	1.66	1.87	19	0.83	203
41010	10.07	8.55	-1.52	1.91	2.16	22	0.81	8.65	-1.42	1.83	2.15	21	0.81	203

SI - scatter index   CC - correlation coefficient

The scatter indices for U_{10}, H_s, and T_p from Tables 2 through 4 are plotted in bar graph

form in Figure 13 to show the relationship between each parameter. The wind speed plot
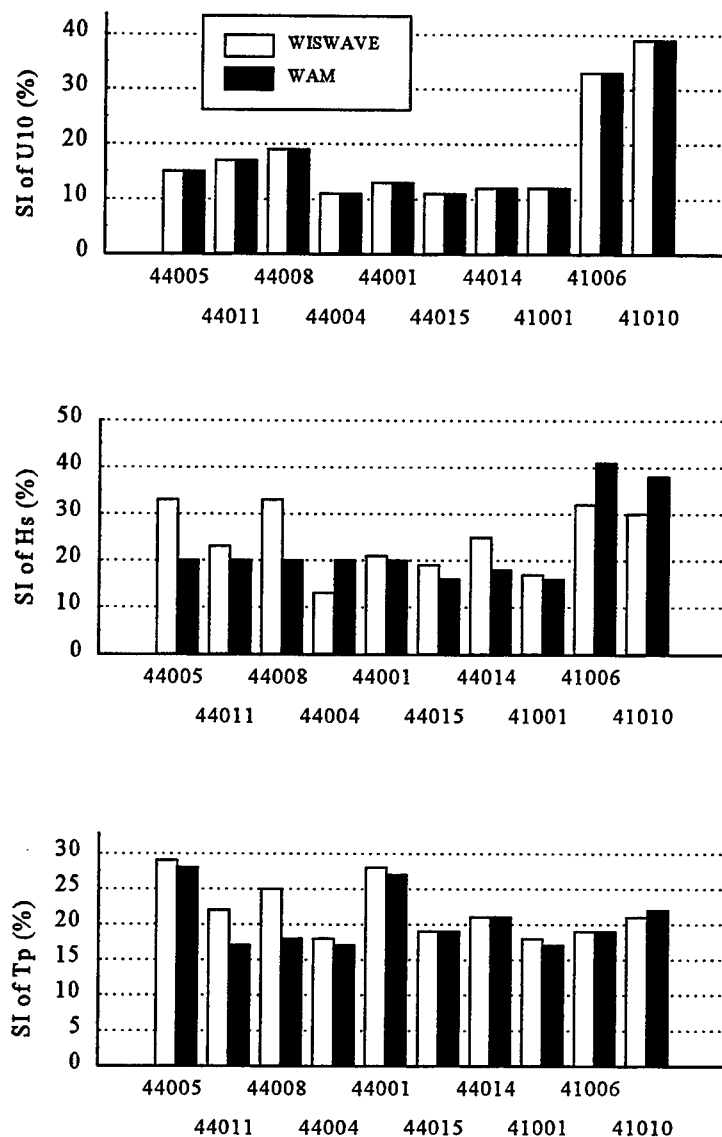
Fig. 13. WAM and WIS U_{10}, H_s, and T_p scatter indexes for IOP1.

shows the southern most locations, 41006 and 41010 with more than 30% scatter. Also note that 44005, 44011, and 44008 have 15% to 20% scatter. The area surrounding these locations are within the KA but have sparse measured data compared to the central SWADE area. The locations within the measured data rich central area, 44004, 44001, 44015, 44014, and 41001 have SI's ranging from 10% to 20 %.

The H_s plot shows that WAM has a SI of less than 20% for all but the two southern most locations. Also note that for these same locations, except for 44004, WAM's SI is less than the WIS SI. This difference is greater than 10% for locations 44005 and 44008. Since depths at buoys 44008 and 44014 are 60 m and 48 m respectively and the maximum T_p at these locations is 12 sec to 13 sec, a portion of the spectral energy at these locations is affected by depth, which is not represented in model simulations. The depth to deepwater wavelength ratio, d/L_o, which 1/3.7 and 1/5.5 for 44008 and 44014 respectively, gives an indication of the degree to which depth affects the spectrum.

The T_p plot shows that both models have similar SIs with the exception of 44008 and 44011. Locations north of 44001, except for 44004, tend to have higher SIs for WIS compared to southern locations. In the case of 44008 and 44005 this might be expected since the WIS H_s SI is also high (over 30%). The WAM T_p SI at 44005 is close to 30% even though the H_sSI, at 20%, is low. Also both models' T_p SIs at 44001 are over 25% while the H_s SIs are about 20%.

d. Non-directional time histories

The following section presents a description of model and measured H_s and T_p time histories for select locations corresponding to non-directional buoys. Locations 44005, 44008, and 44011 are located in the data sparse region and exhibit less accuracy in wind speed than the central SWADE area. Nearly all locations under predict the peak H_s corresponding to the first weather

system. For 44005 (Figure 14) the under prediction of both models is about 1.0 m . Also characteristic of most locations is the under prediction of the T_p during the time leading up to the first system and in the case of 44005 during the passing of the first system. Model T_p ranges from 4 sec to 5 sec while the buoy T_p ranges from 8 sec to 10 sec. Another common characteristic at most of the locations is the over prediction of the peak H_s by WIS and under prediction by WAM during the second system.

The wind time history plots for 44005, in Figure 12, show two wind speed peaks preceding the three main systems which are the focus of this discussion. These two features could have some influence on the wave spectra at this location which is not adequately represented in the simulations since they occur during the model spin-up period. Another unique feature in the northern area can be seen in plots for 44005 and 44011 where the second and third systems have similar peak wind speeds and H_s magnitudes.

Statistics for 44005 showed a large scatter and positive bias for the WIS H_s . This is due to the too rapid growth and over prediction, by more than 1.0 m, during the second system. WIS also has too rapid of an increase in H_s before the peak of the third system although WIS matches the measured H_s peak closely. Both model H_s decrease too slowly toward the end of the second system.

The H_s time history plot for 44011, in Figure 14, indicates similar characteristics to 44005 except for a few differences. First the WIS H_s over predicts the second system peak by a smaller amount, about 1.0 m, while WAM under predicts the same peak by a little more than at 44005, around 0.5 m. Increasing WIS T_p consistently leads the buoy by 3 hours during the growth of the second system. The buoy T_p during the second system oscillates between 10 sec and 11.5 sec. The WIS T_p overshoots to a little over 12 sec and then steadily decreases to around 10 sec by the end of the second system. The WAM T_p for this time period remains at about 11 sec.
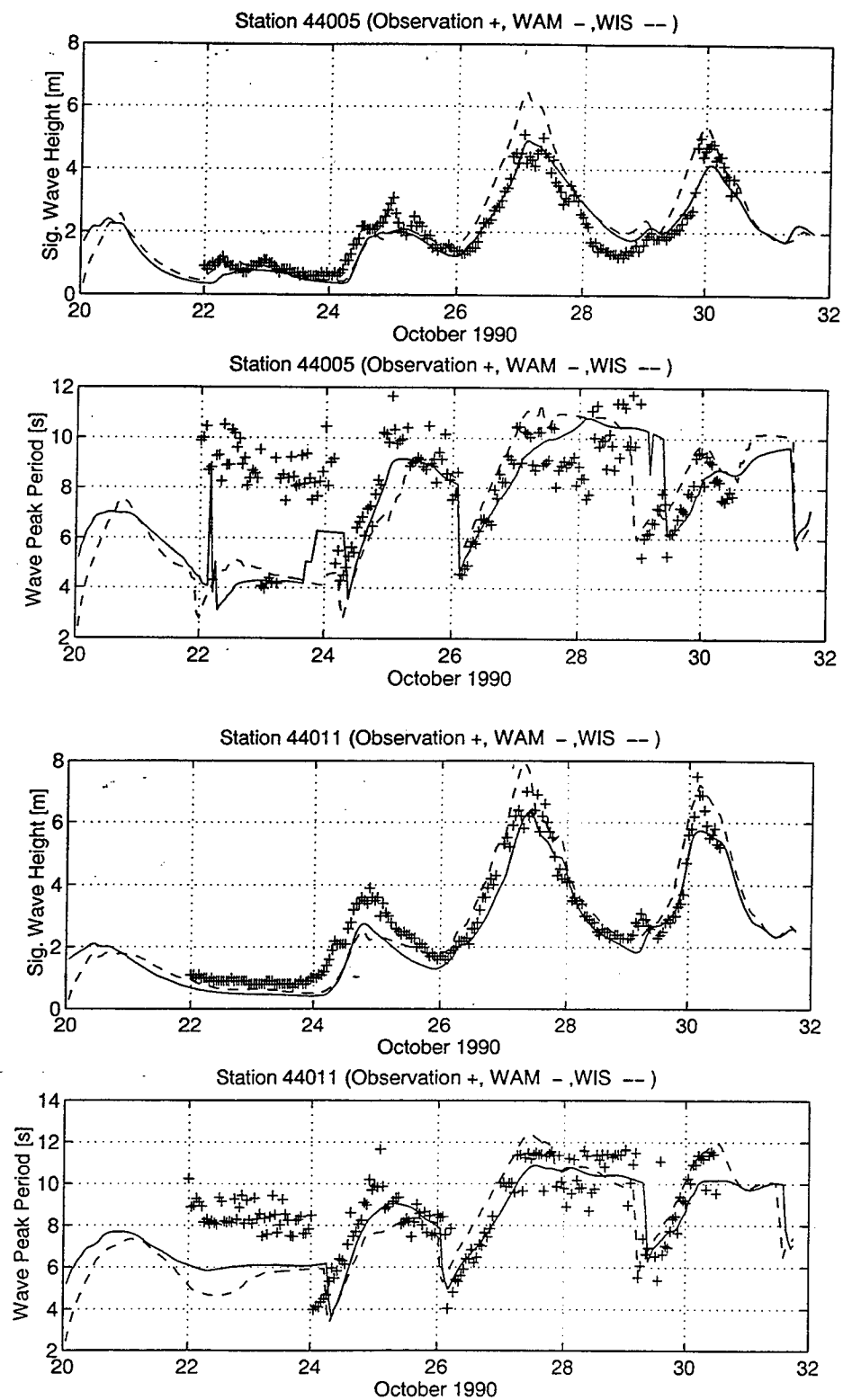
Figure 14. H_s and T_p time histories at 44005 and 44011 for IOP1.
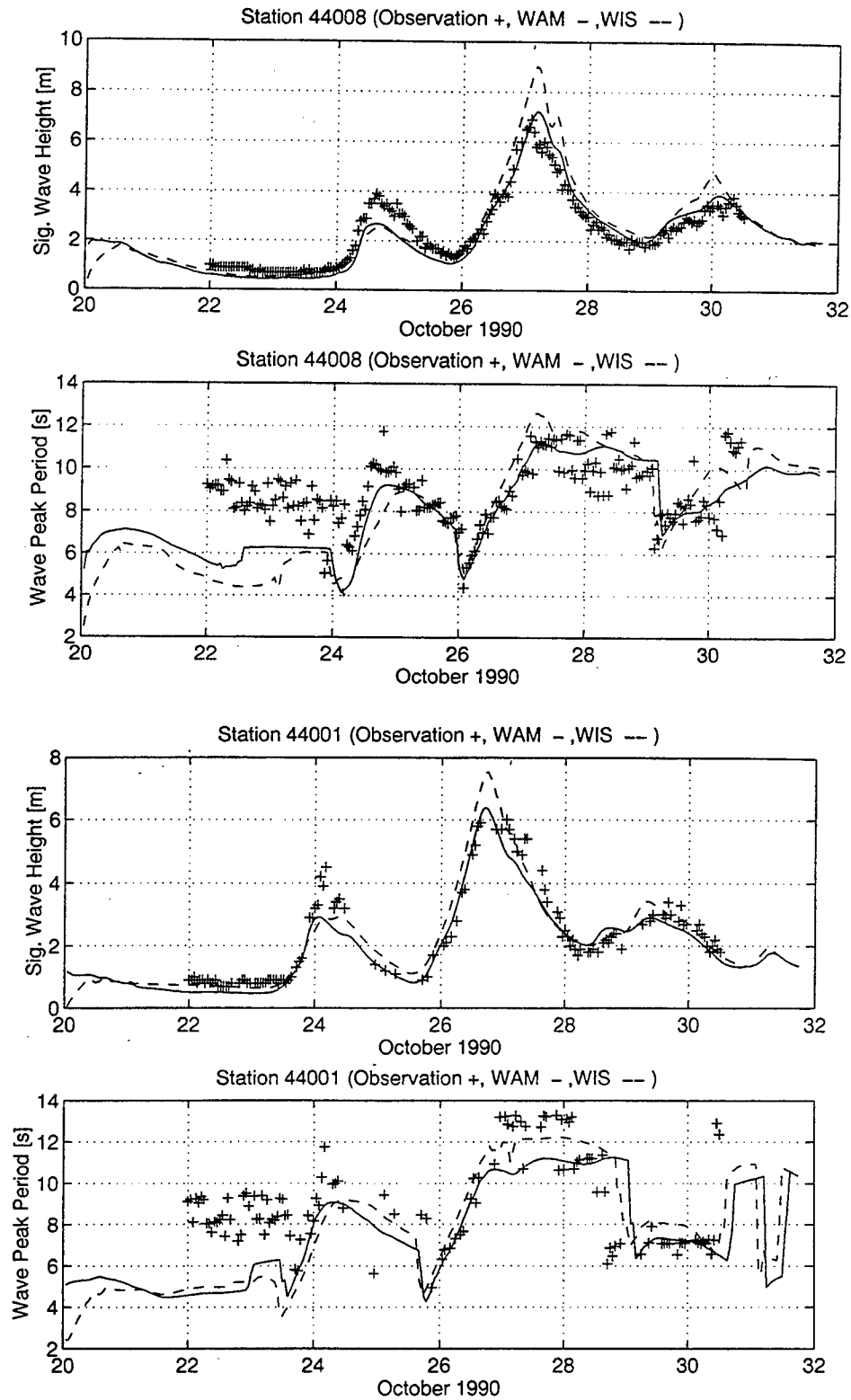
Figure 15. H_s and T_s time histories at 44008 and 44001 for IOP1.

Both models under predict the third system peak H_s.

Figure 15 shows H_s and T_p time histories for 44008 and 44001. The time histories for the models and buoy are similar for both locations, but the buoy peak H_s are about 1.0 m higher at 44008 for the three weather systems. As mentioned previously 44008 has significant depth effects. This could be the reason for both models to over predict the second system peak H_s. WAM over predicts very slightly while WIS over predicts by about 2.0 m. WIS over predicts H_s for the entire growth and decay process of the second system. Also the WAM H_s leads the buoy by several hours. At 44001 WIS over predicts the peak H_s of the second system by 1.5 m while WAM over predicts slightly. WIS over predicts H_s from the decay of the first system to the peak of the second system slightly and then decays too rapidly during the second system. WAM H_s decreases more rapidly than WIS during the second system decay. The maximum T_p reaches 13 sec during the second system and both models under predict. WAM under predicts by 2 sec while WIS under predicts by only 1 sec. Note that with a d/L_o of 1/2.3, depth affects are slight at this location.

Location 44004 is a deepwater location and the very similar performance of both models can be seen in the H_s and T_p time histories shown in Figure 16. Both models show excellent agreement to the buoy H_s throughout the second system but with a small under prediction. At the peak WAM under predicts H_s by 0.25 m while WIS over predicts by about the same amount. During the first and third systems both models under predict the H_s peak. However WIS under predicts by less than WAM throughout the third system. During the decay process of the first system WIS H_s agrees closely with the buoy while WAM is slightly low. The performance of the model T_p is similar to that of locations described previously. Of particular interest, during the second system is the WIS T_p increasing to the maximum T_p of the buoy, around 13 sec, and then decreasing to about 11 sec, also closely matching the buoy results. The WAM T_p on the other hand reaches about 11.5 sec and decreases slightly to 11 sec.
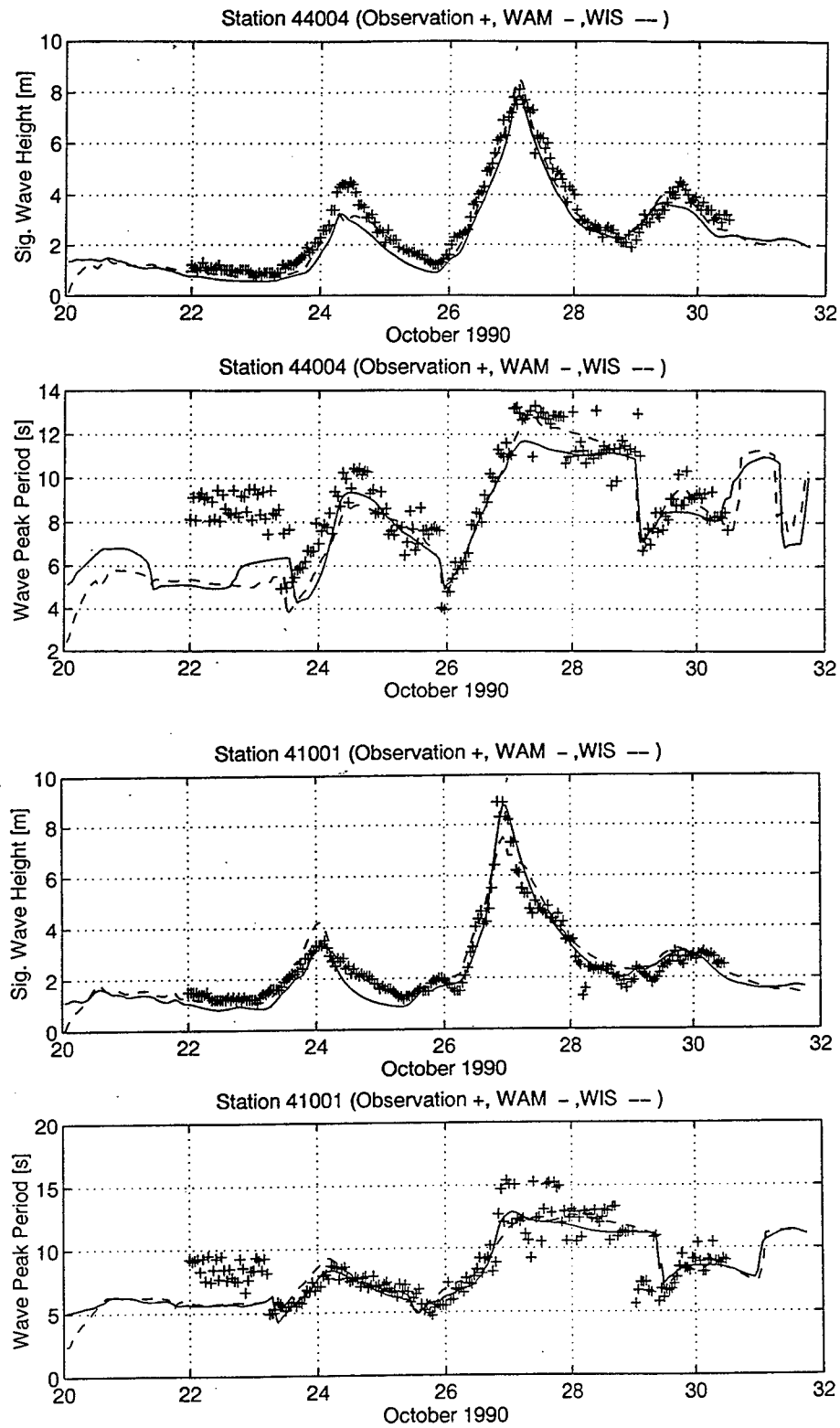
Figure 16. H_s and T_p time histories at 44004 and 41001 for IOP1.

Also shown in Figure 16 are the H_s and T_p time histories for 41001. This location is unique in that it is the only one considered for IOP1 which has good wind specification and is east of the first system track and south of the second system track. This buoy is also a deepwater location and has no depth effects. During the first system WAM matches the peak buoy H_s but decreases too rapidly thereafter. WIS on the other hand, matches the decay but over predicts the peak H_s. During the second system WAM H_s follows the buoy closely throughout while WIS uncharacteristically under predicts the peak H_s by nearly 1.0 m. Both models follow the H_s during the third system reasonably well. For the T_p, both models are very similar and agree with the buoy data except for the portion just before the first system and around the peak of the second system. Around the peak of the second system the maximum buoy T_p is 15 sec while both models are about 12.5 sec.

As mentioned previously 41006 and 41010 are well south of the weather system tracks considered in this study and the KA. These locations experience significantly lower wind speeds and H_s than the other locations. Also since they are outside the KA area the error in the wind field is larger. The maximum wind speed at 41006 is under predicted by 4 m/s. The H_s and T_p time histories for 41006, which is representative of both locations, are shown in Figure 17. Both models have similar performance, under predicting H_s by 1.0 m to 1.5 m from the beginning until just after the only H_s peak. This peak corresponds to the second system. On 27 October both models begin to agree well with the buoy as the decay continues. Both models also have similar performance for the T_p and consistently under predict by 1.0 sec to 4.0 sec before the peak and by 2.5 sec just after the peak. Once the buoy T_p drops from 15 sec to 12.5 sec the models are in agreement with the buoy.

44
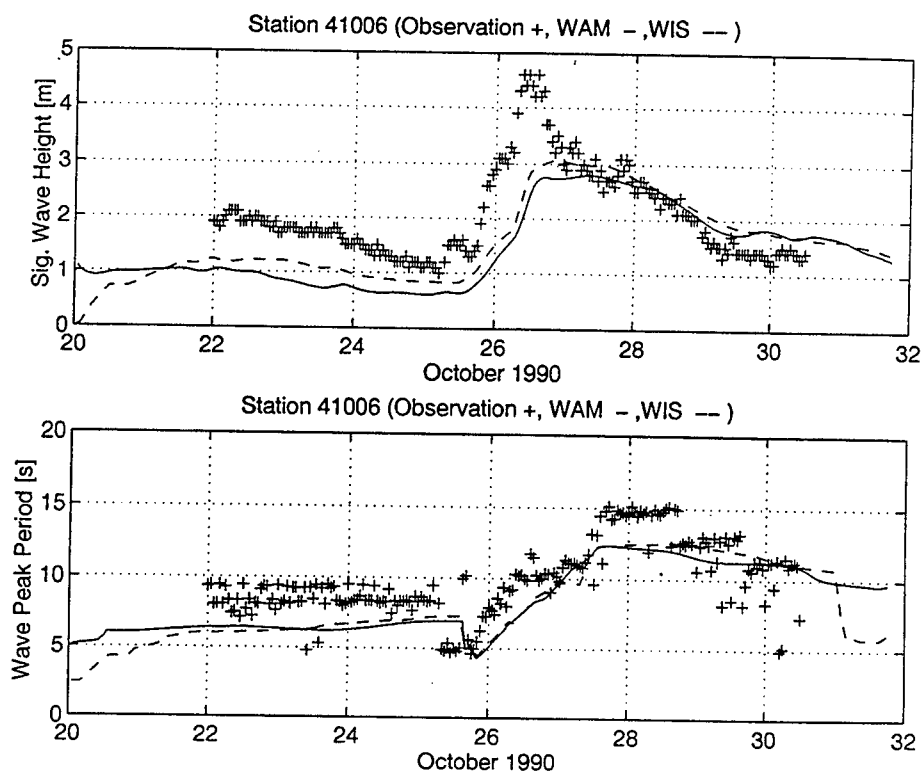
Figure 17. H_s and T_p time histories at 41006 for IOP1.

e. *Directional buoy analysis*

Buoys 44014 and 44015 are directional buoys and allow the comparison of peak wave

direction and directional wave spread in addition to H_s and T_p. At location 44014 the H_s and T_p

time histories, in Figure 18, are similar, for both models, to previous central locations shown.

However this buoy location, with a depth of 48 m, has significant depth effects. This can be seen

at the H_s peak of the second system where both models over predict even though the simulated wind

speed is about 2.0 m/s low. The peak wave direction plot, in Figure 18, shows that both models

have similar skill. However WAM takes about six hours to shift from the northwest to the

southeast on 25 October.

Station 44014 (Observation +, WAM – ,WIS —)

Station 44014 (Observation +, WAM – ,WIS —)

Station 44014 (Observation +, WAM – ,WIS —)
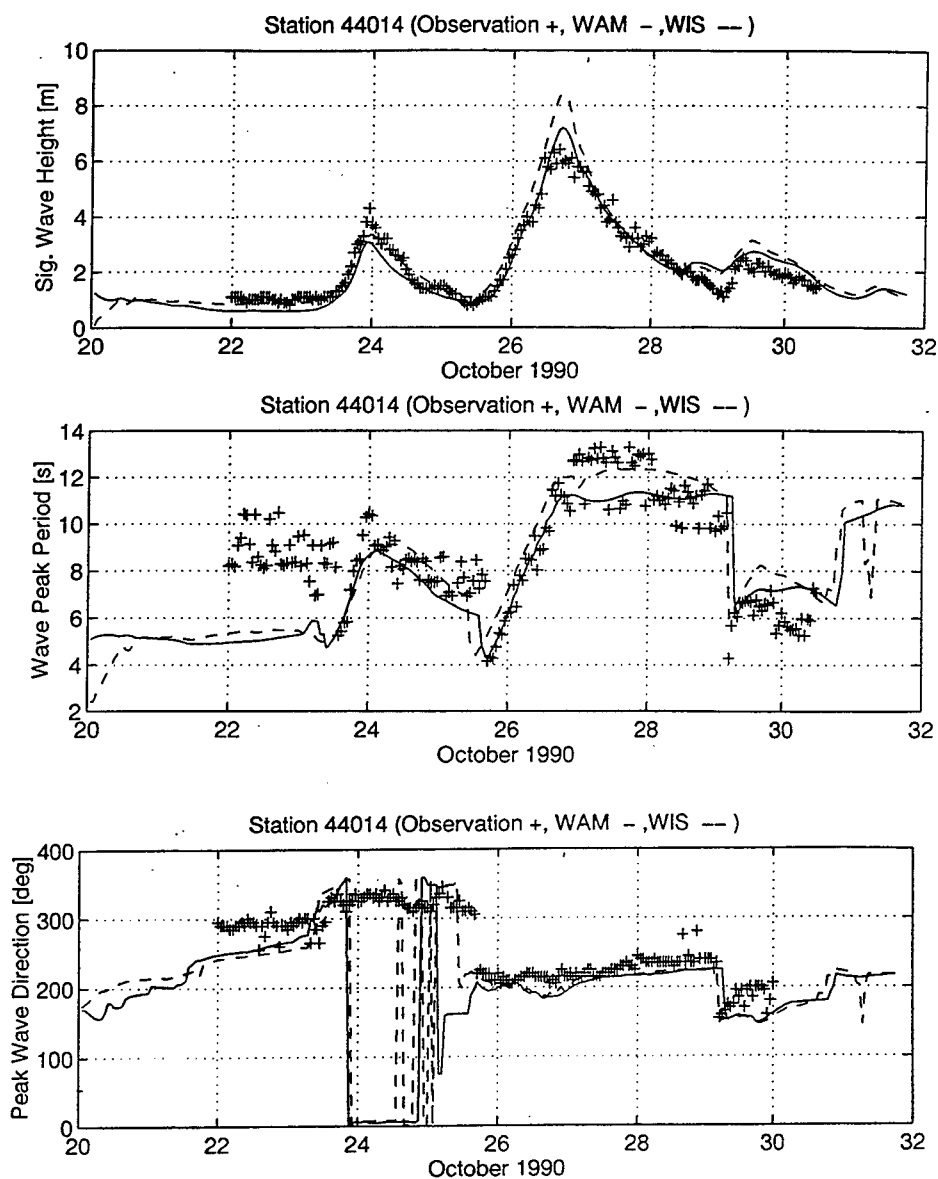
Figure 18. H_s, T_p, and θ_p time histories at 44014 for IOP1.

The directional wave spread, in Figure 19, is reasonably good throughout except for 25 October and 28 October. Beginning on 24 October both models' spreading coefficients begin to increase dramatically. The WAM spread approaches 80° while the WIS spread reaches 60°. During this period the buoy spread remains between 20° and 40°. The large spread in the models
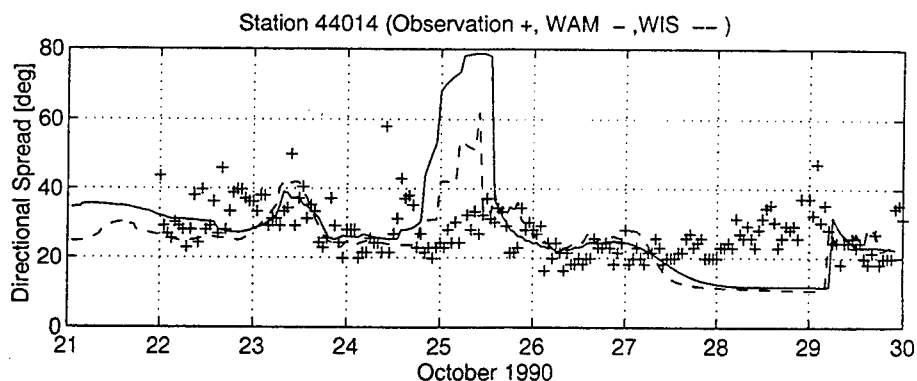
Figure 19. Directional spread time history at 44014 for IOP1.

is related to their inability to properly discretize energy into different frequency bands. The buoy spectrum exhibits a two wave system (2D spectral plots not shown) which have different peak directions, near 180° apart, and two distinct peak frequencies. In the model spectra the two wave systems are present but have the same peak frequency. The model spreads are large because the spreading is calculated at the peak frequency. Since the two wave systems in the model spectra have the same peak frequency, energy from both wave systems is included in the spread. In the buoy spectrum the spread includes only the energy associated with the wave system which has the most energy because the two wave systems have discrete peak frequencies.

After the peak of the second system, on 27 October, the model H_s begins to decrease. During this process the model spread becomes overly narrow, about 10°, compared to a buoy spread of 20° to 40°. This narrow spread persists until the wind from the third weather system causes a shift in peak wave direction from the southwest to the south.

The H_s, T_p, and θ_p plots for location 44015 are shown in Figure 20. This is a deepwater location and shows better model agreement with the buoy than 44014. Most of the same characteristics of H_s and T_p found in the other deepwater locations, are present here. At the peak

of the second system WAM H_s is slightly under predicted and WIS is over predicted. One difference is the slow decline of WIS H_s during the decay process of the first system. Both models under specify T_p at the beginning of the first system and during the decay of the second system. However WIS is closer to the measured T_p during the second system decay.
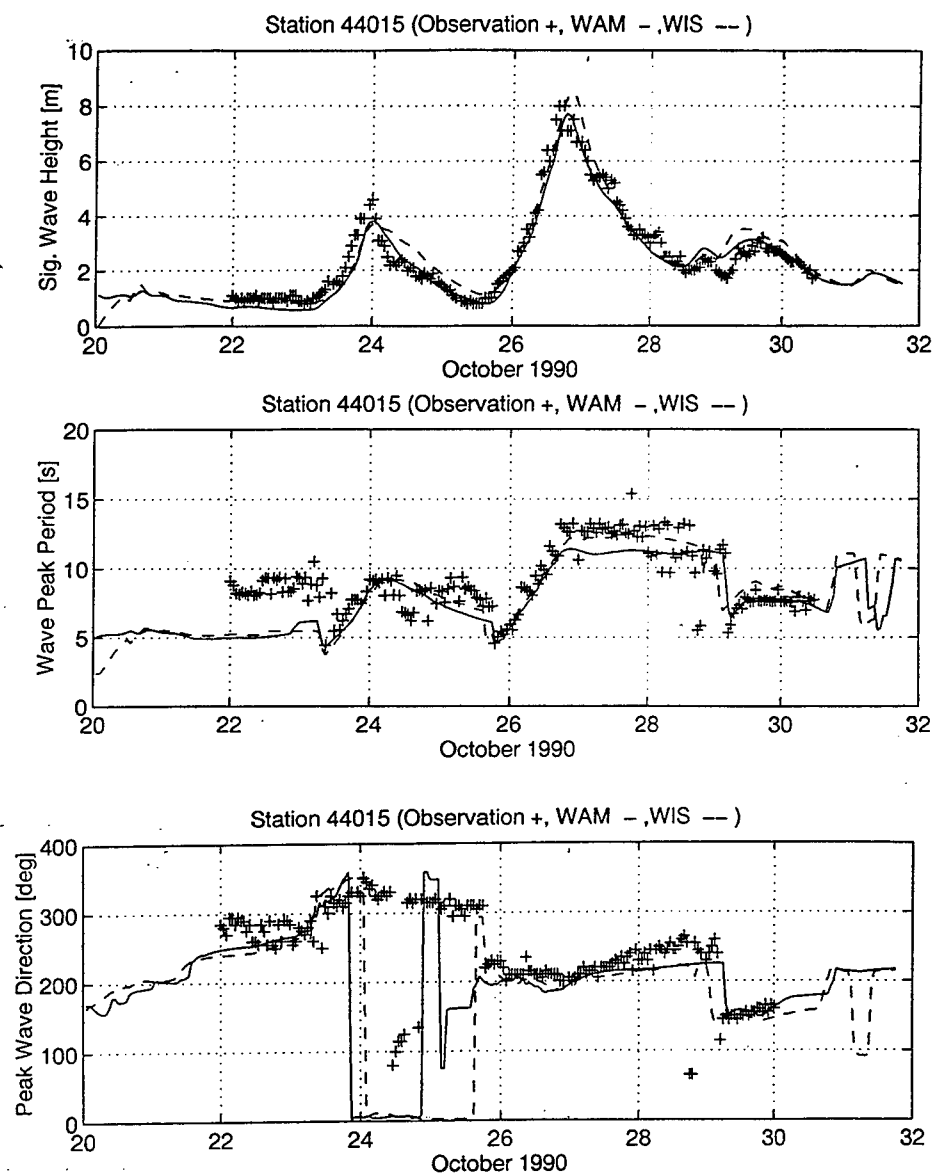
Figure 20. H_s, T_p, and θ_p time histories at 44015 for IOP1.

The plot of peak wave direction is very similar to that of 44014. However, the directional spread for 44015, in Figure 21, has significant differences. Overall the models tend to have a more negative bias than at 44014. This is due in part to generally wider spread in buoy 44015 compared to 44014. This difference could be attributed to the depth effects at 44014. The maximum WAM spread occurs on 25 October and reaches only 60°. The WIS spread matches the buoy spread relatively well during 25 October and reaches a maximum of only 50°, but lags the buoy by several hours. The same overly narrow model spread, about 10°, is evident on 28 October, however the WIS spread oscillates between 10° and 35° toward the later part of 28 October.

The spreading coefficient is formulated to gauge the width of a single mode spectrum. When the spectrum is multi-modal with significant energy peaks in more than one direction the spreading coefficient is not descriptive of the energy distribution in direction. When multi-modal spectra exist the spreading coefficient alone is not sufficient to describe the energy distribution. In addition to the spreading coefficient, kurtosis and skewness parameters were proposed by Kuik et al. (1988) to solve this problem. However, Anctil et al. (1993) showed that these parameters, from higher order moments, when applied to NDBC buoys, do not correlate well with fixed platform measurements.
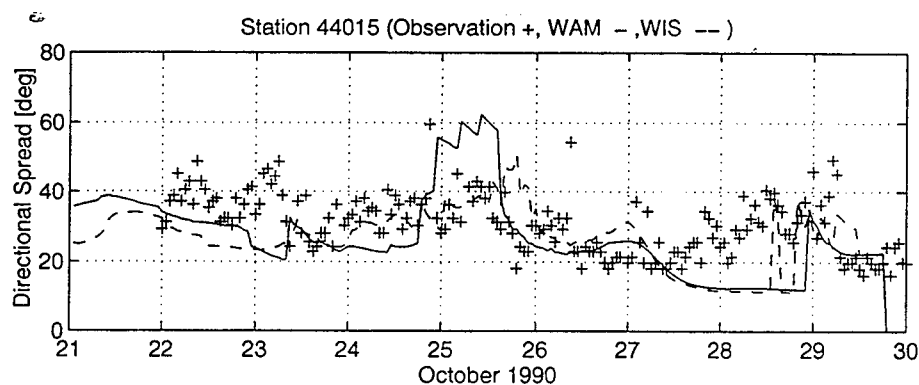
Figure 21. Directional spread time history at 44015 for IOP1.

An alternative method for comparing the model spectral energy distribution to the directional buoy spectra is the pattern correlation method described in Chapter III. This method is concerned only with the relative energy distribution. Recall that adjustments are made to scale the total buoy energy to the model total, rotate the spectrum so that buoy mean direction agrees with the model and shift the buoy spectrum so that the buoy mean frequency matches the model's. The pattern correlation coefficient (PCC) gives an indication of how well the model energy distribution agrees with that of the buoy.

The plots in Figure 22 show the PCC as a function of time for 44014 and 44015. The PCC at both locations have similar characteristics. Midway through 24 October a dramatic decrease of PCC occurs. This corresponds roughly with the large directional spread shown previously. At 44014 the WAM PCC decreases less rapidly than WIS for this period. The WIS PCC also tends to be slightly lower than WAM around the 27th and 28th. These differences between the two locations might be attributed to depth effects at 44014. At 44015 the dramatic drop on the 24th is equally as rapid for both models. The WAM spread at this location and time is still overestimated but WIS agrees with the buoy quite well except for a time lag. So, even though the WAM spread agrees with the buoy the model spectral energy distribution does not correlate well with that of the buoy. Also note that these poor correlations for both models don't correspond to poor H_s and T_p estimates.

Beginning on the 26th the PCC increases back to around 0.8 during the growth cycle of the second weather system. On the 27th, with decay cycle already begun, a more gradual PCC decrease, compared to the 24th, occurs. The gradual decrease continues until midway through the 28th, to about 0.5. After this another abrupt decrease, to about 0.0, occurs and continues until nearly the 29th for 44014 and through the beginning of the 29th for 44015. This decrease in PCC from the 27th to the 29th also corresponds to the very narrow directional spread estimated by the
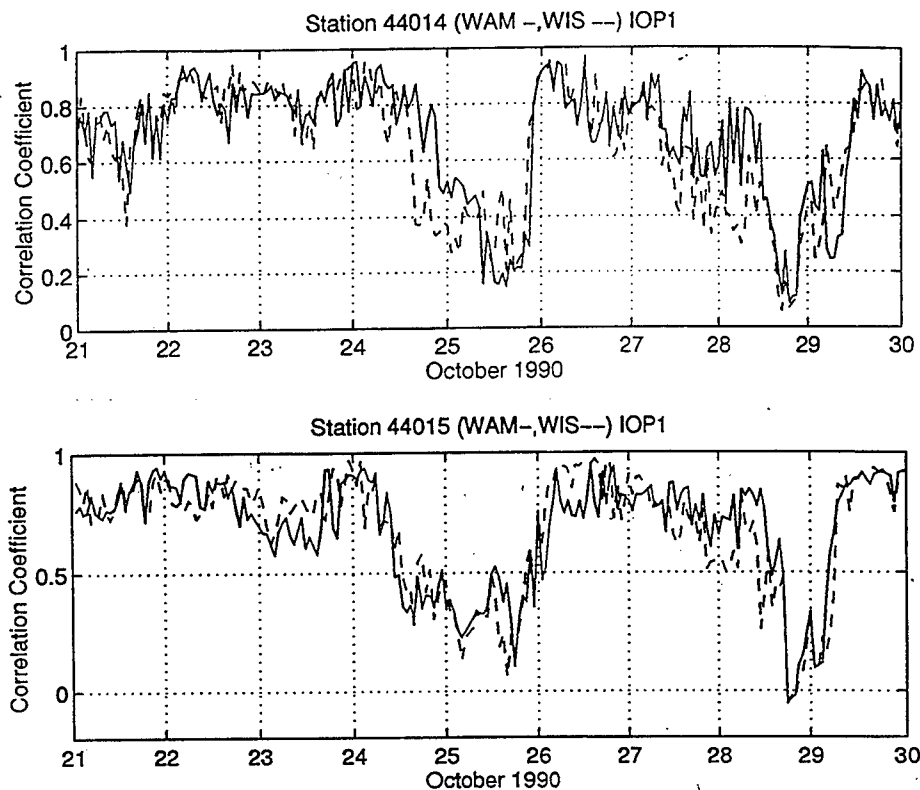
Figure 22. PCC time histories at 44014 and 44015 for IOP1.

models. In general, both models exhibit poor correlation with the buoy spectra during the decay process and transition between the three weather systems.

f. Summary

The IOP1 simulation period is a moderate case in terms of peak wind speeds which were 15 m/s to 25 m/s and has the best simulated winds of the five simulations considered. The wind speed SIs at all locations are below 20% and range from 10% to 19%. The WAM H_s RMS error is about 0.01 m to 0.3 m less than that of WIS, but the WAM H_s has a negative bias ranging to about -0.5 m while WIS has at most a positive bias of about 0.3 m . Also the WAM H_s SI is mostly lower than that of WIS for locations with a low wind speed SI. Both models have a negative

T_p bias, more so for WAM, which ranges from -0.52 sec to -1.37 sec, than for WIS, which ranges from -0.25 sec to -1.08 sec. The WAM T_p RMS Error is generally less than that of WIS with differences ranging from 0.01 sec to 0.42 sec, while the SI is generally similar for both models.

The directional wave spread for both models is too wide at the main peak because two wave systems are present but are not well separated in the frequency domain. During the decay of the storm both models' spread become too narrow. The PCC is relatively good during growth but decreases during decay. The first PCC decline is related to the two lobes of energy, one of which persists longer in the models than the buoy. The second PCC decline is related to the overly narrow spread in both models during the decay of the main storm event.

4.2 IOP2

a. Synoptic weather conditions

The IOP2 meteorological conditions were considerably different from IOP1. Conditions were dominated by low pressure events with associated frontal passages. As many as four significant events are present during the ten day period at some locations. The peak wind speeds associated with these events range from 10 m/s to 18 m/s. Peak wind speeds during IOP1 ranged from 10 m/s to 25 m/s. The IOP2 consist of more dynamic and weaker systems than the main system during IOP1.

On 8 January a high pressure system was centered over New England and Canada while the first major low pressure system was forming well off the Carolina coast. Winds are generally blowing toward the south and southwest, north of the low. On the 9th and 10th the low continues north along the coast passing near Cape Hatteras and then up to Nova Scotia. The wind shifts west ahead of the low on the 9th and then south to southeast behind the low on the 10th.

Figure 23 shows the isobars and track of the low for the 10th. From the 10th to the 12th the winds

turn clockwise from the southeast to the north. By the 12th the second low pressure system has

formed off the New Jersey coast also shown in Figure 23. The winds blow to the northeast and

north in the southern area behind the low and to the northwest to west in the northern area ahead

of the low. By the 13th the low has moved well north off the coast of Nova Scotia.
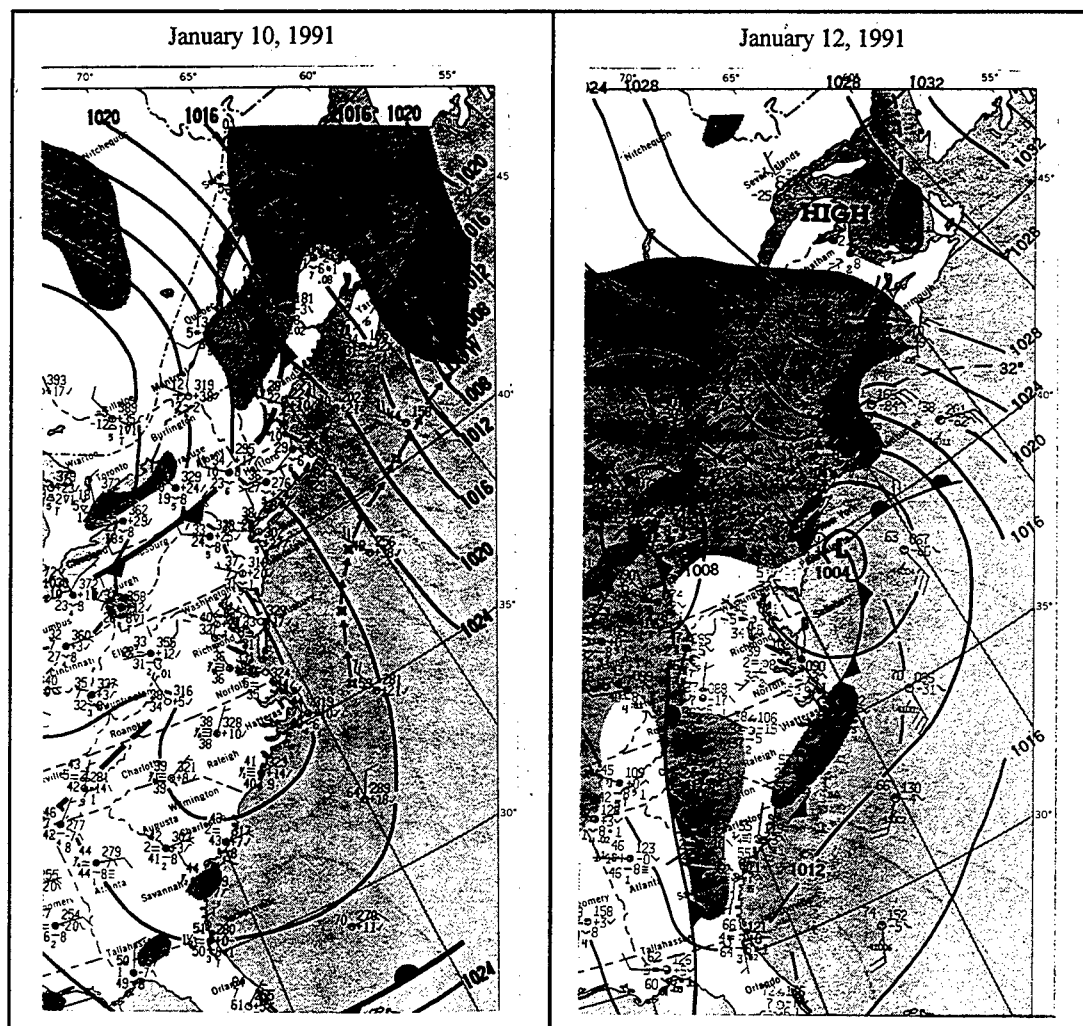
Figure 23. Surface weather maps for the 10th and 12th of January 1991 (National Weather Service, 1991a).

b. Winds

The scatter plots for wind speed and direction at 44001, Figure 24, and wind speed at 44005 and 41006, Figure 25, show the relative quality of the winds for central, northern, and southern locations respectively. As before the southern locations 41006 and 41010 are outside the
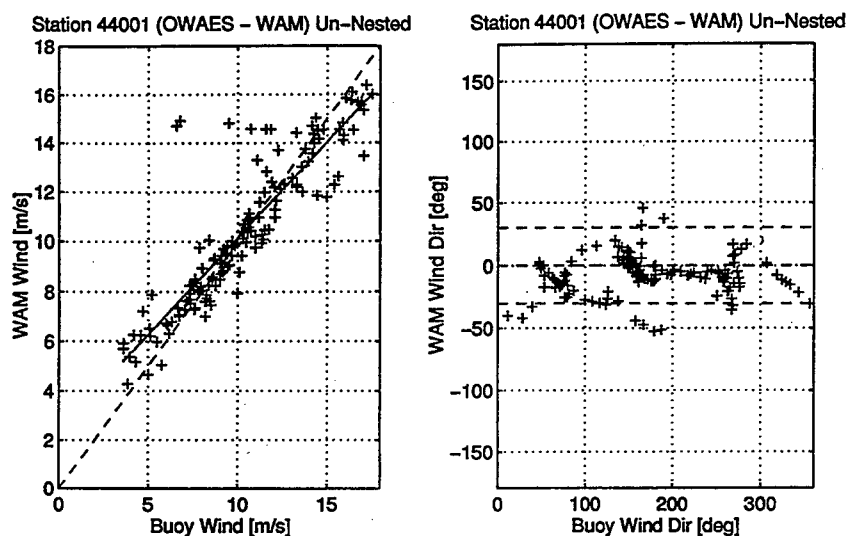
Figure 24. Wind speed and direction scatter plots at 44001 for IOP2.
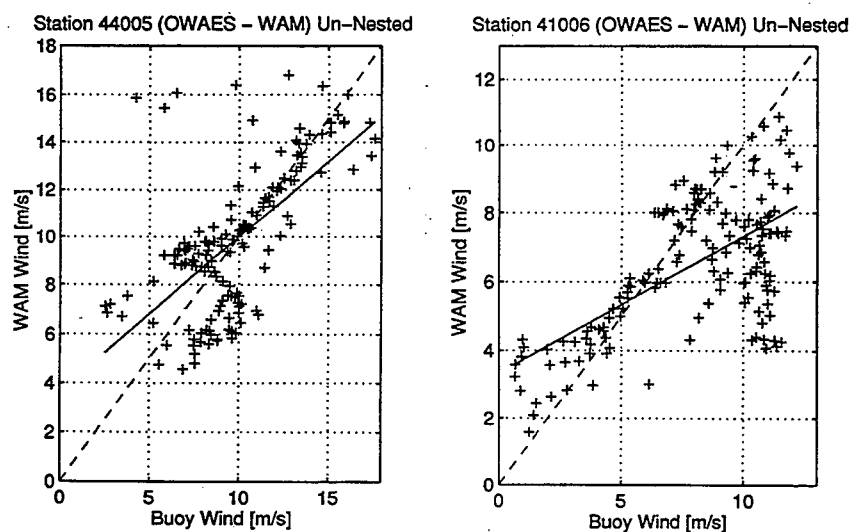
Figure 25. Wind speed scatter plots at 44005 and 41006 for IOP2.

KA area and have the most wind speed scatter with a bias toward the buoy for higher wind speeds. The northern area, which was previously identified as a data sparse region, has slightly more wind speed scatter than the data rich central area. The scatter for wind direction follows a similar trend for each area.

Wind time histories of select locations show several different wind regimes associated with northern, central, and southern areas. Plots for all locations considered in this study are located in Appendix A. The northern area, represented by 44005, in Figure 26, experiences five different wind speed peaks during the simulation, the largest of which reaches a maximum of 18 m/s.
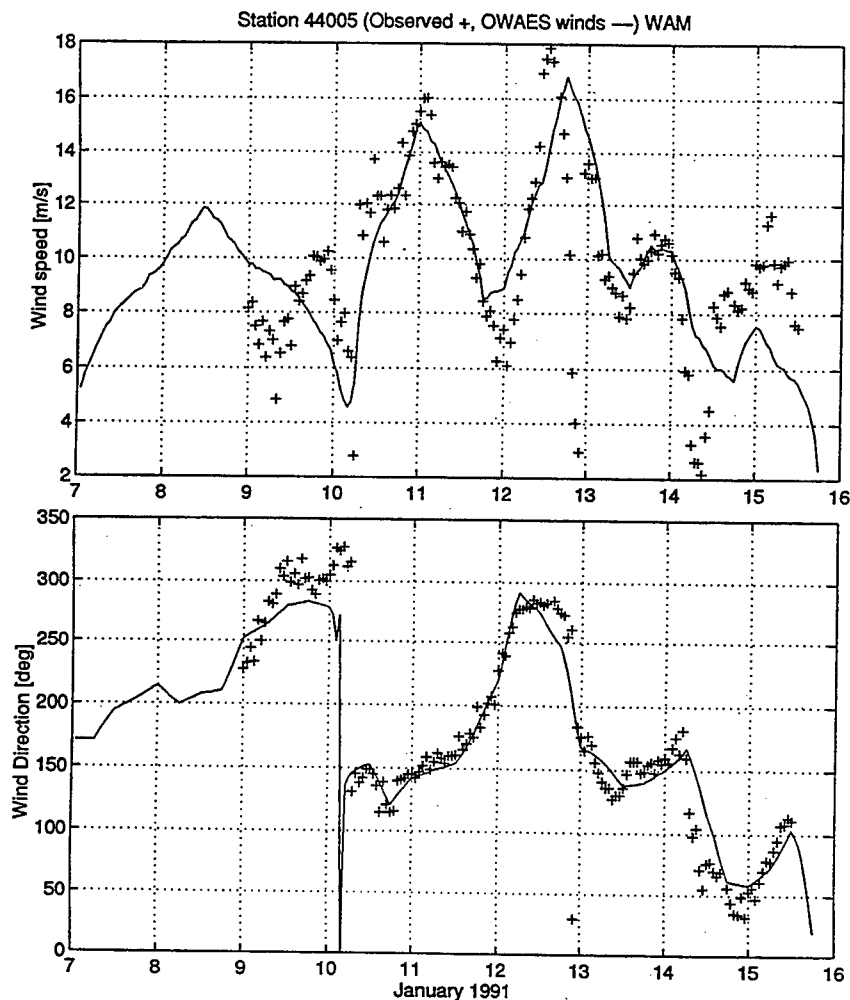
Figure 26. Wind speed and direction time histories at 44005 for IOP2.

Beginning on the 10th the wind abruptly shifts from northwest to southeast with the passing of the front associated with the first low pressure system. Form the 10th to the 11th the wind speed increases to 16 m/s, as the low intensifies. From the 11th to the 12th the wind speed decreases as the wind shifts from southeast to southwest. Beginning on the 12th the second low has formed and wind speed increases to 18 m/s while the wind direction shifts clockwise from southwest to northwest ahead of the low. During the later part of the 12th the wind speed begins to decrease and the wind direction abruptly shifts to the southeast with the passing of the front associated with the second low.

Given the dynamic nature of the wind conditions the simulated winds match the buoy reasonably well. However, there are significant errors such as the underprediction of the two main peaks, by 1 m/s to 2 m/s, and overprediction of the following decreases, in some cases missing the decrease all together, such as the later part of the 12th and beginning of the 14th. The simulated wind direction follows the abrupt shifts in the buoy very well. The largest difference between the simulation and buoy is about 30°.

The central area, represented by 44001, in Figure 27, experiences five wind speed peaks but the maximum wind speed at each peak tends to decrease as the simulation progresses. For this location the wind direction is similar to 44005 but the shift on the 13th is more gradual instead of abrupt. This indicates that there was no strong frontal passage at 44001 on the 13th. The simulated wind speed is improved over the northern area but still underpredicts the first three peaks at 44001 by 2 m/s to 4 m/s and overpredicts some minimum wind speeds. Another location in the central area, 44014, has similar characteristics but the wind speed tends to be more dynamic and oscillates more during the increase and decline associated with the five main peaks.
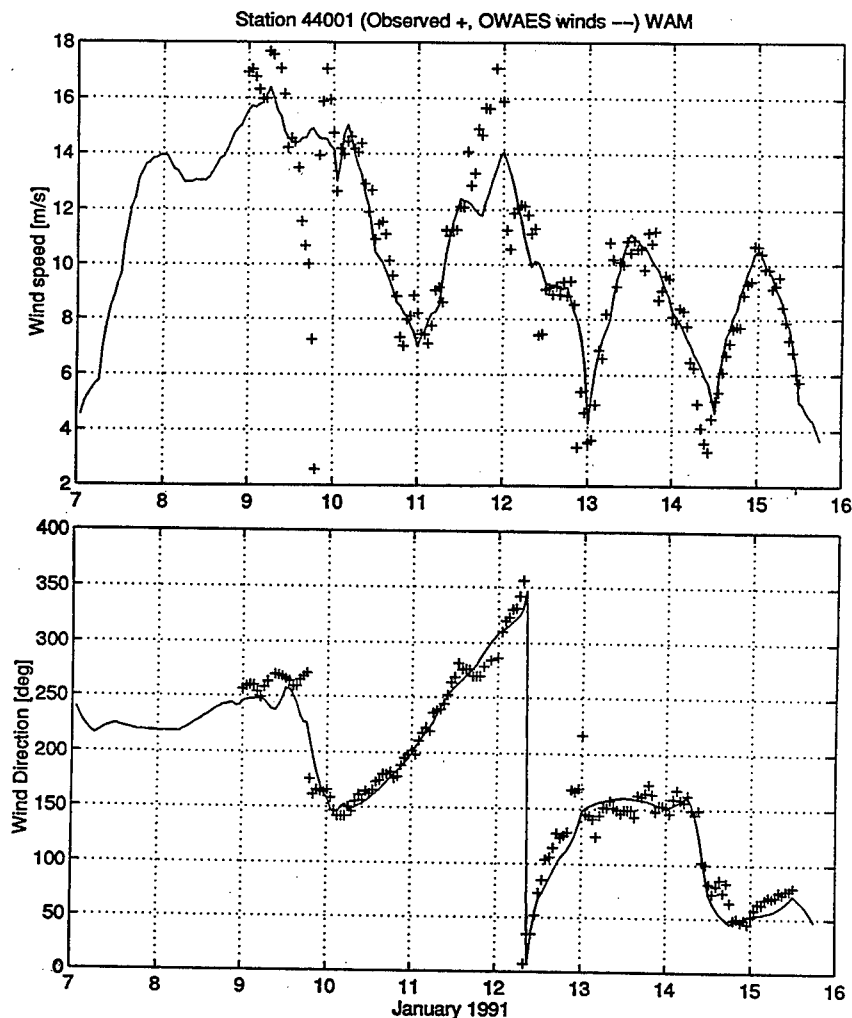
Figure 27. Wind speed and direction time histories at 44001 for IOP2.

Locations 41002, 41006, and 41010 are south of the meteorologic systems which dominate the model domain. Wind time history plots for location 41006 are shown in Figure 28. These locations have more gradual wind speed changes. In general, they have one broad peak with a maximum of 12 m/s from the 9th to the 14th. The wind direction rotates clockwise during the entire simulation beginning near east and turning north then continuing to turn around again to north. Simulated wind speeds at 41006 have considerable error from the 10th to the 12th dropping to 4 m/s compared to 10 m/s to 12 m/s for the buoy.
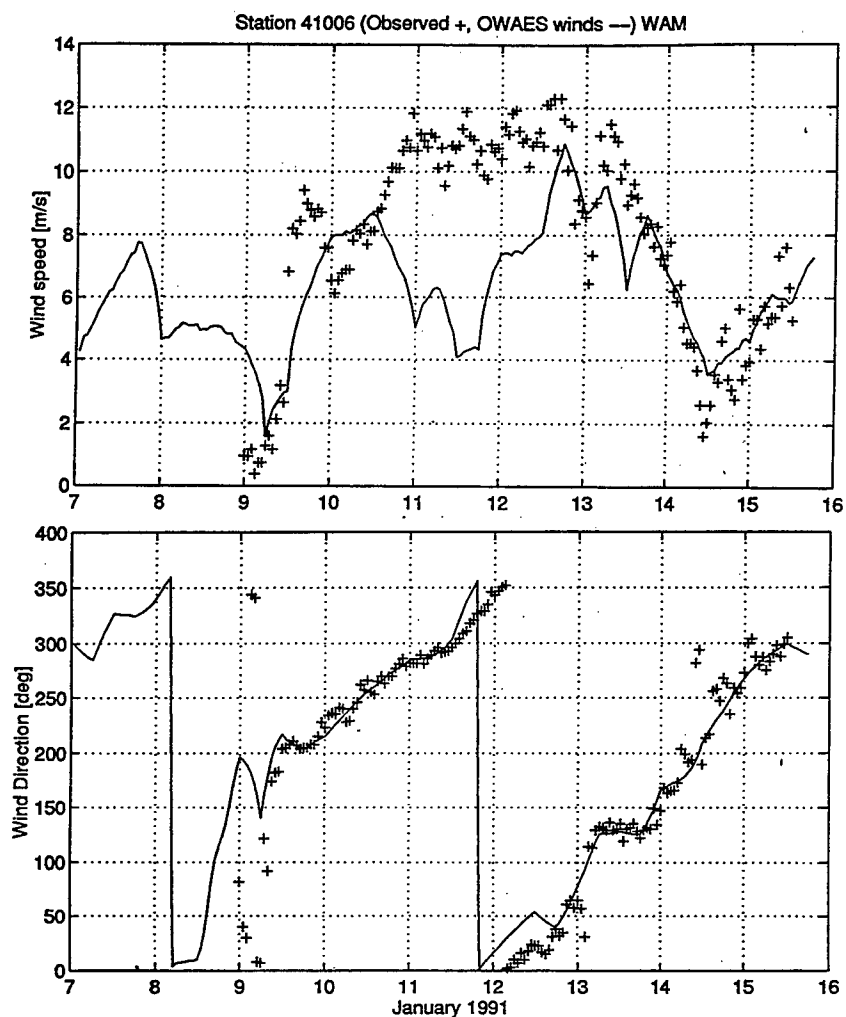
Figure 28. Wind speed and direction time histories at 41006 for IOP2.

c. Wind and wave statistics

The general performance of the models is indicated by the statistics of the integrated properties, wind speed, U_{10}, significant wave height, H_s, and peak wave period, T_p. In Table 5 the quality of the simulated wind speed can be seen in the RMS Error which ranges from 0.89 m/s to 2.83 m/s and the bias which is mostly positive, ranging up to 1.80 m/s. The scatter index (SI) ranges from 11% to 33% and the correlation coefficient (CC) ranges from 0.58 to 0.96. Locations

44011, 41006, and 41010 are excluded from this summary. Location 44011 has too few points and 41006 and 41010 have large errors because they are well south of the KA area. The wind speed statistics here are not quite as good as those for IOP1. This can be attributed to the difficulty in simulating the much more dynamic conditions which existed during IOP2.

Table 6 shows the H_s statistics for WAM and WIS. Considering all but the three locations mentioned previously, the RMS Error tends to be slightly smaller for WIS, ranging from 0.33 m to 0.76 m, than WAM which ranges from 0.59 m to 0.86 m. The difference between the two models' RMS Error ranges from 0.13 m to 0.32 m. WAM has a negative bias, ranging from -0.14 m to -0.73 m, while WIS has a positive bias, except for 41001 which is -0.20 m, ranging from 0.01 m to 0.46 m. The SI for the models is either about equal or lower for WIS. The SI for WIS ranges from 14% to 30%, while the SI for WAM ranges from 22% to 28%. The correlation coefficient (CC) for WIS varies between 0.79 and 0.95 while WAM ranges from 0.65 to 0.95.

Table 5. Statistics of measured and hindcast wind speed for IOP2.

Buoy	Mean Buoy (m/s)	Mean Model (m/s)	Bias (m/s)	Abs Err (m/s)	RMS Err (m/s)	SI (%)	CC	# pts
44005	9.80	9.88	0.08	1.80	2.51	26	0.64	155
44011	8.40	10.09	1.69	2.24	3.07	37	0.80	58
44008	10.20	10.52	0.32	1.53	2.03	20	0.78	156
44004	11.32	11.24	-0.09	0.92	1.20	11	0.94	157
44001	10.28	10.37	0.09	0.94	1.52	15	0.89	154
44014	8.54	9.40	0.86	1.58	2.83	33	0.58	156
41001	9.91	10.05	0.13	1.01	1.27	13	0.94	156
41002	8.06	8.35	0.29	0.66	0.89	11	0.96	156
41006	7.88	6.48	-1.39	2.07	2.80	36	0.63	157
41010	8.11	6.66	-1.45	2.34	3.13	39	0.60	156

SI - scatter index   CC - correlation coefficient

Table 6. Statistics of measured and hindcast H_s for IOP2.

Buoy	WAM							WIS						
	Mean Buoy (m)	Mean Model (m)	Bias (m)	Abs Err (m)	RMS Err (m)	SI (%)	CC	Mean Model (m)	Bias (m)	Abs Err (m)	RMS Err (m)	SI (%)	CC	# pts
44005	2.35	2.02	-0.33	0.50	0.63	27	0.87	2.56	0.21	0.40	0.50	21	0.98	155
44011	2.55	2.24	-0.31	0.46	0.55	22	0.91	2.89	0.33	0.52	0.68	27	0.96	58
44008	2.56	2.42	-0.14	0.53	0.70	28	0.65	3.01	0.46	0.64	0.76	30	0.95	156
44004	3.04	2.59	-0.45	0.48	0.67	22	0.89	3.29	0.25	0.52	0.69	23	0.97	157
44001	2.75	2.36	-0.39	0.47	0.77	28	0.84	2.88	0.13	0.45	0.60	22	0.98	154
44014	2.50	2.18	-0.31	0.37	0.59	23	0.91	2.61	0.12	0.29	0.39	16	0.99	156
41001	3.07	2.35	-0.72	0.72	0.86	28	0.95	2.87	-0.20	0.38	0.54	18	0.99	156
41002	2.30	1.94	-0.36	0.42	0.59	26	0.74	2.31	0.01	0.23	0.33	14	0.99	156
41006	2.28	1.55	-0.73	0.74	0.83	37	0.69	1.82	-0.46	0.55	0.67	29	0.97	157
41010	2.07	1.49	-0.57	0.59	0.73	35	0.78	1.75	-0.32	0.46	0.59	28	0.97	156

SI - scatter index   CC - correlation coefficient

Table 7 shows the T_p statistics for WAM and WIS. Again, excluding the three locations mentioned previously, the statistics are generally similar for both models. WAM exhibits a consistent negative bias, ranging from -0.14 sec to -0.99 sec while WIS has a positive bias for buoys north of 44015 ranging from 0.07 sec to 0.84 sec and a negative bias, ranging from -0.03 sec to -0.37 sec, for buoys south of and including 44015. The RMS Error for both models is very similar in the central area but is lower for WAM except for locations 41001 and 41002 in the southern area. The difference in RMS Error between the models ranges from 0.00 sec to 0.36 sec. The SIs are similar for both models, except for 44008, and range from 13% to 22%. The CC for WAM is higher than that for WIS, except for 44005. The WAM CC ranges from 0.61 to 0.87 and the differences between WAM and WIS CCs vary between 0.06 to 0.15.

Table 7. Statistics of measured and hindcast T_p for IOP2.

	WAM							WIS						
Buoy	Mean Buoy (s)	Mean Model (s)	Bias (s)	Abs Err (s)	RMS Err (s)	SI (%)	CC	Mean Model (s)	Bias (s)	Abs Err (s)	RMS Err (s)	SI (%)	CC	# pts
44005	7.41	7.27	-0.14	1.32	1.59	22	0.61	8.25	0.84	1.19	1.54	21	0.76	155
44011	8.28	7.52	-0.76	1.35	1.64	20	0.47	8.51	0.23	1.70	1.98	24	0.03	58
44008	8.36	7.83	-0.53	1.22	1.47	18	0.53	8.43	0.07	1.46	1.83	22	0.22	156
44004	8.58	7.82	-0.76	0.96	1.29	15	0.72	8.71	0.13	1.03	1.37	16	0.61	157
44001	8.42	7.76	-0.66	1.25	1.54	18	0.64	8.48	0.07	1.17	1.60	19	0.58	154
44014	8.64	7.83	-0.81	1.12	1.57	18	0.78	8.63	-0.02	1.09	1.61	19	0.72	156
41001	8.95	7.96	-0.99	1.07	1.35	15	0.73	8.58	-0.37	0.91	1.24	14	0.61	156
41002	9.15	8.15	-0.99	1.05	1.27	14	0.87	8.84	-0.31	0.81	1.16	13	0.72	156
41006	8.66	8.22	-0.45	1.04	1.31	15	0.75	8.70	0.03	0.83	1.13	13	0.79	157
41010	8.75	8.15	-0.60	1.41	1.61	18	0.69	8.25	-0.50	1.36	1.69	19	0.65	156

SI - scatter index   CC - correlation coefficient

The scatter indices for U_{10}, H_s, and T_p from Tables 5 through 7 are plotted in bar graph form in Figure 29 to show the relationship between each parameter. The wind speed plot shows four locations, 44011, 44014, 41006, and 41010, with more than 30% scatter. The statistics for 44011 are based on about 1/3 of the data points as the other locations and are therefore discarded. Locations 41006 and 41010 are outside the KA area as mentioned previously. Location 44014 is located in the data rich central area. Four locations have wind speed SIs of 20% or less. They are 44004, 44001, 41001, and 41002. The corresponding H_s SIs for WIS are consistently near or below 20% while the H_s SIs for WAM are consistently above 20%. Significant differences, more than 5%, exist between the models' H_s SIs for 44001, 44014, 41001, and 41002 with WIS having the lower value. In the northern area the wind speed SI for 44005 is 26%. This corresponds to a
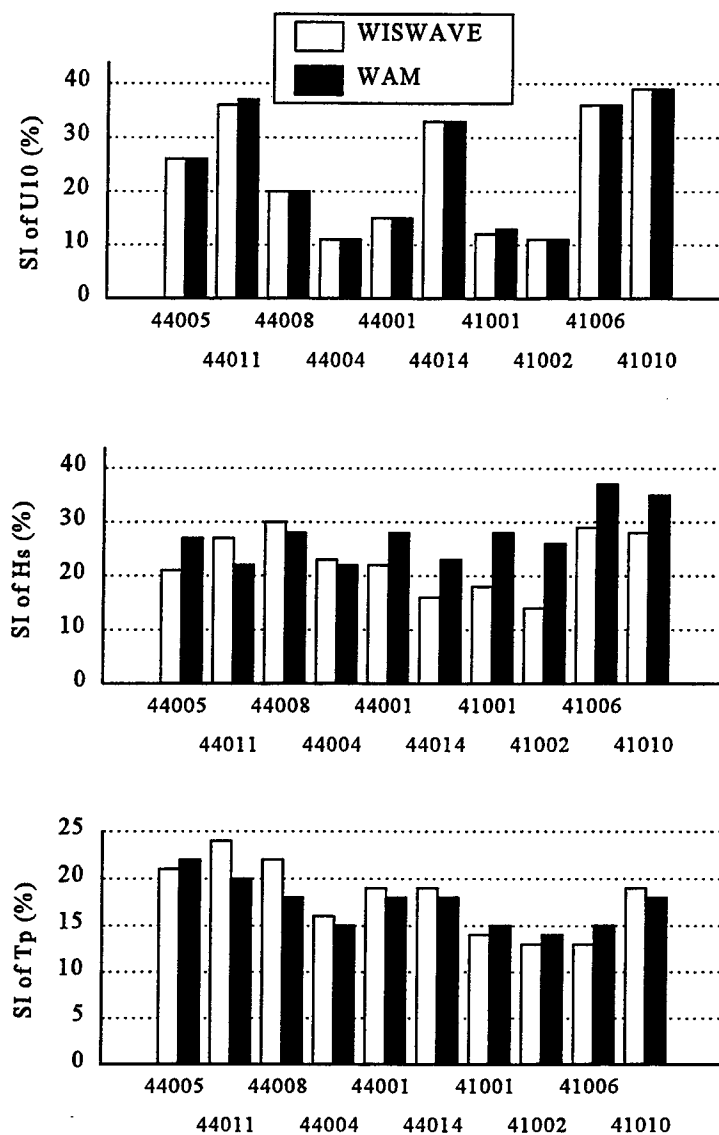
Figure 29. WAM and WIS U_{10}, H_s, and T_p scatter indexes for IOP2.

H_s SI 21% and 27% for WIS and WAM respectively. At location 44008 the wind speed SI is 20% while the H_s SI for both models is near 30%. One reason for this discrepancy between wind speed and H_s is depth effects on the spectrum. The depth to deepwater wavelength ratio, d/L_o, is 1/3.7.

Another apparent discrepancy exists at 44014 where the wind speed SI is over 30% yet the H_s SI is 16% for WIS and 23% for WAM. At the two southern buoys, 41006 and 41010, the high wind speed SI of over 30%, as expected, results in high H_s SIs of 30% or more. The T_p SI is generally below 20% for all but northern locations which are below 25%. In the southern area some locations are below 15%. The difference between the models is small for all locations.

d. Non-directional time histories

The following section presents a description of modeled and measured H_s and T_p time histories for select locations corresponding to non-directional buoys. These locations represent the characteristics found in the northern, central, and southern areas of the model domain.

Locations 44005 and 44008, in Figure 30, represent the northern area. Evident in the H_s plot for 44005, are two peaks associated with the passage of the two low pressure systems. WIS is in good agreement with the buoy throughout the simulation but has a slight overprediction at the first peak. There are several cases where WIS H_s errors can be attributed to wind speed errors. The first example of this is the H_s peak on the 10th which is missed by both models. The wind speed time history plot, in Figure 26, shows that the simulated wind speed also misses this peak. The WIS H_s lag at the first peak is due to a lag in wind speed. WIS H_s begins increasing about 6 hours earlier than the buoy, as does the simulated wind speed, during the growth leading to the second peak. In contrast, WIS H_s matches the buoy at the second peak even though the wind speed is underspecified by 1.0 m/s to 2.0 m/s. WAM H_s , which is less accurate than WIS for this simulation, underpredicts both peaks, the second by 2.0 m/s. The model T_p follows the buoy well but WIS tends to lead and WAM tends to lag by 3 to 6 hours. Both models overpredict by 1.0 sec on the 10th and underpredict on the 13th, WAM by 1.5 sec and WIS by 2.0 sec.
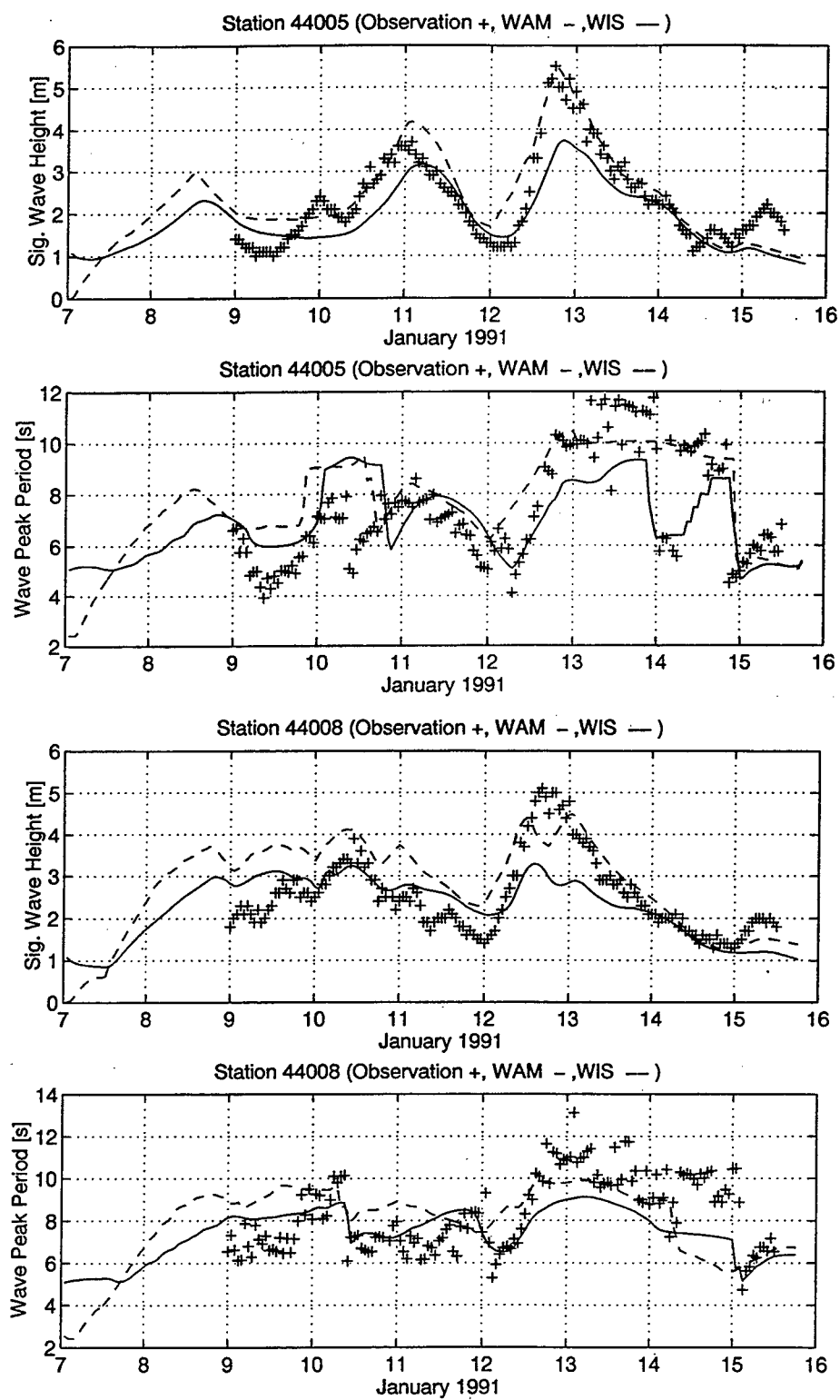
Figure 30. H_s and T_p time histories at 44005 and 44008 for IOP2.

In contrast to 44005, the wind speed at 44008 is more constant varying between 10 m/s and 17 m/s until the 12th. The result of this is that the first H_s peak is less pronounced than at 44005. During this time both model H_s are fairly constant with a H_s for WAM around 3.0 m and 3.5 m to 4.0 m for WIS. WAM matches the buoy better than WIS which overpredicts except at the peak. On the 12th the wind speed increases with the second low approaching. The peak wind speed is underpredicted by 3.0 m/s. This results in an underprediction by both models, WIS by 0.5 m to 1.0 m and WAM by 2.0 m. The d/L_o associated with a T_p of 12 sec is 1/3.7 on the 13th. This depth effect is expected to cause an overprediction of H_s by the models however WIS overpredicts very slightly while WAM underpredicts during this time. The T_p for 44008 has characteristics similar to 44005.

Location 44004 is a deepwater location and is in the central area of the model domain. The wind speed , with a SI of 10%, is in good general agreement with the buoy but underpredicts the second peak by 1.0 m/s to 2.0 m/s. The H_s and T_p plots for 44004 are shown in Figure 31. Between the 9th and 10th the measured H_s is constant at about 4.0 m to 4.5 m while WIS overpredicts by as much as 1.5 m and WAM undepredicts by less than 1.0 m. At the beginning of increasing H_s associated with the approach of the second low WIS begins increasing about 3 hours too soon and peaks about 6 hours early. At the second peak both models underpredict the H_s by 1.0 m and 2.0 m for WIS and WAM respectively. The T_p is underpredicted by both models during both peaks. WIS underpredicts the first peak by 1.0 sec and the second by 2.0 sec. WAM underpredicts the first peak by 1.0 sec to 2.0 sec and the second by 2.0 sec to 3.0 sec.

Location 41001 is on the southern edge of the central area. The H_s and T_p plots are shown in Figure 31. The model H_s shows the four distinct peaks which are also evident in the wind speed. The buoy H_s however does not indicate the peaks as distinctly. Both models begin with
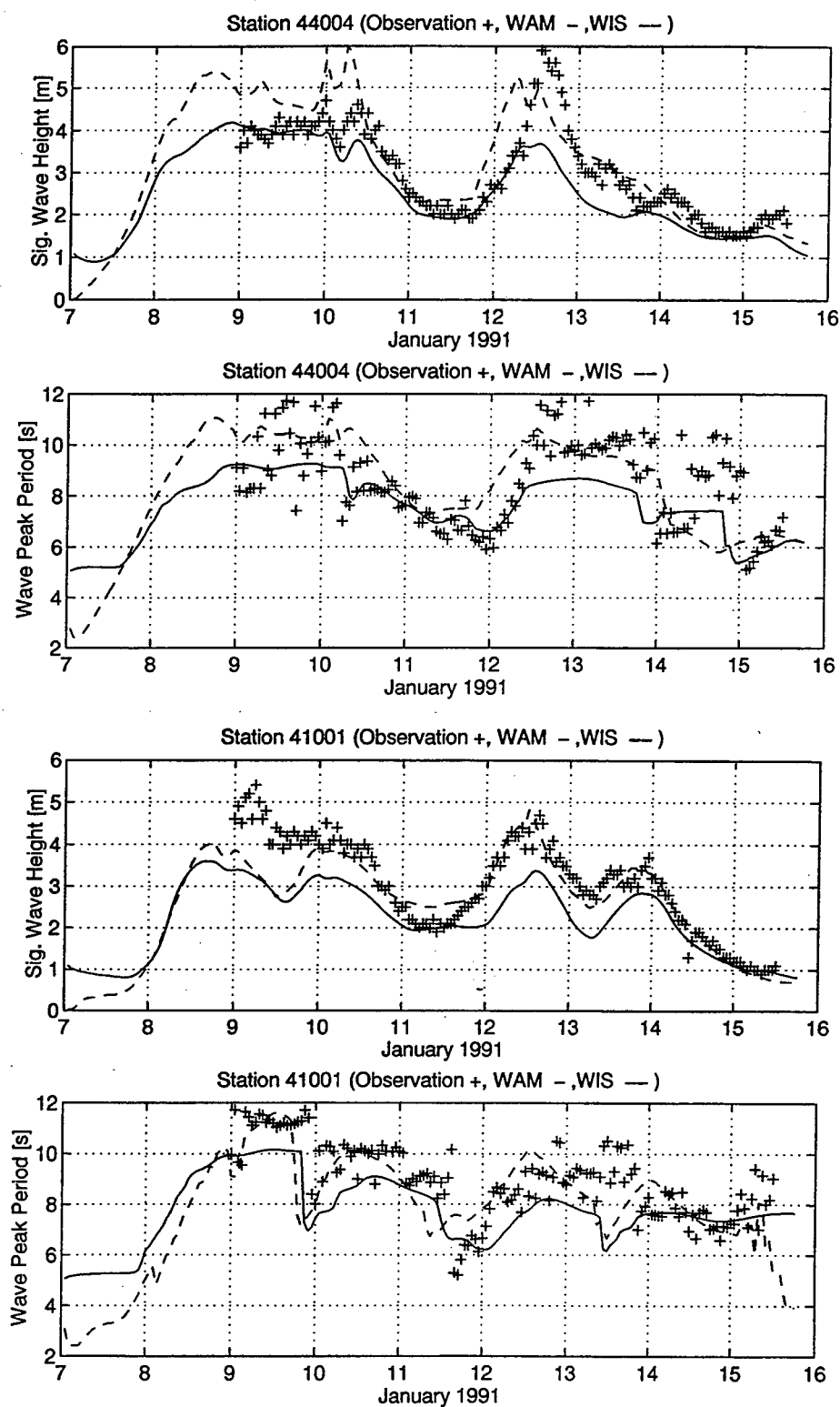
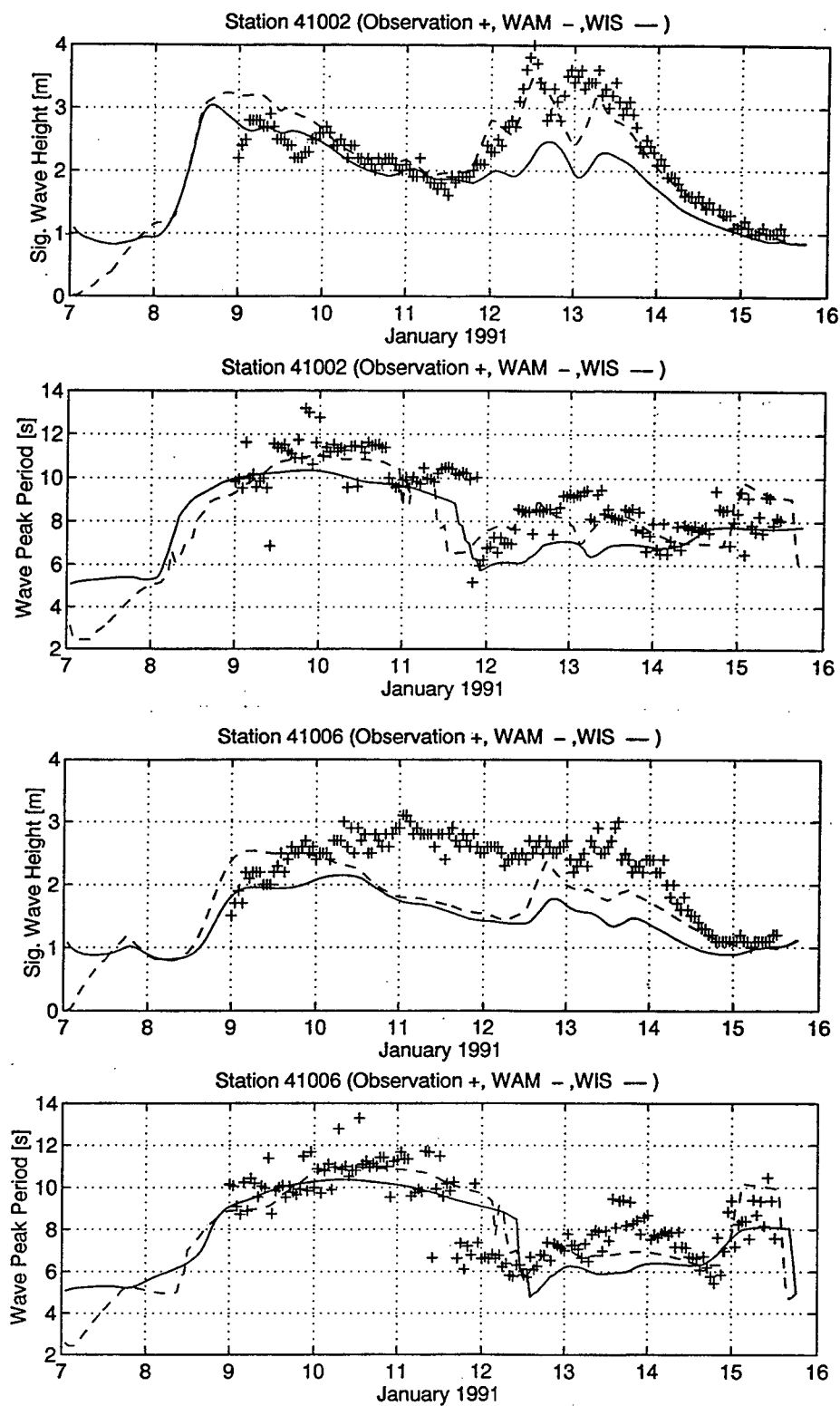**Figure 31.** H_s and T_p time histories at 44004 and 41001 for IOP2.

Figure 32. H_s and T_p time histories at 41002 and 41006 for IOP2.

about a 1.0 m underprediction. WAM continues to underpredict until the 11th while WIS begins to match the buoy on the 10th and continues to match the buoy for the rest of the simulation. WAM underpredicts by 1.5 m on the 12th and by 0.5 m on the 14th. The model T_p is similar to other locations but in this case WIS reaches the maximum T_p for all peaks but is late and decreases too early. WAM underpredicts at the peaks, except for the third one on the 14th, by 1.0 sec to 1.5 sec.

Location 41002, which is in the southern area, has a wind speed time history that gradually increases to two peaks on the 12th and 13th with maximum of 12 m/s. The H_s and T_p plots are shown in Figure 32. WIS H_s matches the buoy reasonably well throughout the simulation except for the peak on the 13th. WIS lags the buoy by 6 hours during the increasing H_s at the beginning of the second peak. WIS underpredicts both peaks by about 0.5 m while WAM underpredicts by 1.5 m. The model T_p is similar to other locations.

Location 41006 is in the extreme southern part of the model domain and as mentioned previously is well outside the KA area. The H_s and T_p plots are shown in Figure 32. Wind speed underprediction by 4.0 m/s to 6 m/s between the 10th and 12th is responsible for the 1.5 m underprediction of H_s during the same time. Also the models are late, by 24 hours, in responding to the decrease in T_p which occurs on the 12th.

e. Directional buoy analysis

Buoys 44001, 44015, and 44014 are directional buoys and allow the comparison of peak wave direction, directional wave spread, and PCC in addition to H_s and T_p. Buoys 44001 and 44015 are deepwater locations while 44014, with a depth of 48 m, has some depth effects. All three locations have similar H_s, T_p and peak wave direction behavior. The H_s, T_p, peak wave direction, directional wave spread, and PCC time histories for 44001 are shown in Figure 33. The comparison begins at the peak of the first low on the 9th. Both model H_s are in good agreement
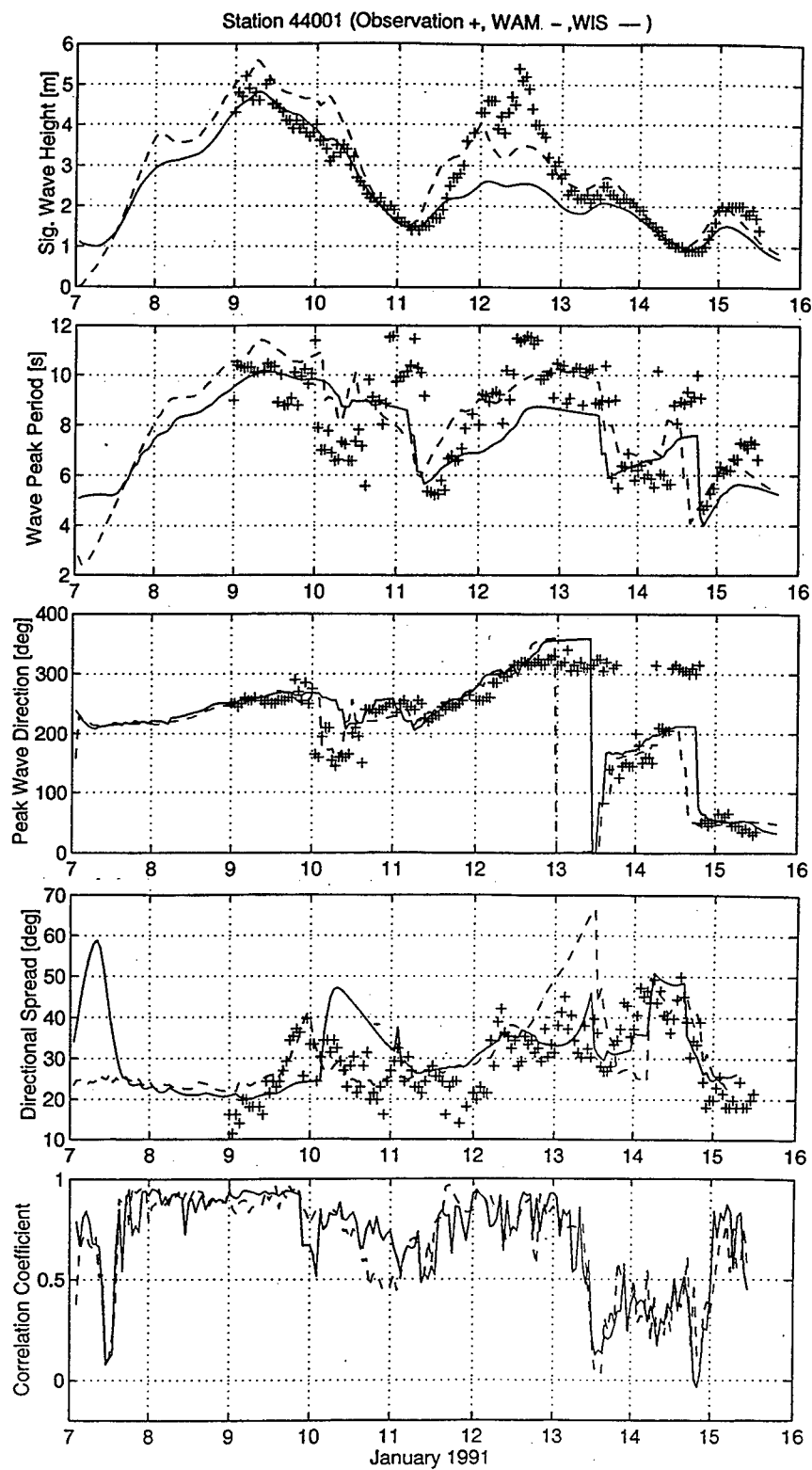
Figure 33. H_s, T_p, θ_p, σ, and PCC at 44001 for IOP2.

with the buoy throughout the subsequent decrease until the 11th except that WIS overpredicts by about 0.5 m. The H_s increases again to a peak on the 12th with the passage of the second low. During this period both models underpredict the peak H_s by 2.0 m and 3.0 m for WIS and WAM respectively. The model T_p are generally similar to the other central locations mentioned previously. The maximum T_p is underpredicted by both models but WIS tends to have longer periods than WAM. Model peak wave direction has relatively good agreement with the buoy except for the 10th, 13th, and 14th. The peak wave direction remains between southwest and northwest except for the shifts to the southeast as the fronts associated with the lows pass.

The model directional wave spread agreement with the buoy is relatively good throughout the simulation except for the end of the decay cycle during each H_s peak. On the 10th WAM reaches nearly 50° about 6 hours after the buoy reaches 40°. WIS follows the buoy's increasing spread particularly well here and matches the buoy's peak value. On the 13th WIS reaches 65° while the buoy reaches only 45°. Both of these overpredictions of spread occur near an abrupt shift in wave direction. The first overprediction occurs after the shift on the 10th while the second overprediction occurs before the shift on the 13th.

The same general characteristics as IOP1 are evident with the PCC decreasing during the wave decay process and increasing or remaining high for the wave growth process. The decrease in the PCC at 44001 corresponds somewhat to the model-buoy disagreement in directional wave spread, although the correspondence isn't always consistent. At times one model has reasonable agreement and the other does not, but both have low PCCs. On the 10th the WIS spread matches the buoy while WAM is too narrow. The PCCs corresponding to this period are higher for WIS (0.75) than for WAM (0.50 - 0.60). After this WIS continues to have good spread and WAM becomes too wide but the PCC for WAM (0.70) is greater than for WIS (0.50). Around the middle of the 11th wave growth has already begun and the PCC improves.

When the improvement begins the corresponding H_s is 2.0 m. On the 13th a more dramatic PCC decline takes places dropping to near 0.0 . The PCC recovers to 0.3 to 0.5 after this as the wave height increases slightly. As the H_s reaches a minimum of 1.0 m the PCC goes to 0.0 . Then the H_s increases to 2.0 m and the PCC improves dramatically to about 0.8 . Each of the declines in the PCC also corresponds to an abrupt shift in the peak wave direction.

The H_s, T_p, peak wave direction, directional wave spread, and PCC time histories for 44015 are shown in Figure 34. The H_s is similar to 44001 except at the peaks it is higher by about 0.5 m. The underprediction of the second peak is by the same margin as 44001. The T_p is very similar to 44001 but longer periods of 13.0 sec as opposed to 11.5 sec are experienced during the first peak. The peak wave direction also has similar characteristics as 44001. Overall the spread at 44015 is in better agreement with the buoy than at 44001 and is also a little wider ranging from 20° to 60°. The overprediction found at 44001 on the 10th doesn't occur here for either model but on the 13th WIS overpredicts. The PCC for 44015 is very similar to 44001 except on he 14th where the models have slightly better correlation. There is very little difference between the PCC for the two models.

The H_s, T_p, peak wave direction, directional wave spread, and PCC time histories for 44014 are shown in Figure 35. This location experiences some depth effects as can be seen in the lower buoy H_s. The buoy H_s is 4.5 m at the second peak which is 1.5 m below the corresponding H_s at 44015. Model performance at the first peak is similar to the other directional locations. However, during the second peak WIS performance is improved to a 1.0 m underprediction while the WAM error is still about a 2.0 m underprediction. The improvement in the WIS performance is undoubtedly due to the lack of depth dependence in the model simulation.
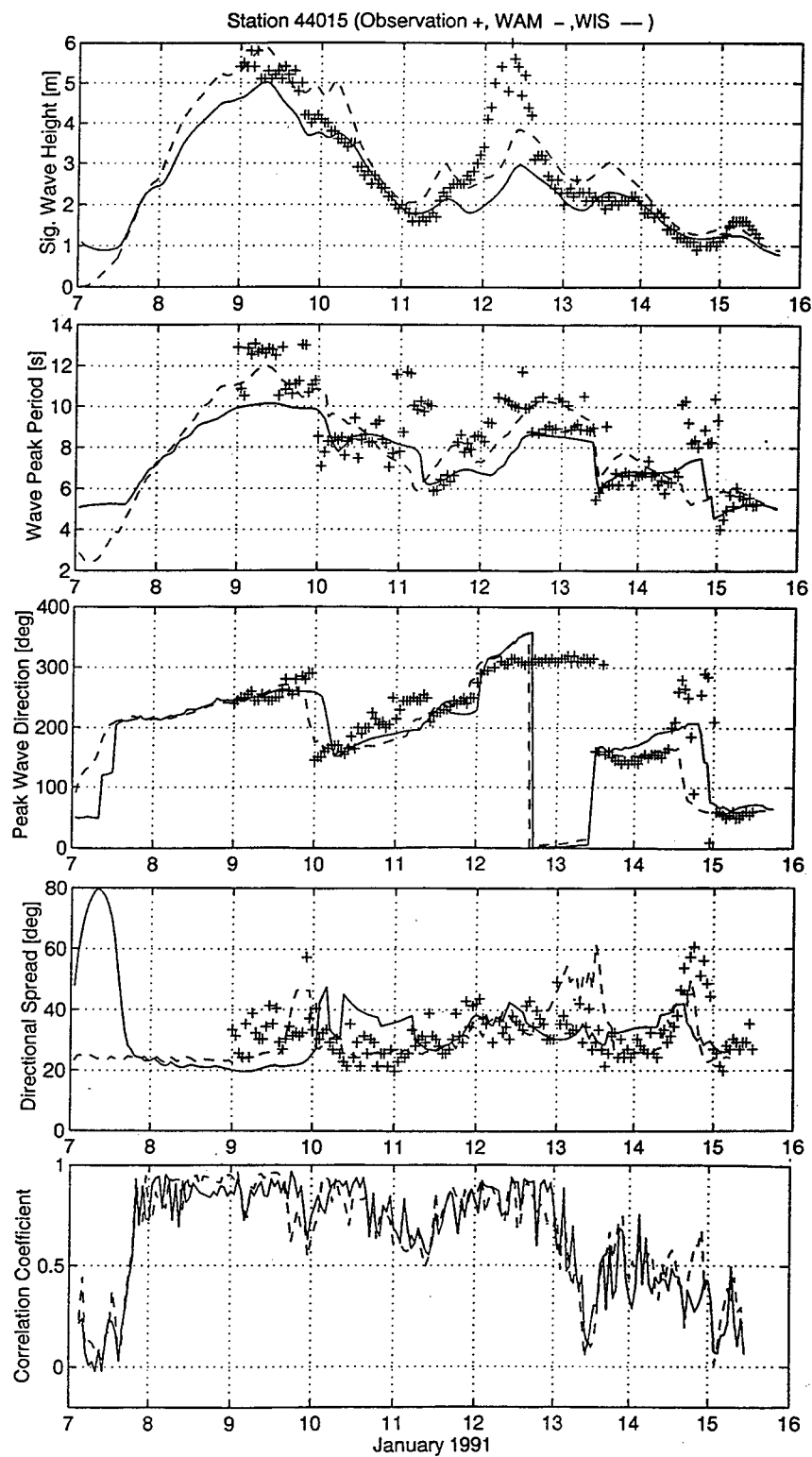
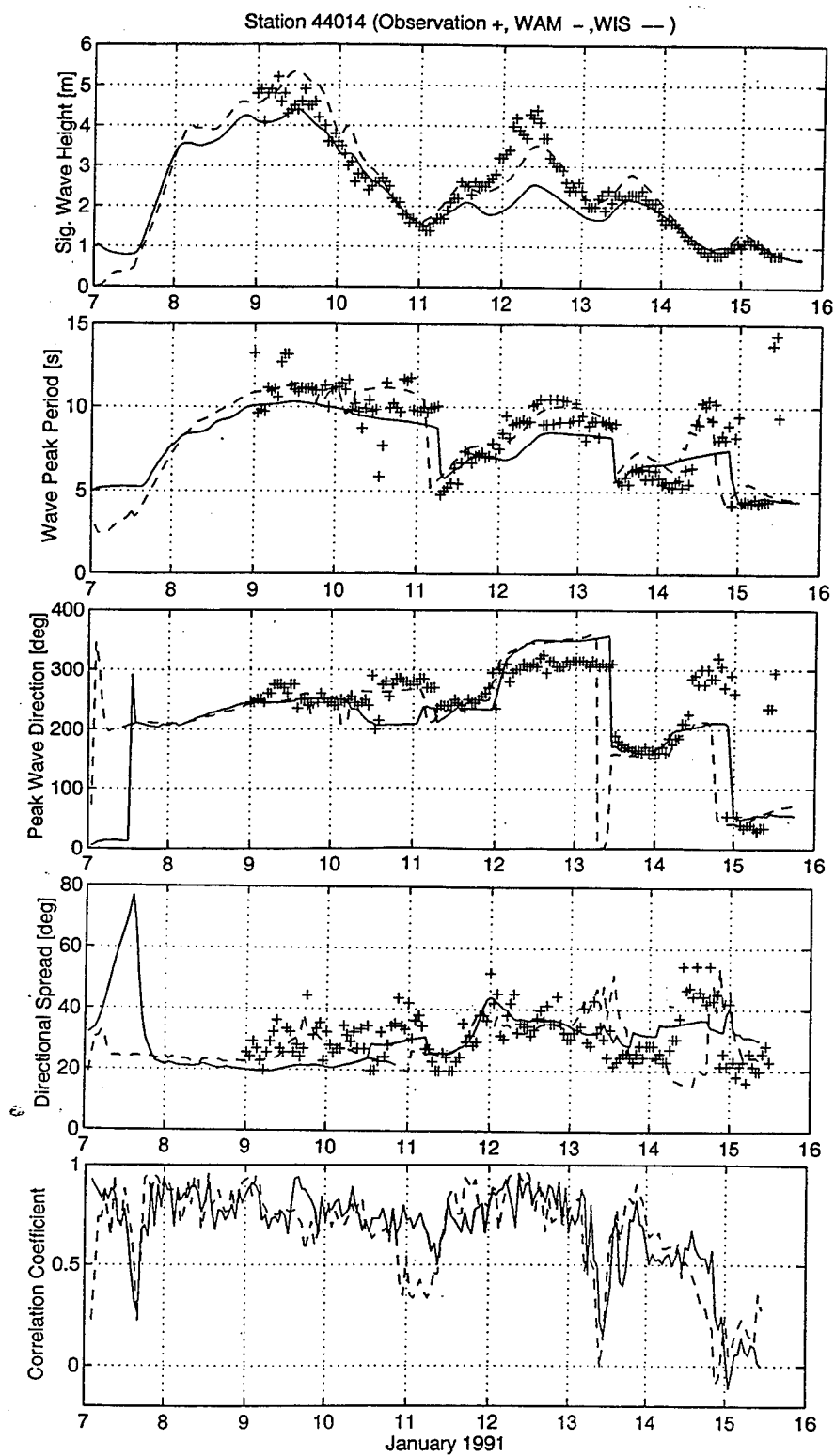Figure 34. H_s, T_p, θ_p, σ, and PCC at 44015 for IOP2.

Figure 35. H_s, T_p, θ_p, σ, and PCC at 44014 for IOP2.

The T_p and peak wave direction are similar to 44015 except for the shift in the wave direction on the 10th. The directional wave spread and PCC for 44014, are both similar to 44015 except on the 11th the WIS PCC (0.4) is less than WAM (0.7 to 0.5) which is also seen at 44001.

f. Summary

The IOP2 simulation is a more dynamic lower energy case with wind speed peaks of 16 m/s to 20 m/s. IOP2 had strong frontal passages and associated abrupt wind shifts. The winds are not as well specified for IOP2 compared to IOP1. This is due to the difficulty in simulating the strong rapid wind shifts associated with the frontal passages. The wind speed RMS Error ranges up to 2.8 m/s and the bias ranged up to 1.8 m/s due to over specification of the low wind speeds. Both models generally underestimate the highest H_s peak. The WAM H_s has a minimum negative bias of -0.73. The WIS H_s bias is mostly positive and ranges up to 0.46 m, but WIS underestimates the higher peaks. The positive bias is due to an overestimate during the beginning of the simulation. The WIS H_s RMS Error is slightly smaller than that of WAM by an average of 0.15 m, and the H_s SI is generally lower for WIS. The T_p bias is negative for both models except for WIS in the northern locations. There is overall good agreement with buoy spread which is between 20° and 40°. There is little difference between each model's PCC and the trend for declining PCC values for the decay portion of storms continues. WIS has a better response to rapidly changing wind speeds and directions. This behavior is evident at 44005 and is similar to the results of test Case III discussed in Chapter II.

5.3 IOP-3

a. Synoptic weather conditions

The IOP3 meteorological conditions are similar to IOP2. Conditions are dominated by three low pressure systems and the associated frontal passages. The storm events are moderate with a maximum wind speed of 18 m/s. The first low forms off the Carolina coast on 24 February and moves northeast. By the 25th the first low is centered just south of location 44004.
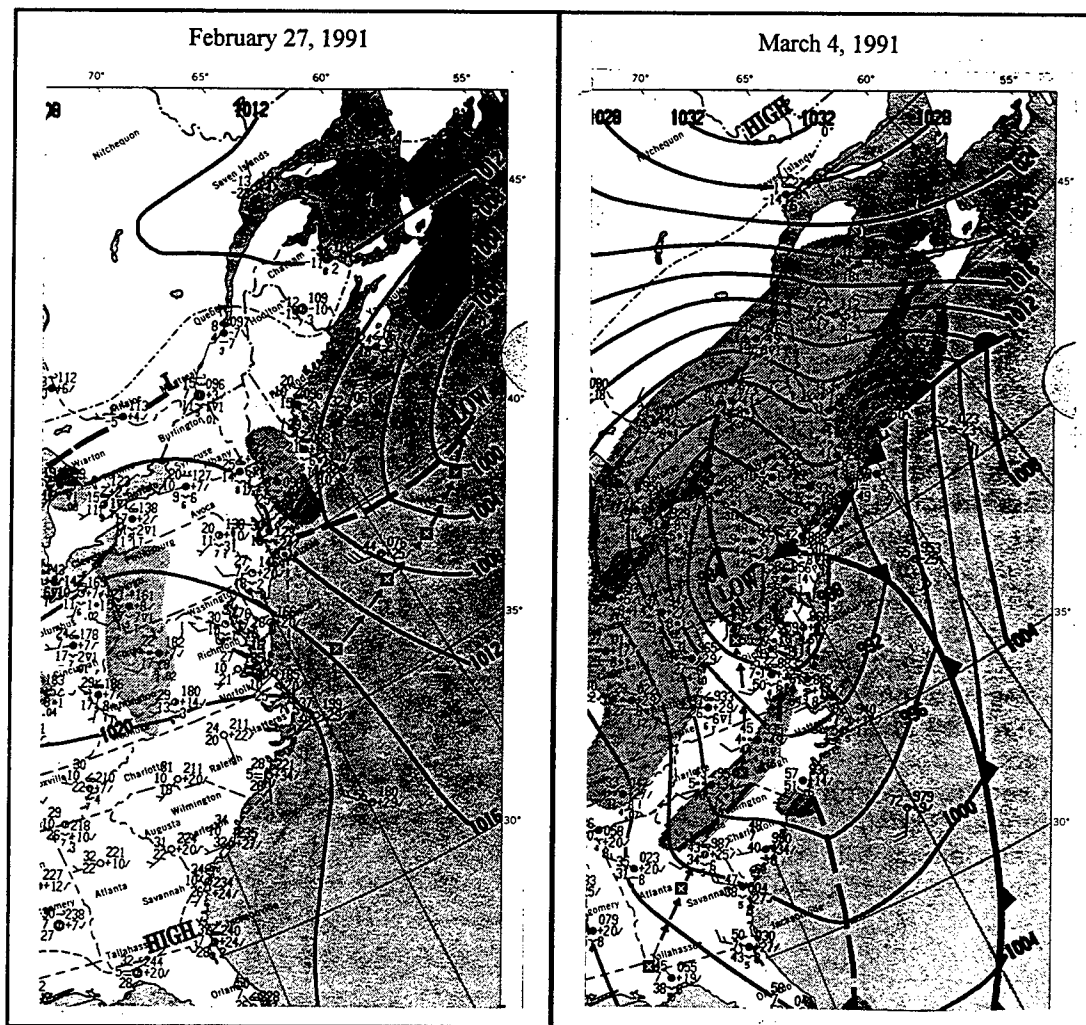

Figure 36. Surface weather maps for February 27th and March 4th, 1991 (National Weather Service, 1991 b,c).

As is typical of low pressure systems along the US Atlantic coast, the wind directions, in general, ahead of the low are to the southwest and below to the northeast. On the 26th the low loses strength and stalls north of Cape Hatteras. On the 27th the low, shown in Figure 36, intensifies and moves to the northeast to just southeast of 44011. With the first low pressure system well out of the area, on the 28th, most of the US Atlantic coast is dominated by a high pressure system. On 1 March a weak front passes through the central and northern part of the model domain. Between the 2nd and 5th the second low pressure system forms over Georgia and moves over land up to Pennsylvania and then off the coast of Nova Scotia. This low pressure system, has a strong front associated with it. The isobars and frontal boundary for the 4th are shown in Figure 36. From the 6th through the 9th the third low pressure system moves across northern Canada and out to the North Atlantic.

b. Winds

The scatter plots of wind speed and direction at 44005, 44001, and 41002, shown in Figure 37, are representative of the northern, central, and southern areas. These plots show the high quality of the winds but indicate a consistent bias toward the simulated winds for the lower wind speeds and more wind direction scatter than seen for IOP1.

The wind time histories of select locations show the different wind regimes associated with northern, central, and southern areas. Plots for all locations considered in this study are located in Appendix A. The northern area, represented by 44005, in Figure 38, shows the dynamic nature of the wind speeds, changing by more than 10 m/s several times per day, especially on the 2nd and 6th of March. The wind direction begins between southwest and northwest and turns counter clockwise to the north, then clockwise through north twice and finally ending southeast. Characteristic of all the buoys during IOP3, most simulated wind speed peaks
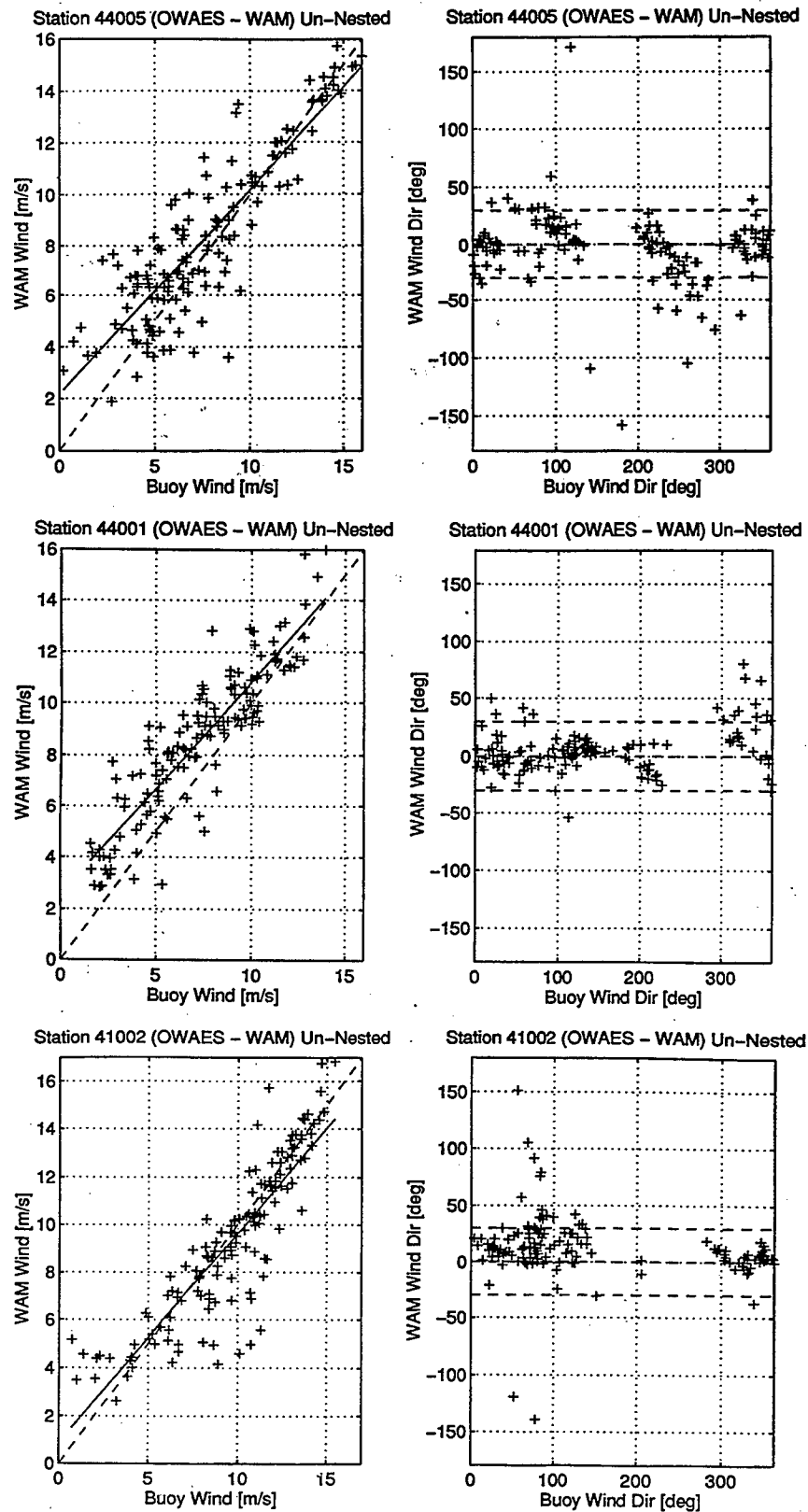
Figure 37. Wind speed and direction scatter plots at 44005, 44001, and 41002 for IOP3.
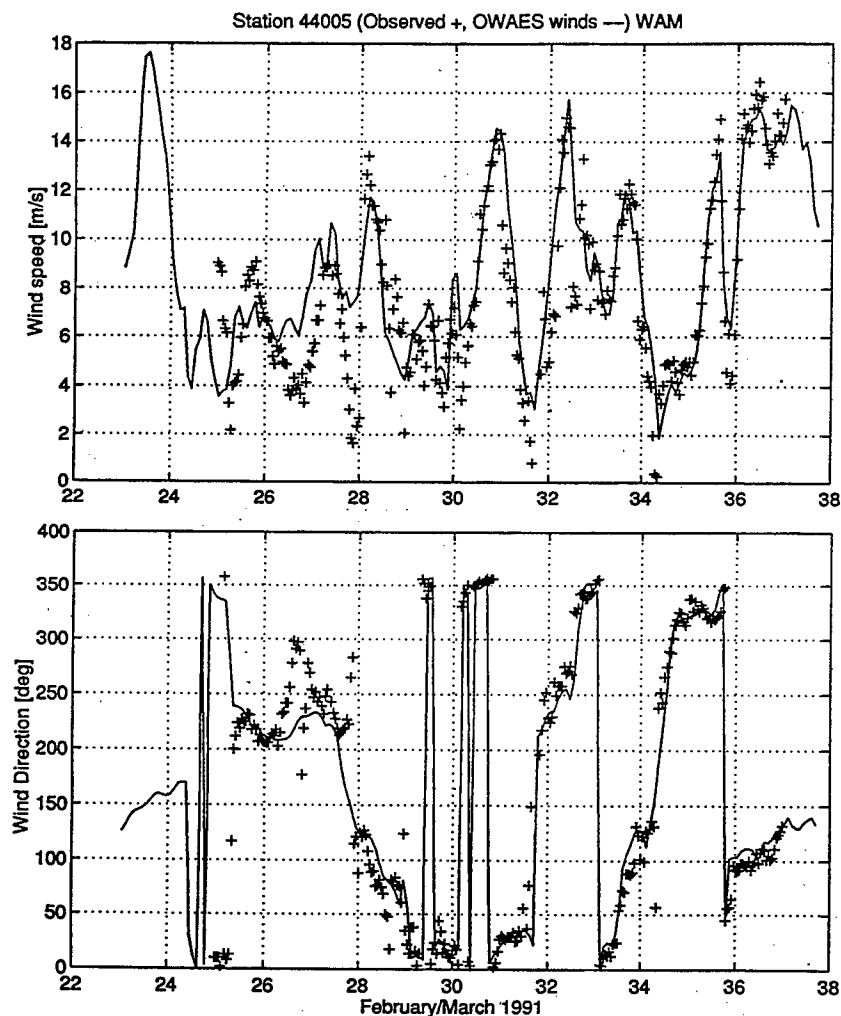
Figure 38. Wind speed and direction time histories at 44005 for IOP3.

match the buoy with less than 2 m/s error but several wind speed minimums are overpredicted by 2 m/s to 4m/s.

The central area, represented by 44001, in Figure 39, has wind speed characteristics similar to the northern locations except the maximum value occurs during the passage of the first low pressure system. The wind direction begins in the southwest to west and turns counter clockwise to the north, then oscillates between north and southeast.

Location 41002, in Figure 40, shows the less dynamic nature of the wind speeds for the
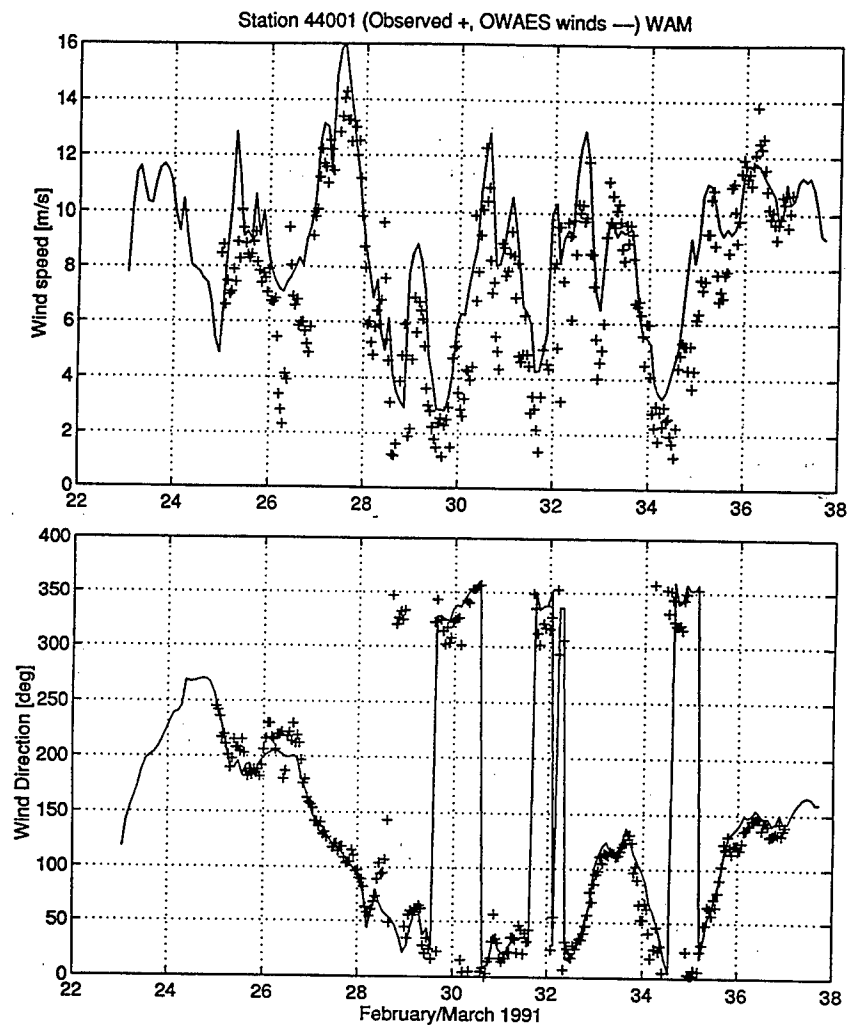
Figure 39. Wind speed and direction time histories at 44001 for IOP3.

southern area with generally a broad increasing trend between the 28 February and 6 March. Between the the 25th and 26th the simulated wind speed is underpredicted by 2 m/s to 4 m/s. The wind direction begins in the northeast then abruptly shifts to the northwest and thereafter is similar to the central locations.
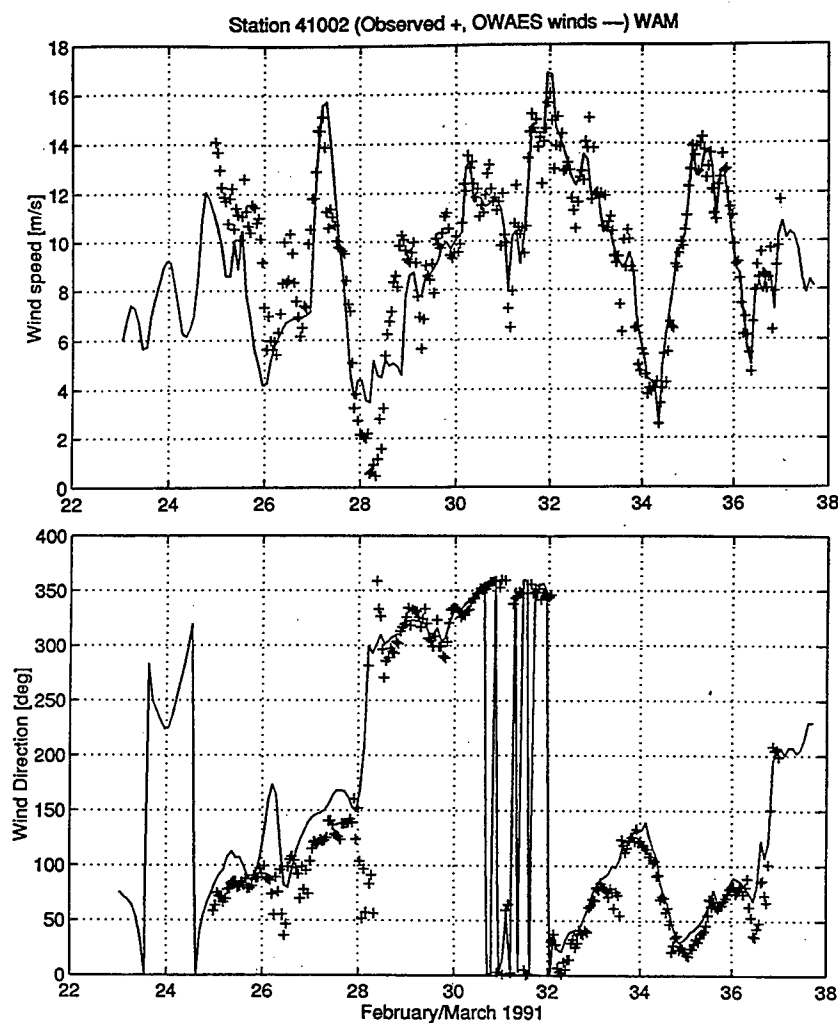
Figure 40. Wind speed and direction time histories at 41002 for IOP3.

c. Wind and wave statistics

The general performance of the models is indicated by the statistics of the integrated

properties, wind speed, U_{10}, significant wave height, H_s, and peak wave period, T_p. In Table 8

the quality of the simulated wind speed can be seen in the RMS Error which ranges from 1.65 m/s

to 2.19 m/s. The bias shows some dependence on the area of the model domain. For the central

to northern locations, 41001 to 44005, the bias is positive, ranging from 0.29 m/s to 1.29 m/s. For

the central to southern locations, 44015 to 41002, the bias is negative except for 44014, and ranged

Table 8. Statistics of measured and hindcast wind speed for IOP3.

Buoy	Mean Buoy (m/s)	Mean Model (m/s)	Bias (m/s)	Abs Err (m/s)	RMS Err (m/s)	SI (%)	CC	# pts
44005	7.64	8.28	0.64	1.38	1.83	24	0.88	143
44011	8.30	8.59	0.29	1.15	1.72	21	0.91	142
44004	9.83	10.47	0.64	1.45	2.19	22	0.85	137
44001	7.22	8.51	1.29	1.56	1.89	26	0.89	142
44015	10.50	10.31	-0.19	1.41	2.01	19	0.83	140
44023	9.52	9.45	-0.07	1.41	1.94	20	0.76	138
44014	8.47	8.84	0.37	1.61	2.01	24	0.81	143
41002	9.60	9.30	-0.31	1.11	1.65	17	0.88	144
41010	7.50	7.15	-0.35	1.84	2.32	31	0.65	144

SI - scatter index   CC - correlation coefficient

from -0.07 m/s to -0.35 m/s. The scatter index (SI) ranges from 17% to 26% and the correlation coefficient (CC) ranges from 0.76 to 0.91. Location 41010 is excluded from the summary of statistics because it is well south of the KA area and consistently has larger error in wind speed than the locations within the KA area.

Table 9 shows the H_s statistics for WAM and WIS. Considering the central locations 44004, 44001, 44015, 44023, and 44014, the RMS Error tends to be slightly smaller for WAM, ranging from 0.35 m to 0.58 m, than WIS which ranges from 0.52 m to 0.68 m . The difference between the two models' RMS Error, for this area, ranges from 0.04 m to 0.24 m. For northern locations, 44005 and 44011, and the southern location , 41002, the WIS RMS Error is smaller and ranges from 0.37 and 0.69 for WIS and 0.43 to 0.93 for WAM. WIS has a positive bias in the central area, ranging from 0.00 m to 0.28 m and a negative bias for the northern and southern

Table 9. Statistics of measured and hindcast H_s for IOP3.

Buoy	WAM							WIS						# pts
	Mean Buoy (m)	Mean Model (m)	Bias (m)	Abs Err (m)	RMS Err (m)	SI (%)	CC	Mean Model (m)	Bias (m)	Abs Err (m)	RMS Err (m)	SI (%)	CC	
44005	2.17	1.90	-0.27	0.33	0.43	20	0.95	2.15	-0.03	0.29	0.37	17	0.93	143
44011	2.93	2.25	-0.68	0.73	0.93	32	0.92	2.62	-0.31	0.49	0.69	23	0.89	142
44004	2.95	2.68	-0.27	0.41	0.55	18	0.88	3.04	0.09	0.41	0.67	23	0.81	137
44001	2.27	2.07	-0.20	0.44	0.58	26	0.89	2.26	0.00	0.47	0.62	27	0.81	142
44015	2.63	2.45	-0.17	0.43	0.54	21	0.88	2.70	0.08	0.49	0.68	26	0.79	140
44023	2.22	2.15	-0.06	0.27	0.35	16	0.90	2.38	0.16	0.37	0.52	23	0.83	138
44014	1.97	2.02	0.05	0.31	0.40	20	0.85	2.25	0.28	0.47	0.64	32	0.77	143
41002	2.55	2.12	-0.43	0.58	0.75	30	0.81	2.43	-0.13	0.49	0.62	24	0.82	144
41010	1.88	1.42	-0.45	0.64	0.73	39	0.61	1.64	-0.24	0.57	0.64	34	0.59	144

SI - scatter index   CC - correlation coefficient

locations. WAM has a negative bias, for all but 44014, ranging from -0.06 m to -0.68 m. The SI for WAM is lower than WIS for the central area and higher than WIS in the northern and southern areas. The SI for WIS ranges from 17% to 32%, while the SI for WAM ranges from 26% to 32%. The correlation coefficient (CC) for WAM varies between 0.81 and 0.95 and is consistently higher than WIS, which ranges from 0.77 to 0.93, except for 41002.

Table 10 shows the T_p statistics for WAM and WIS. In addition to location 41010, 44004 is excluded from the summary of T_p statistics because errors were present in the buoy data. WAM exhibits a consistently negative bias, ranging from -0.11 sec to -0.66 sec while WIS has a positive bias for buoys except 44014 and 41002, ranging from -0.02 sec to -0.84 sec. The WIS bias is generally smaller than the WAM bias for the central locations. The RMS Error for WAM

Table 10. Statistics of measured and hindcast T_p for IOP3.

Buoy	WAM							WIS						
	Mean Buoy (s)	Mean Model (s)	Bias (s)	Abs Err (s)	RMS Err (s)	SI (%)	CC	Mean Model (s)	Bias (s)	Abs Err (s)	RMS Err (s)	SI (%)	CC	# pts
44005	8.18	8.07	-0.11	1.25	1.71	21	0.72	7.54	-0.64	0.93	1.25	15	0.90	143
44011	9.07	8.41	-0.66	1.16	1.39	15	0.79	8.23	-0.84	1.13	1.40	15	0.83	142
44004	9.71	8.33	-1.38	1.56	3.66	38	0.11	8.61	-1.10	1.55	3.71	38	0.06	137
44001	8.47	8.02	-0.46	1.32	1.60	19	0.65	8.36	-0.11	1.50	1.87	22	0.49	142
44015	8.51	8.06	-0.45	1.03	1.28	15	0.76	8.49	-0.02	1.23	1.63	19	0.54	140
44023	8.63	8.03	-0.60	1.27	1.65	19	0.56	8.43	-0.20	1.41	2.01	23	0.31	138
44014	8.40	8.05	-0.35	1.16	1.62	19	0.48	8.57	0.17	1.41	2.12	25	0.18	143
41002	7.95	7.46	-0.49	1.39	1.75	22	0.32	7.99	0.04	1.56	1.99	25	0.16	144
41010	8.43	6.70	-1.74	2.07	2.57	31	0.01	7.54	-0.90	2.19	2.72	32	0.25	144

SI - scatter index   CC - correlation coefficient

is lower than WIS in the central area and ranges between 1.28 sec and 2.12 sec for both models. The difference in RMS Error between the models ranges from 0.01 sec to 0.50 sec. The SI for WAM is lower than WIS, by about 5% in the central area, except for 44005 and 44011, and ranges from 15% to 25%. The CC for WAM is higher than that for WIS, except for 44005 and 44011. The WAM CC ranges from 0.32 to 0.79 and the differences between WAM and WIS CCs varies between 0.04 to 0.30.

The scatter indices for U_{10}, H_s, and T_p from Tables 8 through 10 are plotted in bar graph form in Figure 41 to show the relationship between each parameter. For the central area,

the wind speed SI is within 2% of 20% except for 44001 and 44014. Of these locations, only the

WAM H_s SI at 44004, 44015, 44023, and 44014 are near or below 20%. Note that 44014 and

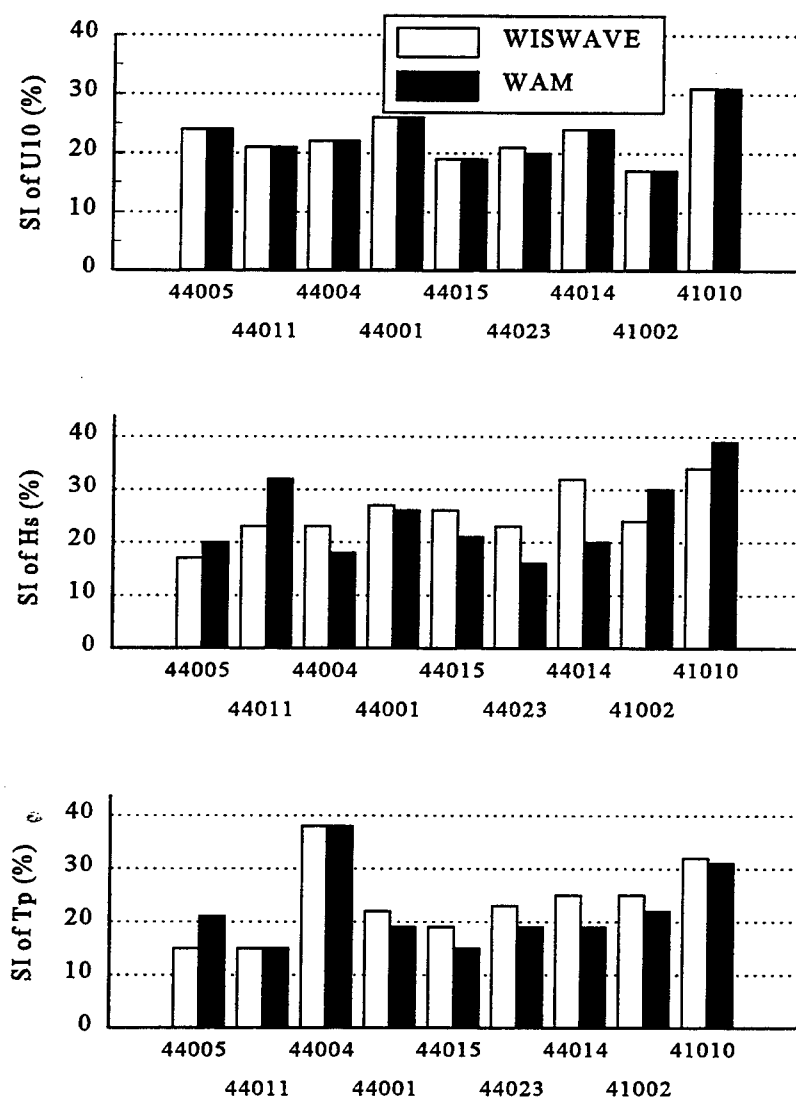44023 are expected to have significant depth effects with a d/L_o, associated with maximum T_p,

Figure 41. WAM and WIS U_{10}, H_s, and T_p scatter indexes for IOP3.

of 1/4.7 and 1/6.6 respectively. The WIS H_s SI in the central area is consistently above 20%. The only location which has a WIS H_s SI below 20% is 44005. The difference between the model H_s SIs for the central locations is about 5%, except for 44001 where both model H_s SIs are about 26%. In the northern and southern locations, as seen in the previous simulations, the WIS H_s SI is smaller than WAM. For all locations, except 44005, the WAM T_p SI is equal to or lower than WIS. Note that buoy 44004 contains errors and is excluded from the T_p discussion. With the exception just noted the WAM T_p is below 20% for the central locations.

d. Non-directional time histories

The following section presents a description of modeled and measured H_s and T_p time histories for select locations corresponding to non-directional buoys. These locations represent the characteristics found in the northern, central, and southern areas of the model domain.

Location 44005, in Figure 42, represents the northern area. The H_s plot shows four main peaks associated with the four meteorological systems which affected the area. The highest H_s, 4.5 m, occurs at the 3rd and 4th peaks. There is overall good agreement with the buoy except for an underprediction at the first peak on 28 February, the third peak on 4 March, and the fourth peak on 8 March. At the first peak WIS underpredicts H_s by 0.5 m and WAM by 1.0 m. During the second peak both models follow the buoy closely with WIS slightly overpredicting and WAM slightly underpredicting. Between the second and third peaks the WIS H_s stops declining at 2.5 m 12 hours early while the buoy and WAM continue to decline to 2.0 m. The third meteorologic system has a double H_s peak with the second being larger. Both models underpredict the first peak by about 0.5 m and the second by less than 0.5 m for WIS and 1.0 m for WAM. At the fourth main H_s peak both models underpredict by about the same margin, 0.5 m for WIS and 1.0 m for WAM. The model T_p follows the buoy reasonably well with a few exceptions. On the 26th WAM
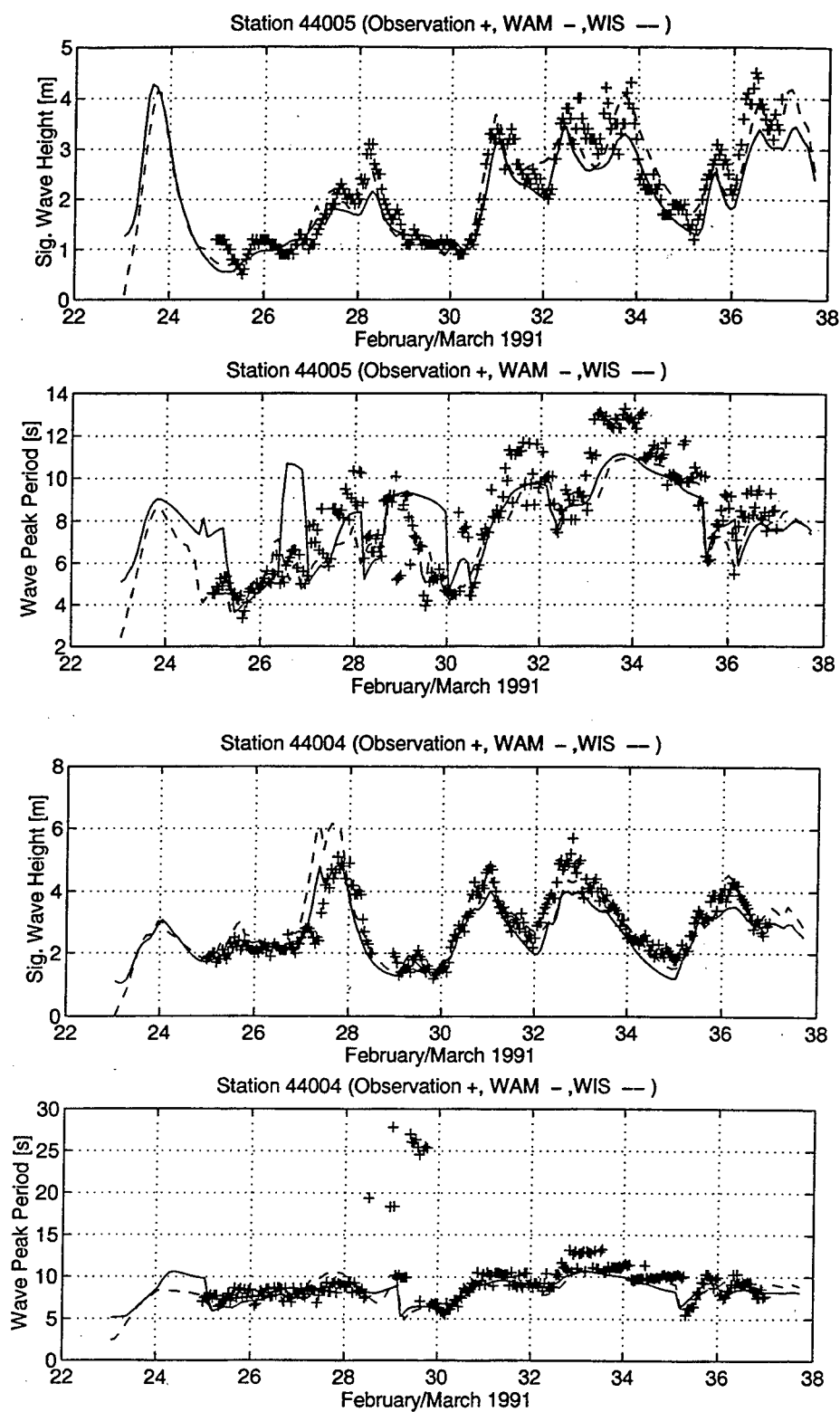
Figure 42. H_s and T_p time histories at 44005 and 44004 for IOP3.

overpredicts the buoy by 3.0 sec while WIS is only slightly under the buoy. The WAM T_p is late by 24 hours in declining on 1 March. During the second and third H_s peak the maximum T_p is underpredicted by both models by about 2.0 sec.

Location 44004, in Figure 42, represents the central area. The H_s plot shows four main peaks associated with the four meteorological systems which affected the area. The highest H_s, 5.5 m, occurs at the third peak. There is overall good agreement with the buoy except for an overprediction by WIS at the first peak on 27 February, and underpredictions by one or both models at the second, third, and fourth peaks. On the 27th the increasing WIS H_s leads the buoy by about 6 hours and overpredicts the peak by 1.0 m. This is caused by an overspecified wind speed which also leads and overpredicts the buoy wind speed. While the WAM H_s also leads the buoy, but by only about 3 hours, the peak is predicted to within 0.25 m. WIS underpredicts the H_s at the third peak by 1.5 m while WAM is under by just less than 2.0 m. WIS matches the buoy H_s at the second and third peaks while WAM is under by about 1.0 m. The T_p shows characteristics similar to 44005 with a 2.0 sec underprediction at the third peak by both models. Note the buoy data contain unrealistically long periods around 1 March.

Location 41002, in Figure 43, represents the southern area. The H_s plot shows only three main peaks for this area. The highest H_s, 5.5 m, occurs at the second peak. Both models overpredict the H_s at the peak on the 26th even though the wind speeds are well specified at this peak. There is, however, some lag in both model H_s due to a lag in decreasing wind speed. Both WIS and WAM underpredict during the second peak due to an early decline in model H_s by about 24 hours compared to the buoy. Both models also underpredict the third peak, WAM by 1.5 m and WIS by 0.5 m. The T_p plot shows an overprediction by both models during the increase and decline of the first H_s peak. Both models also underpredict T_p during the early decline of model H_s on 4 March.
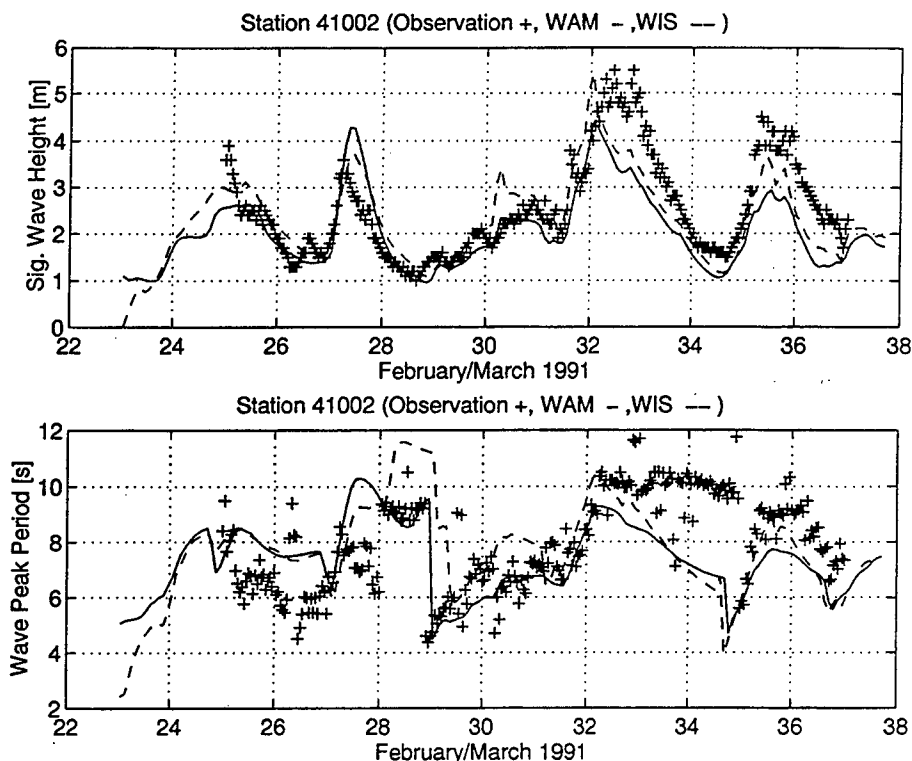
Figure 43. H_s and T_p time histories at 41002 for IOP3.

e. Directional buoy analysis

Buoys 44001, and 44015 are directional buoys and allow the comparison of peak wave direction, directional wave spread, and PCC in addition to H_s and T_p. Buoys 44001 and 44015 are deepwater locations. Both locations have similar H_s, T_p, peak wave direction, spread and PCC. The time histories of these parameters for 44001 are shown in Figure 44. The four main peaks are evident in the H_s plot. With the wind speed overpredicted by 2 m/s at the first peak WIS H_s is overpredicted by 1.5 m while WAM matches the buoy well. During the second and third peaks both models underpredict H_s by about 2.0 m. The T_p for both models underpredicts at the third peak on 4 March by 2.0 sec. The peak wave direction for both models has an error of 100° on the
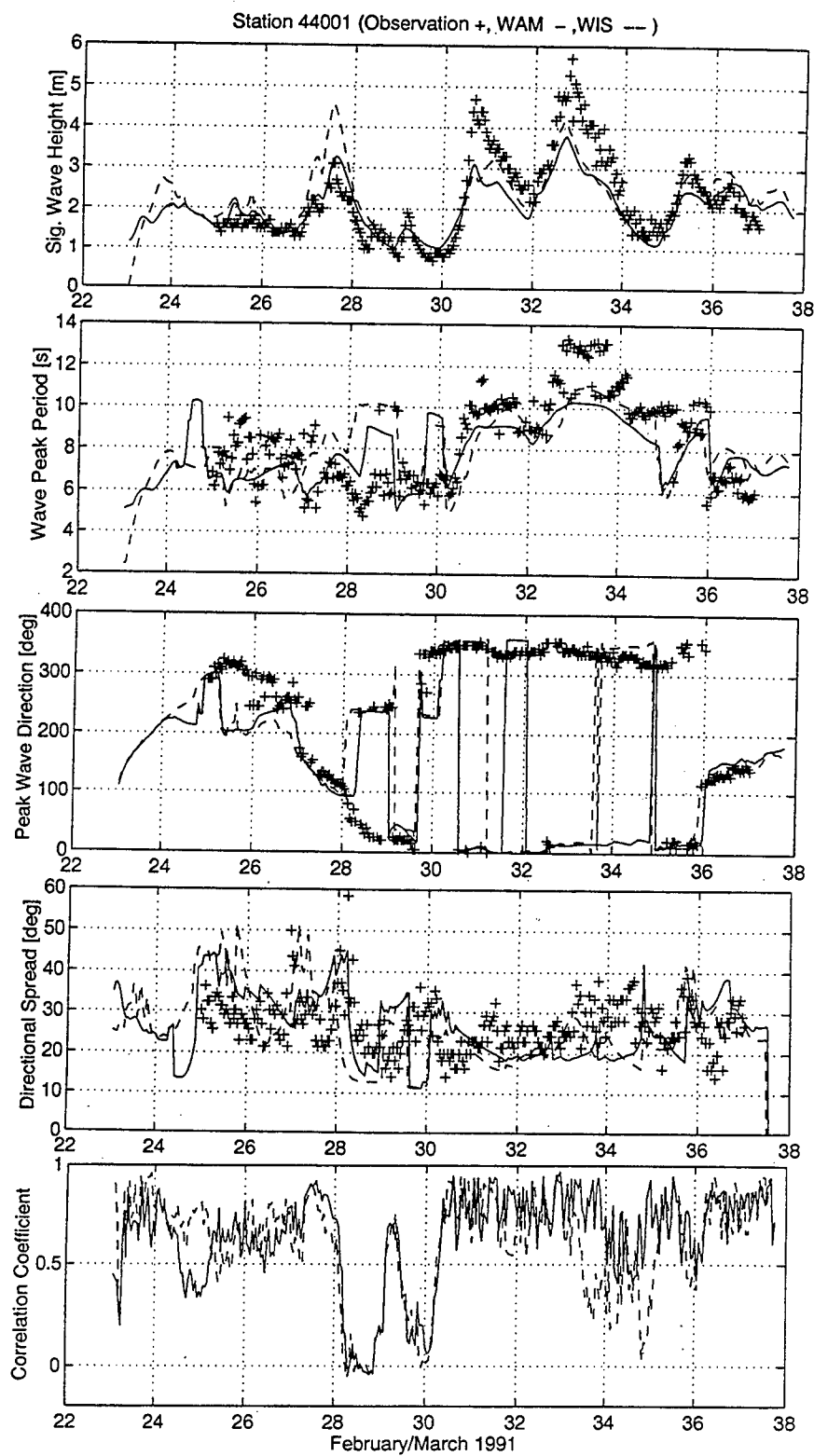
Figure 44. H_s, T_p, θ_p, σ, and PCC at 44001 for IOP3.

25th but has reasonable agreement during the remainder of the simulation. The wave spread has relatively good agreement with the buoy and ranges between 10° and 50°. Both of the models' PCCs decrease during the decline in H_s on the 28th to 0.0 and then recover briefly to 0.75 as the H_s increases on 1 March. Following this small increase the H_s decreases again along with the PCC. The PCC recovers to a range of 0.9 to 0.6 with the beginning of the growth of the second peak. Also note that the model peak wave direction shifts abruptly during this period and the buoy peak wave direction oscillates between northeast and southwest. This suggests that there are two distinct wave systems present. During the decline of H_s on the 5th the PCC also decreases for both models. The WIS PCC however decreases 12 hours earlier than WAM and decreases more than WAM to 0.2 to 0.0 as opposed 0.7 to 0.5 for WAM. The PCC decline in this case is not associated with an abrupt shift in peak wave direction.

The time histories of the integrated parameters and PCC for 44015 are shown in Figure 45. All the quantities plotted are similar to 44001 with a few exceptions noted here. Similar to 44001 there is an overprediction of windspeed of just less than 2 m/s on the 27th but in this case both models overpredict the H_s by 2.0 m for WIS and by 0.25 m for WAM. The second and third H_s peaks are underpredicted by both models, but by less than at 44001 (1.0 m or less for WIS and 1.5 m for WAM), even though the wind speed is underpredicted by 2 m/s to 3 m/s at both peaks. Recall that there was little or no underprediction of wind speed at 44001 but that the maximum wind speeds at the peaks were 2 m/s to 6 m/s below that of 440015. The buoy H_s for 44015 are less than 0.25 m higher at the peaks than 44001. The T_p is similar to 44015 with a 2.0 sec underprediction at the third peak on 4 March. The peak wave direction is also very similar to that of 44001. The wave spread is similar to 44001 but has a slightly wider range, 20° to 50°, than 44001. For 44015 there is a consistent underprediction by 5° to 20° in the last half of the simulation for WAM. The PCC for 44015 is also very similar to 44001.
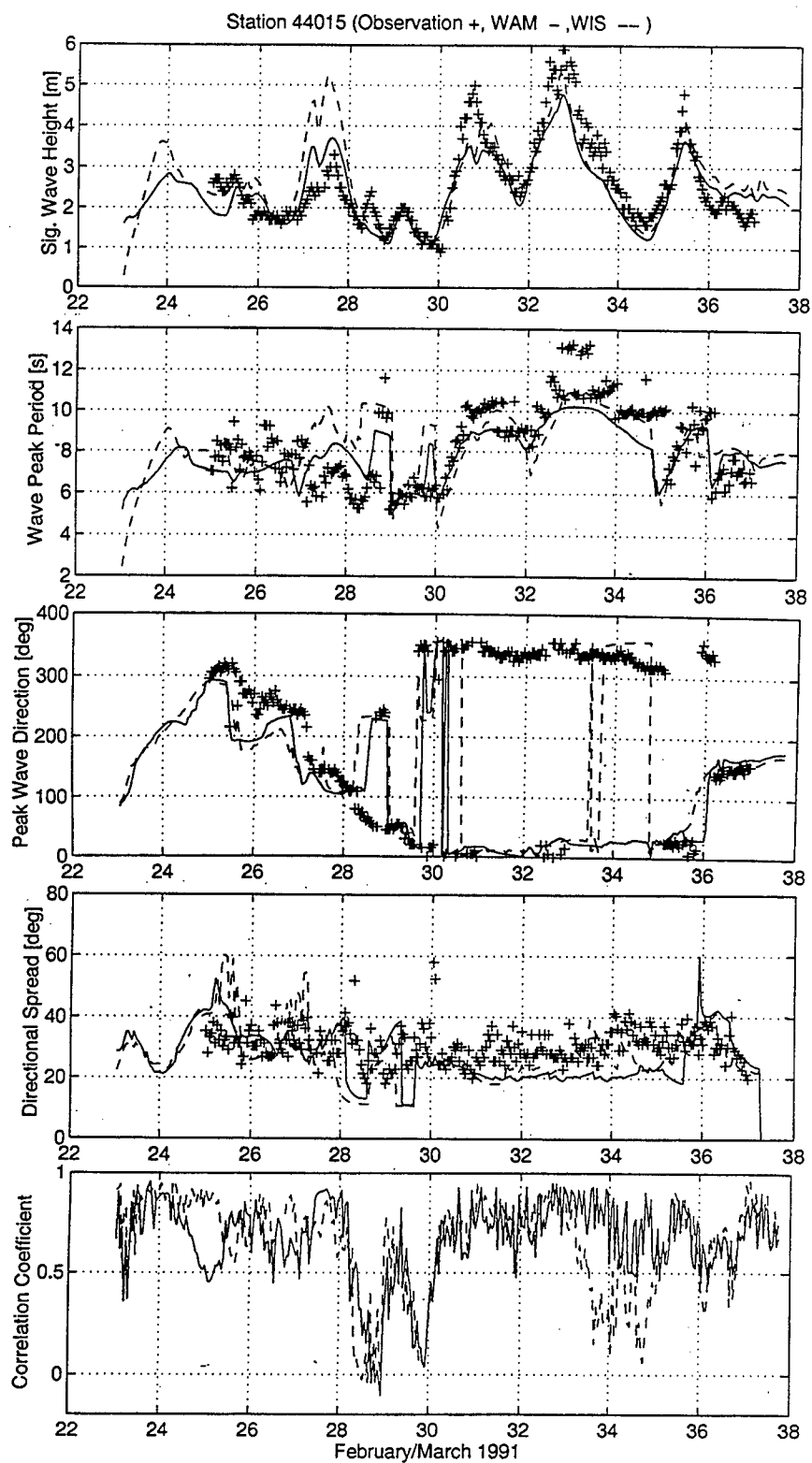
Figure 45. H_s, T_p, θ_p, σ, and PCC at 44015 for IOP3.

f. Summary

The IOP3 simulation is similar to IOP2 but with somewhat lower wind speeds (12 m/s to 18 m/s) and weaker frontal passages. Similar to the simulated wind speeds in IOP2 the simulated wind speeds in IOP3 are not as well specified as IOP1. The wind speed SI ranges from 17% to 26%. Also similar to IOP2 both models underestimate H_s at the peaks although by a smaller margin and WAM underestimates more than WIS. Both models underestimate the T_p at the maximum storm peak and at times the model peak wave direction doesn't agree very well with the measured values. This is probably due to a bi-modal spectrum. The PCC decreases with some decay cycles but not all. In some cases low PCCs are associated with overly narrow spread. There is little difference between the model PCCs.

5.4 Halloween Storm

a. Synoptic weather conditions

In this section a general description of the meteorological systems which affected the model domain during the Halloween Storm (HOS) is presented. A more detailed description may be found in Cardone et al. (1996). The HOS was an extreme event with maximum wind speeds of 27 m/s and maximum H_s of 12 m considering the NDBC buoys available for this period. The maximum wind speed and wave height for the storm occurred further north outside the area covered by NDBC buoys for this event.

The main meteorological features present during this period were the subtropical storm, Hurricane Grace, and an extratropical storm. The tracks of these events are shown in Figure 46. The subtropical system formed on the 25th and strengthened to become Hurricane Grace by the 26th located about 26°N, 62°W. The hurricane moved northwest then eastward and northeast until about the 30th when it was absorbed by the extratropical system to the north. The extratropical
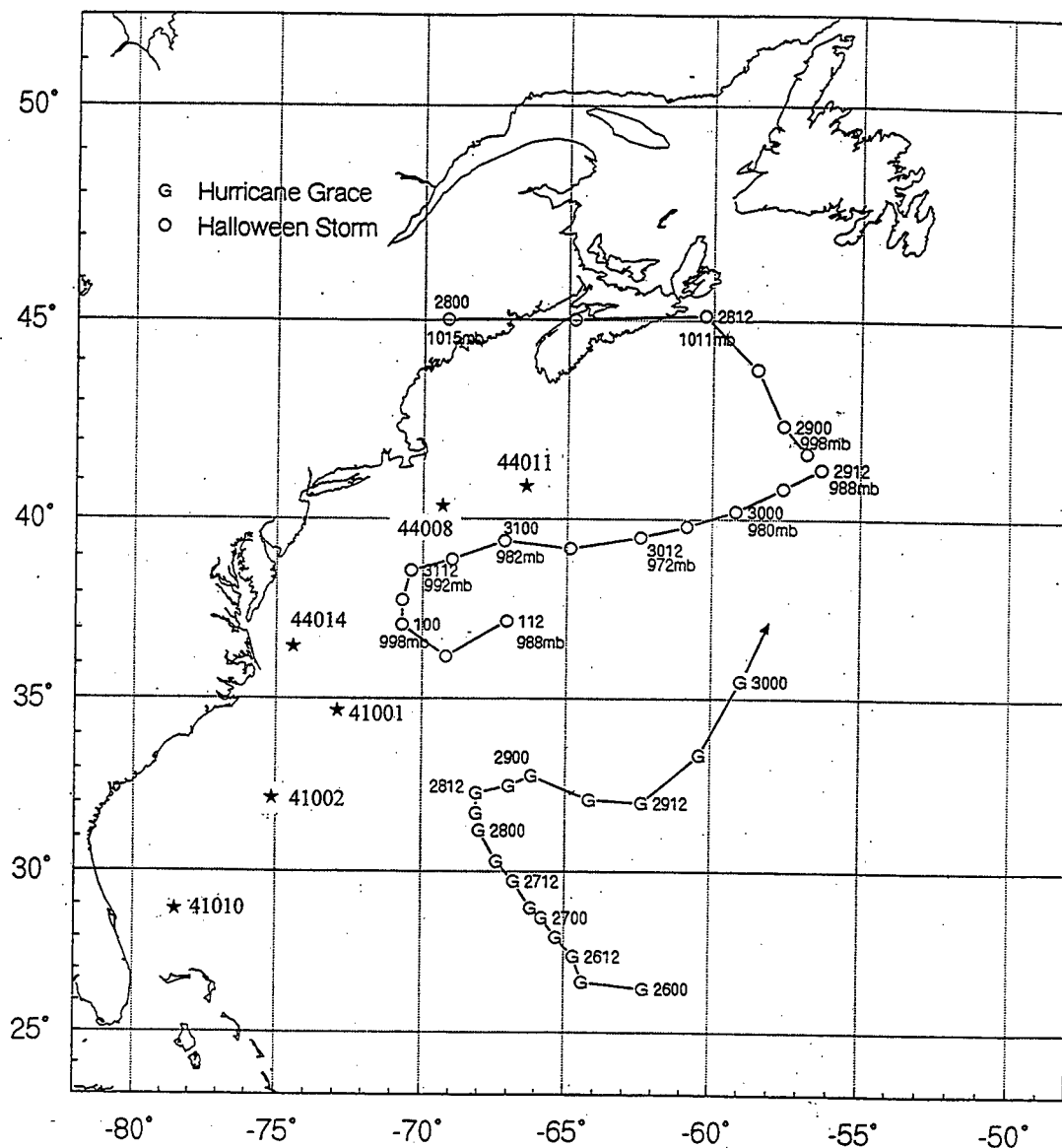
92

Figure 46. Track and central pressure of the Halloween Storm and Hurricane Grace. Buoy locations indicated by ★ (adapted from Cardone et al. 1996).

system formed over New England and moved off the coast of Nova Scotia on the 28th. The system moved southward and began to intensify late on the 28th. On the 29th the system turned to the southwest and continued until the 31st. Maximum wind speeds, at 44011 and 44008, of 25 to 27

m/s were reached by the later part of the 30th and early on the 31st. During the maximum wind speeds the wind direction was predominantly to the southwest over most of the area.

b. Winds

The scatter plots of wind speed and direction at 44011 and 44014, in Figure 47, and 41002, in Figure 48, are representative of the northern, central, and southern areas. These plots indicate
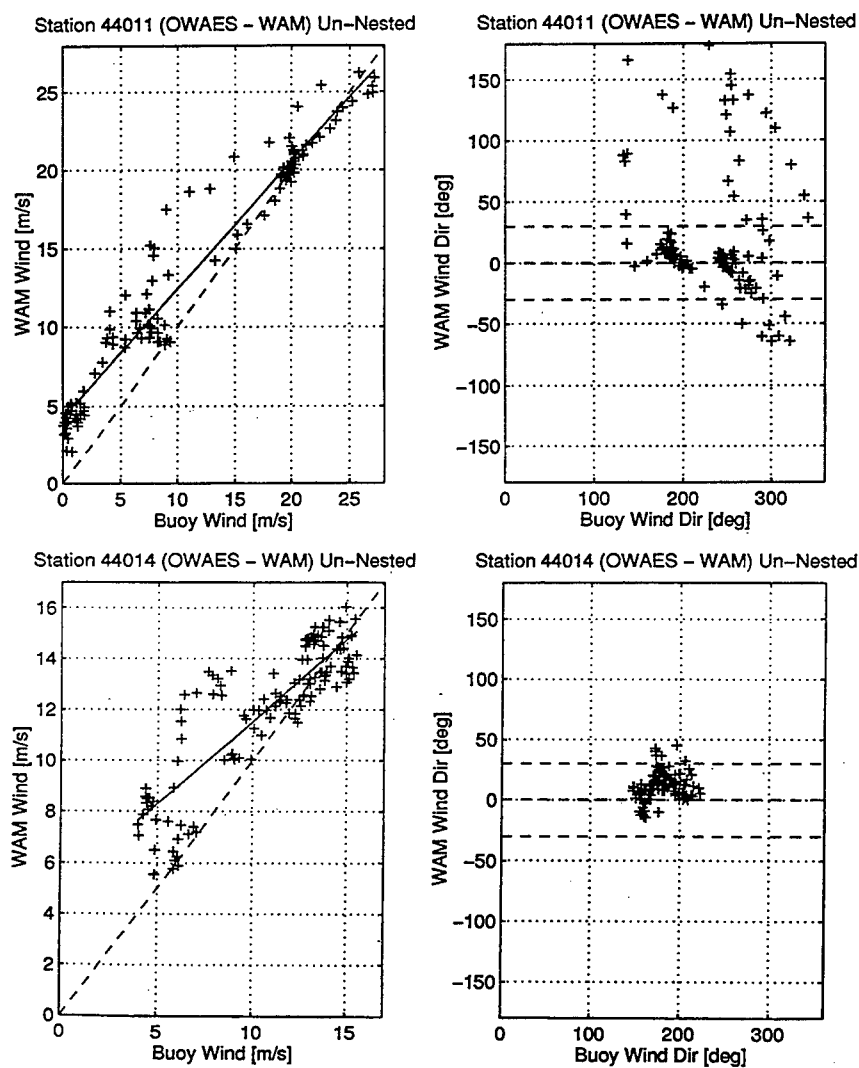
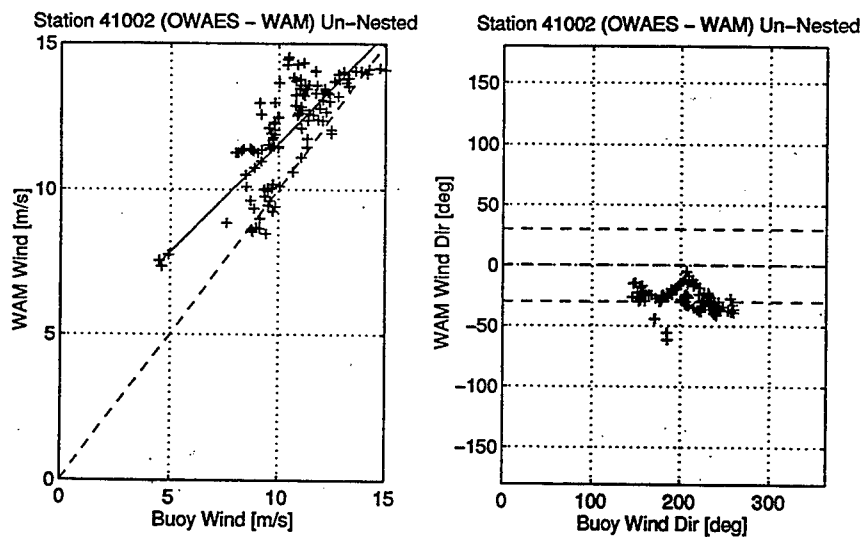Figure 47. Wind speed and direction scatter plots at 44011 and 44014 for HOS.

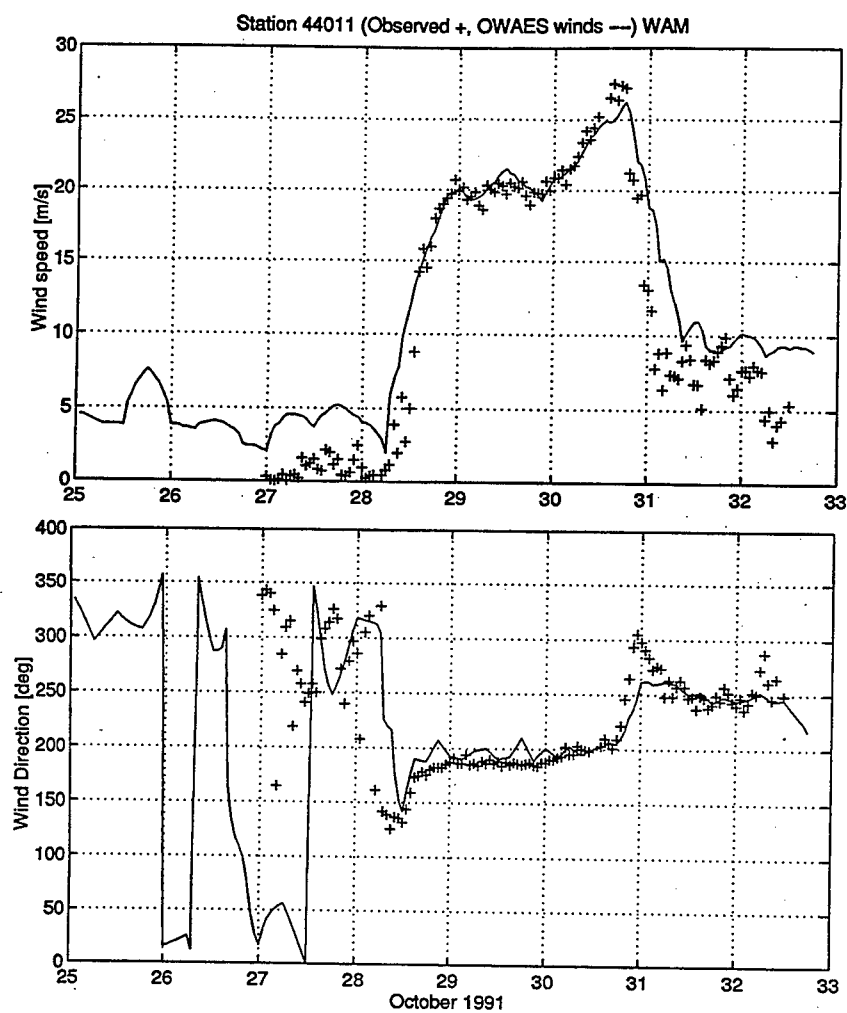Figure 48. Wind speed and direction scatter plots at 41002 for HOS.

Figure 49. Wind speed and direction time histories at 44011 for HOS.

a consistent bias toward the simulated wind speeds especially for the lower wind speeds. The wind direction scatter is small for 44014 and 41002.

The wind time histories of these locations are shown in Figures 49 through 51. Plots for all locations considered in this study are located in Appendix A. The wind speed plot for 44011, in Figure 49, shows the rapid increase in wind speed as the extratropical storm intensifies on the 28th. On the 29th the wind speed is nearly constant at about 20 m/s. Then on the 30th the wind speed increases to 27 m/s before a decline back to 10 m/s. The wind direction plot for 44011, in
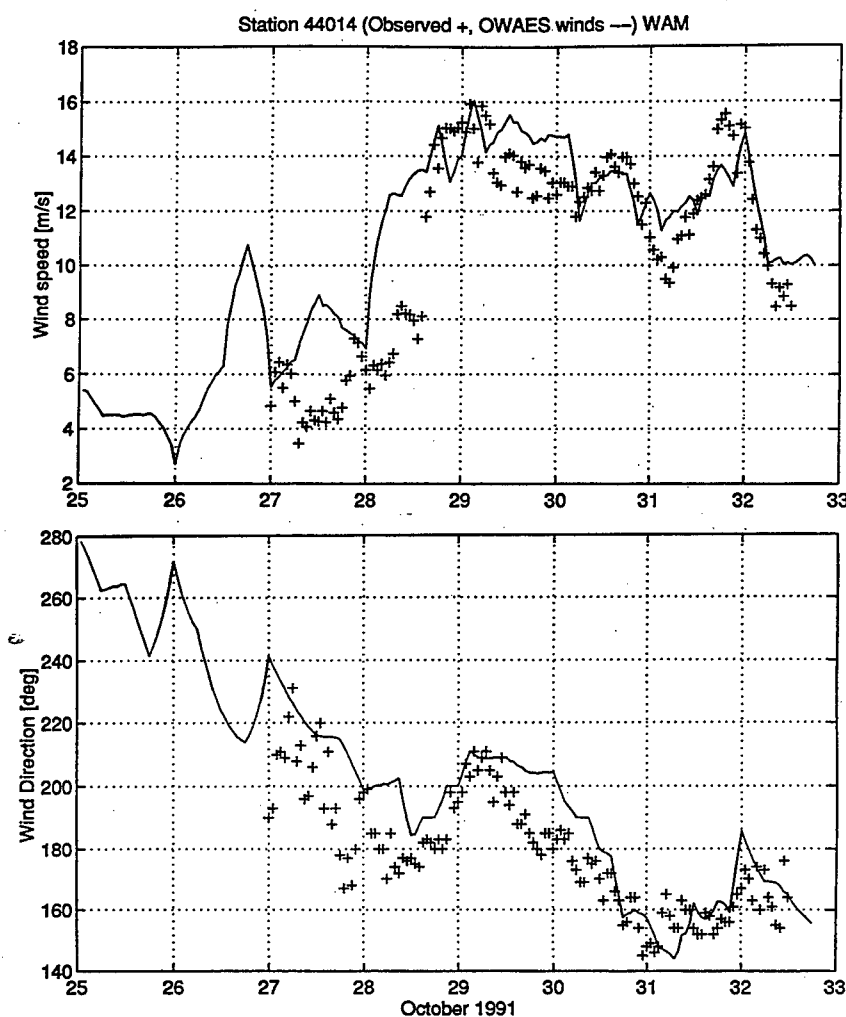

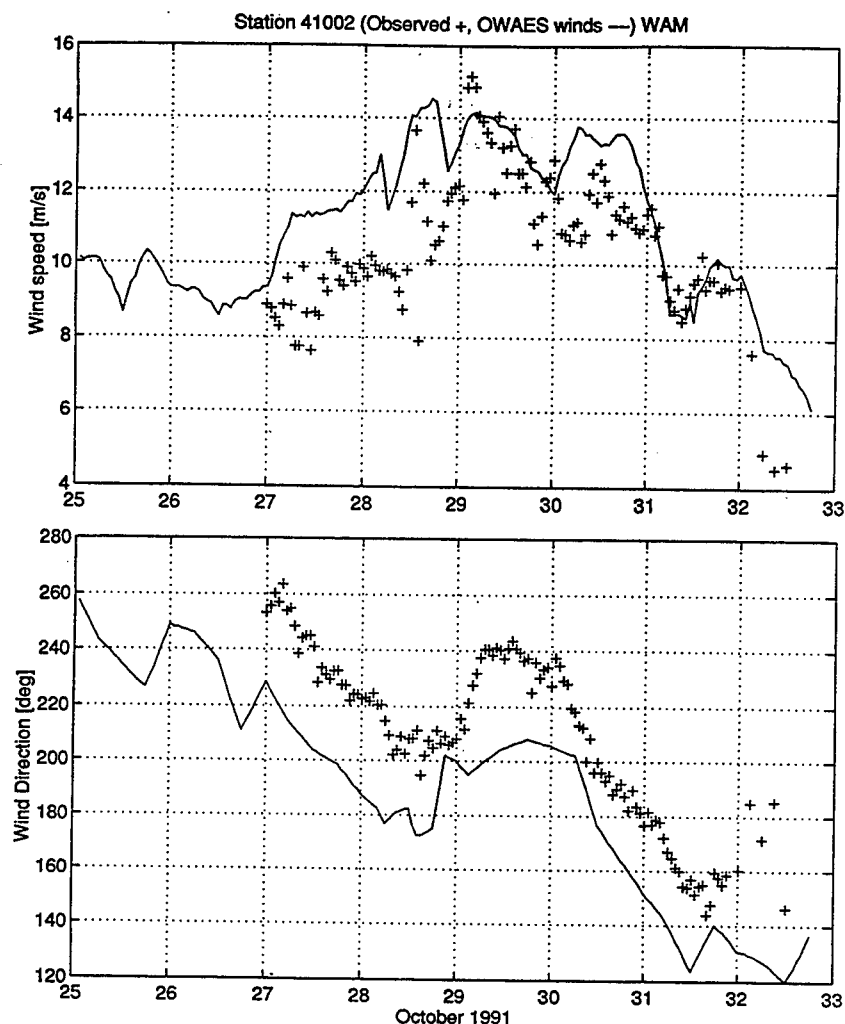Figure 50. Wind speed and direction time histories at 44014 for HOS.

Figure 51. Wind speed and direction time histories at 41002 for HOS.

Figure 49, shows that once the system begins to intensify the wind direction remains constant at south-southwest until the wind speed begins to decline. As the wind speed drops the wind direction shifts to a more southwest direction.

The wind speed plot at 44014, in Figure 50, shows a similar increase in wind speed on the 28th but the maximum is only 16 m/s. Then the wind speed gradually declines to 10 m/s before increasing back to near 16 m/s on the 31st. The wind direction plot shows a steady turning of the winds throughout the simulation from southwest to southeast.

The wind speed plot for 41002, in Figure 51, shows a more gradual increase and decline

in wind speed and a maximum of 15 m/s on the 29th which is associated with the subtropical system. The wind direction plot, in Figure 51, is similar to 44014 in that the direction shifts gradually from the west to the southeast in a counter clockwise direction, but also shows a gradual shift in the opposite direction on the 29th before returning to the overall trend. This wind direction change on the 29th is associated with the passage of the subtropical system.

c. Wind and wave statistics

The general performance of the models is indicated by the statistics of the integrated properties, wind speed, U_{10}, significant wave height, H_s, and peak wave period, T_p. In Table 11 the quality of the simulated wind speed can be seen in the RMS Error which ranges from 1.89 m/s to 3.39 m/s. The bias is positive, ranging from 0.30 m/s to 2.19 m/s. The scatter index (SI) ranges from 15% to 28% and the correlation coefficient (CC) ranges from 0.69 to 0.97.

Table 11. Statistics of measured and hindcast wind speed for HOS.

Buoy	Mean Buoy (m/s)	Mean Model (m/s)	Bias (m/s)	Abs Err (m/s)	RMS Err (m/s)	SI (%)	CC	# pts
44011	11.35	13.53	2.19	2.41	3.15	28	0.97	130
44008	12.08	13.77	1.69	2.77	3.39	28	0.95	128
44014	10.81	12.05	1.24	1.64	2.23	21	0.86	133
41001	13.28	14.52	1.24	1.67	1.95	15	0.80	133
41002	10.55	12.00	1.45	1.55	1.89	18	0.77	123
41010	7.91	8.21	0.30	1.73	2.16	27	0.69	133

SI - scatter index   CC - correlation coefficient

Table 12 shows the H_s statistics for WAM and WIS. The RMS Error tends to be slightly smaller for WIS, with the exception of 44014 and 41002, ranging from 0.61 m to 1.21 m, than WAM which ranges from 0.70 m to 1.41 m. The difference in RMS Error between the two models, ranges from 0.04 m to 0.58 m. The RMS Error at 44008 for both models, 1.41 m and 1.21 m for WAM and WIS respectively, is significantly higher than the other locations. The RMS Error for wind speed is the highest at 44008 but is not significantly higher than 44011. WIS has a positive bias at the two northern most locations, of 0.00 m and 0.70 m and a negative bias for the remaining locations, ranging from -0.01 m to -0.32 m. WAM has a positive bias, for all but 44011 and 41002, ranging from -0.05 m to -0.79 m. The SIs for WAM and WIS are all below or near 20% except for 44008. The only significant differences between the models are at 44011 where the WIS SI is 6% lower and at 41002 where WAM is 6% lower. The SI for WIS ranges from 12% to 27%, while the SI for WAM ranges from 15% to 32%. The correlation coefficient (CC) for WAM varies between 0.86 and 0.98 and is consistently higher than WIS, which ranges from 0.81 to 0.99, except for 44011.

Table 12. Statistics of measured and hindcast H_s for HOS.

Buoy -	WAM							WIS						
	Mean Buoy (m)	Mean Model (m)	Bias (m)	Abs Err (m)	RMS Err (m)	SI (%)	CC	Mean Model (m)	Bias (m)	Abs Err (m)	RMS Err (m)	SI (%)	CC	# pts
44011	5.28	5.23	-0.05	0.79	0.95	18	0.98	5.29	0.00	0.53	0.63	12	0.99	130
44008	4.42	5.21	0.79	1.00	1.41	32	0.98	5.12	0.70	0.94	1.21	27	0.97	128
44014	4.13	4.36	0.22	0.68	0.78	19	0.95	3.86	-0.27	0.62	0.82	20	0.86	133
41001	5.32	5.35	0.02	0.64	0.79	15	0.95	5.32	-0.01	0.54	0.69	13	0.87	133
41002	4.62	4.53	-0.09	0.61	0.72	16	0.88	4.30	-0.32	0.66	1.03	22	0.77	123
41010	3.37	3.37	0.00	0.61	0.70	21	0.86	3.11	-0.27	0.53	0.61	18	0.81	133

SI - scatter index   CC - correlation coefficient

Table 13 shows the T_p statistics for WAM and WIS. WAM and WIS exhibit a consistently negative bias with the exception of 44008 (0.48) for WAM, ranging from -0.75 sec to -1.58 sec for WAM and from - 0.89 sec to -2.42 sec for WIS. The WIS bias is generally larger than the WAM bias. The RMS Error for WAM ranges between 1.87 sec and 2.84 sec and from 2.34 sec

Table 13. Statistics of measured and hindcast T_p for HOS.

	WAM							WIS						
Buoy	Mean Buoy (s)	Mean Model (s)	Bias (s)	Abs Err (s)	RMS Err (s)	SI (%)	CC	Mean Model (s)	Bias (s)	Abs Err (s)	RMS Err (s)	SI (%)	CC	# pts
44011	12.10	11.32	-0.78	1.54	1.87	15	0.86	10.15	-1.95	2.13	2.57	21	0.80	130
44008	11.16	11.64	0.48	2.25	2.77	25	0.68	10.19	-0.97	1.82	2.42	22	0.61	128
44014	13.21	11.85	-1.36	2.00	2.50	19	0.87	10.79	-2.42	2.61	3.11	24	0.86	133
41001	13.02	12.26	-0.75	2.43	2.84	22	0.69	12.13	-0.89	1.96	2.34	18	0.74	133
41002	13.91	12.32	-1.58	1.94	2.33	17	0.88	11.65	-2.25	2.30	2.80	20	0.86	123
41010	14.00	12.47	-1.53	1.87	2.29	16	0.88	12.61	-1.39	2.00	2.61	19	0.75	133

SI - scatter index   CC - correlation coefficient

to 3.11 sec for WIS. The difference in RMS Error between the models ranges from 0.32 sec to 0.70 sec. The SI for WAM ranges from 16 % to 25% and from 18% to 24% for WIS. Differences between the model SIs range from 3% to 6 %. The CC for WAM is higher than that for WIS, except for 41001. The WAM CC ranges from 0.68 to 0.88 and the differences between WAM and WIS CCs varies between 0.01 to 0.13.

The scatter indices for U_{10}, H_s, and T_p from Tables 11 through 13 are plotted in bar graph form in Figure 52 to show the relationship between each parameter. For the central to southern area, the wind speed SI is near or below 20%. The wind speed SI for the two northern locations and the extreme southern location are over 25%. Of these locations, only the H_s SI at 44008 is much above 20% with an SI of around 30%. Note that 44011, 44008 and 44014 are

expected to have significant depth effects with a d/L_o, associated with the maximum T_p, of 1/8.7,
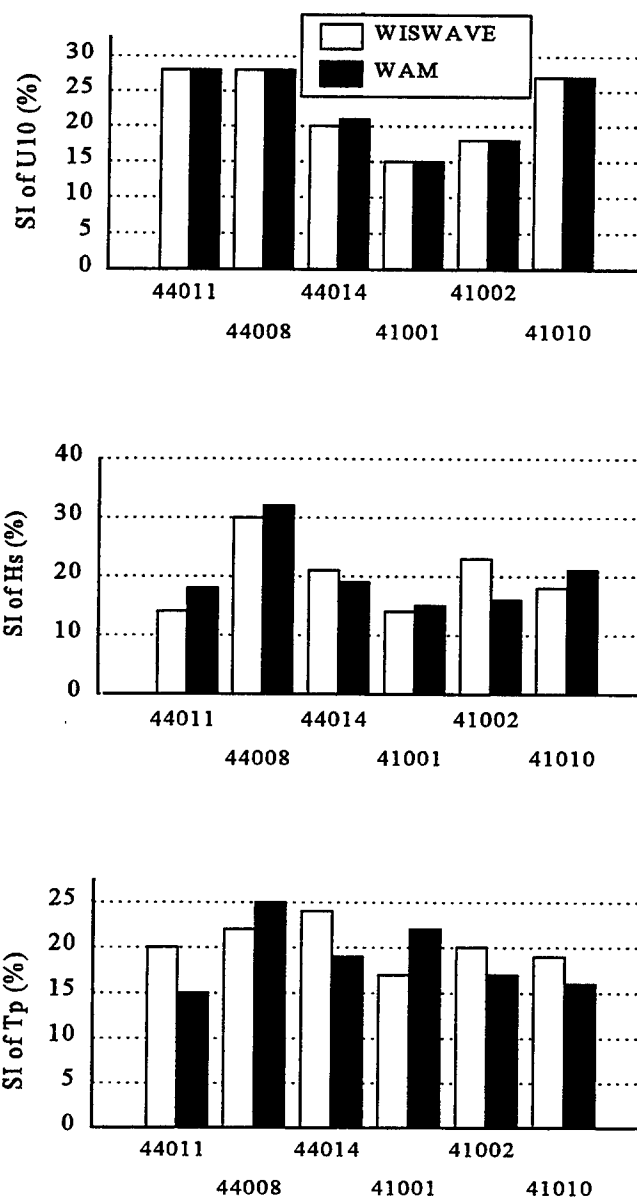
1/7.5 and 1/10.5 respectively.

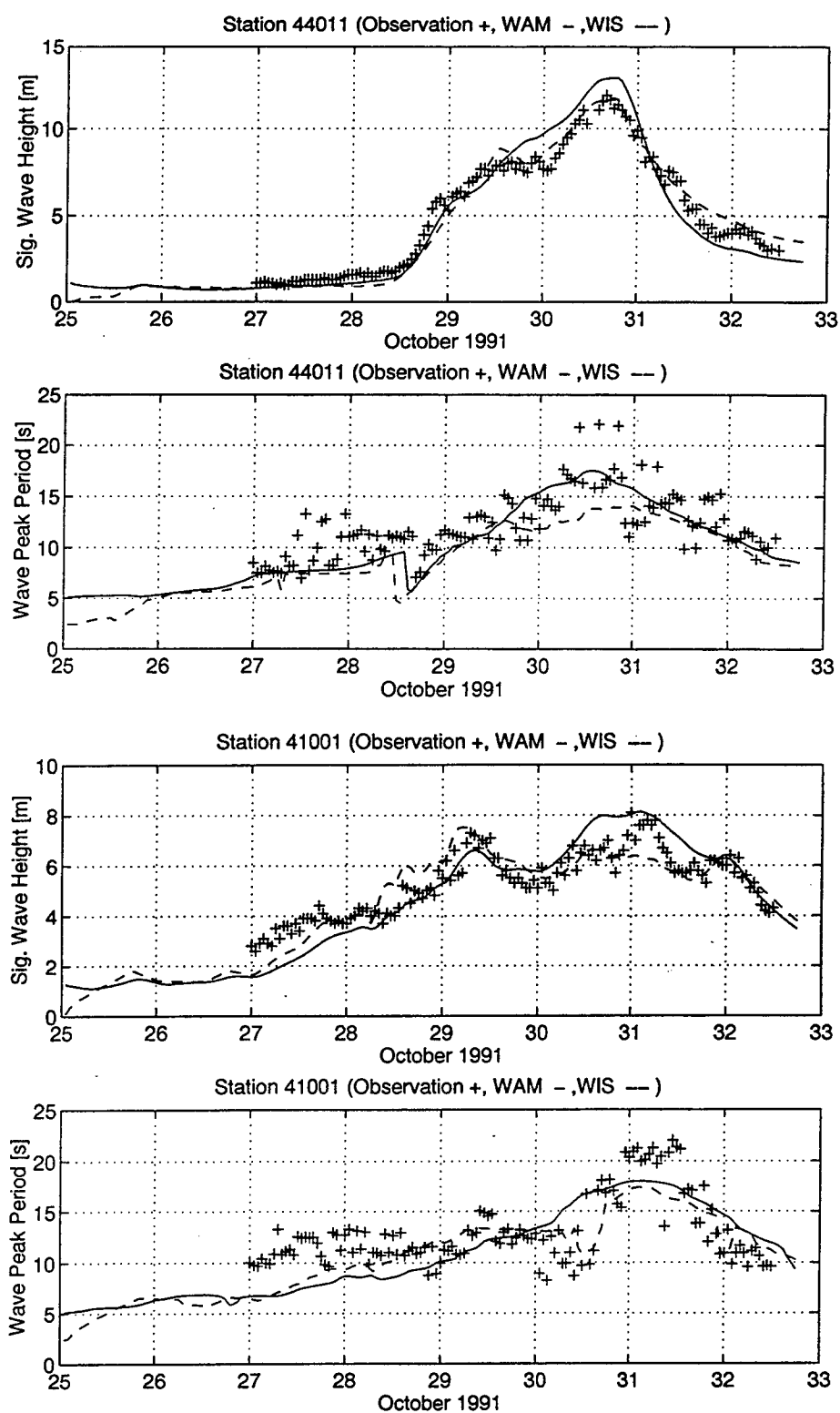Figure 52. WAM and WIS U_{10}, H_s, and T_p scatter indexes for HOS.

Station 44011 (Observation +, WAM – ,WIS —)

Station 44011 (Observation +, WAM – ,WIS —)

Station 41001 (Observation +, WAM – ,WIS —)

Station 41001 (Observation +, WAM – ,WIS —)

Figure 53. H_s and T_p time histories at 44011 and 41001 for HOS.

d. Non-directional time histories

The following section presents a description of modeled and measured H_s and T_p time histories for select locations corresponding to non-directional buoys. Location 44011, shown in Figure 53, is expected to have some depth effects. The location is south of the maximum wave heights and experiences primarily swell conditions. Both models predict the H_s well during the entire simulation however WAM has about a 1.0 m overprediction beginning on the 29th and continuing until just past the peak even though the wind speed is well specified. Both models underpredict the T_p through much of the simulation but WAM is closer to the buoy during the peak
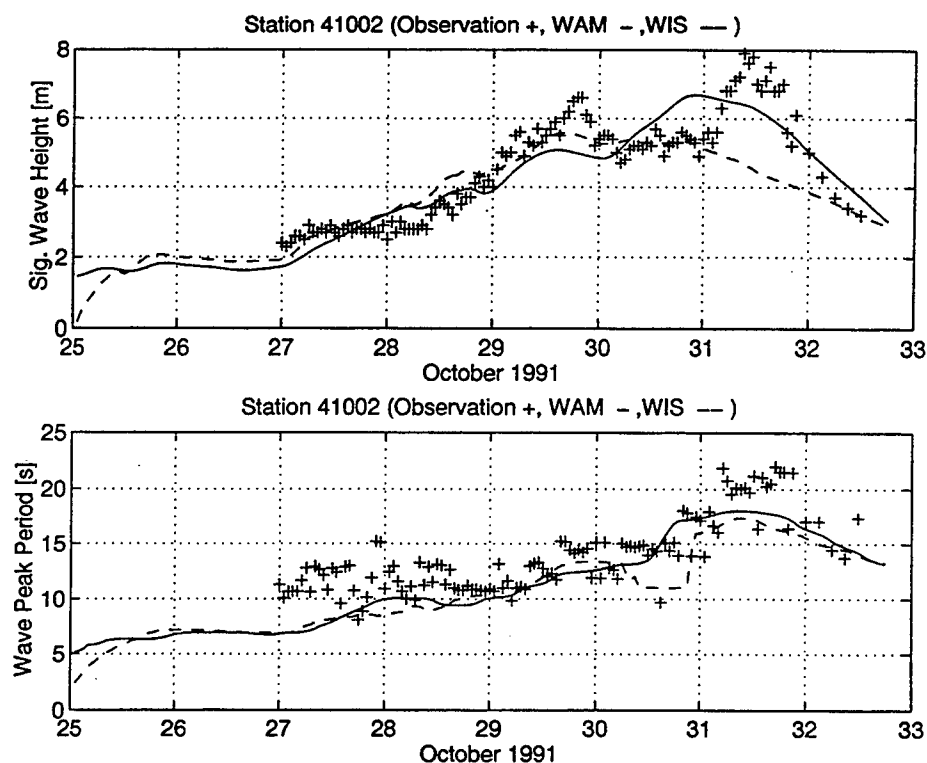
Figure 54. H_s and T_p time histories at 41002 for HOS.

of the storm. At 41001, in Figure 53, which is strictly deepwater, both models have good agreement with the buoy H_s with WAM overpredicting by 1.0 m but matching at the peak and WIS underpredicting the peak by 1.5 m. Also evident at this location are the effects of Hurricane Grace on the 29th where WIS is slightly high and WAM is slightly low. The model T_p at this location are similar to 44011 but the buoy maximum is only 20 sec. Model performance is reduced at 41002, shown in Figure 54 with both underpredicting by 2.0 m.

e. Directional buoy analysis

Buoy 44014 , in Figure 55, is a directional buoy and allows the comparison of peak wave direction, directional wave spread, and PCC in addition to H_s and T_p . This location is expected to have considerable depth effects as noted previously. The model performance is also reduced as the model H_s follows a much broader trend than the buoy near the main peak. Again model T_p are underpredicted at the peak by 4 to 5 sec. The buoy peak wave direction moves between 200° and 300° for the entire simulation and suggest a two wave system. The model peak wave direction remains near 200° after the 29th. The model spread is reasonably close to the buoy until the 29th and then becomes too narrow afterward although WIS is a little closer until the 30th. Unlike the previous simulations the PCC remains high until the more rapid growth occurs on the 30th and reaches a minimum of mostly 0.4 before the peak H_s .

f. Summary

The HOS simulation represents an extreme event with a peak wind speed of 27 m/s. WIS estimates of H_s during the storm are consistently below that of WAM and usually underestimate the buoy H_s while WAM has a tendency to overestimate the buoy H_s during the storm. This is
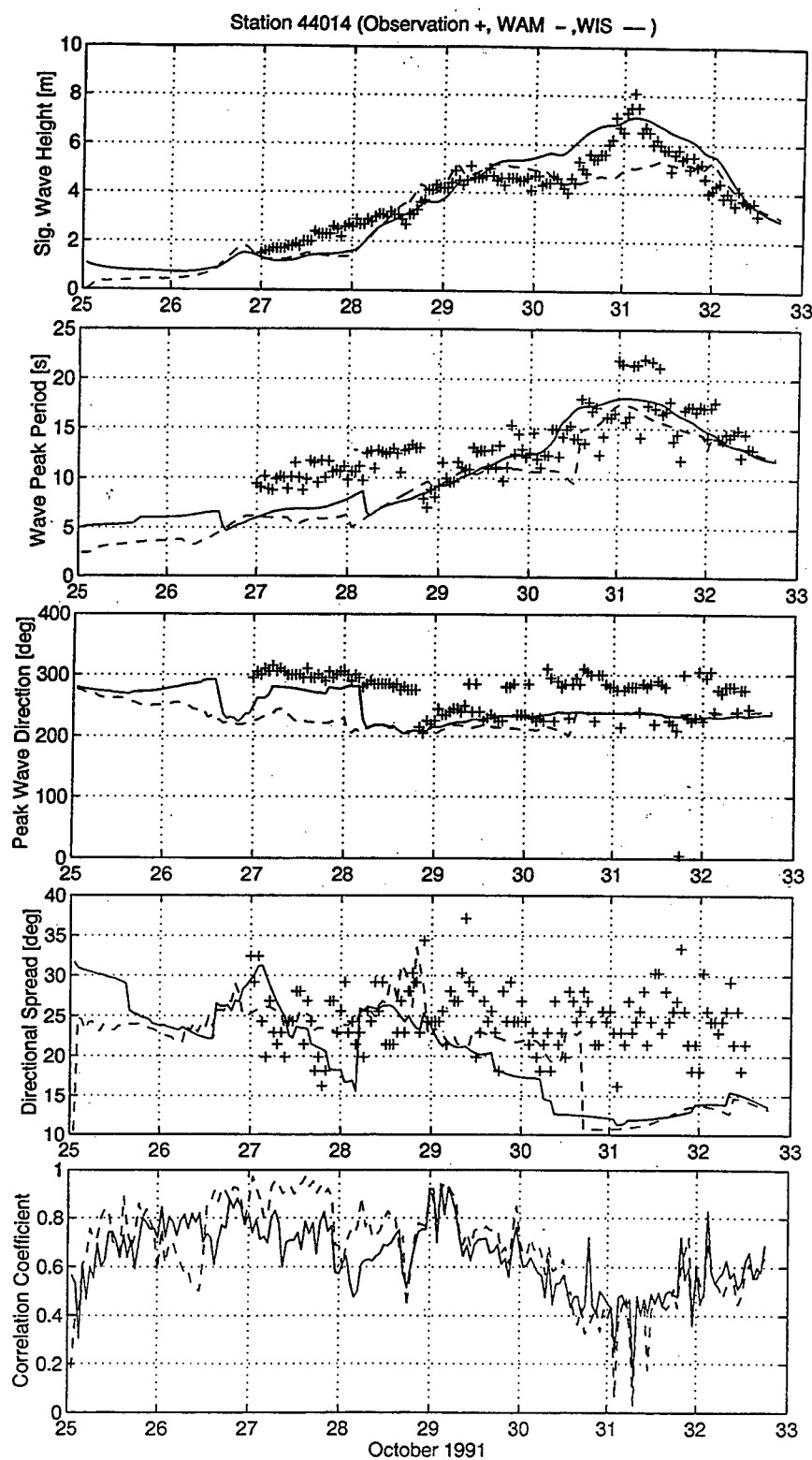
Figure 55. H_s, T_p, θ_p, σ, and PCC at 44014 for HOS.

opposite the trend found in the previous three simulations where WIS usually estimated H_s higher than WAM and overestimated the storm peaks. Both models underestimate the T_p near the peak of the storm but WIS is closer than WAM. Both model peak wave directions in some cases have large errors due to bi-modal spectrum. The model wave spread becomes too narrow during the decay and both models underestimate most of the time. The PCC for both models is not as good as previous simulations during the first three days. This suggests a need for longer spin up or energy originating from outside the grid domain is present. Also unlike other simulations the PCC begins to decline as H_s increases.

5.4 Storm of the Century

a. Synoptic weather conditions

The SOC is the most extreme event among the cases considered in this study with a maximum wind speed of 27 m/s and a maximum H_s of 15 m considering the NDBC buoys available for this period. A more detailed description of this event may be found in Cardone et al. (1996). The maximum wind speed and wave height for the storm occurred further north outside the area covered by NDBC buoys for this event.

The SOC began with the development of a low pressure system in the Gulf of Mexico off the Texas coast on 12 March 1993. Figure 56 shows the storm track. Over the next 48 hours this low pressure strengthened and moved northeast across the Florida panhandle and then along the eastern US coast. By 15 March the system moved into Canada and weakened considerably. As the storm moved along the US coast the strongest winds were east of the track and were from the southwest to southeast.
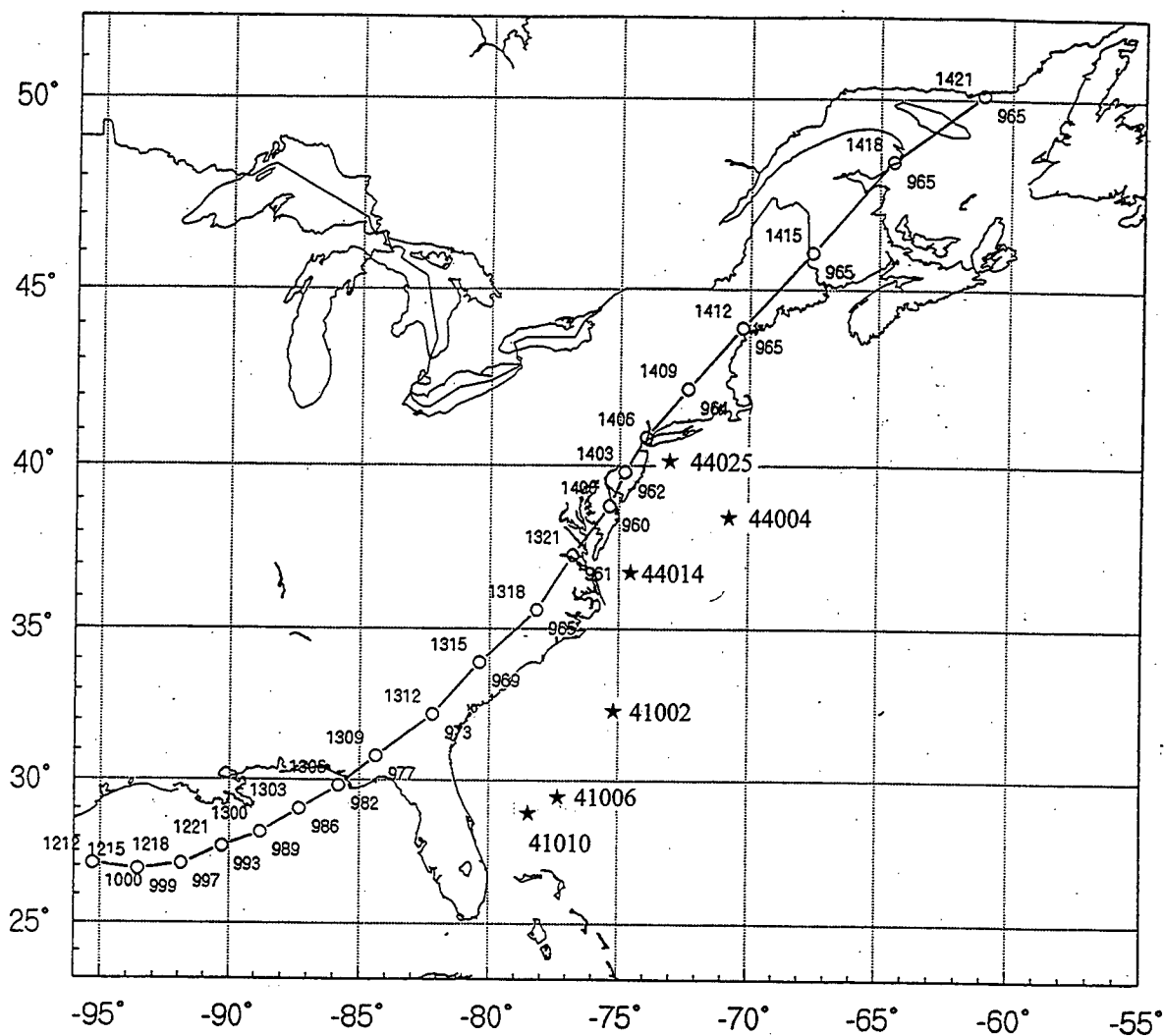
Figure 56. Track and central pressure of the Storm of the Century. Buoy locations indicated by ★ (adapted from Cardone et al. 1996).

b. Winds

The scatter plots of wind speed and direction at 41010, 44004, and 44025 are shown in Figure 57. The wind speed bias is smaller for 41010, the southern most location, than the central and northern locations. The wind direction shows a similar trend with the simulated direction remaining within ± 50° of the measured direction for 41010 while the differences at 44004 and 44025 are slightly larger.
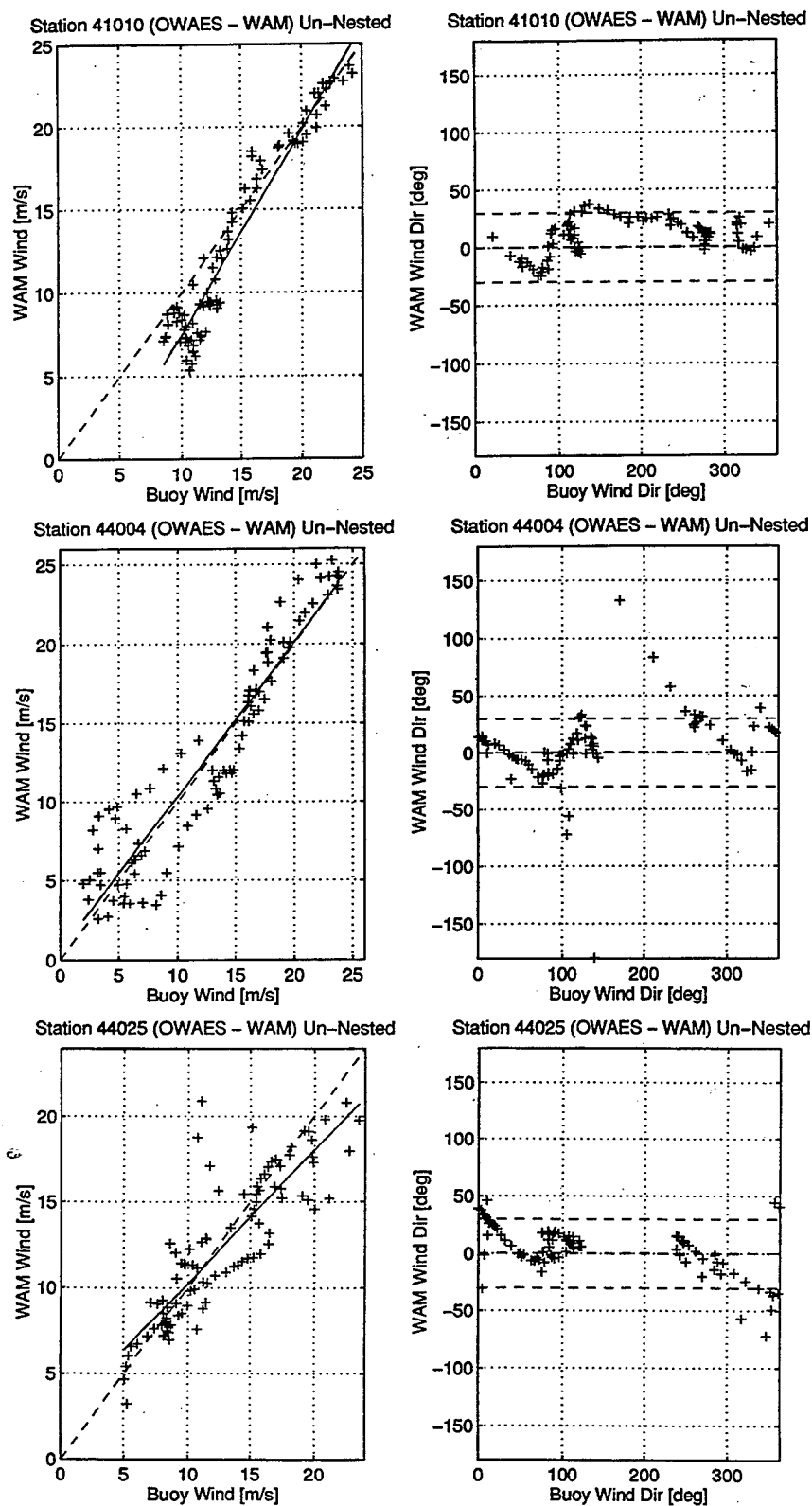
Figure 57. Wind speed and direction scatter plots at 41010, 44004, and 44025 for SOC.
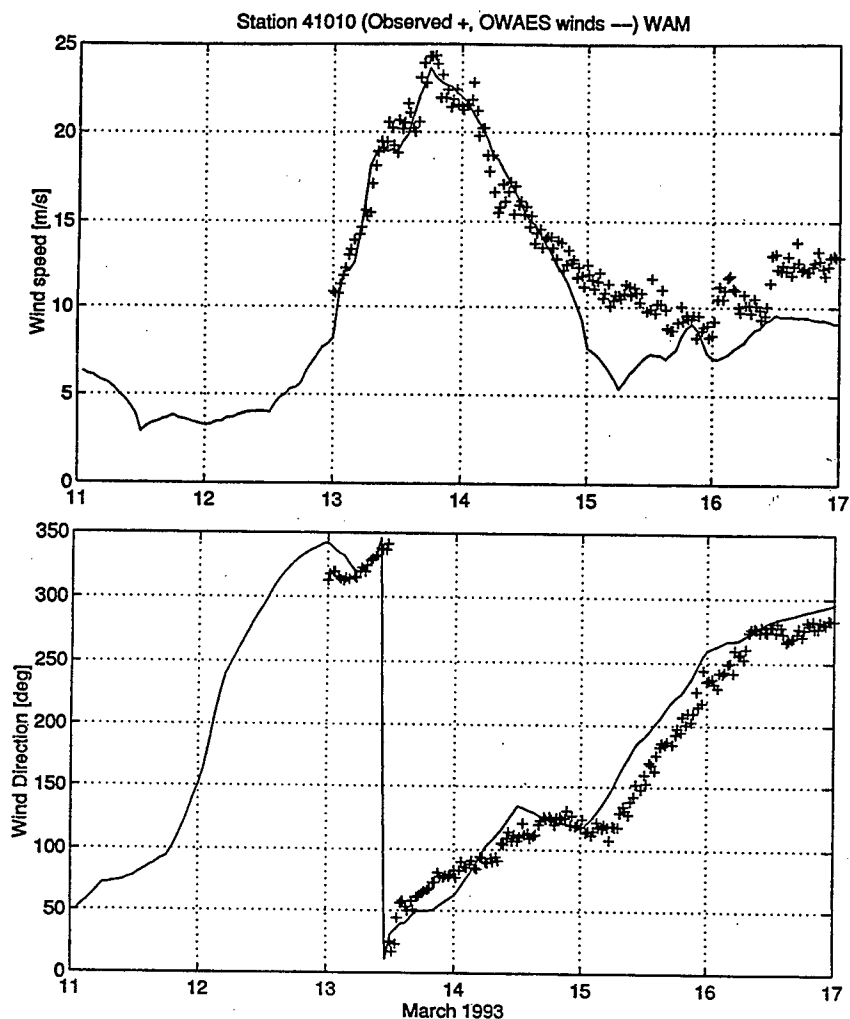
Figure 58. Wind speed and direction time histories at 41010 for SOC.

The wind time histories for locations 41010, 44004, and 44025 are representative of the model domain. Since this is a large storm event in which the track followed the coast the wind speed and direction time histories are very similar for all locations. Beginning on the 13th the wind speed began to increase from about 5 m/s to 25 m/s to 30 m/s by the end of the 13th or beginning of the 14th and then decreased to about 5 m/s to 10 m/s by the 15th. The wind speed time history has a more distinct peak for the southern locations, represented by 41010 in Figure 58, where the storm was most intense. The wind speed time history has a broader more complex peak for the
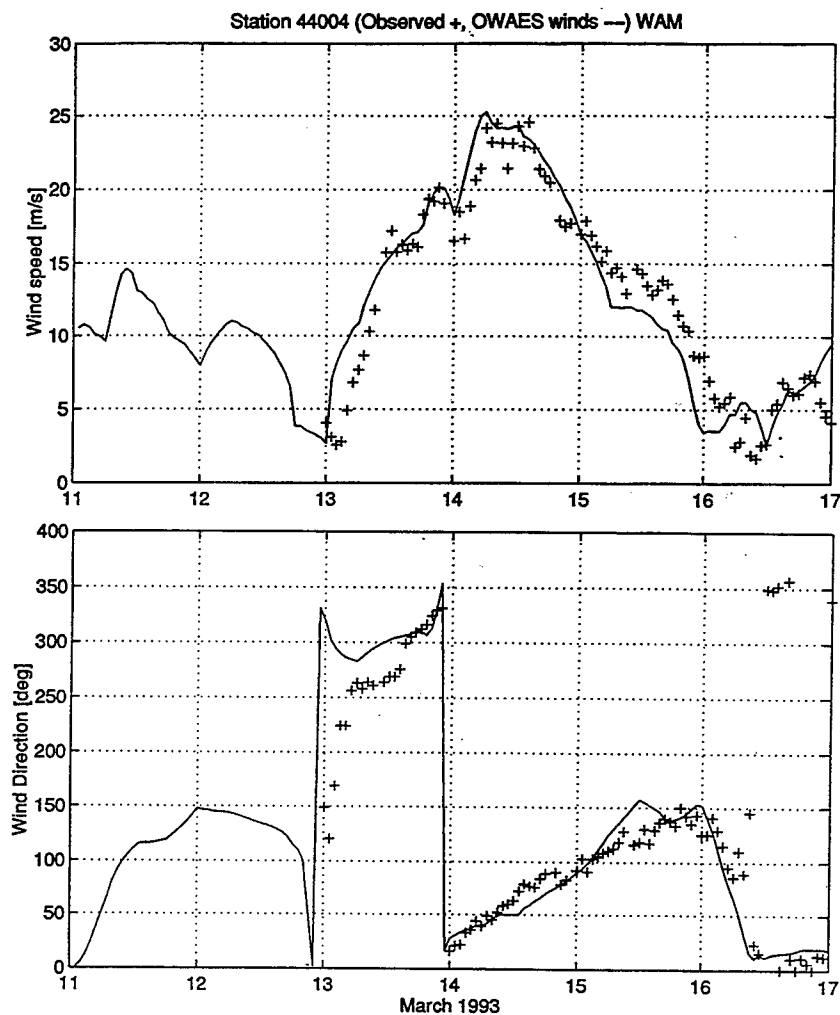
Figure 59. Wind speed and direction time histories at 44004 for SOC.

central and northern locations, represented by 44004 in Figure 59 and 44025 in Figure 60 respectively. The wind direction is generally toward the north to northwest at the beginning of the storm and gradually turns clockwise back to the northwest for the southern locations. The wind directions at the central and northern locations are toward the north to northwest in the beginning and turn clockwise to the southeast before turning counter clockwise back to the north.
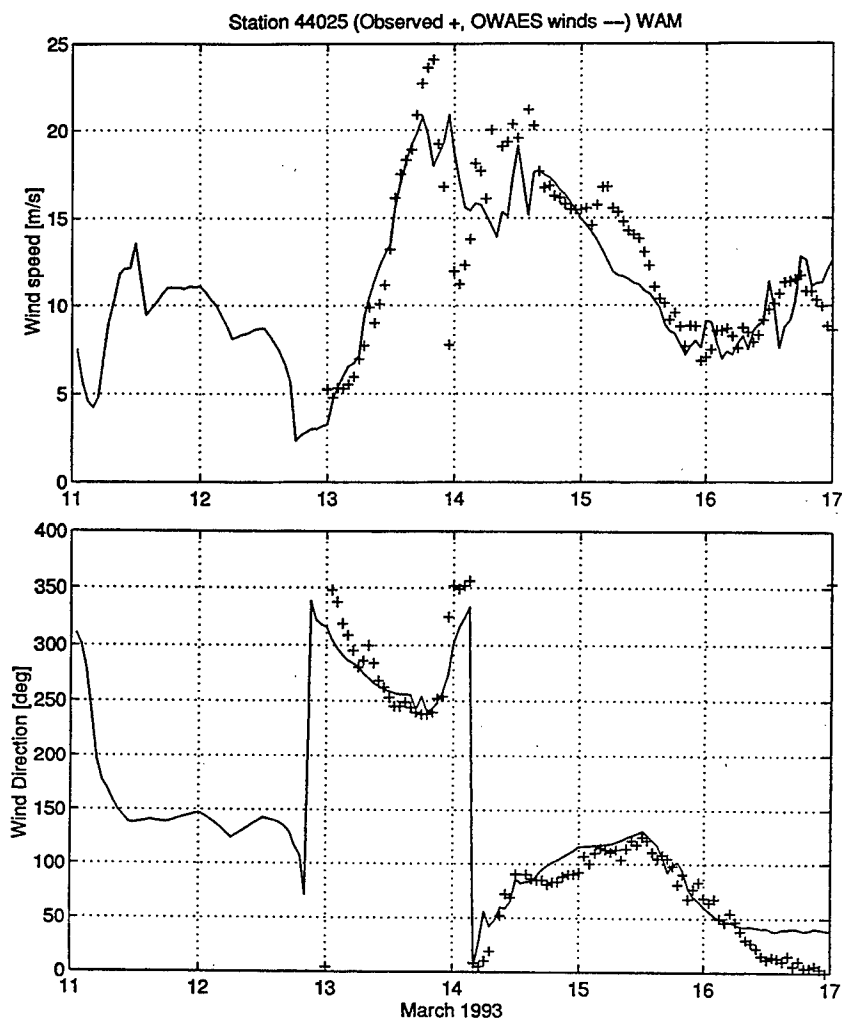
Figure 60. Wind speed and direction time histories at 44025 for SOC.

c. Wind and wave statistics

The general performance of the models is indicated by the statistics of the integrated properties, wind speed, U_{10}, significant wave height, H_s, and peak wave period, T_p. Table 14 shows the quality of the simulated wind speed with an RMS Error which ranges from 2.34 m/s to 3.46 m/s. The bias ranges from -1.53 m/s to 0.38 m/s. The SI ranges from 17% to 31% and is below 20% for all locations except 44014 (31%) and 41002 (23%). The CC ranges from 0.85 to 0.96 .

Table 14. Statistics of measured and hindcast wind speed for SOC.

Buoy	Mean Buoy (m/s)	Mean Model (m/s)	Bias (m/s)	Abs Err (m/s)	RMS Err (m/s)	SI (%)	CC	# pts
44025	12.76	12.37	-0.39	1.75	2.47	19	0.85	95
44004	12.78	13.05	0.27	1.86	2.34	18	0.94	92
44014	11.09	11.47	0.38	2.38	3.46	31	0.86	97
41002	14.77	13.56	-1.20	2.21	3.33	23	0.89	90
41006	14.03	12.56	-1.48	1.75	2.46	18	0.95	97
41010	14.20	12.66	-1.53	1.85	2.38	17	0.96	95

SI - scatter index   CC - correlation coefficient

Table 15 shows the H_s statistics for WAM and WIS. The only clear trend evident form consideration of all the locations is a negative bias for strictly deepwater locations and a positive bias for the shallower locations 44014 and 44025. These locations also have relatively larger RMS Errors, between 1.21 m and 1.74 m, except for WIS at 44025, than the deepwater locations and significantly larger SI, between 32% and 66%. This trend is present, with the exception noted, in both model results.

Considering only the deepwater locations the statistics for WIS are slightly better than those for WAM at the southern most locations, 41010 and 41006, with differences in RMS Error, bias, and SI within 0.16 m, 0.21 m, and 5% respectively. For 41002 and 44004 WAM statistics are better than WIS with differences in RMS Error, bias, and SI within 0.18 m, 0.27 m, and 4% respectively. The CCs are relatively high for both models at all locations with WIS having the edge for all but 41002. The difference between the CCs range from 0.01 to 0.05.

Table 16 shows the T_p statistics for WAM and WIS. Similar to the H_s results, the T_p statistics for 44014 and 44025 are considerably worse than for the other locations.

Table 15. Statistics of measured and hindcast H_s for SOC.

	WAM							WIS						
Buoy	Mean Buoy (m)	Mean Model (m)	Bias (m)	Abs Err (m)	RMS Err (m)	SI (%)	CC	Mean Model (m)	Bias (m)	Abs Err (m)	RMS Err (m)	SI (%)	CC	# pts
44025	2.79	3.34	0.55	0.93	1.21	43	0.89	3.32	0.53	0.74	0.88	32	0.94	94
44004	5.01	4.83	-0.18	0.47	0.78	16	0.98	4.56	-0.45	0.59	0.89	18	0.99	92
44014	2.62	3.60	0.98	1.11	1.74	66	0.91	3.43	0.81	0.97	1.57	60	0.93	97
41002	5.15	4.60	-0.55	0.60	0.84	16	0.99	4.58	-0.57	0:75	1.02	20	0.98	90
41006	3.83	3.55	-0.29	0.62	0.71	19	0.97	3.71	-0.13	0.44	0.55	14	0.98	97
41010	3.63	3.32	-0.31	0.63	0.76	21	0.96	3.54	-0.10	0.50	0.61	17	0.98	95

SI - scatter index   CC - correlation coefficient

Table 16. Statistics of measured and hindcast T_p for SOC.

	WAM							WIS						
Buoy	Mean Buoy (s)	Mean Model (s)	Bias (s)	Abs Err (s)	RMS Err (s)	SI (%)	CC	Mean Model (s)	Bias (s)	Abs Err (s)	RMS Err (s)	SI (%)	CC	# pts
44025	6.75	10.30	3.56	4.24	5.41	80	0.34	8.80	2.06	2.67	3.77	56	0.57	94
44004	9.62	10.43	0.80	1.73	2.11	22	0.86	9.62	-0.01	1.70	2.19	23	0.81	92
44014	7.60	9.93	2.33	3.21	4.10	54	0.43	9.37	1.77	3.02	3.89	51	0.40	97
41002	9.59	9.49	-0.10	0.93	1.13	12	0.95	9.27	-0.32	0.89	1.22	13	0.95	90
41006	8.75	8.67	-0.08	0.61	0.73	8	0.96	8.54	-0.22	0.55	0.74	9	0.95	97
41010	8.42	8.33	-0.10	0.74	0.92	11	0.91	8.28	-0.14	0.62	0.84	10	0.90	95

SI - scatter index   CC - correlation coefficient

The T_p RMS Error, bias, and SI for 44014 and 44025 range between 3.77 sec and 5.41 sec, 1.77 sec and 3.56 sec, and 51% and 80% respectively , with WIS having the better statistics. The T_p RMS Error, bias, and SI for the remaining locations range between 0.73 sec and 2.19 sec, -0.32 sec and 0.80 sec, and 1% respectively. The only significant difference between the two models at

the deepwater locations is a tendency for the WIS T_p to have a more negative bias than WAM. The CCs for both model T_p are similar and are relatively high for the deepwater location, ranging from 0.81 to 0.96 and relatively low for the more shallow locations, ranging from 0.34 to 0.57.
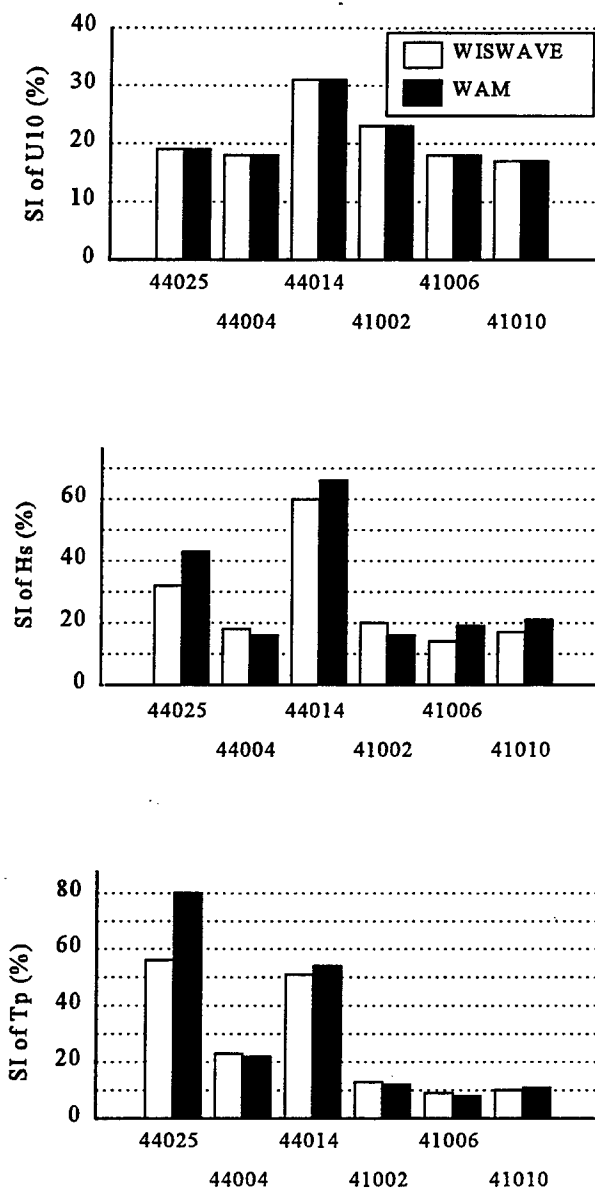

Figure 61. WAM and WIS U_{10}, H_s, and T_p scatter indexes for SOC.

The scatter indices for U_{10}, H_s, and T_p from Tables 14 through 16 are plotted in bar graph form in Figure 61 to show the relationship between each parameter. Wind speed SIs, for both models, are below 20% for all locations except 44014 (31%) and 41002 (23%). The H_s SIs are below 20% for all but the shallower locations, 44014 (60% - 66%) and 44025 (32%- 43%). Even though the wind speed SI at 41002 is somewhat high, the H_s SI is below 20% for both models. Similar to the H_s SIs, the T_p SIs are near or below 20% for all but locations 44014 and 44025 which are above 50% for both models.

d. Non-directional time histories

The following section presents a description of modeled and measured H_s and T_p time histories for locations corresponding to non-directional buoys. At locations 41010 and 41006, in Figure 62, both model H_s are very similar and follow the buoy results closely except at the peak. WAM underestimates the peak by 0.5 m to 1.0 m while WIS matches the measured peak closely, even though the simulated wind speed is underestimated by 1 m/s to 2 m/s. The model T_p at these locations are also in good agreement with the buoy with an underestimate of about 1 sec to 2 sec at the peak of the storm. Also the WAM T_p is slightly longer than WIS during the storm decay.

At 41002, in Figure 63, both model H_s are underestimated at the peak by about 2 m to 3 m, while the T_p is underestimated by 2 sec to 3 sec. This underestimate is due in part to an underspecified wind speed at the peak of the storm of 2 m/s to 3 m/s. This wind speed underestimate can not account completely for a 2 m to 3 m underestimate of H_s. This relatively large error may be due to underspecified wind speeds in the area upwind or southeast of this location. At 44004, in Figure 63, both models' H_s lag the increasing buoy H_s before the peak of the storm. In contrast to most of the cases considered WIS underestimates H_s by 1.5 m, while WAM is within 0.5 m. No lag in simulated wind speed is present at this location.
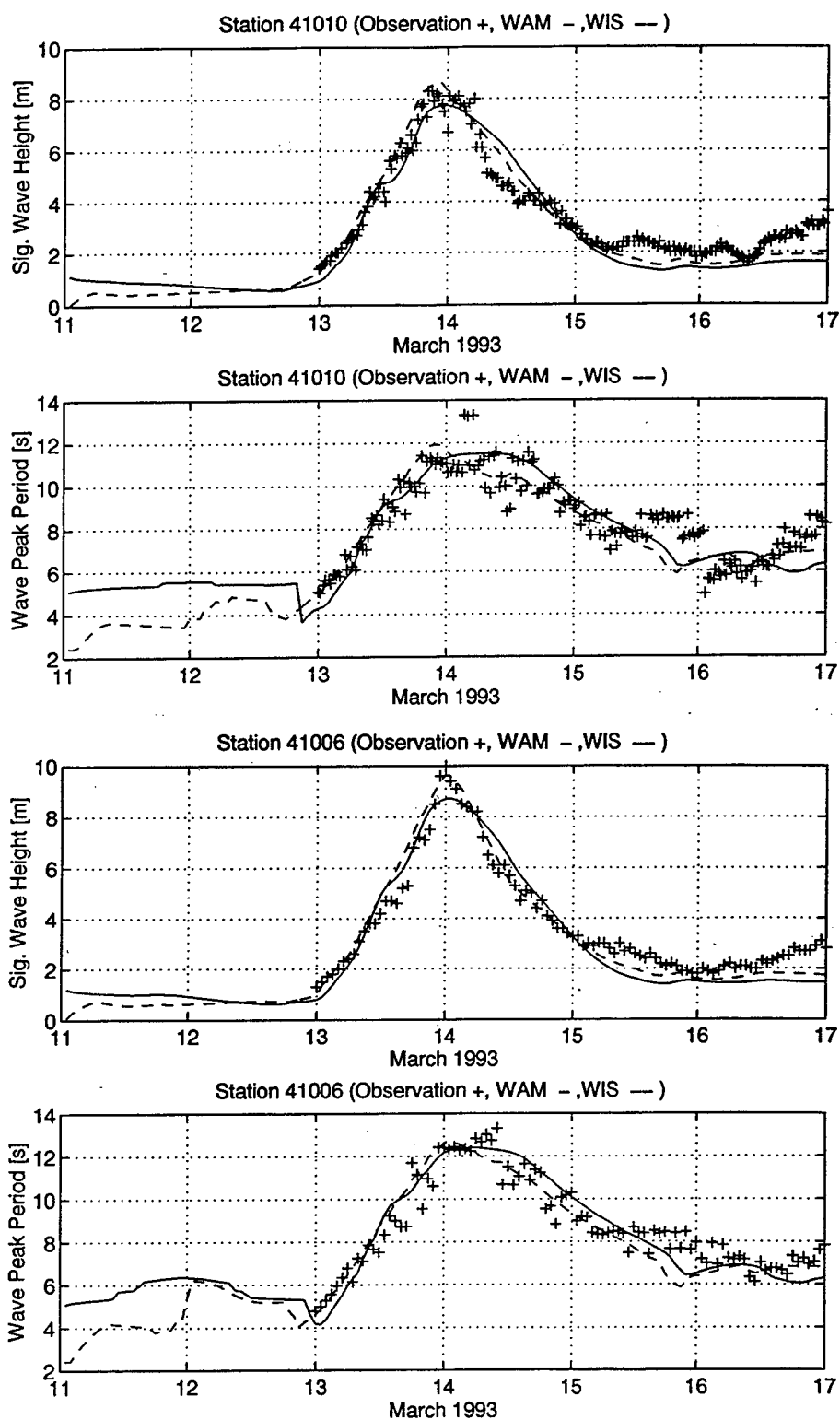
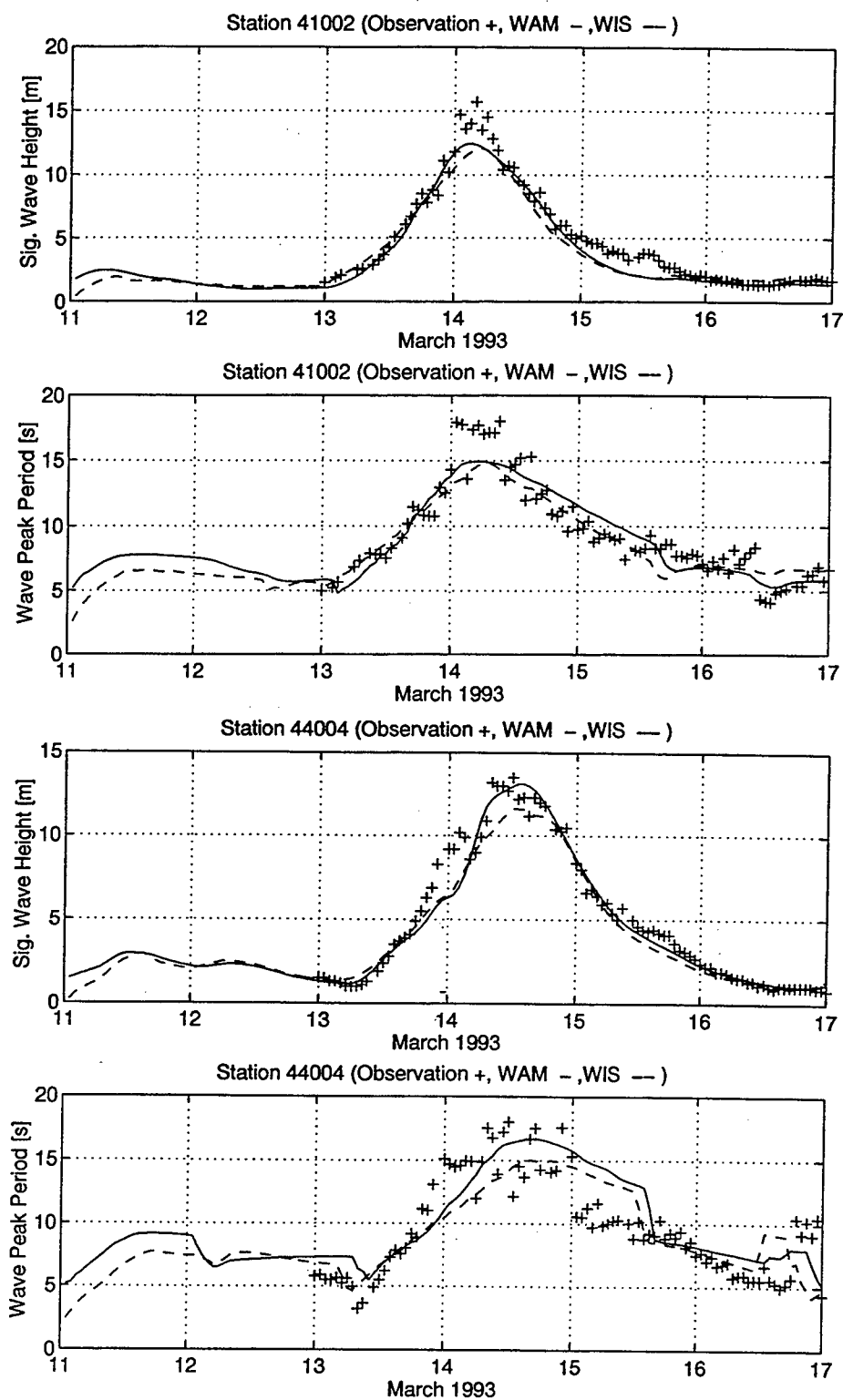Figure 62. H_s and T_p time histories at 41010 and 41006 for SOC.

Figure 63. H_s and T_p time histories at 41002 and 44004 for SOC.

e. Directional buoy analysis

      Buoys 44014 and 44025 are directional buoys and allow the comparison of peak wave direction, directional wave spread, and PCC in addition to H_s and T_p. Both locations are near the coast and experience more complex wind conditions than the other locations. This contributes to the poor performance of both models at these locations.

      The buoy wind speed at 44014 on the 13th decreases to 10 m/s and 5 m/s after reaching 15 m/s while the simulated wind speed continues to increase. The simulated wind speed is overspecified by 5 m/s to 10 m/s for more than 12 hours until the beginning of the 14th. The wind direction, which is reasonably well simulated, also shifts about 70° from west to northwest within several hours.

      Plots for 44014 are shown in Figure 64. The over specification of wind speed for an extended period of time accounts for the 2.0 m overestimation of H_s at the peak. However, the growth of the simulated H_s is expected to lead that of the measured since the simulated wind speed increases faster than the measured wind speed. But the modeled H_s growth follows the buoy closely, with a slight lag during the first part of growth. Very little difference between the two model H_s exist, however the WIS H_s decreases slightly faster than WAM.

      The model T_p are very similar also. The increase in model T_p lags the measured T_p increase, by about 6 hours, during the 13th but reaches the same maximum. The maximum model T_p also persist longer than the maximum measured T_p by about 12 hours. The mode peak wave directions are similar but WIS leads WAM in direction shifts on the 13th and 15th. Both models' peak wave direction have nearly 100° of error during the decay of the storm. The model wave spreads are similar during the storm event and generally underestimate the measured spread on the 14th and 15th during the storm decay.
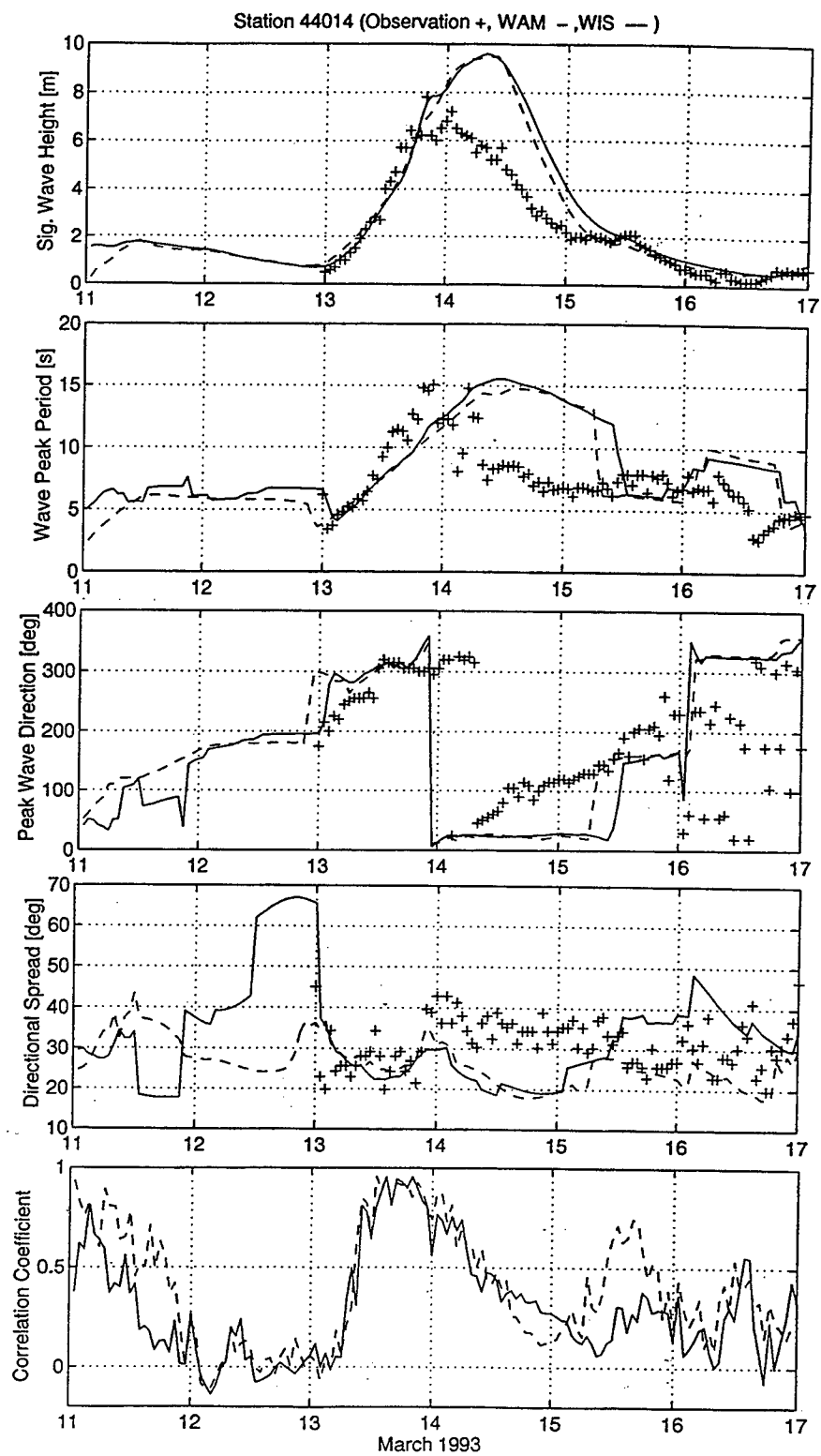
Figure 64. H_s, T_p, θ_p, σ, and PCC at 44014 for SOC.

The PCC for this case follows a trend similar to the previous cases considered. The PCC declines to near 0.0 during the spinup as H_s decreases from 2.0 m to less than 1.0 m. The PCC increases to near 1.0 during the growth stage of the storm and then declines below 0.5 during the decay. The only significant difference between the model PCCs is the brief increase in the WIS PCC, to 0.75, on the 15th while the WAM PCC remains below 0.5.

The measured wind time history at 44025 also exhibits oscillations in wind speed and shifts in direction during the storm passage. At the first maximum measured wind speed the simulated wind speed underspecifies by 4 m/s. Then the measured wind direction shifts about 100° from west to northwest and the increased wind speed drops to below 10 m/s. While the simulated wind direction is in good agreement with the measured, the simulated wind speed drops to only 15 m/s. Next another wind speed maximum, of 20 m/s, occurs in the measured and simulated wind speed, followed by a gradual decrease, over the next 36 hours, to 8 m/s.

The effect of this wind speed behavior on the H_s is a 1.0 m underestimate of the measured peak by both models. Plots for 44025 are shown in Figure 65. Both models' H_s increase to near the measured peak 6 hours later with the WIS H_s being about 0.25 m below that of WAM. The WIS H_s begins decreasing slightly earlier than the WAM H_s because of the slightly reduced peak value. The WIS H_s also begins increasing during the growth of the storm several hours earlier than that of WAM. The T_p at this location is similar to that of 44014 but the WAM T_p overestimates by 2 sec. The WAM T_p also persists in overestimating about 24 hours longer than WIS. Similar to 44014 both model peak wave directions are in reasonable agreement except that WIS shifts 6 hours earlier than WAM on the 13th. Both model wave spreads are similar and follow the measured spread well except for an underestimation of 10° to 20° during the storm decay. Little difference exists between the model PCCs. The trend is similar to 44014 but the increase and decrease of the PCCs is more abrupt during the growth and decay of the storm.
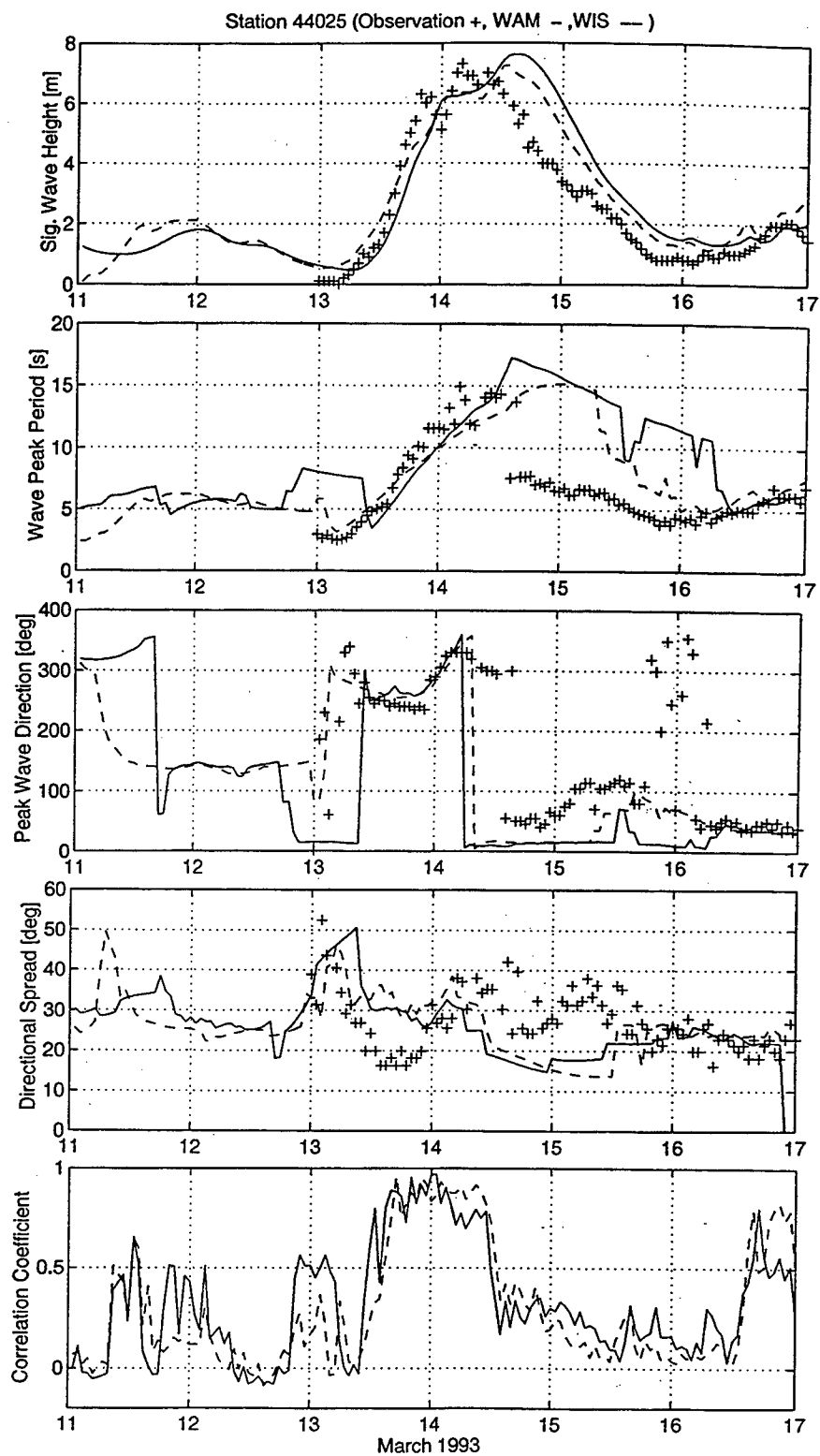
Figure 65. H_s, T_p, θ_p, σ, and PCC at 44025 for SOC.

f. Summary

The SOC represents an extreme event with a peak wind speed of 27 m/s. The simulated wind speeds have a negative bias but are reasonably well specified as shown by SIs below 20% except for one location. Errors in the wind speed and possibly depth effects cause considerable errors in H_s and T_p at several locations. Both models estimate H_s well at the two southern most location (41006 and 41010) but significant errors exist for the more central locations. The PCC for both models is very low except for the growth stage of the storm.

CHAPTER V

SUMMARY AND CONCLUSIONS

The objective of this study is to assess the relative performance of a *second generation* (2G) model, WISWAVE (Hubertz 1992), and a *third generation* (3G) model, WAM (WAMDI 1988), in deep water. High-quality wind fields, with detailed spatial and temporal resolution, were used to force both models in an effort to isolate differences between their formulations. Statistical tests were used to compare these models to in situ measurements over a variety of meteorological scenarios.

Even though previous studies (Cardone et al. 1996) have compared these models, this study is the first direct comparison where frequencies and directions have been discretized identically, no wind field interpolation was used and wave model grids are not nested. Nesting the grid of primary interest inside a larger domain grid allows the use of boundary conditions to represent wave energy originating from outside the primary grid but this adds another source of error in comparing the models' performance. The wind fields used in this study are the highest quality available for wave modeling, which minimizes errors in the wave models due to wind input, allowing direct insight into wave model deficiencies.

Five extra-tropical storm events which occurred along the US Atlantic coast were selected for comparison. All five historical wind fields were developed using kinematic analysis and objective techniques (Cardone et al. 1980 ; Cardone 1992). These storm events were selected because of the availability of high-quality winds and their variety of conditions ranging from extreme events to more moderate and variable events characterized by sea and swell, shifting

winds, and passage of cold fronts. Three of the storms occurred during the Surface Wave Dynamics Experiment (SWADE) (Weller et al. 1991) intensive operation periods (IOP) and are IOP1, IOP2, and IOP3. The remaining two storms, the "Halloween Storm" (HOS) and the "Storm of the Century" (SOC), were significant events causing flooding and damage along the Atlantic seaboard.

Each model was driven by identical wind fields, gridded to 1/2° latitude and longitude spatial resolution and 1-hour temporal resolution. Each model also had identical frequency bands, direction bands, and time steps. Both models were run in the deepwater mode since shallow water effects were not investigated in this study. Model results for these storms were compared to National Data Buoy Center (NDBC) buoy wave measurements.

The analysis of the results is divided into three steps. First, a qualitative comparison is made between model predictions and buoy data for the mean parameters: significant wave height H_s, mean wave period T_m, peak wave period T_p, peak wave direction θ_p, directional spreading coefficient, wind speed, and wind direction. Second, a series of statistical tests of the wave parameters was developed, including mean, bias, and RMS Error . In addition to the standard statistical parameters, a pattern correlation between model and measured 2-D spectra is presented.

The five simulations run for this study can be categorized into moderate storm conditions, dynamic lower energy conditions associated with frontal passages, and large extreme storm events. The IOP1 simulation represents a moderate case in terms of peak wind speeds which were 15 m/s to 25 m/s and has the best simulated winds of the five simulations considered. The wind speed scatter index (SI) at all locations is below 20% and ranges from 10% to 19%. The WAM H_s RMS Error is 0.01 m to 0.3 m less than that of WIS, but the WAM H_s has a negative bias ranging to about -0.5 m while WIS has at most a positive bias of about 0.3 m. Also the WAM

H_s SI is mostly lower than that of WIS for locations with a low wind speed SI. Both models have a negative T_p bias, more so for WAM, which ranges from -0.52 sec to -1.37 sec, than for WIS, which ranges from -0.25 sec to -1.08 sec. The WAM T_p RMS error is generally less than that of WIS with differences ranging from 0.01 sec to 0.42 sec, while the SI is generally similar for both models.

The directional wave spread for both models is wider than that of the buoy at the main peak of IOP1 because two wave systems are present but are not well separated in the frequency domain. During the decay of the storm both models' spread becomes too narrow. The pattern correlation coefficient (PCC) is relatively high during growth but decreases during decay. The first PCC decline is related to the two lobes of energy, one of which persists longer in the models than at the buoy location. The second PCC decline is related to the overly narrow spread in both models during the decay of the main storm event.

IOP2 and IOP3 represent dynamic conditions with frontal passages and peak wind speeds of 12 m/s to 20 m/s. The winds are not as well specified for IOP2 and IOP3 compared to IOP1. This is due to the difficulty in simulating the strong rapid wind shifts associated with the frontal passages. Both models underestimate H_s at the peaks although by a smaller margin and WAM underestimates more than WIS. Both models underestimate the T_p at the maximum storm peak and at times the model peak wave direction doesn't agree very well with the measured values. In both cases WIS appears to have a better response to rapidly changing wind speeds and directions.

The HOS and SOC simulations represent extreme events with peak wind speeds of 27 m/s. During the HOS, WIS estimates of H_s are consistently below that of WAM and usually underestimates the buoy wave heights while WAM has a tendency to overestimate the buoy measurements. This is opposite the trend found in the previous three simulations where WIS usually estimated H_s higher than WAM and overestimated the storm peaks. Both models

underestimate the T_p near the peak of the storm, but WIS is closer than WAM. Both model peak wave directions in some cases have large errors due to bi-modal spectra. The model wave spread becomes too narrow during the decay and both models underestimate spread most of the time. The PCC for both models is not as good as the three previous simulations during the first three days. This suggests a need for longer spin-up, or a presence of energy originating from outside the grid domain. Also, unlike other simulations, the PCC begins to decline as H_s increases.

For the SOC, simulated wind speeds have a negative bias but are reasonably well specified as shown by SIs below 20% except for one location. Errors in the wind speed and possibly depth effects cause considerable errors in H_s and T_p at several locations. Both models estimate H_s well at the two southern most buoy locations (41006 and 41010), but significant errors exist for the more central locations. The PCC for both models is very low except for the growth stage of the storm.

In order to summarize some of the differences found between the models, a series of scatter plots is presented which includes all storms. Figure 66 shows the model H_s plotted against the buoy H_s for WAM and WIS, at location 44014. Note that the depth for this location is 48 m and the models may have errors due to neglect of depth effects. Comparison of the two plots shows that, in general, the WAM H_s has slightly less scatter than that of WIS. For IOP1 the small scatter for both models indicates that this was the best simulation for both models except for the error at the largest H_s which may be due to the neglect of depth effects. In this simulation WAM has the least scatter and WIS is more positively biased. For IOP2 WAM is more negatively biased including the largest H_s while the largest H_s for WIS are positively biased. The models are very similar for IOP3 but WIS has more scatter and is positively biased. Dramatic differences are evident for HOS with WIS being limited to about a 5 m H_s while the WAM H_s is within 1 m of the buoy H_s of about 8 m. Both models have very large scatter for the SOC which is due to wind errors and possibly some depth effects.
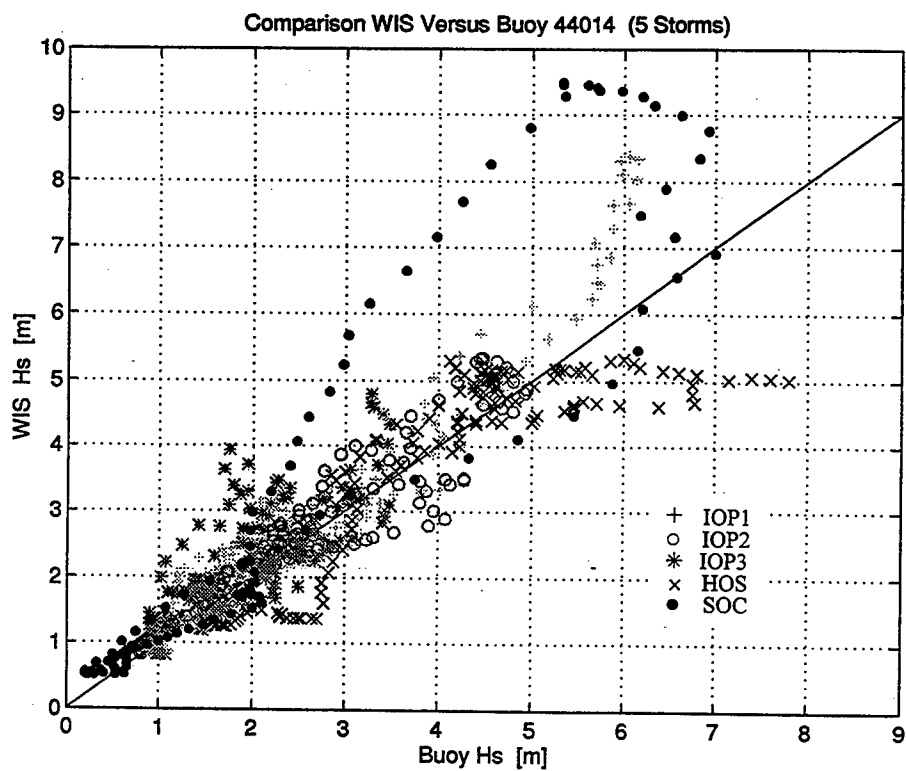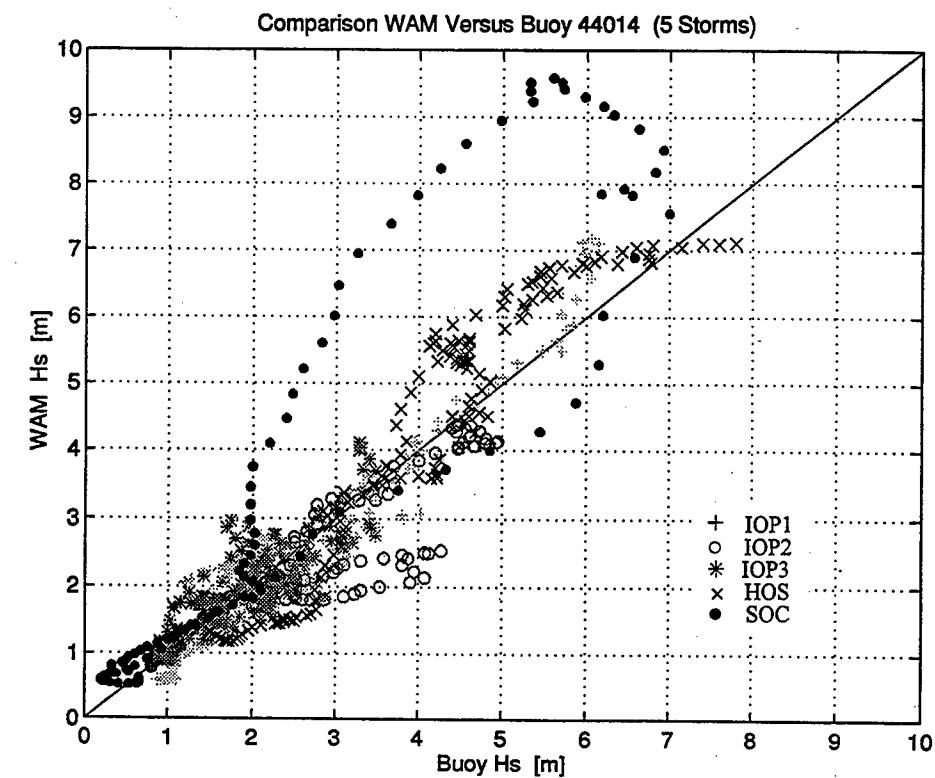
Figure 66. WAM and WIS H_s versus buoy H_s at 44014 for all storms.
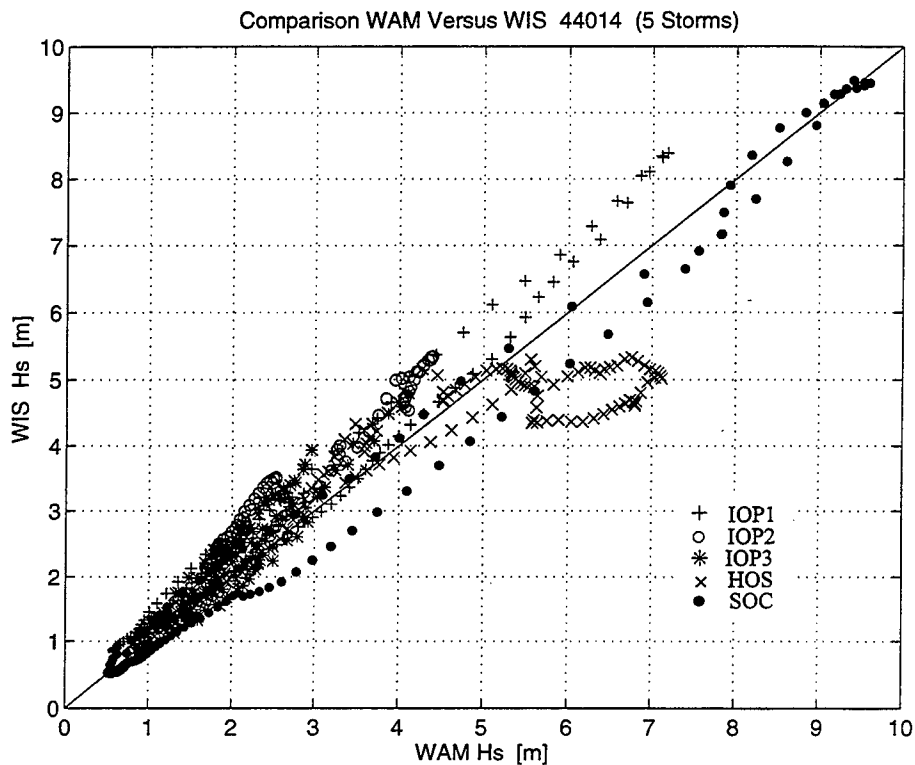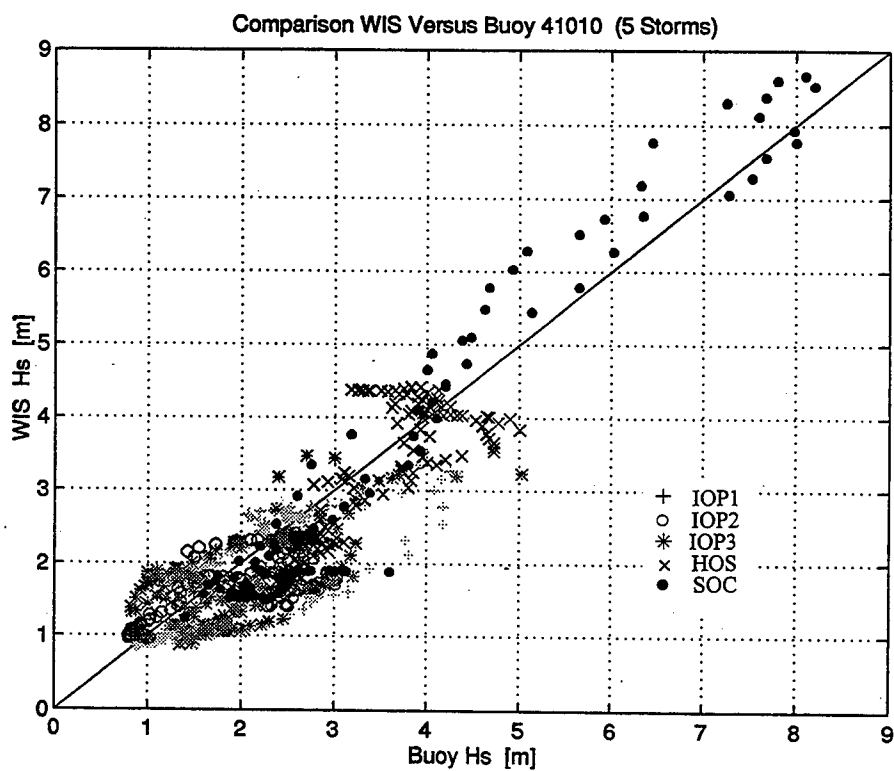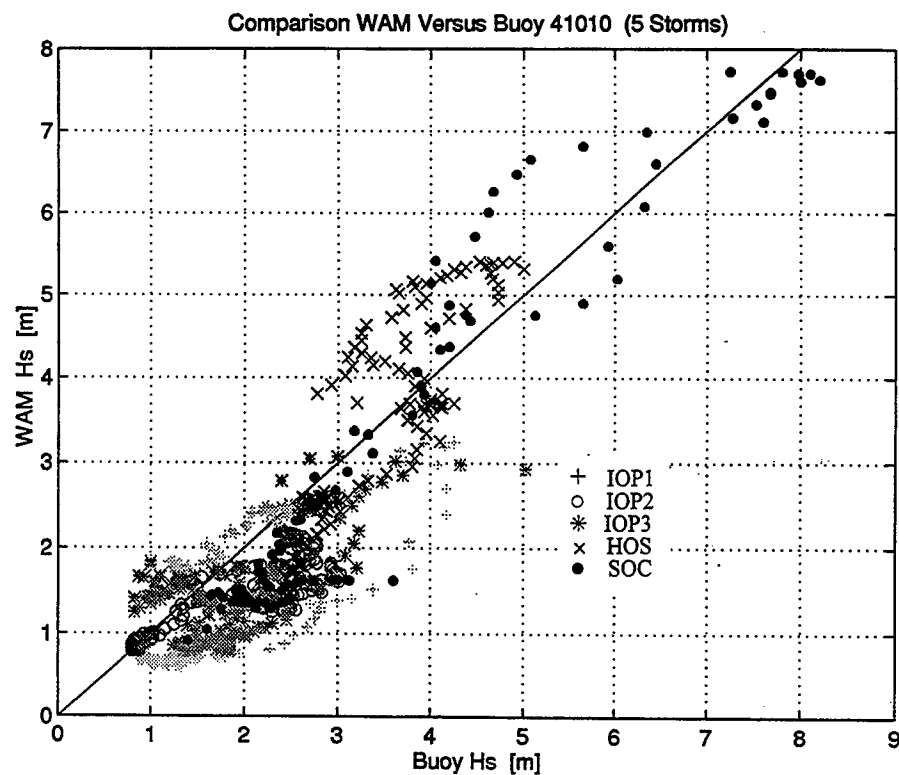
Figure 67. WAM H_s versus WIS H_s at 44014 for all storms.

Differences between the two models can be seen more readily in the plot of WAM H_s versus WIS H_s at 44014, shown in Figure 67. Overall, H_s is increasingly biased toward WIS with increasing H_s except for the HOS and SOC, the two extreme events.

Figure 68 shows the model H_s plotted against the buoy H_s for WAM and WIS, at location 41010. Both models show very similar H_s scatter which is similar to the results for IOP1, IOP2, and IOP3. For these simulations this location is well south of the storms and in most cases shows large underestimates of wind speeds which leads to large negative H_s biases. Again the limit to the WIS H_s can be seen for HOS. For SOC this location is in an area that is dominated by active wave

Figure 68. WAM and WIS H_s versus buoy H_s at 41010 for all storms.
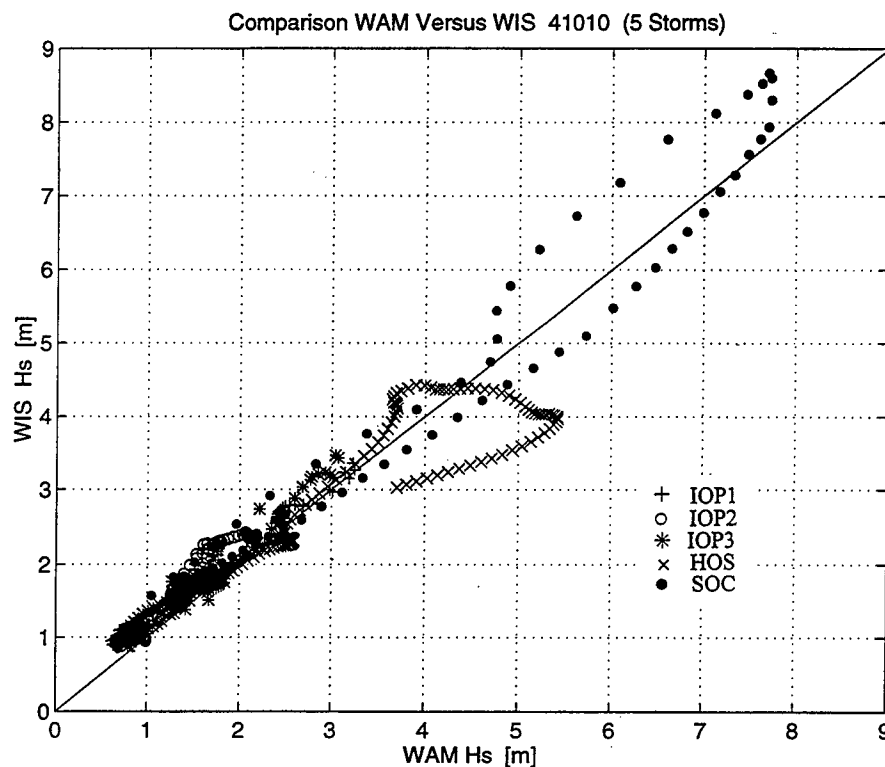
Figure 69. WAM H_s versus WIS H_s at 41010 for all storms.

growth. In this case WIS has less scatter than WAM but is positively biased while WAM has a small negative bias for the largest H_s. Figure 69 shows the WAM H_s versus the WIS H_s at 41010. The most significant events at this location were the SOC and the HOS. For the HOS this location is outside the area of the main storm and is affected primairly by swell. The plot shows that there is a 1.5 m bias toward WAM during the later part of the simulation. During the SOC 41010 is in an area of active wave generation as the storm moves off the coast into this area. The model H_s are similar except for a 1 m bias toward WIS during the growth portion of the simulation.

The following discussion presents two of the more consistent tendencies found in the models' performance. Figure 70 shows the relationship between wind speed bias and model H_s bias for both models and includes all locations and storms. For a well behaved wave model the H_s

Wind Speed Versus Wave Height Bias (WAM [+] WIS [o])
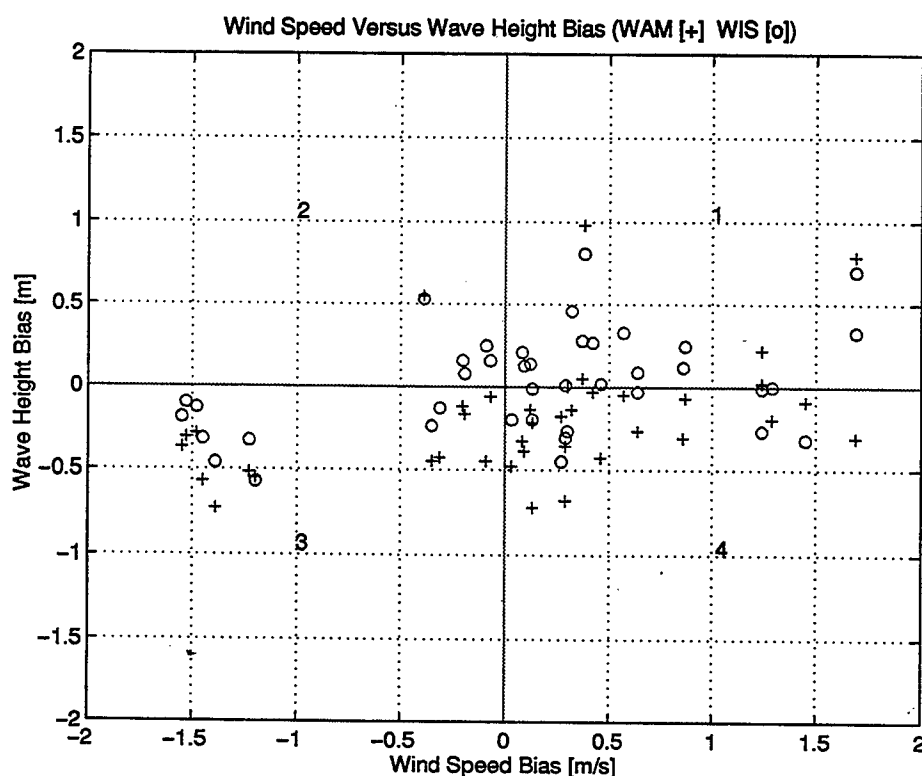
Figure 70. Wind speed bias versus H_s bias for all storms and locations.

bias should correspond to the wind speed bias. That is, for a positive wind speed bias the H_s bias should be positive (quadrant 1), and for a negative wind speed bias the H_s should also be negatively biased (quadrant 3). For wind speeds with a positive bias of up to 2 m/s there is a tendency for the WIS H_s to be biased positively while WAM tends to be more negatively biased. This suggests that, over all, WIS will tend to slightly overestimate H_s and WAM will slightly underestimate H_s and this is what occurs in many cases where wave growth is the dominant process.

Similarly, Figure 71 shows the wind speed bias verses the model T_p bias which, for a well behaved wave model, should fall in quadrant 1 or 3. The general trend here is for both models to have negatively biased T_p and this is what is shown in the statistics and time series plots especially around the peak H_s.
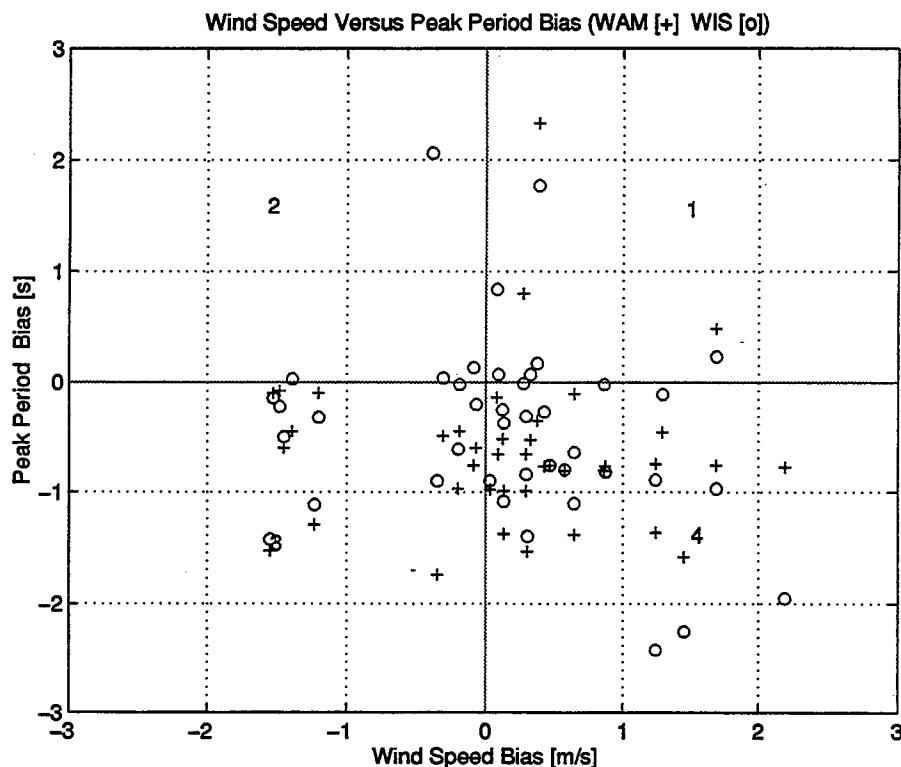
Figure 71. Wind speed bias versus T_p bias for all storms and locations.

A simplified test to determine the response of the wave models to rapidly turning winds was presented in Chapter II. This test showed that the WIS peak wave direction responded at twice the rate of WAM. This faster response can be seen in the better estimation of H_s by WIS for IOP2 and to a lesser extent for IOP3. The differences are less dramatic for IOP3 because the frontal passages were not as strong for this event. In some cases the WIS H_s leads the buoy even though the modeled wind speed is in phase or lags the buoy. This may be due to an over sensitivity to the wind input, or wind errors upwind of the buoy.

During the HOS simulation a situation with constant a 20 m/s wind speed and constant wind direction of 200° lasting for 24 hours existed. This is very similar to the fetch and duration limited growth test presented in Chapter II and similar behavior is expected between the test and

simulation. However the opposite trend occurs in the simulation where the WIS H_s is slightly higher than WAM in the beginning and is eventually exceeded by the WAM H_s within 24 hours. The behavior of the models during the simulation is influenced by previously existing conditions and it is likely that swell propagation as well as wave growth existed at this location and time.

In areas where propagated swell becomes an increasingly more significant part of the spectrum both models have a tendency to under specify H_s. In the HOS, WIS consistently underestimates H_s more than WAM for these swell influenced areas. It appears that WIS is more dissipative than WAM in this case however this trend is not evident in the SOC. This difference between the two simulations may be due to the complexity of HOS, which included a hurricane, an extratropical storm, and longer wave periods, with a maximum T_p of 22 sec for the HOS while the SOC had a maximum T_p of 17 sec.

Several disadvantages in model setup and analysis methods should be considered in the interpretation of the simulation results. Some cases have been identified in which wave model errors are due to the implementation of the model. These include the presence of energy coming from outside the model domain which was not represented in the models since there was no boundary condition input and an inadequate spin up period to allow the model spectrum to reach the conditions indicated by the measurements.

A better understanding of the mechanisms responsible for the model differences could be gained through a spatial analysis of the wind and wave parameter distributions for each model. From this information fetch estimates could be made for comparison to the fetch limited growth test.

In this study differences and similarities between WIS and WAM performance have been shown for a variety conditions and some explanation for the cause of these differences and similarities are offered. In conclusion some guidance for the usage of these models and suggestions

for improvements are given.

Even though WAM was formulated, in part, to improve performance over 2G models during rapidly turning winds found in hurricanes, small cyclones, and frontal passages, WIS performs better in the two cases considered in this study, IOP2 and IOP3, which contain rapidly turning winds associated with frontal passages. Directional relaxation rates have been computed for previous versions of WAM (Young et al. 1987) and were consistent, although slower for lower frequencies, with rates inferred from airborne radar observations (Jackson and Jensen 1995). The cause for the deficiency in WAM during rapid wind shifts should be investigated by comparing directional relaxation rates from the present version of WAM (Cycle 4) to the previous version and to rates inferred from observations. The changes implemented in Cycle 4 may have reduced the response of WAM to rapid wind shifts.

WIS consistently performs better than WAM in cases where the winds are not well specified. This would correspond to wind speed SIs greater than about 25%. This suggests that WIS would be a better choice than 3GWAM: Cycle 4 for practical applications in which wind fields are not usually as accurate as those used in this study. On the other hand, WIS underestimates some H_s peaks during the HOS extreme event most likely due to dissipative swell propagation. This is a significant disadvantage considering WIS is used to establish design conditions for coastal structures.

Any efforts toward improving model performance will probably be directed to the more advanced WAM model. Several researchers have suggested higher order numerical schemes to improve model performance (Tolman 1992; Lin and Huang 1996; Bender 1996). Given that the numerics can affect the growth rate, response to shifting winds, propagation of swell and the

interaction between wind sea and swell, all processes that show varying degrees of apparent error in the model simulations of this study, the next investigation should implement a higher order numerical scheme in 3GWAM: Cycle 4 and determine the effect on the wave processes.

NOMENCLATURE

Abs Err	$=$	absolute error ;
a_1	$=$	first Fourier coefficient ;
B	$=$	refers to statistics of buoy wave parameters ;
b_1	$=$	second Fourier coefficient ;
CC	$=$	correlation coefficient ;
CPSD	$=$	cross power spectral density ;
c_g	$=$	group wave velocity ;
d	$=$	water depth ;
E_b	$=$	energy per bin of the buoy wave spectrum ;
E_b'	$=$	energy per bin of the model wave spectrum ;
$E(f)$	$=$	frequency spectrum ;
F	$=$	two dimensional wave spectrum ;
f	$=$	frequency ;
f_m	$=$	mean wave frequency ;
f_p	$=$	peak wave frequency ;
H_s	$=$	significant wave height ;
HOS	$=$	Halloween Storm ;
IOP1	$=$	Intensive Operation Period 1 ;
IOP2	$=$	Intensive Operation Period 2 ;
IOP3	$=$	Intensive Operation Period 3 ;
KA	$=$	kinematic analysis ;
L_o	$=$	deep water wavelength ;
MLM	$=$	maximum likelihood method ;
m_1	$=$	first centered Fourier coefficient ;
PCC	$=$	pattern correlation coefficient ;
U	$=$	wind speed ;
U_{10}	$=$	wind speed at 10 m elevation ;
U_*	$=$	frictional velocity ;
UTC	$=$	Universal Time Coordinate ;
$RMSE$	$=$	root mean square error ;
SI	$=$	scatter index ;
SOC	$=$	Storm of the Century ;
S_{ds}	$=$	wave dissipation source term ;
S_i	$=$	source terms ;
S_{in}	$=$	wind input source term ;
S_{nl}	$=$	nonlinear wave-wave interaction source term ;
T_m	$=$	mean wave period ;
T_p	$=$	peak wave period ;
t	$=$	time ;
α	$=$	Phillips equilibrium constant ;
θ	$=$	wave direction ;
θ_m	$=$	mean wave direction ;

$$\theta_o \quad = \quad \text{vector mean wave direction ;}$$
$$\theta_p \quad = \quad \text{peak wave direction ;}$$
$$\sigma \quad = \quad \text{directional wave spread ;}$$
$$\lambda \quad = \quad \text{longitude ;}$$
$$\phi \quad = \quad \text{latitude ;}$$

REFERENCES

Anctil, F., M. A. Donelan, G. Z. Forristal, K. E. Steele, and Y. Ouellet, 1993: Deep water field evaluation of NDBC-SWADE 3-m discus directional buoy. *J. Atmos. and Ocean. Tech.*, **10**, 97-112.

Bender, L. C., 1996: Modification of the physics and numerics in a third-generation ocean wave model. *J. Atmos. and Ocean. Tech.*, **13**, 726-750.

Bretschneider, C. L., 1952: Revised wave forecasting relationships. *Proc. 2nd International Conf. on Coastal Engr*, Berkley, CA, ASCE, 1-5.

Brissette, F. P., I. K. Tsanis, 1994: Estimation of wave directional spectra from pitch-roll buoy data. *J. Water, Port, Coastal, Ocean Eng.*, **120**, 93-113.

Capon, J., 1969: High-resolution frequency-wavenumber spectrum analysis. *Proc. IEEE, 57*, 1408-1418.

Cardone, V. J., A. J. Broccoli, C. V. Greenwood and J. A. Greenwood, 1980: Error characteristics of extratropical storm wind fields specified from historical data. *J. Petrol. Tech.*, **32**, 872-880.

_____, 1992: On the structure of the marine surface wind field. *3rd International Workshop of Wave Hindcasting and Forecasting*, Montreal, Quebec, May 19-22, 54-66.

_____, H. C. Grabber, R. E. Jensen, S. Hasselmann, and M. J. Caruso, 1995: In search of the true surface wind field in SWADE IOP-1: ocean wave modeling perspective. *The Global Atmos. and Ocean Sys.*, **3**, 107-150.

_____, R. E. Jensen, D. T. Resio, V. R. Swail, and A. T. Cox, 1996: Evaluation of contemporary ocean wave models in rare extreme events: "Halloween Storm" of October, 1991; "Storm of the Century" of March, 1993. *J. Atmos. and Ocean. Tech.*, **13**, 198-230.

Donelan, M.A. and W.J. Pierson, 1983: The sampling variability of estimates of spectra of wind-generated waves, *J. Geophys. Res.*, **88**, 4381-4392.

Gelci, R., H. Cazale, and J. Vassal, 1957: Prevision de la houle. La methode des densites spectroangularies. *Bull. Infor. Comite Central Oceangr. d'Etude Cotes*, **9**, 416-435.

Hasselmann, K. 1962: On non-linear energy transfer in a gravity-wave spectrum - Part 1. *J.Fluid Mech.*, **12**, 481-500.

_____, 1963a: On the non-linear energy transfer in a gravity-wave spectrum - Part 2. *J. Fluid Mech.*, **15**, 273-281.

_____ , 1963b: On the non-linear energy transfer in a gravity-wave spectrum - Part 3. *J. Fluid Mech.*, **15**, 385-398.

_____ , T.P. Barnett, E. Bouws, H. Carlson, D.E. Cartwright, K. Enke, J.A. Ewing, D.E. Hasselmann, P. Kruseman, A. Meerburg, P. Muller, K.J. Olbers, K. Richter, W. Sell, and W.H. Walden, 1973: Measurements of wind-wave growth and swell decay during the Joint North Sea Wave Project (JONSWAP). *Deutsche Hydrograph, Zeit., Erganzung-self Reihe* **A 8**(12).

Hasselmann, S., K. Hasselmann, J. H. Allender, and T. P. Barnett, 1985: Computations and parameterizations of the nonlinear energy transfer in a gravity-wave spectrum. Part II: Parameterization of the non-linear transfer for application in wave models. *J. Phys. Oceanogr.*, **15**, 1378-1391.

Hubertz, J.M., 1992: User's guide to the wave information studies (WIS) wave model, version 2.0. WIS Report 27, U.S. Army Engineer Waterways Experiment Station, Vicksburg, MS. 28pp.

_____ , R.M. Brooks, W.A. Brandon, and B.A. Tracy, 1993: Hindcast wave information for the US Atlantic Coast, WIS Report 30, U.S. Army Engineer Waterways Experiment Station, Vicksburg, MS. 20 pp.

Isobe, M., K. Kondo, and K. Horikawa, 1984: Extension of the MLM for estimating directional wave spectrum. *Symp. on Desc. and Model. of Direc. Seas,* Tech. University, Denmark, A-6, 1-15.

Jackson, F.C. and R.E. Jensen, 1995: Wave field response to frontal passages during SWADE. *J. Coastal Res.*, **11**, 34-67.

Janssen, P. A. E. M., 1991: Quasi-linear theory of wind wave generation applied to wave forecasting. *J. Phys. Oceanogr.*, **21**, 745-754.

Kuik, A. J., G. P. VanVledder, and L. H. Holthuijsen, 1988: A method for the routine analysis of pitch and roll buoy wave data. *J. Phys. Oceangr.*, **18**, 1020-1034.

Large, W. and S. Pond, 1981: Open ocean momentum flux measurements in moderate to strong winds. *J. Geophys. Res.*, **11**, 324-336.

Lin, R. Q., N. E. Huang, 1996: The Goddard Coastal Wave Model. Part I: Numerical method. *J. Phys. Oceanogr.*, **26**, 833-847.

Longuet-Higgins, M. S., D. E. Cartwright and N. D. Smith, 1961: Observations of directional spectrum of sea waves using the motions of a floating buoy. *Ocean Wave Spectra,* Englewood Cliffs, NJ, Prentice-Hall, Inc. pp 111-132.

Miles, J.W., 1957: On the generation of surface waves by shear flows. *J. Fluid Mech,* **3**, 185-204.

Mitsuyasu, H. 1968: On the growth of the spectrum of wind-generated waves 1. *Rep. Res. Inst. Appl. Mech., Kyushu University*, **16,** 459-465.

_____. 1969: On the growth of the spectrum of wind-generated waves. 2. *Rep. Res. Inst. Appl. Mech., Kyushu University*, **17,** 235-248.

National Weather Service, 1991a: Daily weather maps, January 7-13, 1991. U.S. Department of Commerce, National Oceanic and Atmospheric Administration, Washington, DC, 8 pp.

_____, 1991b: Daily weather maps, February 25 - March 3, 1991. U.S. Department of Commerce, National Oceanic and Atmospheric Administration, Washington, DC, 8 pp.

_____, 1991c: Daily weather maps, March 4 - 10, 1991. U.S. Department of Commerce, National Oceanic and Atmospheric Administration, Washington, DC, 8 pp.

Phillips, O.M. 1957: On the generation of waves by turbulent wind. *J. Fluid Mech.*, **2,** 417-445.

_____. 1958: The equilibrium range in the spectrum of wind-generated waves. *J. Fluid Mech.*, **4,** 426-434.

Pierson, W. J., G. Neuman, and R. W. James, 1955: Observing and forecasting ocean waves by means of wave spectra and statistics. Pub. No. 603, U.S. Navy Hydrographic Office, Washington, DC, 284 pp.

_____, W.J. and L. Moskowitz 1964: A preposed spectral form for fully developed wind seas based on the similarity theory of S.A. Kitiagordskii. *J. Geophys. Res.*, **9,** 5181-5190.

Resio, D. T., and W. Perrie, 1989: Implications of an f^4 equilibrium range for wind-generated waves. *J. Phys. Oceanogr.*, **19,** 193-204.

Shay, L. K., P. C. Zhang, H. C. Grabber, and E. J. Walsh, 1996: Simulated surface wave current interactions during SWADE. *The Global Atmos. and Ocean Sys.*, **5,** 125-150.

Sverdrup, H. U., and W. H. Munk, 1947: Wind, sea and swell: theory of relations for forecasting. Pub. No. 601, U.S. Navy Hydrographic Office, Washington, DC, 44 pp.

The SWAMP Group, 1985: Sea wave modelling project (SWAMP). An intercomparison study of wind wave prediction models, Part1: Principal results and conclusions. *Ocean Wave Modeling*, Plenum, NY, Plenum Press, 256 pp.

Tolman, H. L., 1992: Effects of numerics on the physics in a third-generation wind-wave model. *J. Phys. Oceanogr.*, **22,** 1095-1111.

WAMDI Group, 1988: The WAM model - a third generation wave prediction model. *J. Phys. Oceanogr.*, **18,** 1775-1810.

Weller, R.A., M.A. Donelan, M. G. Briscoe, and N. E. Huang, 1991: Riding the crest: A tale of two wave experiments. *Bull. Amer. Meteor. Soc.*, **72**, 163-183.

Wu, J., 1982: Wind-stress coefficients over the sea surface from breeze to hurricane. *J. Geophys. Res.*, **87**, 9704-9706.

Young, I.R., S. Hasselmann and K. Hasselmann, 1987: Computations of the response of a wave spectrum to a sudden change in wind direction. *J. Phys. Oceanogr.*, **17**, 1317-1338.

APPENDIX A

WIND TIME HISTORIES

142
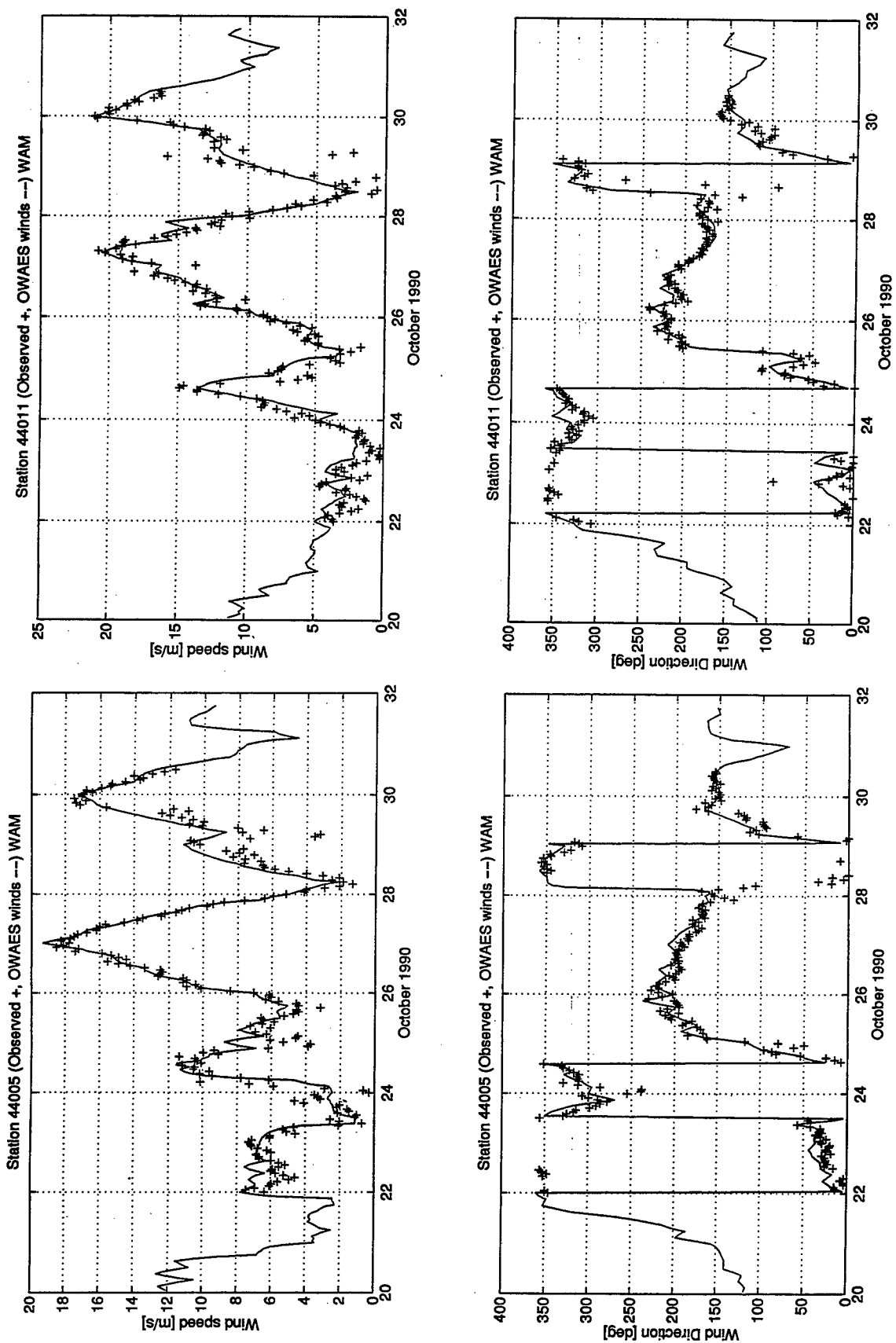
Figure A-1. Wind speed and direction time histories at 44005 and 44011 for IOP1.
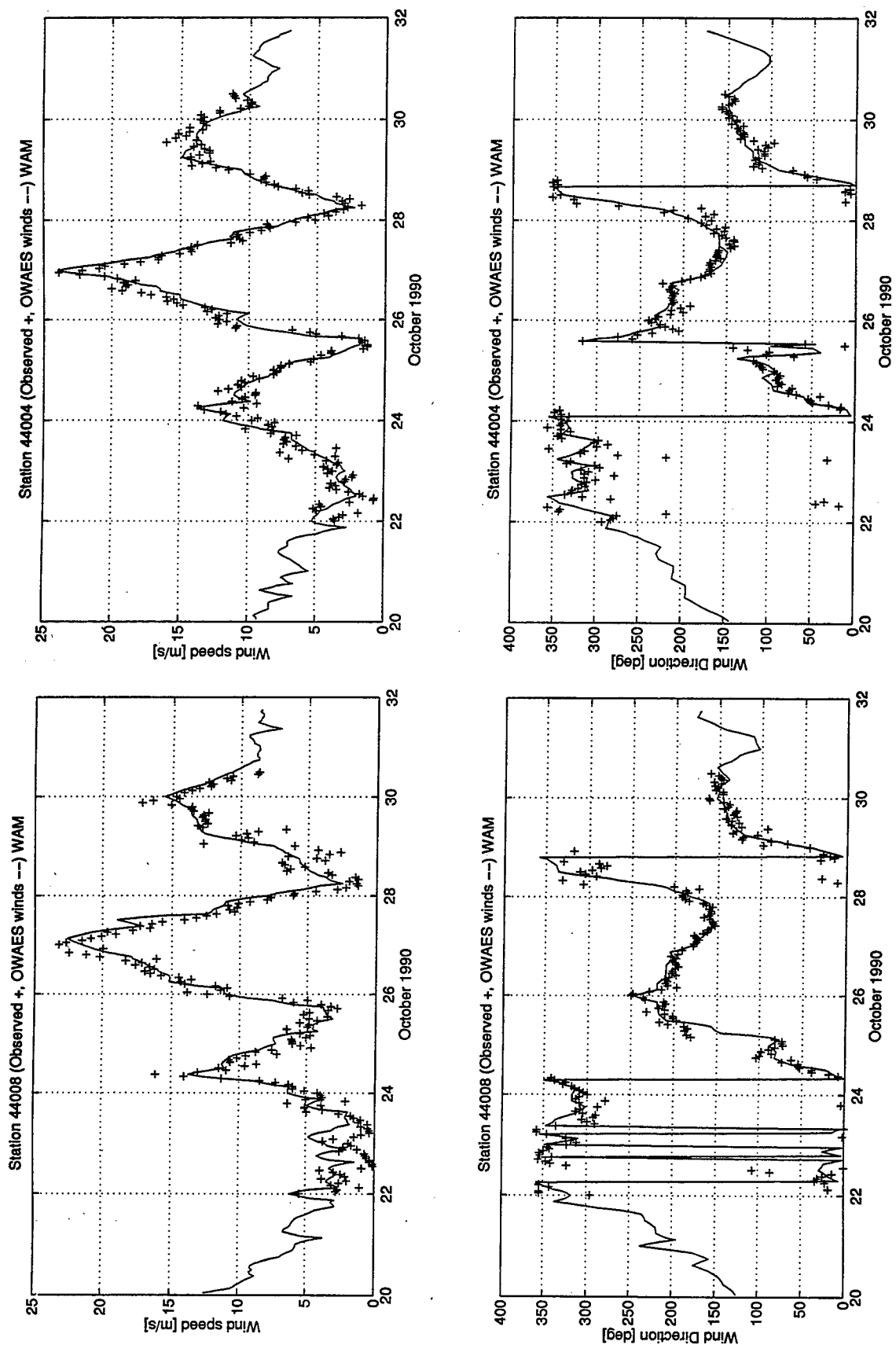
Figure A-2. Wind speed and direction time histories at 44008 and 44004 for IOP1.
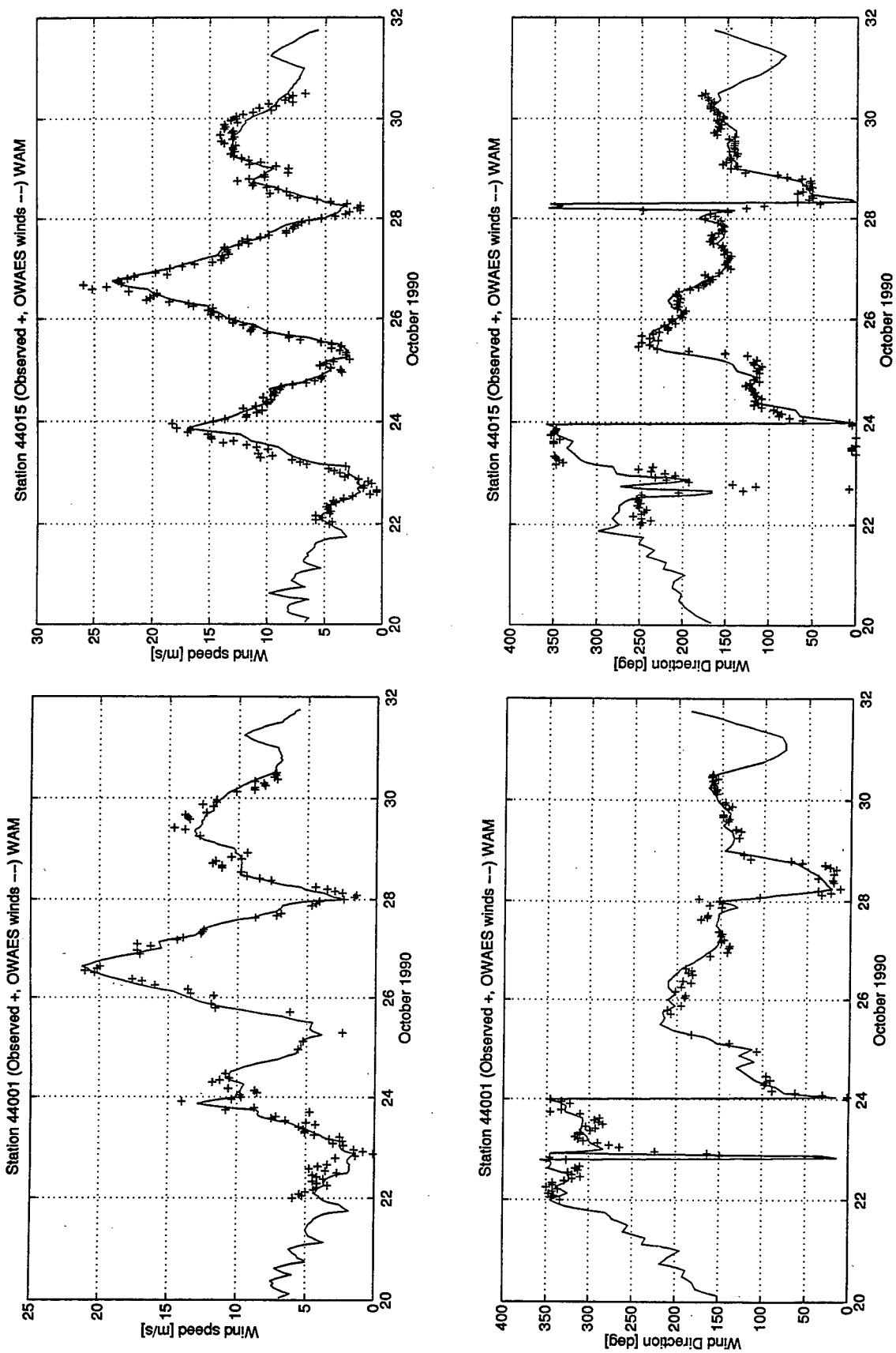
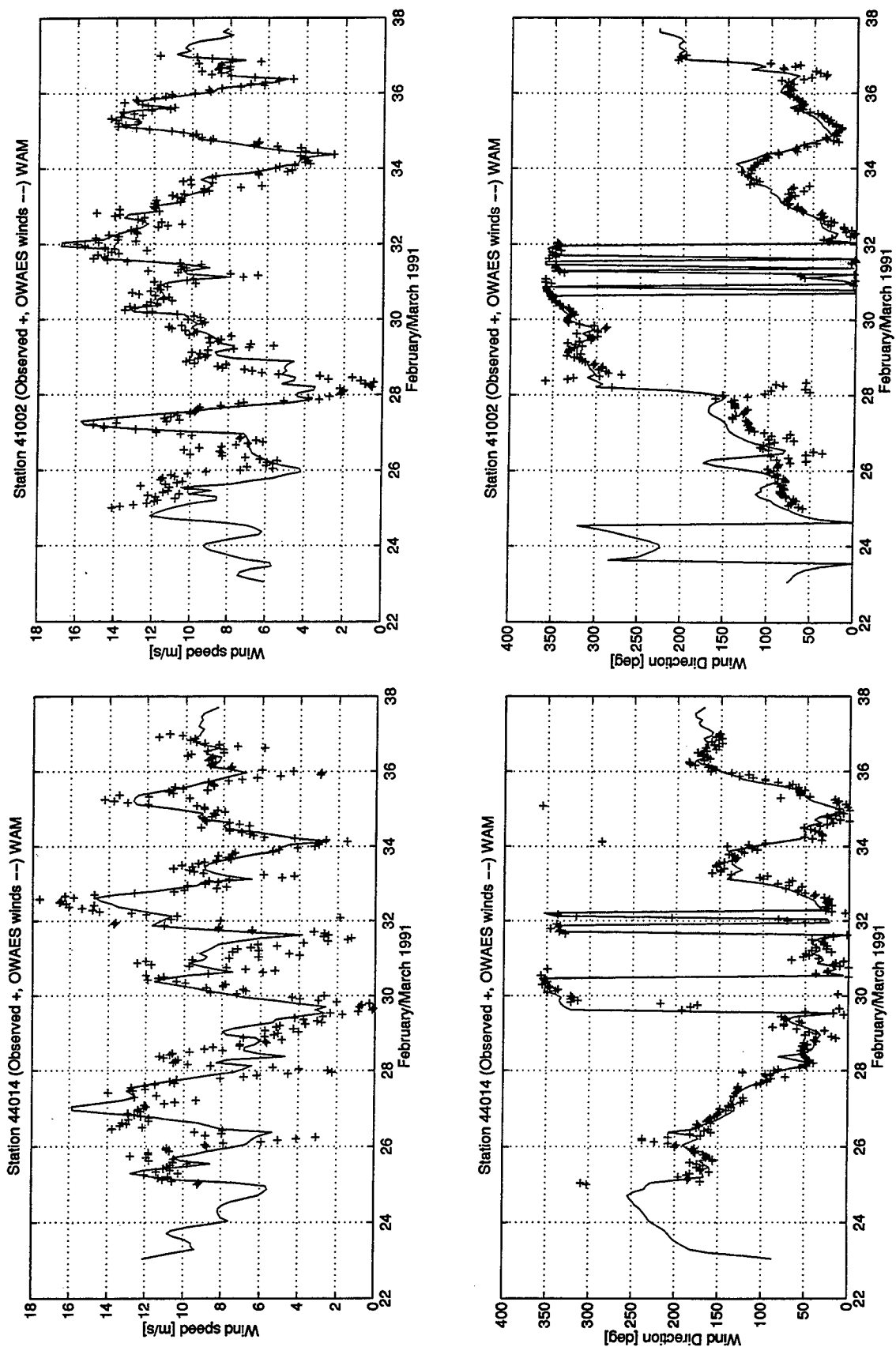Figure A-3. Wind speed and direction time histories at 44001 and 44015 for IOP1.
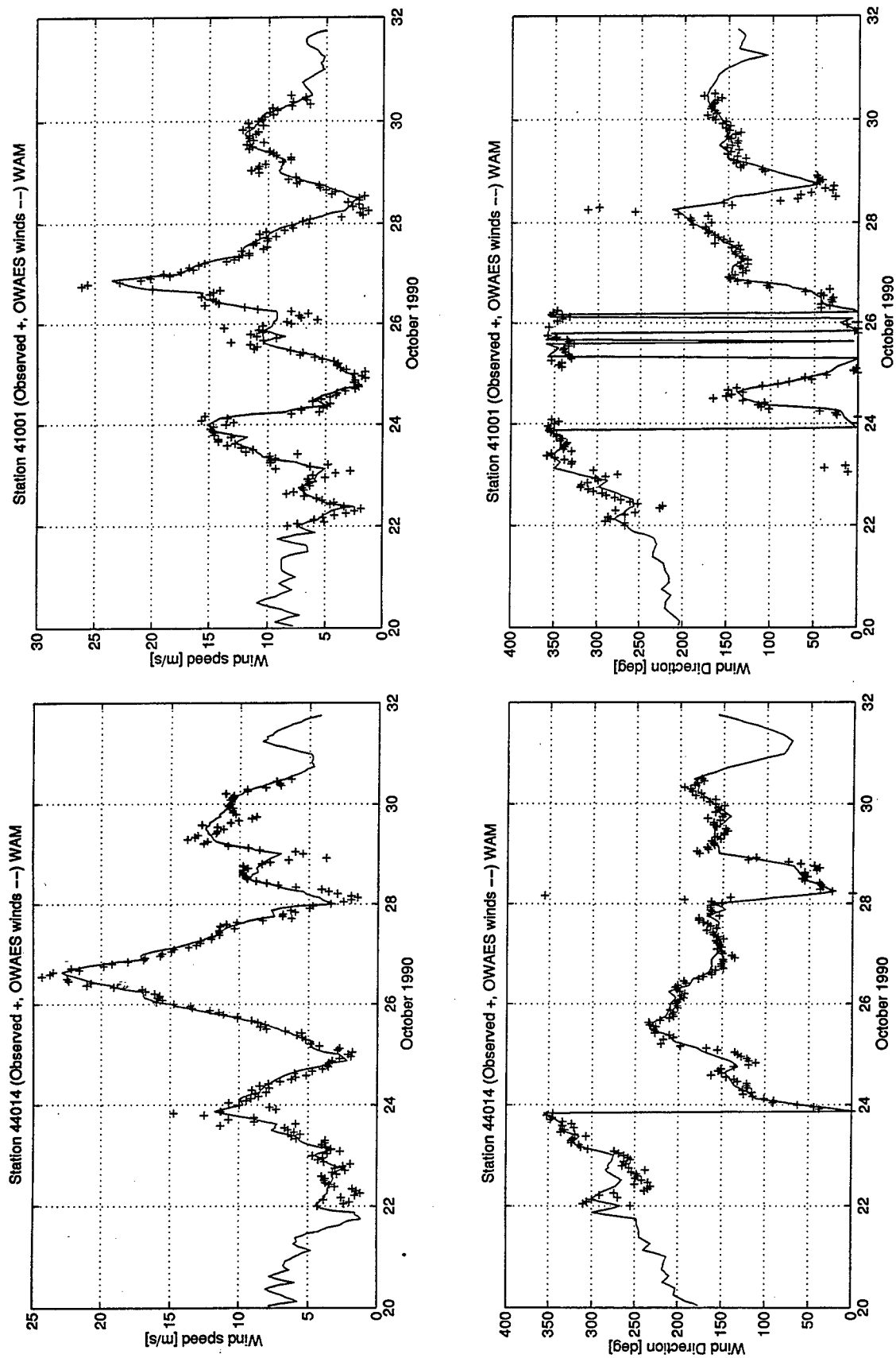
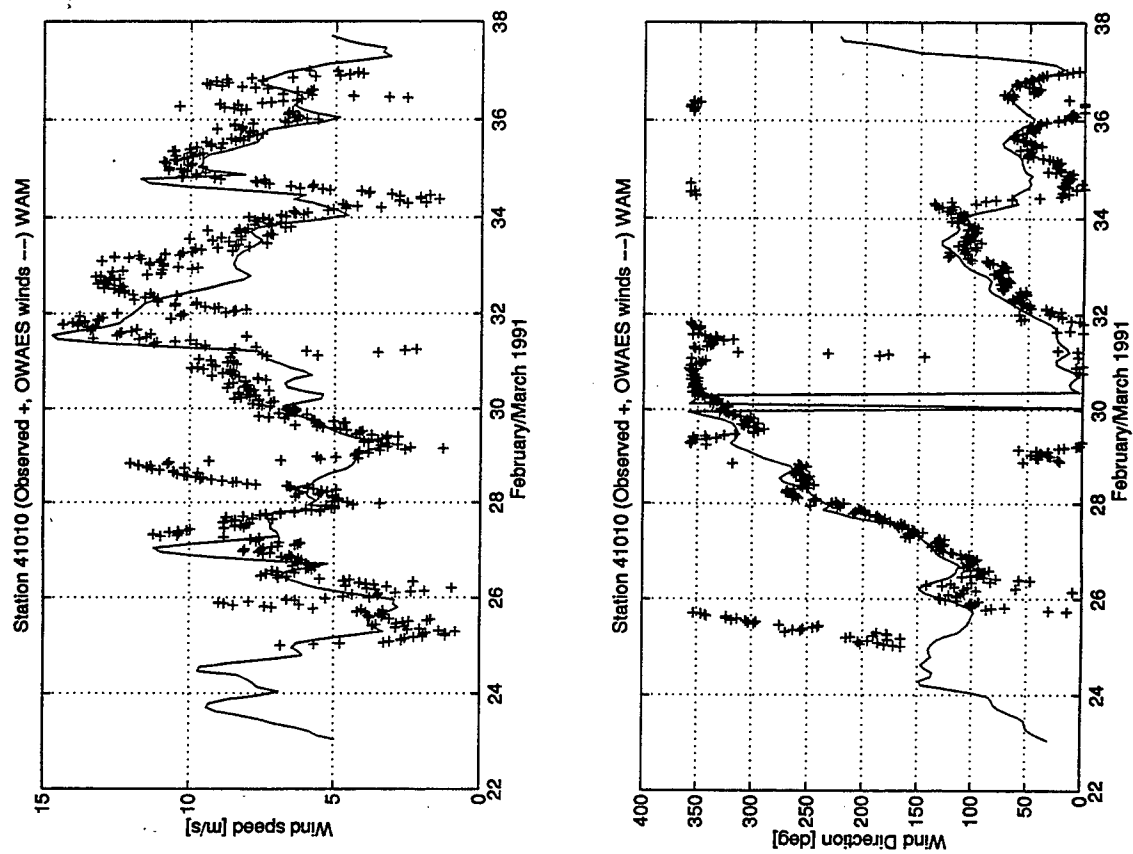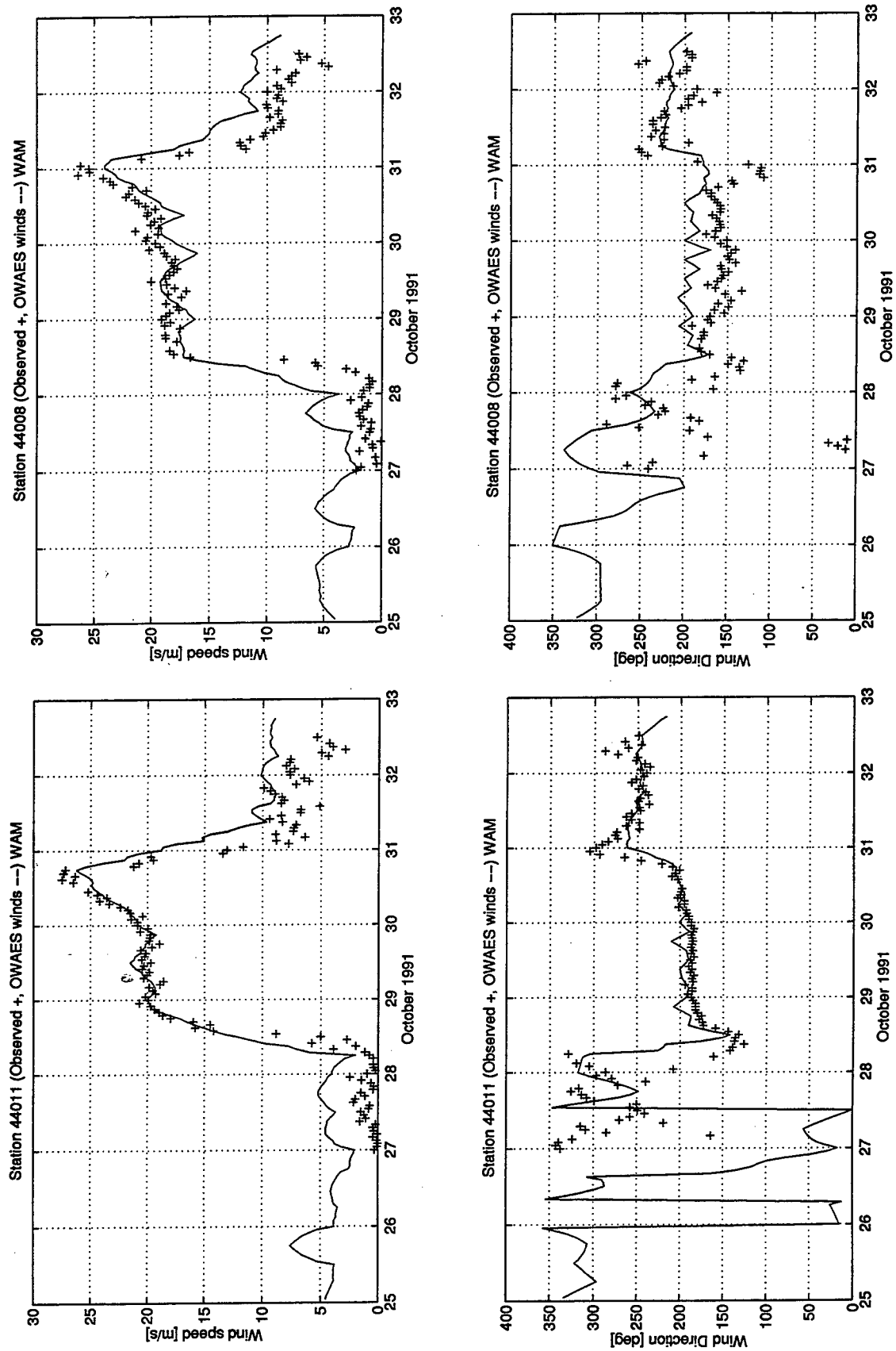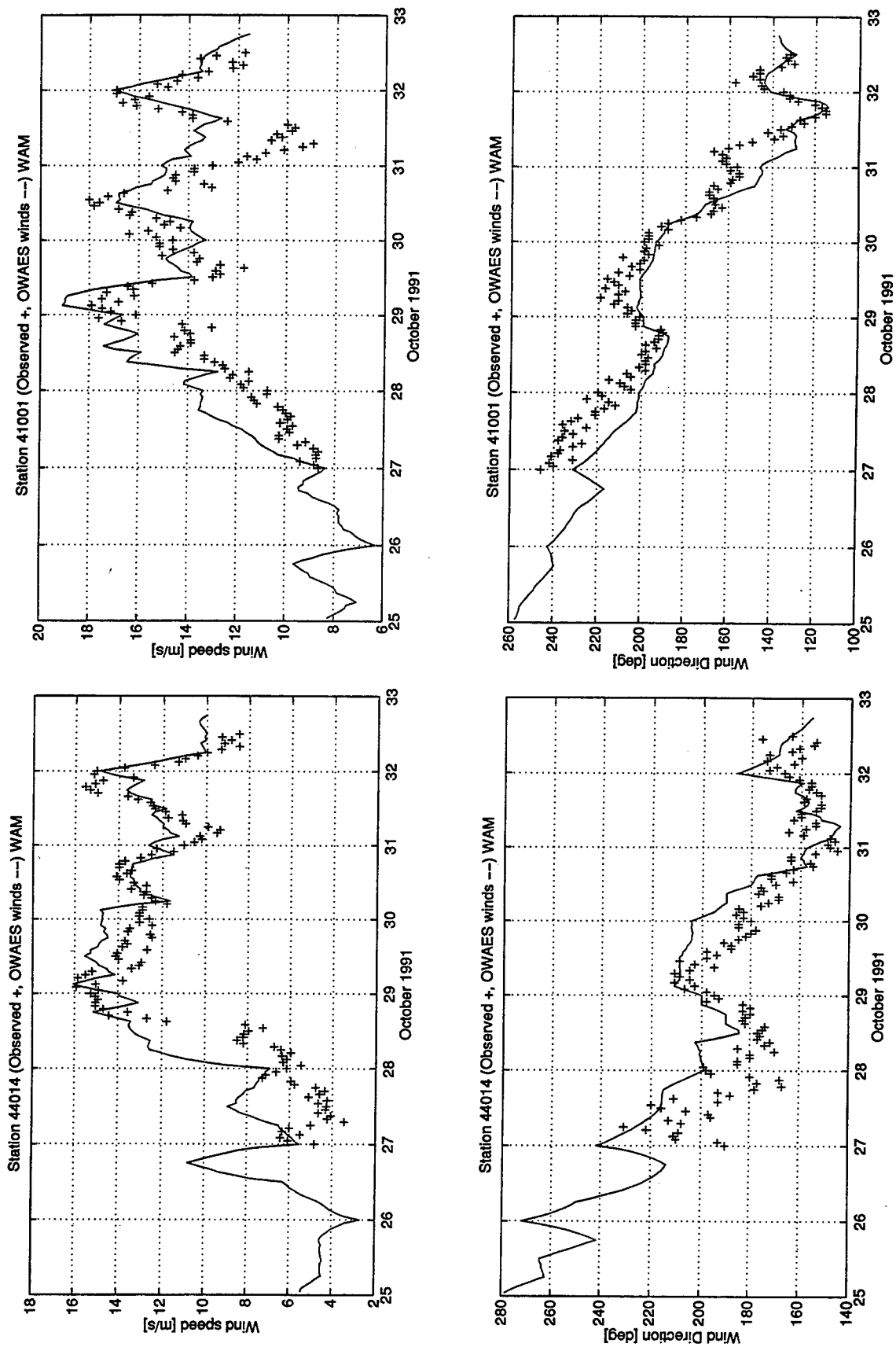Figure A-4. Wind speed and direction time histories at 44014 and 41001 for IOP1.
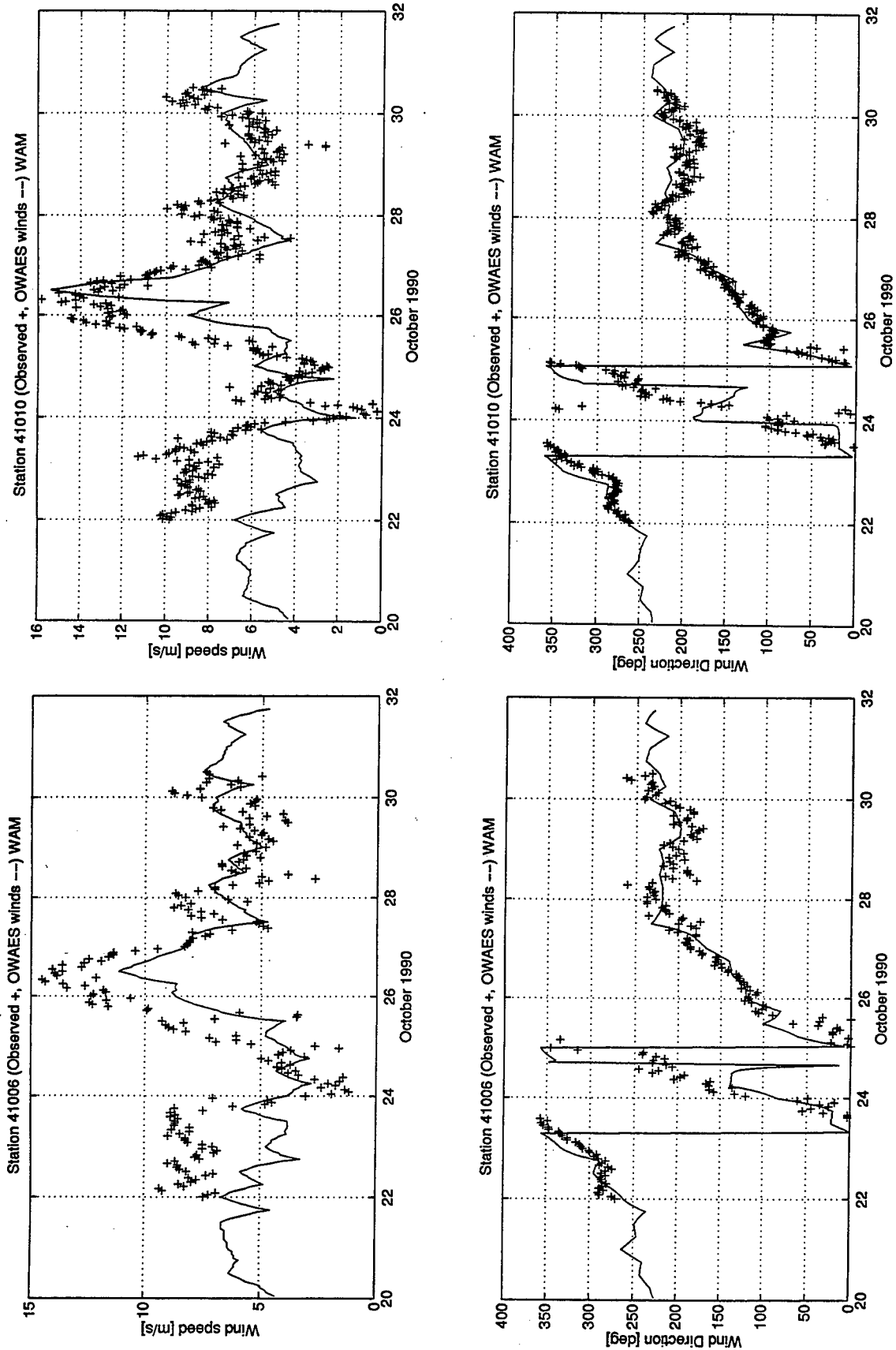
Figure A-5. Wind speed and direction time histories at 41006 and 41010 for IOP1.
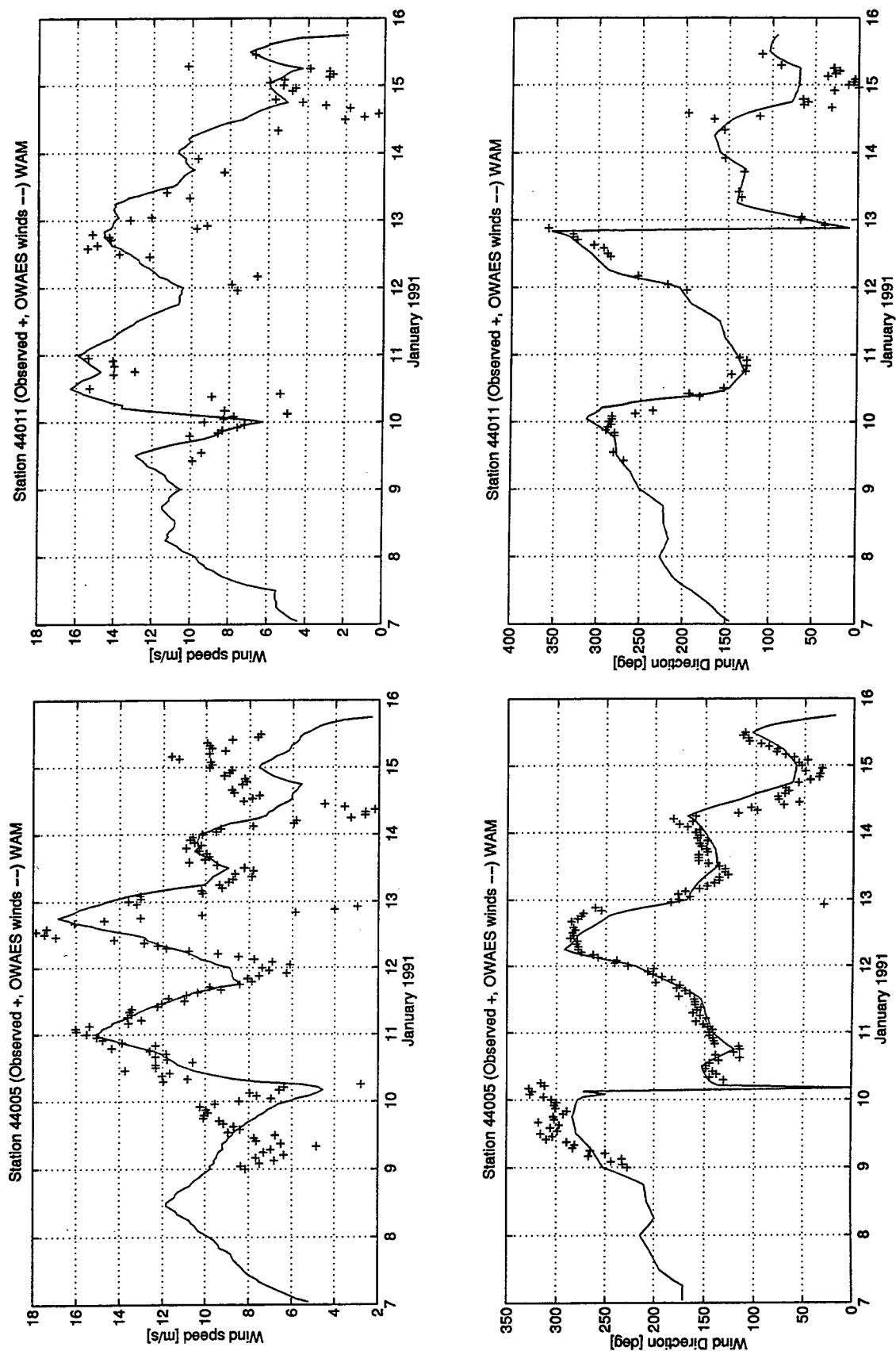
Figure A-6. Wind speed and direction time histories at 44005 and 44011 for IOP2.
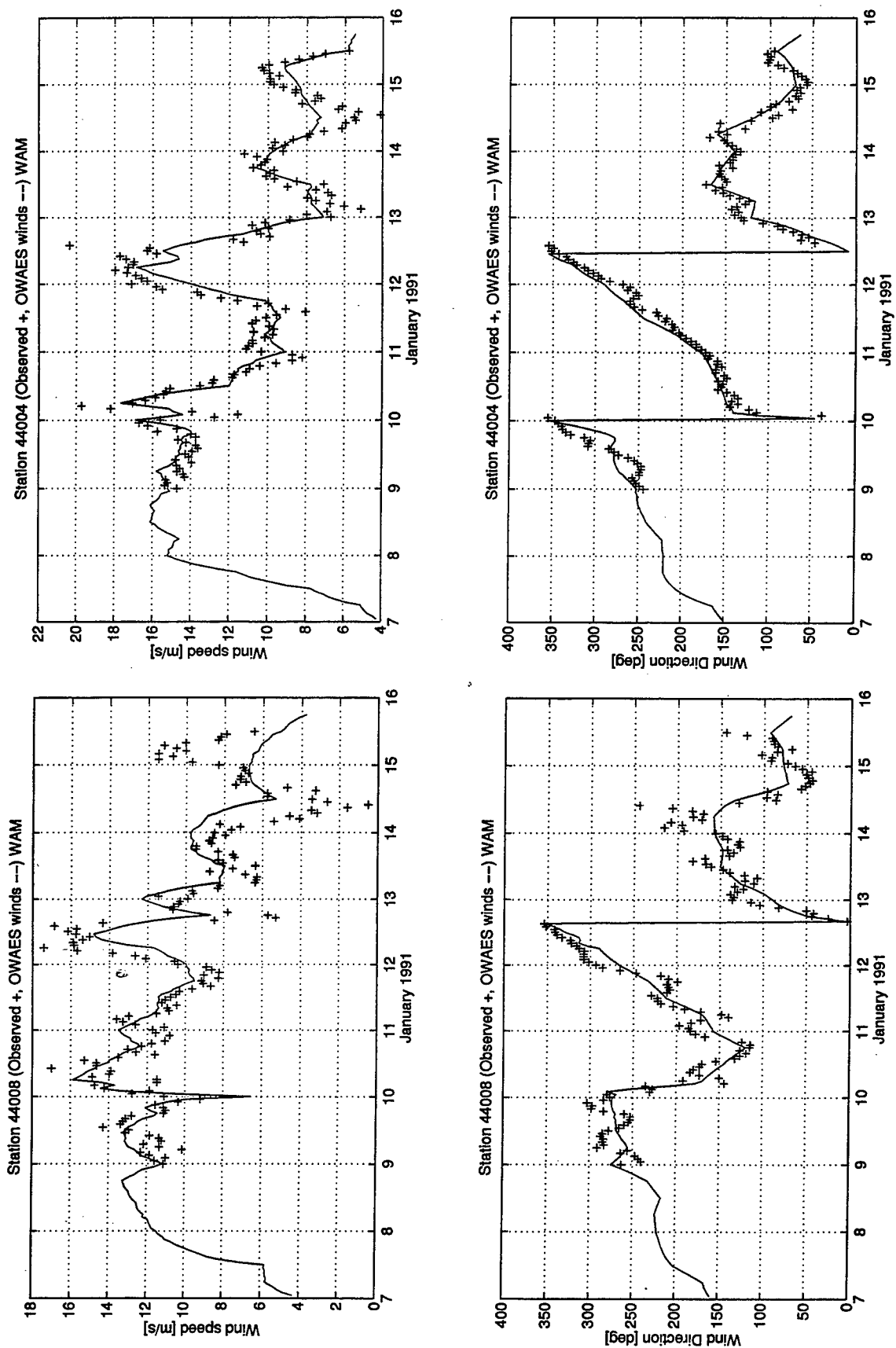
Figure A-7. Wind speed and direction time histories at 44008 and 44004 for IOP2.
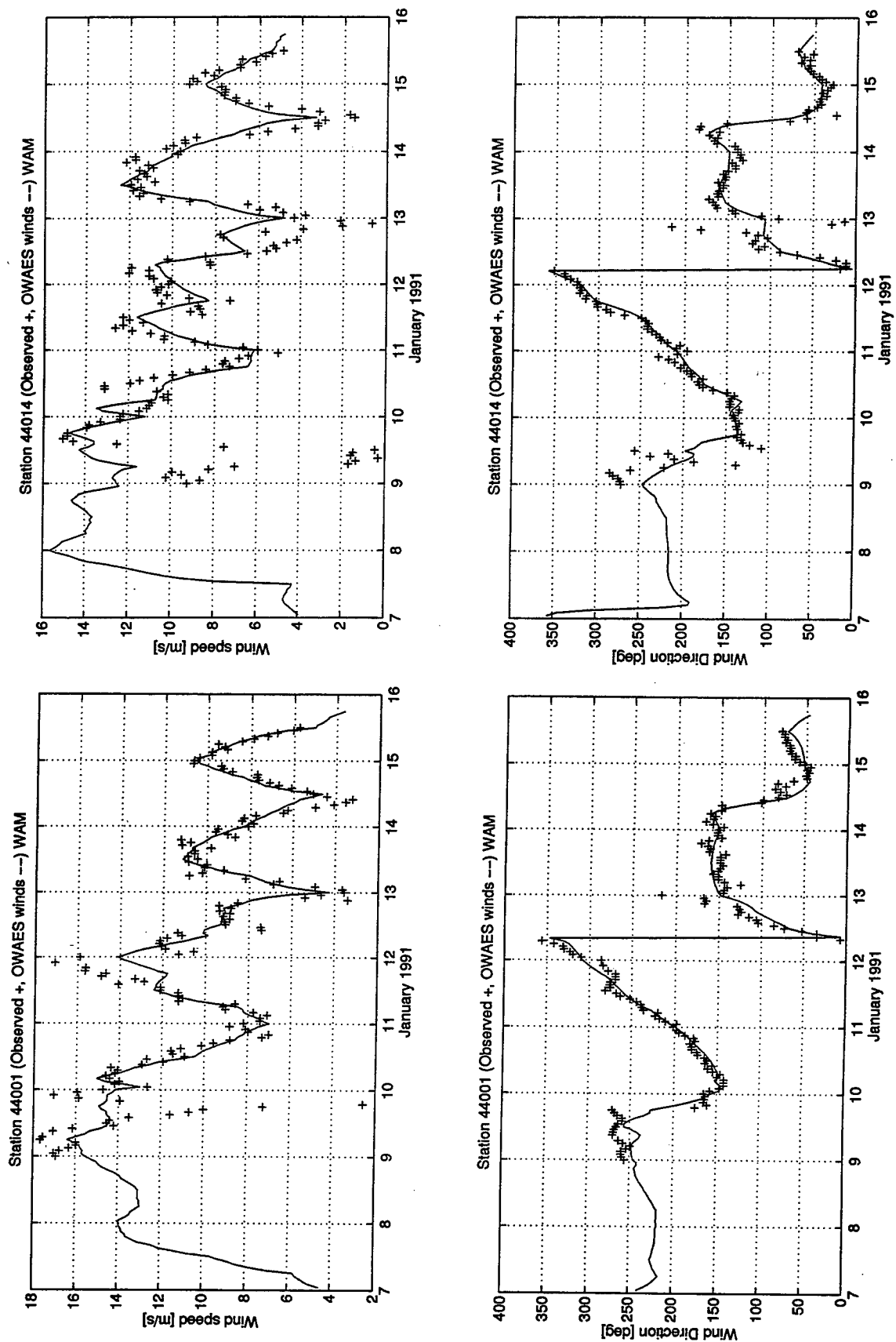
Figure A-8. Wind speed and direction time histories at 44001 and 44014 for IOP2.

149
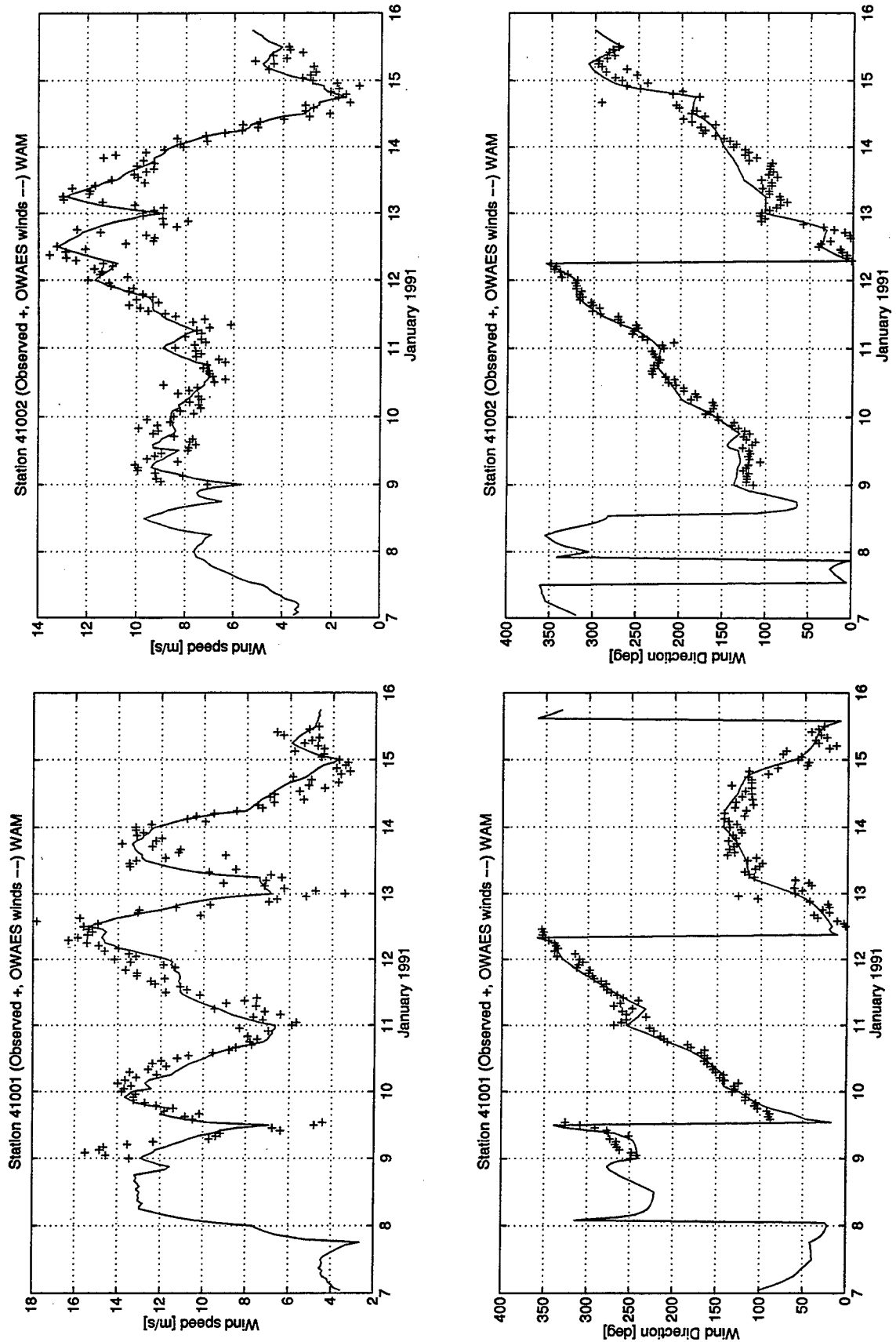
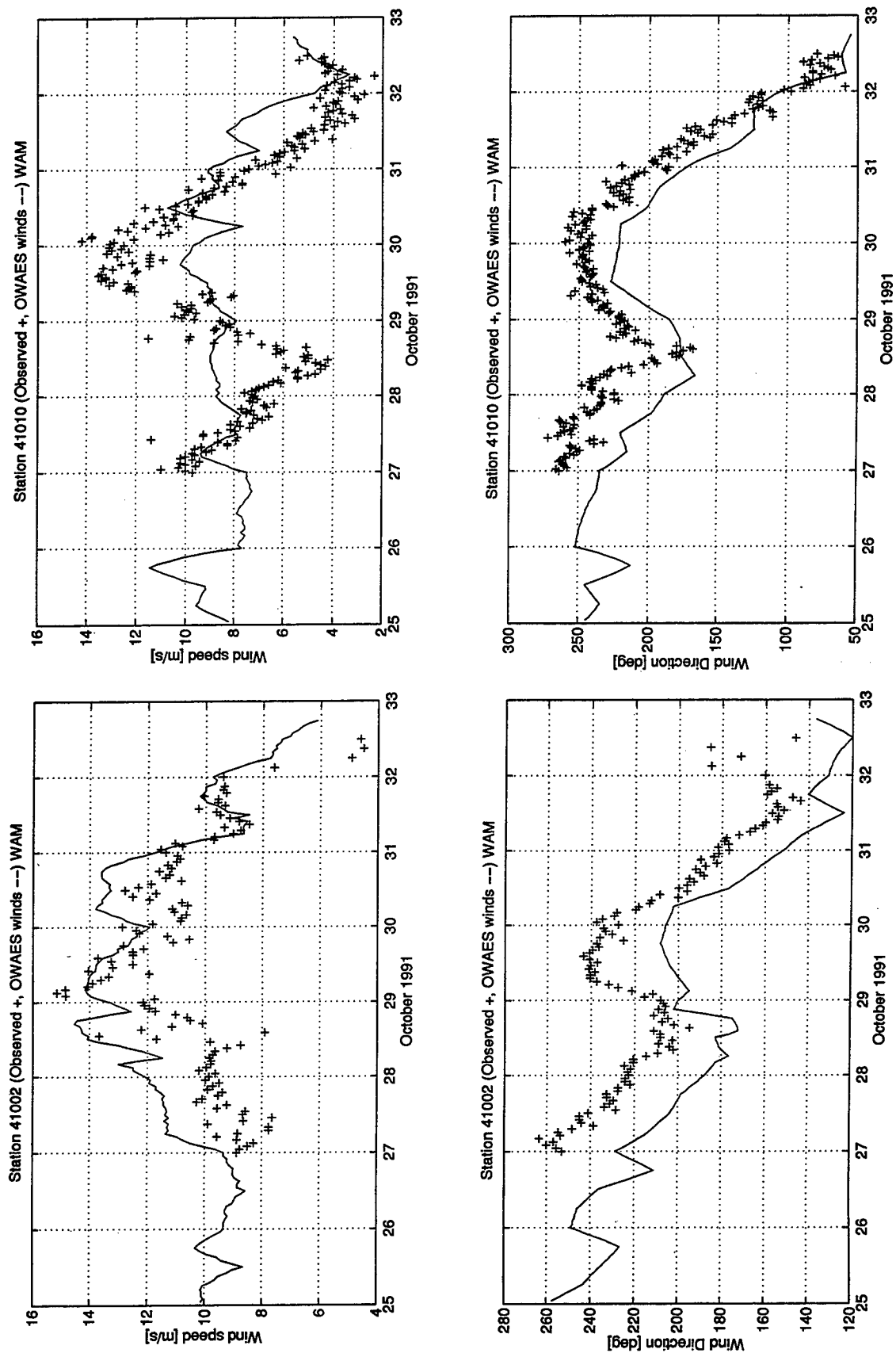Figure A-9. Wind speed and direction time histories at 41001 and 41002 for IOP2.
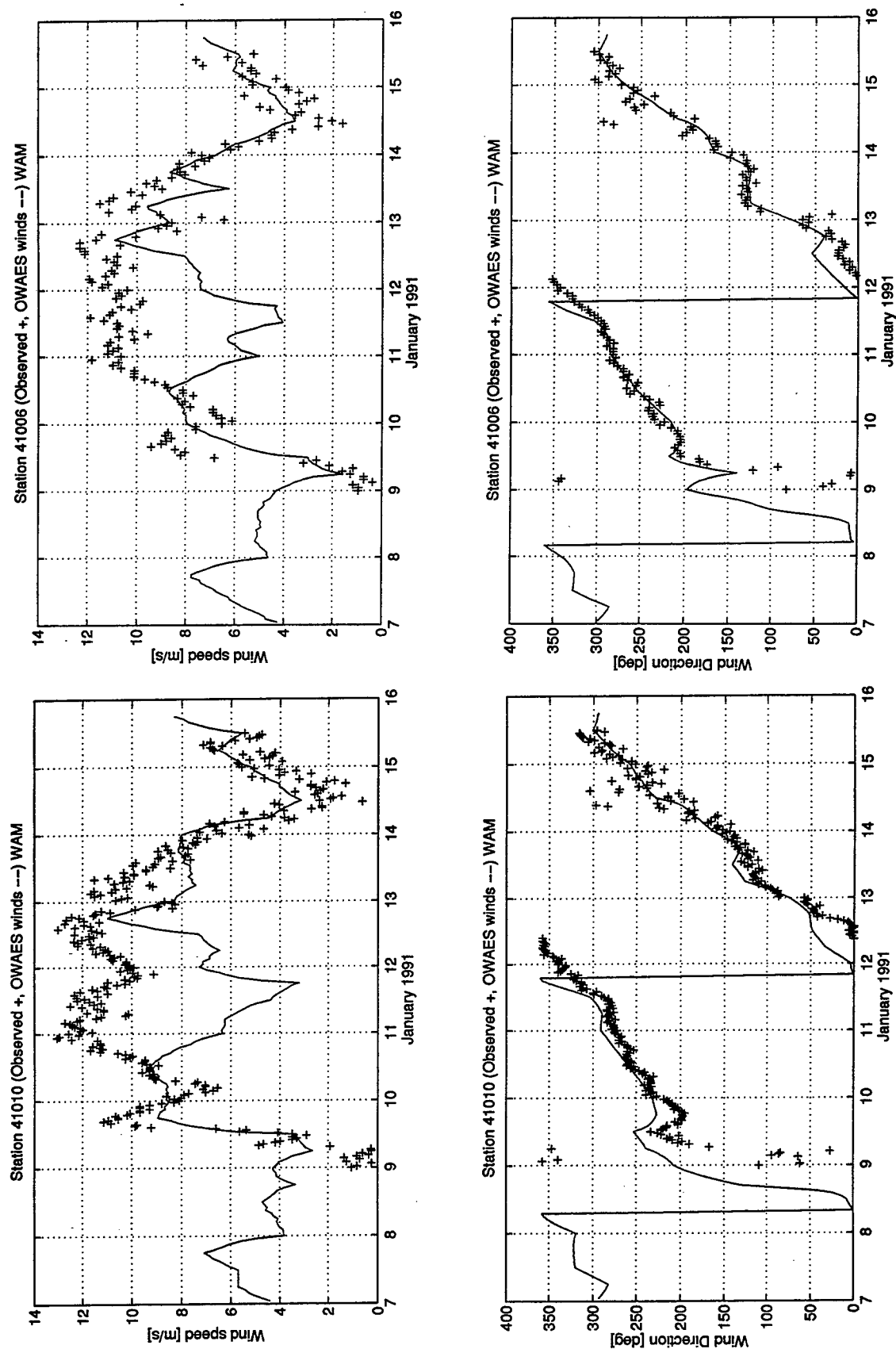
Figure A-10. Wind speed and direction time histories at 41010 and 41006 for IOP2.
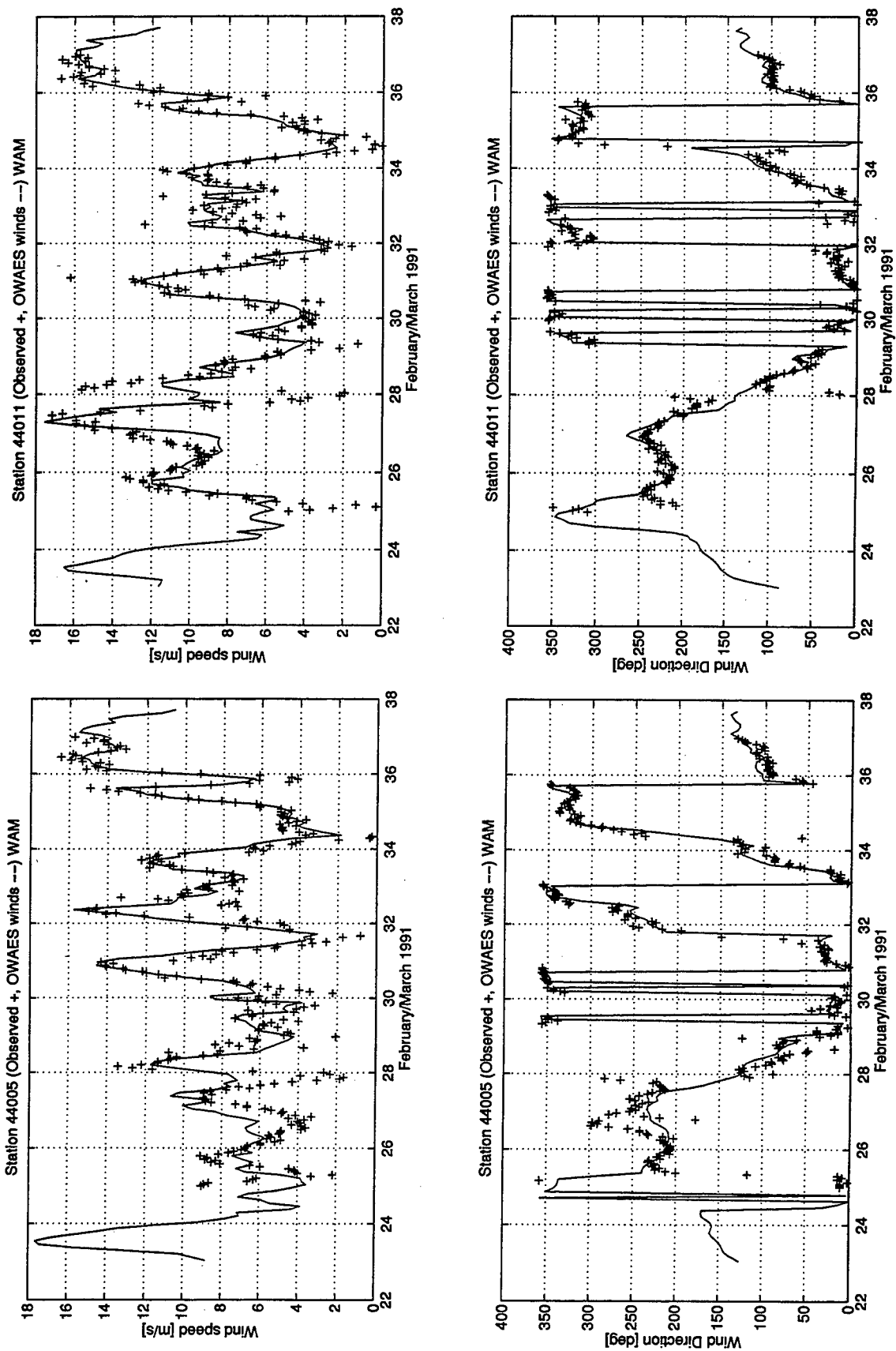
Figure A-11. Wind speed and direction time histories at 44005 and 44011 for IOP3.
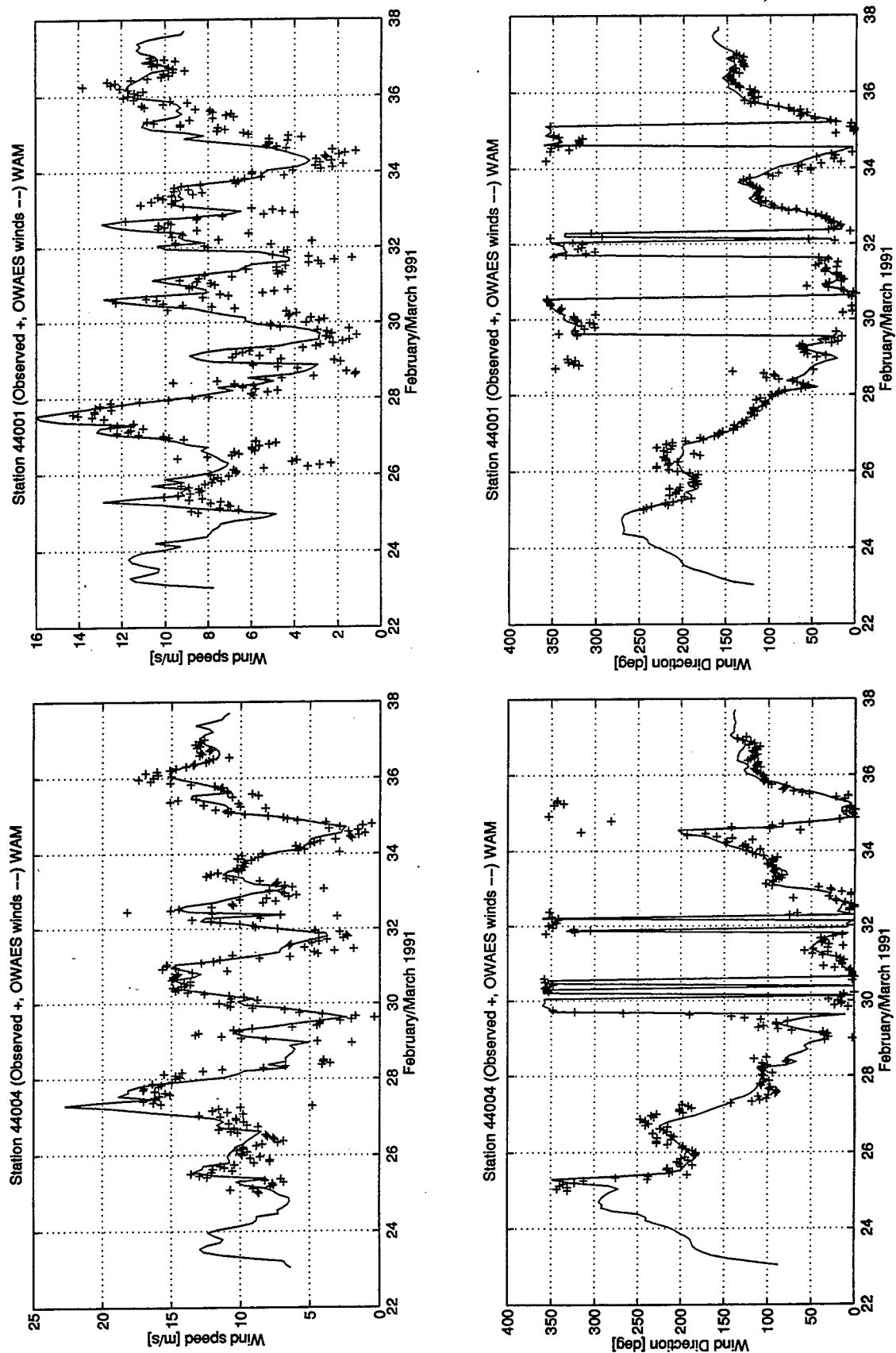
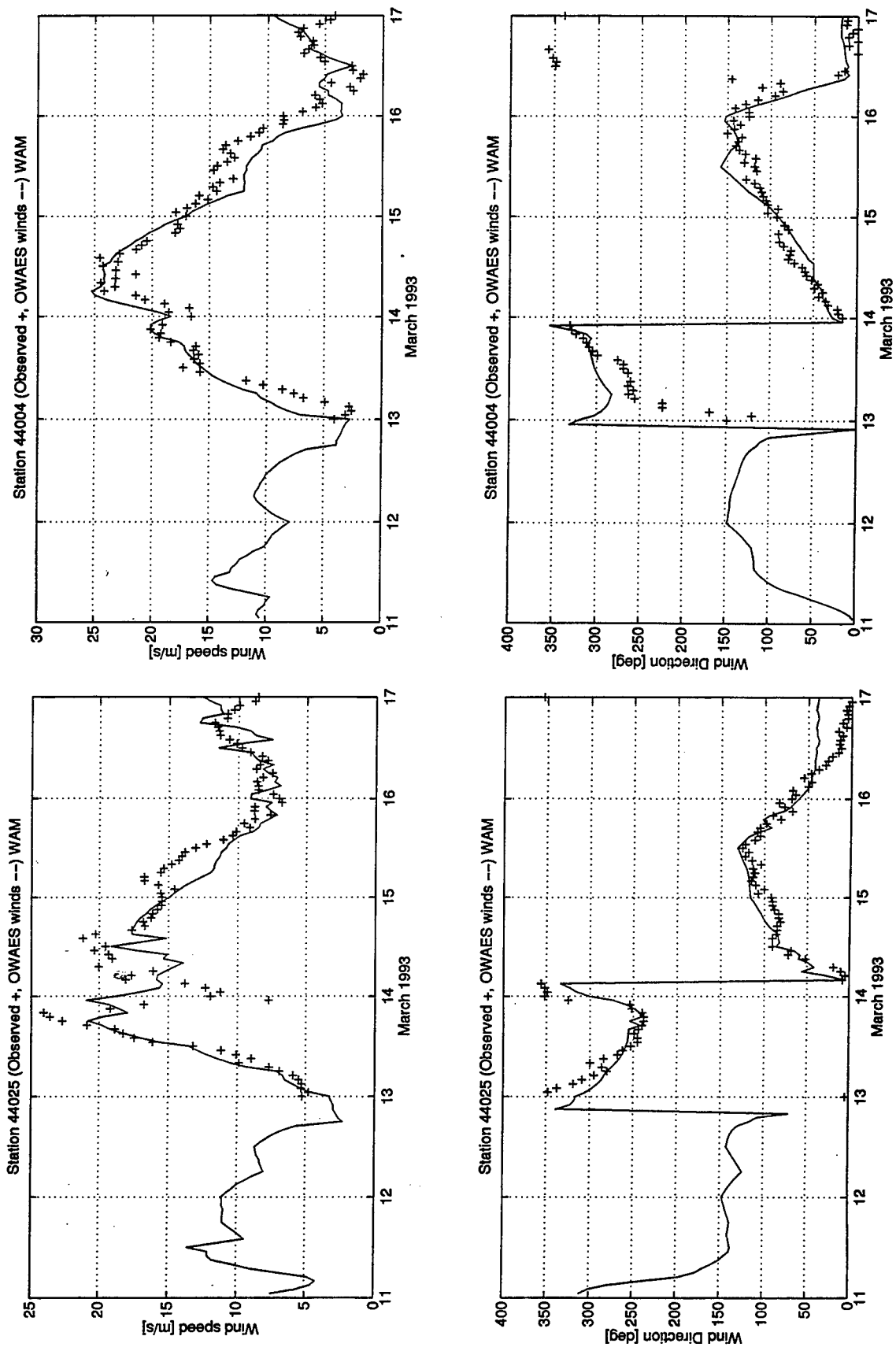Figure A-12. Wind speed and direction time histories at 44004 and 44001 for IOP3.

154
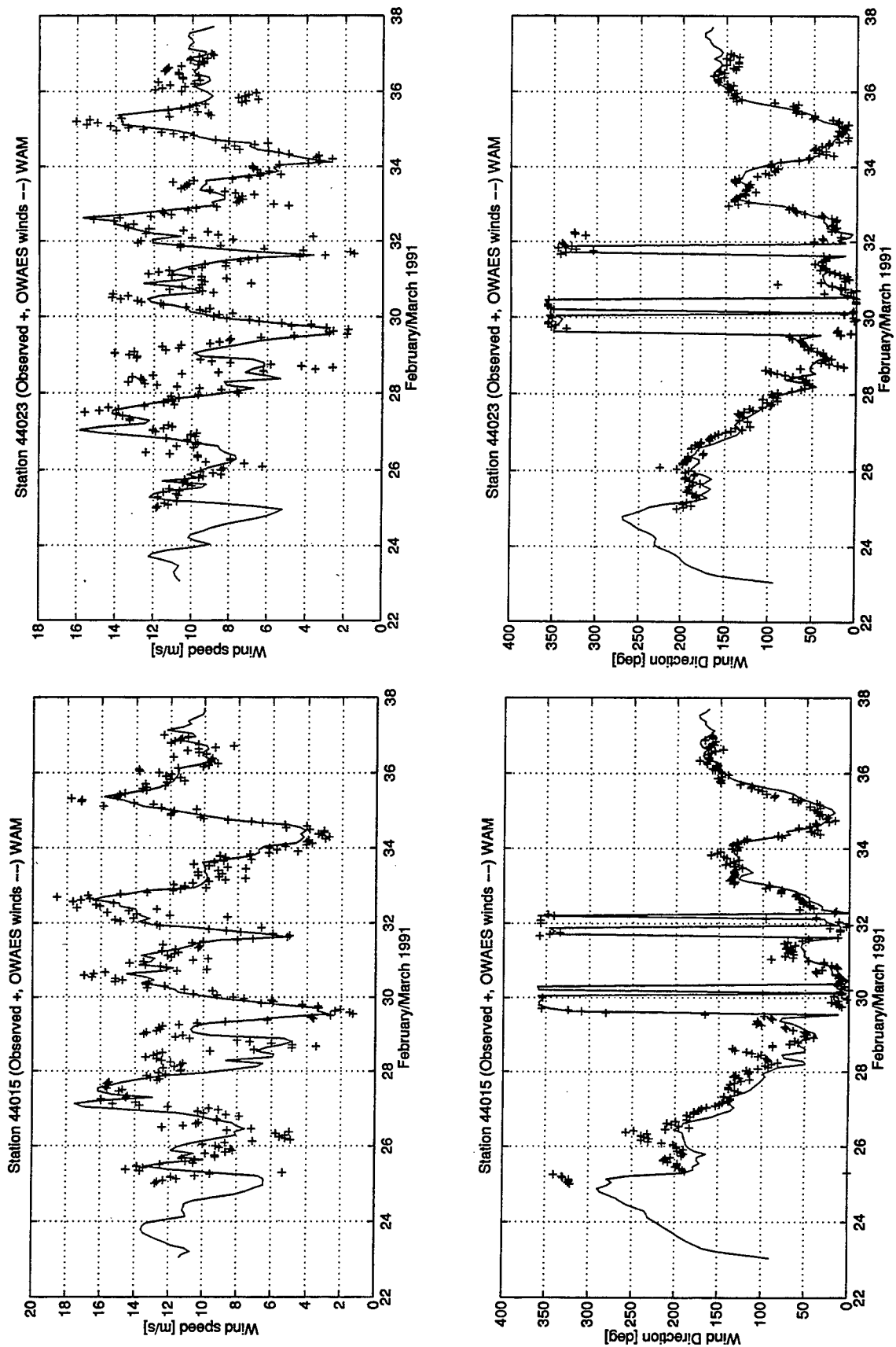
Figure A-13. Wind speed and direction time histories at 44015 and 44023 for IOP3.
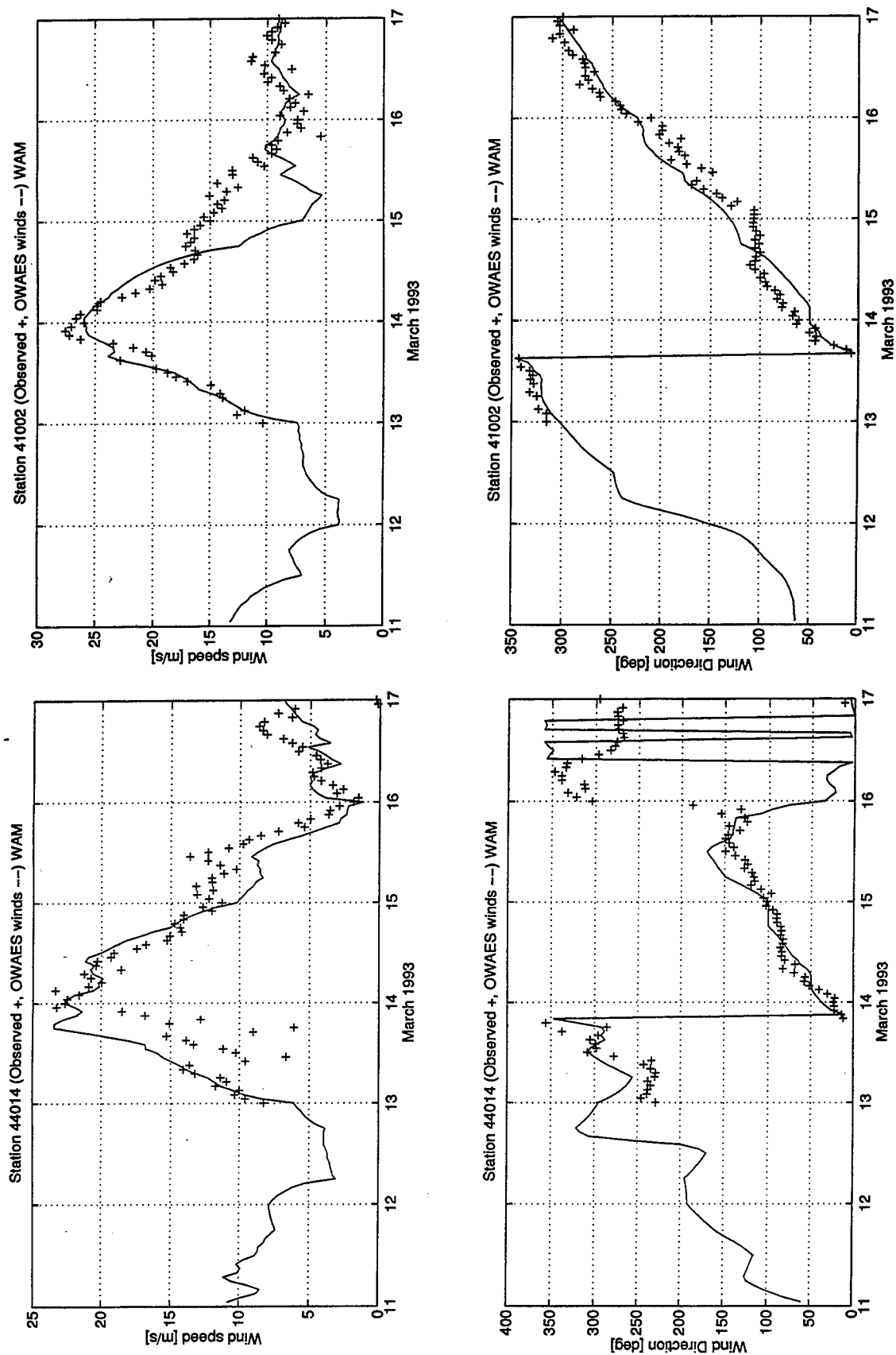
Figure A-14. Wind speed and direction time histories at 44014 and 41002 for IOP3.

Figure A-15. Wind speed and direction time histories at 41010 for IOP3.

Figure A-16. Wind speed and direction time histories at 44011 and 44008 for HOS.

Figure A-17. Wind speed and direction time histories at 44014 and 41001 for HOS.

Figure A-18. Wind speed and direction time histories at 41002 and 41010 for HOS.

Figure A-19. Wind speed and direction time histories at 44025 and 44004 for SOC.

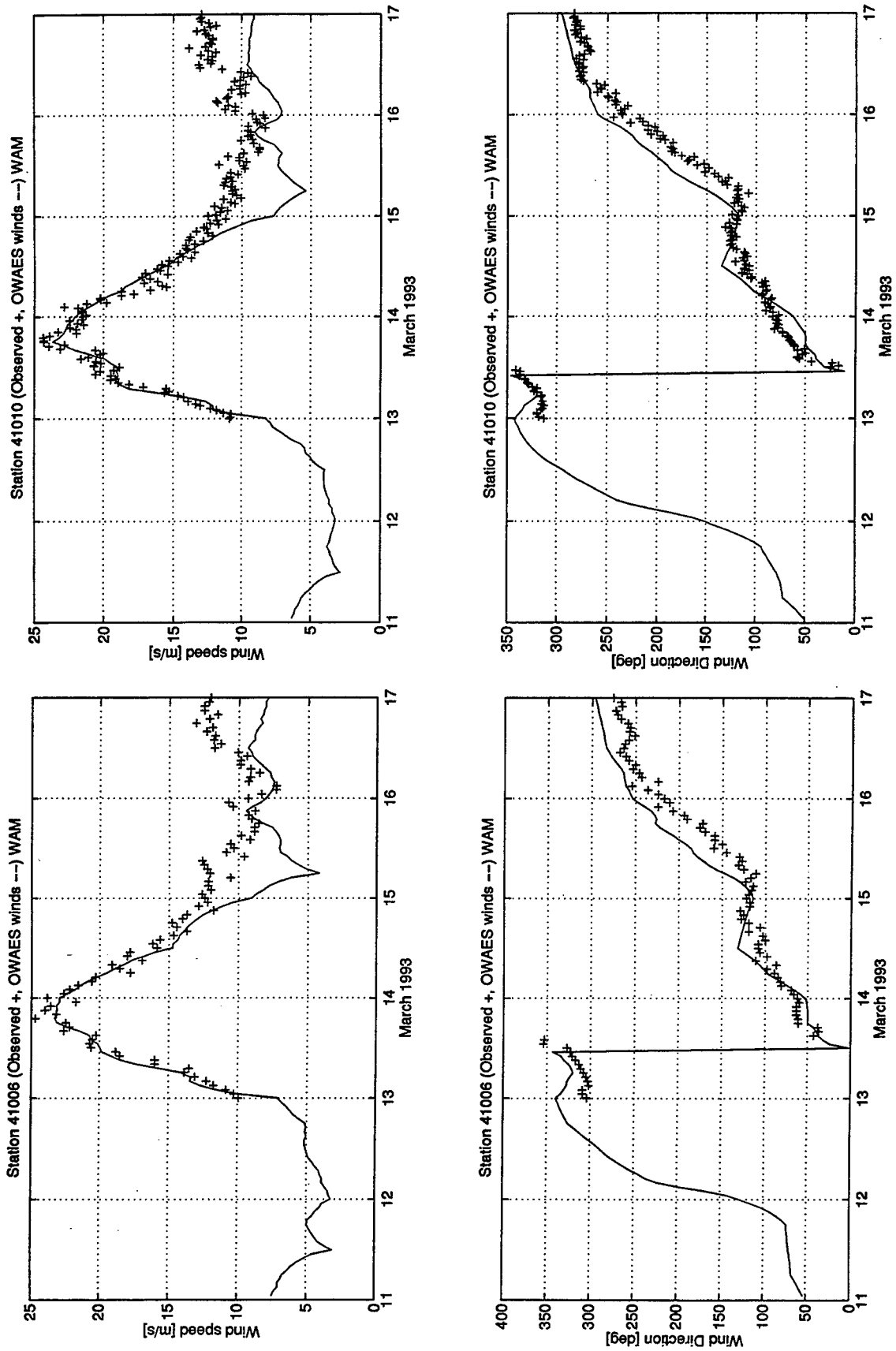Figure A-20. Wind speed and direction time histories at 44014 and 41002 for SOC.

Figure A-21. Wind speed and direction time histories at 41006 and 41010 for SOC.

1. AGENCY USE ONLY (Leave blank)	2. REPORT DATE September 1998	3. REPORT TYPE AND DATES COVERED Final report

4. TITLE AND SUBTITLE
Comparison Between Third- and Second-Generation Ocean Wave Models

5. FUNDING NUMBERS

6. AUTHOR(S)
Steven M. Bratos

7. PERFORMING ORGANIZATION NAME(S) AND ADDRESS(ES)
U.S. Army Engineer Waterways Experiment Station
3909 Halls Ferry Road, Vicksburg, MS 39180-6199

8. PERFORMING ORGANIZATION REPORT NUMBER
Technical Report CHL-98-25

9. SPONSORING/MONITORING AGENCY NAME(S) AND ADDRESS(ES)
U.S. Army Corps of Engineers
Washington, DC 20314-1000

10. SPONSORING/MONITORING AGENCY REPORT NUMBER

11. SUPPLEMENTARY NOTES
Available from National Technical Information Service, 5285 Port Royal Road, Springfield, VA 22161.

12a. DISTRIBUTION/AVAILABILITY STATEMENT
Approved for public release; distribution is unlimited.

12b. DISTRIBUTION CODE

13. ABSTRACT (Maximum 200 words)

The objective of this study is to assess the relative performance of a second-generation (2G) model, WISWAVE, and a third-generation (3G) model, WAM, in deep water. High-quality wind fields, with detailed spatial and temporal resolution, were used to force both models in an effort to isolate differences between their formulations. Even though previous studies have compared these models, this study is the first direct comparison where frequencies and directions have been discretized identically; no wind field interpolation was used, and wave model grids are not nested.

Five extratropical storm events that occurred along the U.S. Atlantic coast were selected for comparison. All five historical wind fields were developed using kinematic analysis and objective techniques. These storm events were selected because of the availability of high-quality winds and their variety of conditions ranging from extreme events to more moderate and variable events characterized by sea and swell, shifting winds, and passage of cold fronts. Three of the storms occurred during the Surface Wave Dynamics Experiment (SWADE) intensive operation periods (IOP) and are IOP1, IOP2, and IOP3. The remaining two storms, the "Halloween Storm" and the "Storm of the Century," were significant events causing flooding and damage along the Atlantic seaboard.

(Continued)

14. SUBJECT TERMS

Frequency-direction spectra	Statistics	WISWAVE
Numerical wave modeling	Third generation	
Second generation	WAM	

15. NUMBER OF PAGES
175

16. PRICE CODE

17. SECURITY CLASSIFICATION OF REPORT UNCLASSIFIED	18. SECURITY CLASSIFICATION OF THIS PAGE UNCLASSIFIED	19. SECURITY CLASSIFICATION OF ABSTRACT	20. LIMITATION OF ABSTRACT

13. (Concluded).

Each model was driven by identical wind fields and gridded to 1/2° latitude and longitude spatial resolution and 1-hr temporal resolution. Both models were run in the deepwater mode. Model results for these storms were compared with National Data Buoy Center (NDBC) buoy wave measurements.

The analysis of the results is divided into three steps. First, a qualitative comparison is made between model predictions and buoy data for the mean parameters: significant wave height, mean wave period, peak wave period, peak wave direction, directional spreading coefficient, wind speed, and wind direction. Second, a series of statistical tests of the wave parameters was developed, including mean, bias, and root-mean-square error. In addition to the standard statistical parameters, a pattern correlation between model and measured two-dimensional spectra was presented.